Targeting FGFR signalling to disrupt cellular cross-talk in pancreatic cancer

Abigail Shirley Coetzee

Submitted in partial fulfilment of the requirements of the Degree of Doctor of Philosophy

August 2019

Queen Mary University of London

Barts Cancer Institute

Centre for Tumour Biology

John Vane Science Centre

Charterhouse Square

London

EC1M 6BQ

Declaration of authorship

I, Abigail Shirley Coetzee, confirm that the research included within this thesis is my own work or that where it has been carried out in collaboration with, or supported by others, that this is duly acknowledged below and my contribution indicated. Previously published material is also acknowledged below.

I attest that I have exercised reasonable care to ensure that the work is original, and does not to the best of my knowledge break any UK law, infringe any third party's copyright or other Intellectual Property Right, or contain any confidential material.

I accept that the College has the right to use plagiarism detection software to check the electronic version of the thesis.

I confirm that this thesis has not been previously submitted for the award of a degree by this or any other university.

The copyright of this thesis rests with the author and no quotation from it or information derived from it may be published without the prior written consent of the author.

Signature: Abigail Shirley Coetzee

Date: 28th August 2019

List of publications

Coetzee A., Grose R., Kocher H. 2019. Pancreatic cancer organotypic models. *Curr Top Microbiol Immunol.*

Neuzillet C., Tijeras-Raballand A., Ragulan C., Cros J., Patil Y., Martinet M., Erkan M., Kleeff J., Wilson J., Apte M., Tosolini M., **Wilson A.S.**, Delvecchio F.R., Bousquet C., Paradis V., Hammel P., Sadanandam A., Kocher H.M. 2018. Inter-and intra-tumoral heterogeneity in cancer-associated fibroblasts of human pancreatic ductal adenocarcinoma. *The Journal of Pathology*, 248**,** 51-65.

Clayton N.S., **Wilson A.S.**, Laurent E.P., Grose R.P., Carter E.P. 2017. Fibroblast growth factor-mediated crosstalk in cancer etiology and treatment. *Developmental Dynamics*, 246**,** 493-50.

Carapuça E.F., Gemenetzidis E., Feig C., Bapiro T.E., Williams M.D., **Wilson A.S.**, Delvecchio F.R., Arumugam P., Grose R.P., Lemoine N.R., Richards F.M., Kocher H.M. 2016. Anti-stromal treatment together with chemotherapy targets multiple signalling pathways in pancreatic adenocarcinoma. *The Journal of Pathology*, 239**,** 286-296.

Acknowledgements

Firstly, I would like to thank both Richard and Hemant for giving me the opportunity to complete this project. I really appreciate all of the invaluable advice, support, encouragement and guidance that they have given me throughout my PhD. I would also like to thank Pancreatic Cancer Research Fund for funding the project for the last four years.

I feel so lucky to have had the opportunity to complete my PhD in the Centre for Tumour Biology. Everyone within the department has been so friendly, kind and helpful, both inside and outside of the lab. Debbie and Erwin, you are superstars that keep the laboratory running, thank you. There are so many people to thank, but in particular Ami, Claire, Zareen, Liz, Alex, Caz, Banu, Sophie, Ivan, Brynna, Amelia, Lauren, Litsa, Marina, George, Rachel, Sara and Bakouche, thank you so much for being great friends and for the chats and laughter. You all made me feel so welcome at the start of my PhD and have kept me smiling throughout. Thanks also to everyone in G23, you have kept me constantly entertained and fed throughout my thesis writing! I feel really grateful to have such a positive and friendly office to work in.

I have had the great opportunity to be part of two wonderful teams throughout my time at BCI. Thank you so much to Beta, who gave me such good training and advice at the start of my PhD. To the pancreas crew new and old – thank you for making my time in the lab so enjoyable. You helped the long hours slip by with laughter and beautiful singing! Prabs, Cindy, Francesca, Abhirup, Vickna, Michelle, Gabriel, Ahmet, Christine, Rachel and Daniel, I feel so lucky to have been able to share the lab area with you all over the last four years. To the extended pancreas group: Sara, Bakouche, Sophie, Minal, Lavanya, Rhiannon, Archana and Tom, you all have been

so kind and helpful to me both scientifically and personally and for that I am truly grateful.

The FGF group have been equally as amazing and supportive throughout the last four years. To the FGF 4 life gang (Ed, Tash and Yasmine), thanks for getting me through the majority of the PhD. You are all amazing friends who were there for me through all the ups and downs of lab life, thank you so much. To the new Grose group, Ed, Lucía, Chris, Demi, Shayin, Reza and Nick, thank you for all your support over the last part of my PhD and for keeping my spirits up even in the depths of Mass Spec harvesting or thesis writing!

I would like to say an additional thank you to all the post docs that have given me so much help and guidance over the last 4 years. Ed, Tash, Michelle, Chris and Lucía, thank you for all the advice and ideas that have helped me to complete the PhD.

Finally, to all my friends and family, thank you so much for being understanding and encouraging over the last four years. The many missed plans or late arrivals, you have all been a network of support for me personally throughout the journey. Especially Amy, Shree, Ellie and Sophie who helped me to plan a wedding alongside all the PhD madness, you are all stars. My lovely family, Mum, Dad, Sophie and Josh, thank you for trying to understand what I do, always being so proud and keeping my spirits up. Nathan, there are no words to describe my gratitude for your support. Your love and understanding nature for the last four years has been incredible and you have made this journey so much easier for me.

Abstract

Pancreatic ductal adenocarcinoma (PDAC) has a poor prognosis with a 5 year survival rate of less than 5 %. PDAC tumours consist of a desmoplastic stroma, which limits the effectiveness of chemotherapy. Pancreatic stellate cells (PSCs), which form a key part of this stroma, become activated in response to tumour development. Activated PSCs enter a cross-talk with cancer cells to induce tumour cell proliferation and invasion, leading to metastatic spread. Nuclear fibroblast growth factor receptor 1 (nFGFR1) has been found in PSCs at the invasive edge of PDAC tumours. Inhibition of FGFR1 prevents its nuclear translocation in PSCs, which results in decreased invasion in 3D *in vitro* PDAC models. Nuclear translocation of FGFR1 in PSCs appears to be a vital mechanism that triggers the transcription of key proteins involved in PDAC invasion.

We have used a powerful combination of chromatin immunoprecipitation (ChIP-seq) and sub-cellular mass spectrometry to determine the transcriptional targets of nFGFR1 and consequent sub-cellular protein flux. These techniques have allowed us to dissect the functional consequences of FGFR1 knockdown or inhibition in the PSCs. Candidate drivers of invasion are being validated in state-of-the-art 3D *in vitro* PDAC models. We have extended these functional studies to combination therapy with the clinical agent gemcitabine (targeting cancer cells) and all-trans retinoic acid (ATRA, modulating PSCs), providing translational relevance for our findings. We are validating this novel strategy using *in vivo* co-culture xenograft models with specific reference to FGFR1. Effectively disrupting the cross-talk between the tumour and stroma, either alone or in combination with other therapies, could translate to improved therapeutic responses in PDAC patients in the clinic.

Table of Contents

List of Figures

List of Tables

List of acronyms

4-MU	4-methylumbelliferone
5-FU	Fluorouracil
ADEX	Aberrantly differentiated endocrine exocrine
α	Alpha
α-SMA	α-Smooth muscle actin
ADM	Acinar-to-ductal metaplasia
ANXA2	Annexin A2
AP-1	Activator protein-1
AsPC-1	Pancreatic cancer cell line
ATRA	All-trans retinoic acid
AZD4547	FGFR tyrosine kinase inhibitor
B2M	Beta-2 microglobulin
BAG3	Bcl2-associated athanogene 3
β	Beta
BMP8A	Bone morphogenetic protein 8A
BSA	Bovine serum albumin
CA19-9	Carbohydrate antigen 19-9
CAF	Cancer associated fibroblast
CAR T	chimeric antigen receptor T
CBL	Casitas B-lineage lymphoma
CBP	Cyclic AMP responsive element-binding protein
CEA	Carcinoembryonic antigen
cfDNA	Cell-free DNA
ChIP	Chromatin immunoprecipitation
COLO 357	Pancreatic cancer cell line
CREs	cAMP-response elements

CT	Computed Tomography
ctDNA	Circulating tumour DNA
DAB	3,3'-diaminobenzidine
DAPI	4,6-diamidino-2-phenylindole
DAG	Diacylglycerol
δ	Delta
dCMPDA	Deoxycytidine monophosphate deaminase
dFdCDP	gemcitabine diphosphate
dFdCTP	gemcitabine triphosphate
DHH	Desert hedgehog
DMEM	Dulbecco's modified Eagle's medium
DMSO	Dimethyl sulfoxide
dNTPs	Deoxynucleotide triphosphates
Dox	Doxycycline
DTT	Dithiothreitol
DUSP6	Dual-specificity phosphatase 6
EBI3	Epstein barr virus induced 3
ECM	Extra-cellular matrix
EGF (R)	Epidermal growth factor (receptor)
EMT	Epithelial to mesenchymal transition
ER	Oestrogen receptor
ERAD	ER-associated protein degradation
EZR	Ezrin
FAMMM	Familial atypical multiple mole melanoma syndrome
FAP	Fibroblast activation protein
FBS	Foetal bovine serum
FDA	Food and Drug Administration
FGF (R)	Fibroblast growth factor (receptor)

FGF-BP	Fibroblast growth factor binding protein
FGFR1-HT	Fibroblast growth factor receptor 1 – HaloTag construct
FHOD1	Formin homology-2-domain containing protein 1
FOP	FGFR1 oncogene partner
FRS2	FGFR substrate 2
FTSECS	Fallopian tube secretory epithelial cells
GAB1	GRB2-associated binding protein 1
GAPDH	Glyceraldehyde 3-phosphate dehydrogenase
γ	Gamma
Gem	Gemcitabine
GFAP	Glial fibrilliary acidic protein
GFP	Green Fluorescent Protein
GI_{50}	Drug concentration at which 50 % of the cell growth is inhibited
GPER	G protein-coupled oestrogen receptor
GPX1	Glutathione peroxidase 1
GRB2	Growth factor receptor-bound 2
GRINA	glutamate ionotropic receptor NMDA type subunit associated protein 1
HA	Hyaluronic acid
HEK293T	Human embryonic kidney cells
HES1	Hairy and enhancer of split-1
HGF	Hepatocyte growth factor
HGSC	High grade serous carcinoma
HIER	Heat induced epitope retrieval
HNF3b	Hepatocyte nuclear factor 3-beta
HNSCC	Head and neck squamous cell carcinoma
HPRT-1	Hypoxanthine Phosphoribosyltransferase 1
HSC	Hepatic stellate cell

HSC70	Heat shock cognate 70
HSPG	Heparan sulphate proteoglycans
hTERT	Human telomerase reverse transcriptase
HUAEC	Human umbilical arterial endothelial cells
HUVEC	Human umbilical venous endothelial cells
IAA	Iodoacetamide
Ig	Immunoglobulin
IGF	Insulin-like growth factor
IL	Interleukin
INFS	Integrative nuclear fibroblast growth factor receptor 1 signalling
iNOS	Inducible nitric oxide synthase
IP_3	Inositol-1,4,5-triphosphate
IP-10	Interferon-inducible protein 10
IPMN	Intraductal papillary mucinous neoplasms
JAK/STAT	Janus kinase/signal transducer and activator of transcription
KRTAP5-6	Keratin associated protein 5-6
LGALS3BP	Galectin-3-binding protein
LOX	Lysyl oxidase
LYVE1	Lymphatic vessel endothelial hyaluronan receptor 1
M1090T	Primary cancer-associated stellate cell (sub-type A)
M1245	Primary cancer-associated stellate cell (sub-type A)
MARCKSL1	Myristoylated alanine-rich c-kinase substrate-like protein 1
MCN	Mucinous cystic neoplasms
MDM2	Mouse double minute 2
MEM	Minimum essential medium
MIA PaCa-2	Pancreatic cancer cell line
miRs	MicroRNAs
MUC2	Mucin 2

MYO15A	Myosin XVA
MMPs	Matrix metalloproteinases
NaCl	Sodium Chloride
$NaHCO_3$	Sodium bicarbonate
N-cadherin	Neuronal cadherin
N-CAM	Neural cell-adhesion molecule
NChIP	Native chromatin immunoprecipitation
nFGFR1	Nuclear FGFR1
NF-κB	Nuclear factor kappa B
NSG	Non-obese diabetic (NOD) severe combined immunodeficiency (scid) gamma mice
PANC-1	Pancreatic cancer cell line
PanINs	Pancreatic intraepithelial neoplasias
PARP	Poly (ADP-ribose) polymerase
PBS	Phosphate buffered saline
PBS (T)	Phosphate-buffered saline (0.05 % (v/v)Tween 20)
PCDHB15	Protocadherin beta 15
PCNA	Proliferating cell nuclear antigen
PD	Pancreaticoduodenectomy
PDAC	Pancreatic Ductal Adenocarcinoma
PDC	Pyruvate dehydrogenase complex
PDGF (R)	Platelet-derived growth factor (receptor)
PDHK1	Pyruvate dehydrogenase kinase 1
PDX1	Pancreatic and duodenal homeobox 1
PED	Pancreatic expression database
PHLDA1	Pleckstrin homology like domain family A member 1
PI3K	Phosphoinositide 3-kinase
PIP_2	Phosphatidylinositol-4,5-bisphosphate

PKC	Protein kinase C
PLCγ	Phospholipase Cγ
PPPD	Pylorus-preserving pancreaticduodenectomy
PRSS27	Serine protease 27
PS1	Pancreatic stellate cell line
PS1-HT	PS1 cell line with inducible expression of the FGFR1-HT construct
PSC	Pancreatic stellate cell
PTB	Phosphotyrosine-binding
QM	Quasi-mesenchymal
qPCR	Quantitative polymerase chain reaction
RARs	Retinoic acid receptors
REG1A	Regenerating islet-derived 1 alpha
RHAMM	receptor for hyaluronan-mediated motility
RON	Recepteur d'origine nantais
ROS	Reactive oxygen species
RSK1	Ribosomal S6-kinase 1
RTK	Receptor tyrosine kinase
RXRs	Retinoid acid receptors
SAM	Sterile α motif
SCRIB	Scribble planar cell polarity protein
SDS	Sodium dodecyl sulphate
SDS-PAGE	Sodium dodecyl sulphate polyacrylamide gel electrophoresis
SEF	Similar expression to FGF
SEM	Standard error of the mean
SERPINI2	Serpin peptidase inhibitor, clade I (pancpin) member 2
SH2	Src homology 2
SFN	Stratifin

Shh	Sonic hedgehog
shRNA	Inducible PS1 FGFR1 short hairpin RNA knockdown cells
siRNA	Small interfering RNA
SPARC	Secreted protein acidic and rich in cysteine
SPRY	Sprouty
SOS	Son of Sevenless
SOX9	SRY-related HMG-box gene 9
STR	Short tandem repeat
sTRA	Sialylated tumour-related antigen
STRING	Search Tool for the Retrieval of Interacting Genes/Proteins
TACC	Transforming acidic coiled-coil
TBS (T)	Tris-buffered saline (0.1 % (v/v) Tween-20)
TEA	Trimethylamine
TEAB	Triethylammonium bicarbonate
TFF1	Trefoil factor 1
TG2	Tissue transglutaminase 2
TGF (-β)	Transforming growth factor (beta)
TGFBI	Transforming growth factor beta induced
TKIs	Tyrosine kinase inhibitors
TMR	Tetramethyl rhodamine
TMT	Tandem Mass Tag
UA	Urea buffer
UCHL1	Ubiquitin carboxyl-terminal esterase L1
UGT	UDP-glucuronosyltransferase
VEGF (R)	Vascular endothelial growth factor (receptor)
VOCs	Volatile organic compounds
XChIP	Cross-linked chromatin immunoprecipitation
ZFC3H1	Zinc finger C3H1 domain-containing protein

Chapter 1: Introduction

1.1 The Pancreas

1.1.1 Pancreatic development

Embryonically the pancreas develops from two distinct buds of the endoderm: dorsal and ventral. As the duodenum rotates, the ventral bud with the bile duct also rotates such that the two buds fuse together at about 6-7 weeks gestation (Pan and Brissova, 2014). Further differentiation of the cells within the pancreas occurs through signalling between mesenchymal cells and epithelial cells. Some of the main pathways involved in this process are Fibroblast Growth Factor (FGF), retinoic acid, Notch and Sonic Hedgehog (Shh) signalling (Gittes, 2009, Johannesson et al., 2009, Mfopou et al., 2010).

1.1.2 Adult Pancreas

The adult pancreas performs two main functions. The exocrine compartment is involved in the secretion of many digestive enzymes, such as pancreatic lipase, amylase and proteases, into the duodenum. This compartment is made up of acinar and ductal cells, which release enzymes into ductal structures before they are further secreted into the digestive tract. The endocrine function of the pancreas involves release of hormones that can mainly control blood glucose levels amongst other functions. The endocrine pancreas is comprised of islets, formed of alpha (α), beta (β), delta (δ) and gamma (Ɣ) cells. The α cells secrete glucagon, the β cells secrete insulin, the δ cells secrete somatostatin and the Ɣ cells secrete pancreatic polypeptide (Figure 1.1) (Bardeesy and DePinho, 2002).

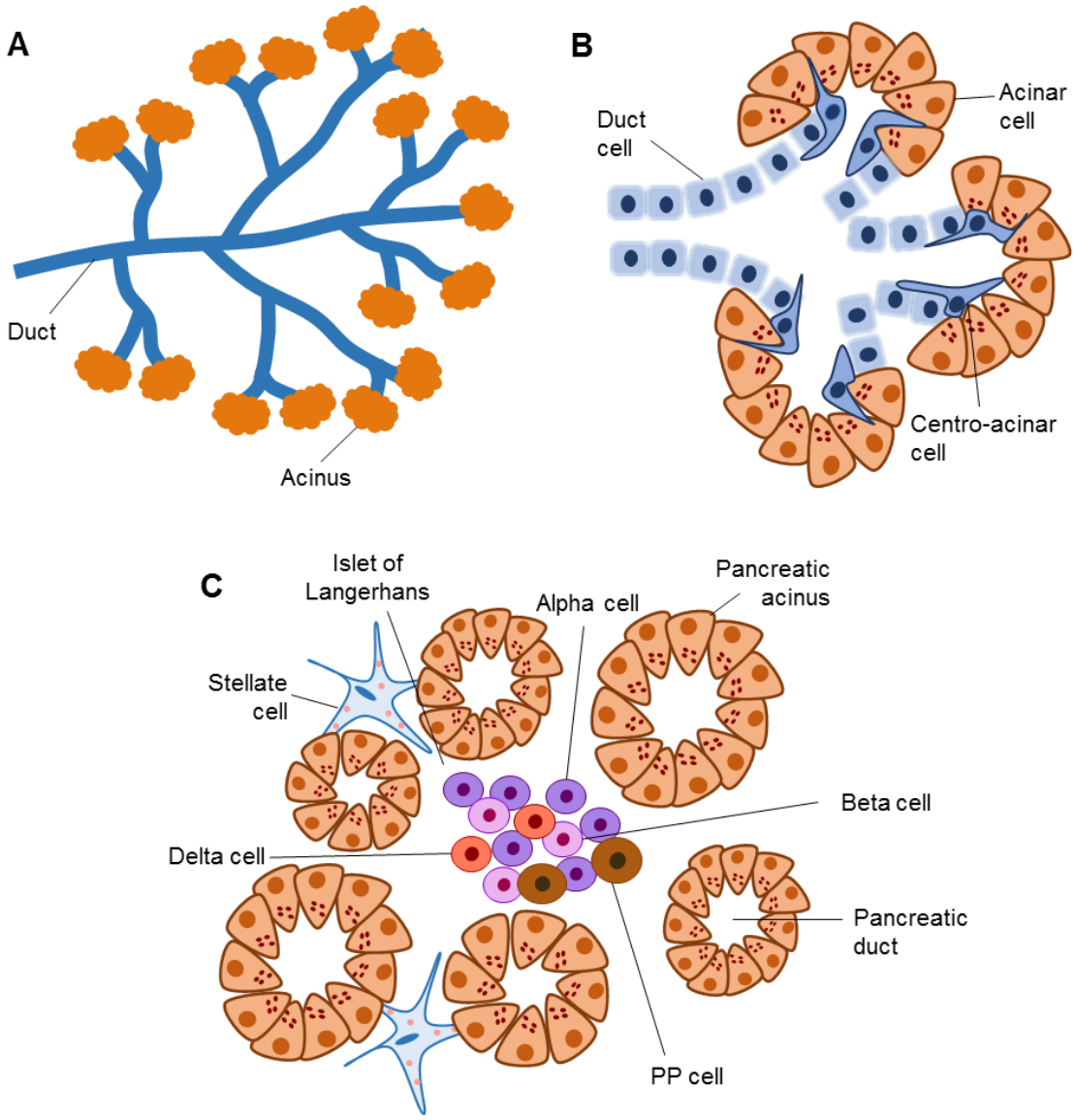

Figure 1.1 Structure of the pancreas

A. *Ductal structure with acini at the end of each branch.* ***B.*** *Acini made up of acinar cells producing digestive enzymes, which are then secreted into the ducts lined by the ductal cells. Centro-acinar cells have an indeterminate function and may represent, at least partly, the stem cells of the exocrine pancreas.* ***C.*** *The islets of Langerhans (made up of alpha, beta, delta and gamma cells) are interspersed between acini and carry out key endocrine functions to regulate blood glucose levels. Stellate cells, newly recognised interstitial pancreatic parenchymal cells which are of indeterminate origin, are also found surrounding the pancreatic acini.*

1.2 Pancreatic Ductal Adenocarcinoma

1.2.1 Epidemiology

Pancreatic cancer is one of the leading causes of cancer-related death worldwide. The five-year survival rate for patients is below 5 % and there have been no significant advances in diagnosis or treatments in recent years (Bosetti et al., 2013, Siegel et al., 2018). Pancreatic Ductal Adenocarcinoma (PDAC) arises from the exocrine compartment and is the most common tumour (~90 %) to occur within the pancreas (Hariharan et al., 2008, Rawla et al., 2019). Other rare exocrine tumours can also occur (~<5 %), such as acinar cell carcinoma, solid pseudopapillary neoplasm and pancreatoblastoma. Pancreatic neuroendocrine tumours arise from the endocrine compartment of the pancreas, however these are much less common (~5 %) and tend to have a better patient prognosis than PDAC (Brooks et al., 2019, Ilic and Ilic, 2016). PDAC is predicted to become the third most common cause of cancer related death in the USA by 2030 (Rahib et al., 2014), making it a cancer of unmet clinical need and a focus of research. I will discuss PDAC only from now onwards.

1.2.2 Risk factors

There are a number of factors that can increase the risk of developing PDAC. The risk increases with the number of first degree relatives that have suffered from the disease (Becker et al., 2014). Furthermore, some familial conditions can be linked with development of PDAC; for example, Lynch syndrome (hereditary non-polyposis colorectal cancer), which is underpinned by mutations in DNA mismatch repair genes, or familial adenomatous polyposis, characterised by mutations in the *APC* gene (Elkharwily and Gottlieb, 2008, Kastrinos et al., 2009). Familial *BRCA* mutations can cause an increased risk in many cancers, including PDAC (Greer and Whitcomb, 2007). Patients suffering from Peutz-Jeghers syndrome, caused by mutations in

STK11/LKB1, and familial atypical multiple mole melanoma syndrome (FAMMM), caused by mutations in *P16INK4A/CDKN2A*, have an increased risk of developing PDAC. Other conditions that have been linked with PDAC include cystic fibrosis, ataxia-telangiectasia and chronic pancreatitis (Becker et al., 2014).

However, despite these links with hereditary conditions, 90 % of PDAC cases are sporadic. As with most tumours, the risk of developing PDAC increases with age, with the highest incidence occurring between the ages of 65-75 years (Lowenfels and Maisonneuve, 2006). Smoking, drinking alcohol and obesity can all increase the likelihood of developing PDAC. There is also an increased risk found in diabetic patients (Becker et al., 2014). This could be due to increased levels of insulin and insulin-like growth factors (IGFs), which can stimulate cell proliferation. Also diabetic patients have increased oxidative stress and inflammation within the pancreas, which can promote tumour development (Li, 2012).

1.2.3 Clinical symptoms

Many tumours are asymptomatic until they are advanced, meaning that most patients are diagnosed during the late stages of the disease. Patients may present with non-specific abdominal pain, anorexia, weight loss and obstructive jaundice. Diagnosis is usually made through a Computed Tomography (CT) scan and subsequent biopsy. The tumour markers carcinoembryonic antigen (CEA) and carbohydrate antigen 19-9 (CA19-9) may be elevated in PDAC, however, these alone are not specific enough for use in detecting the presence of PDAC. For example, CA19-9 can also be elevated in other gastrointestinal cancers and in non-malignant pancreatic conditions, such as chronic pancreatitis (Ryan et al., 2014).

1.2.4 PDAC biomarkers

Due to the lack of suitable biomarkers, biomarker discovery is currently a major area of research. Earlier diagnosis of patients could significantly improve treatment options and therefore survival rates.

1.2.4.1 Serum biomarker panels

PDAC patients have elevated levels of vascular endothelial growth factor (VEGF) and FGF2 in their serum, compared to healthy controls (Pistol-Tanase et al., 2008). A serum biomarker panel including interferon-inducible protein 10 (IP-10), interleukin 6 (IL-6), platelet-derived growth factor (PDGF) and CA19-9 was able to distinguish patients with PDAC from those with benign pancreatic diseases (Shaw et al., 2014). The clinical utility of biomarkers can be assessed by sensitivity and specificity. Sensitivity measures the fraction of people with the disease that will be tested positive. Specificity measures the fraction of people without the disease that will be tested negative. A comparison of the glycan sialylated tumour-related antigen (sTRA) and CA19-9 levels in serum demonstrated that sTRA is more specific for detecting PDAC. This test was improved by combining two sTRA detection panels with CA19-9 in a specificity optimised panel, obtaining 95 % specificity and 54 % sensitivity (Staal et al., 2019). A panel of biomarkers may improve the chance of reliably detecting PDAC compared to a single biomarker. Subsequently a panel of 25 serum biomarkers has been developed that can reliably differentiate patients with PDAC from healthy controls and patients with other pancreatic diseases, such as chronic and autoimmune pancreatitis (Wingren et al., 2012).

1.2.4.2 Metabolomics

Metabolomics offers another promising method of identifying patients with cancer. For example, a panel of four metabolites (xylitol, 1,5-anhydro-D-glucitol, histidine and inositol) in serum from 59 patient samples compared to controls, has been shown to have a higher sensitivity in detecting PDAC, compared to CA19-9 and CEA (Sakai et al., 2016). Furthermore, palmitic acid presence in serum has been reported to distinguish between patients with malignant and benign lesions in 40 patient samples (Di Gangi et al., 2016). Other metabolite and amino acid serum panels have demonstrated sensitivity that can distinguish between healthy controls, pancreatitis, precursor lesions and PDAC (Leichtle et al., 2013, Yuan et al., 2016). These metabolomic approaches need to be tested in a wider cohort to confirm if any of them would make a suitable clinical biomarker panel for PDAC.

1.2.4.3 Cell-free DNA

Cell-free DNA (cfDNA) has been shown to be significantly increased in patients with cancer, making it a potential source of clinical biomarkers. Advances in sequencing techniques and droplet digital PCR have made it possible to isolate cfDNA and accurately analyse it for mutations or epigenetic changes specific to tumours. As *KRAS* mutation is an early event in PDAC development, identifying this mutation in cfDNA could be a useful early-stage diagnostic biomarker. In a study of 155 plasma samples from PDAC patients, the detection rate of circulating tumour DNA (ctDNA) was only 48% in localised disease, compared to over 80% in metastatic disease (Bettegowda et al., 2014). Another study found the same *KRAS* mutations in the primary tumour and in cfDNA in 35% of the patients analysed (Uemura et al., 2004). Circulating exosomes could also be used as a diagnostic tool, for example 43.6% of early-stage PDAC patients had detectable *KRAS* mutations in their exosomes (Allenson et al., 2017). Another study has shown increased levels of $KRAS^{G12D}$ in

exosomes isolated from PDAC patients (39.6%), compared to patients with IPMN precursor lesions (28.6%) or healthy controls (2.6%) (Yang et al., 2017).

Methylation status of cfDNA could also be used as a biomarker to predict the presence of PDAC. A study looking at cfDNA in 30 patient plasma samples discovered a panel of 17 gene promoters whose methylation could distinguish between chronic pancreatitis, pancreatic cancer and healthy controls (Liggett et al., 2010). The methylation profile of the *BNC1* and *ADAMTS1* promotors in cfDNA has been described as a potential early-stage PDAC biomarker, with a sensitivity of 81% and a specificity of 85% (Yi et al., 2013).

1.2.4.4 Non-invasive biomarkers

The presence of cell free microRNAs (miRs) in urine can also be a potential biomarker test for detecting cancer. Four miRNAs (miR-143, miR-223, miR-30e and miR-204) have been identified as being overexpressed in PDAC, compared to healthy controls (Debernardi et al., 2015). Furthermore, a three-biomarker panel, Lymphatic vessel endothelial hyaluronan receptor 1 (LYVE-1), Regenerating islet-derived 1 alpha (REG1A) and Trefoil factor 1 (TFF1), discovered in urine was shown to distinguish early stage PDAC (stage I-II) from healthy controls (Radon et al., 2015). This could be very useful to detect tumours at an earlier stage when treatment is more effective. Further work has shown detection of volatile organic compounds (VOCs) in urine can reliably discriminate between healthy controls and PDAC patients with either early or late stage disease. A urine biomarker test would be an easy, non-invasive method to check for the presence of PDAC in the clinic (Arasaradnam et al., 2018).

A miR panel extracted from stool samples has also been shown to be a potential PDAC biomarker. Three miRs (miR-21, miR-155 and miR-216) were present at higher levels in stools from PDAC patients, compared to patients with chronic pancreatitis and healthy controls. Stool samples provide an equally easy and non-invasive method of screening for PDAC in the clinic (Yang et al., 2014). All of the discussed biomarkers require further wide-scale validation to assess their suitability for clinical use to detect PDAC (Zhang et al., 2018).

1.2.5 PDAC development and progression

The development of PDAC is considered to begin with genetic mutations and the appearance of precursor lesions within the pancreas. The most well-described precursor lesions are pancreatic intraepithelial neoplasias (PanINs), which progress from grade 1 to 3 before cancer develops (Figure 1.2). The early frequent oncogenic changes that occur during the development of PanIN lesions are *K-RAS* activating mutations (>90 %), *HER2* amplification (30-40 %), the deactivation of *p16* (~90 %) and telomere shortening (>90%). Subsequently, there may be a loss of tumour suppressor proteins and the inactivation of DNA repair genes, such as *TP53* (~70 %) and *BRCA1/2* (~4-14 %) (Cicenas et al., 2017, Hezel et al., 2006, Qiu et al., 2011, Shibata et al., 2018, van Heek et al., 2002).

Other cystic precursor lesions that could lead to PDAC are intraductal papillary mucinous neoplasms (IPMNs) or mucinous cystic neoplasms (MCNs). IPMNs can develop from a main or a branch duct, depending on the location of the lesion, and progress from low grade to high grade dysplasia (Grützmann et al., 2011). Immunohistochemical staining can be used to further characterise these lesions into intestinal, pancreatobiliary, oncocytic and gastric subtypes (Distler et al., 2013,

Furukawa et al., 2005). MCNs are less common, occur mostly in women and tend to arise in the pancreatic body and tail (Crippa et al., 2008). These lesions can be classified into low, moderate and high grade dysplasia. Generally, if any precursor lesion is found in a scan, it will be surgically resected to prevent any risk of progression to invasive cancer (Distler et al., 2014).

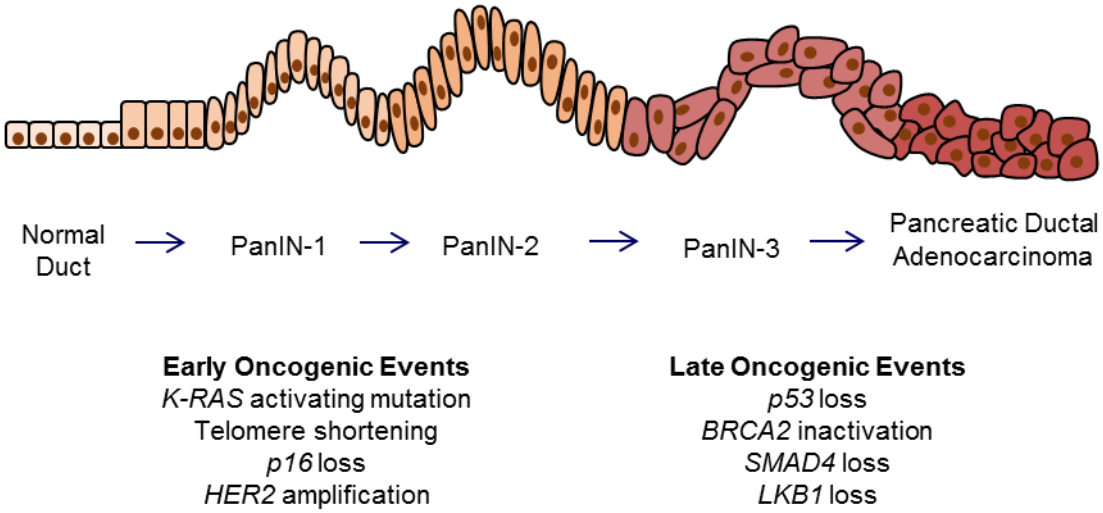

Figure 1.2 Phenotypic and genetic development of PDAC

The progression of pancreatic intraepithelial neoplasia (PanIN) lesions that can lead to the development of PDAC. Throughout the progression, the lesions become more irregular and gain increasing genetic mutations. Early events include the activation of the oncogene K-RAS and loss of p16. Late events involve the loss of tumour suppressor genes, such as TP53 and the inactivation of DNA repair proteins, such as BRCA2 (Hezel et al., 2006).

1.2.6 PDAC surgery

Currently the only potentially curative treatment for PDAC is surgical resection of the tumour. Unfortunately, only 10-15 % of patients are eligible for surgery, due to either the advanced stage of the disease at diagnosis, or due to increased risk factors, such as age or tumour proximity to major blood vessels (Ryan et al., 2014). The surgical resection procedure depends on the location of the tumour within the pancreas. Tumours that are located in the head are treated with pancreaticoduodenectomy (PD or Whipple), during which the head of the pancreas is removed, along with the duodenum, the gall bladder, part of the bile duct and the lower part of the stomach. Patients can also be treated with pylorus-preserving pancreaticduodenectomy (PPPD), which is the same as the PD operation except that none of the stomach is removed. Tumours that are present in the tail of the pancreas are treated by distal pancreatectomy, which removes the body and tail of the pancreas, along with the spleen. These surgeries are complex and can leave patients with complications such as diabetes or insufficient pancreatic enzyme production (Scavini et al., 2015, Strobel et al., 2019). Adjuvant chemotherapy and, sometimes, radiotherapy is given to these patients. However tumour recurrence is still common. Once the tumour has spread to distant organs, the patient has a poor prognosis (Hariharan et al., 2008).

1.2.7 Chemotherapy

Chemotherapy is often given to patients to extend life, however this has a limited effect. The poor response to drug treatment is due to the hypoxic environment within tumours and drug resistance of the tumour cells (Mahadevan and Von Hoff, 2007, Mohammed et al., 2014).

1.2.7.1 Gemcitabine

The current standard chemotherapy treatment that is used to treat PDAC is the nucleoside analogue gemcitabine. It is incorporated into the cellular DNA in place of cytosine to inhibit DNA synthesis. Gemcitabine is a pro-drug, which is taken up by cells to be converted into the active nucleotide analogues: gemcitabine diphosphate (dFdCDP) and triphosphate (dFdCTP) (Marangon et al., 2008, Mini et al., 2006), whereby it inhibits DNA polymerase and thymidylate synthase, causing increased cellular toxicity. Gemcitabine metabolites can be incorporated into RNA as well as DNA, causing chain termination (Plunkett et al., 1995a, Plunkett and Gandhi, 1996). This method of action allows drug damage to avoid detection by DNA repair enzymes and increases the level of drug induced apoptosis (Heinemann et al., 1988).

Gemcitabine also decreases the level of competing deoxyribonucleotides by inhibiting the enzyme ribonucleotide reductase. Other affected enzymes include the drug metabolising enzyme deoxycytidine monophosphate deaminase (dCMPDA), leading to increased levels of active metabolites within the cells (Mini et al., 2006, Plunkett et al., 1995b). This drug can cause toxic side effects, as it targets all cells; however tumour cells divide more frequently than other cells, making them vulnerable to the treatment, therefore increasing the therapeutic index in patients.

1.2.7.2 Nab-paclitaxel

Despite gemcitabine treatment, the median overall survival of patients is 6 months (Sun et al., 2014). There have been many clinical trials to develop more effective chemotherapy regimens in these patients. One drug that has been approved for use is nanoparticle albumin-bound paclitaxel (nab-paclitaxel). This is a formulation of the taxane: paclitaxel, which binds to microtubules preventing depolymerisation and,

therefore, prevents effective cell mitosis. Nab-paclitaxel contains the hydrophobic drug bound to albumin to form soluble nanoparticles, which reduces the side-effects of paclitaxel drug formulation. It has also been shown that nab-paclitaxel can reach higher concentrations in xenograft tumours compared to traditional formulations of paclitaxel (Desai et al., 2006). Another factor which could be responsible for increased drug response in tumours is that nab-paclitaxel could destroy the stroma surrounding the tumour. In a tumour xenograft study (Von Hoff et al., 2011), mice injected with nab-paclitaxel had decreased levels of collagen fibres and an increase in the presence of endothelial cells within the tumour mass. Furthermore, in the genetically engineered KPC (LSL-Kras(G12D) (/+);LSL-Trp53(R172H) (/+);Pdx-1-Cre) mouse model, it was reported that nab-paclitaxel caused a reduction in the levels of the gemcitabine metabolising enzyme cytidine deaminase, through the production of reactive oxygen species (ROS). This could lead to higher levels of gemcitabine triphosphate within the tumour cells, thereby increasing the cytotoxic effect of the combination treatment (Frese et al., 2012, Olive and Tuveson, 2006). Combination chemotherapy of gemcitabine and nab-paclitaxel has been shown, in clinical trials, to increase patient survival by nearly 2 months over gemcitabine treatment alone (Von Hoff et al., 2013).

1.2.7.3 Combination chemotherapy

Other chemotherapy regimens can be used in the clinic, usually combining a number of different drugs to give increased patient response. The combination chemotherapy regimen FOLFIRINOX has been shown to increase patient survival within groups of PDAC patients with a good performance status (Conroy et al., 2011). FOLFIRINOX comprises folinic acid (a vitamin B derivative that increases the effects of 5-FU by further inhibiting the activity of the thymidylate synthase enzyme), fluorouracil (5-FU, a pyrimidine analogue which is incorporated into the DNA and binds to thymidylate

synthase, preventing DNA replication and causing cell apoptosis), irinotecan (a topoisomerase 1 inhibitor which prevents effective DNA unwinding and replication) and oxaliplatin (a platinum based drug that intercalates in the DNA causing inter- and intra-strand cross-links, causing ineffective DNA replication and transcription) (Longley et al., 2003, Raymond et al., 2002, Robert and Rivory, 1998). There is also a nanoparticle formulation of irinotecan that has been approved by the Food and Drug Administration (FDA) to be used in combination with 5-FU and folinic acid as a second-line therapy in patients, after gemcitabine resistance (Hsueh et al., 2016). Capecitabine is an oral pro-drug of 5-FU which is also given to patients along with gemcitabine, decreasing side effects (Cunningham et al., 2009). Another oral pro-drug of 5-FU that has been approved for use as adjuvant chemotherapy following surgery in PDAC patients in Japan is S-1. This formulation improves the activity of 5-FU by inhibiting dihydropyrimidine dehydrogenase, which is the key enzyme of 5-FU catabolism (Sudo et al., 2014, Uesaka et al., 2016).

Despite all these therapeutic options, PDAC patients consistently show a poor response to chemotherapy. This could be due to the desmoplastic stroma and hypoxic environment within the tumour, the advanced stage of the tumour at diagnosis, the performance status of the patients or due to intrinsic drug resistance in the tumour cells. Consequently there is an urgent need for new therapeutic strategies for these patients.

1.2.8 PDAC sub-groups

Attempts have been made to categorise PDAC patients into sub-groups (Figure 1.3), allowing treatment options to become more tailored and hopefully improve patient response. Gene expression microarray data from PDAC tumours could divide

patients into three main sub-groups (Collisson et al., 2011). The quasi-mesenchymal (QM) group showed high levels of mesenchymal gene expression and was associated with worse prognosis. The exocrine sub-group showed a high expression of tumour cell derived digestive genes and the classical sub-group had higher expression of epithelial and adhesion genes (Collisson et al., 2011).

The sub-groups identified in 2011 were refined further by RNA expression profiling of PDAC patients to determine four sub-groups (Bailey et al., 2016). The features in these groups were matched with histopathological and genetic mutation data to further characterise these populations of patients. The four groups determined from this analysis were squamous, pancreatic progenitor, immunogenic and aberrantly differentiated endocrine exocrine (ADEX). The squamous, pancreatic progenitor and ADEX groups overlapped with the QM, classical and exocrine-like groups respectively. The immunogenic group was a newly classified sub-group within this analysis. The squamous sub-group had notably poor survival compared to the other three groups and was characterised by gene networks involved in inflammation, hypoxia response, metabolic reprogramming, autophagy and TGF-β signalling. Additionally, this sub-group was characterised by *TP53* mutations and increased expression of *TP63*, which has been shown to cause a more metastatic phenotype in genetically engineered mice ($Kras^{G12D/+}$; $Trp53^{fl/+}$; $TAp63^{fl/fl}$ KPC mice) (Miller et al., 2015). Indeed, there was an increase in expression of genes related to metastasis within this group, such as *lysyl oxidase* (*LOX)*, which could indicate tumours with a higher metastatic potential and therefore a worse prognosis for these patients. Whereas, the pancreatic progenitor subtype had increased expression of pancreatic endoderm cell-fate determination transcription factors, such as *pancreatic and duodenal homeobox 1 (PDX1)*, as well as fatty acid oxidation, drug metabolism and hormone biosynthesis pathways. The immunogenic sub-group had expression of

similar pathways to pancreatic progenitor, with an enriched immune infiltrate signature. The ADEX sub-group had enriched expression of pathways related to exocrine and endocrine pancreatic lineage differentiation.

An alternative approach combined a genetic signature for the tumour cells with either activated or non-activated stroma to form four sub-groups of patients (Moffitt et al., 2015). In this study, virtual microdissection was used to separate the gene expression signatures from the tumour cells and the stromal cells. Two sub-groups of tumour cells emerged from this analysis, named basal-like and classical, alongside the two sub-groups of stroma, activated or normal. It was found that the basal-like tumour with activated stroma signature gave the worst prognosis, whereas classical tumour with normal stroma had the best overall survival. The basal-like tumour sub-group most strongly associated with the squamous sub-group from the Bailey analysis, with half of the samples falling into this category and the rest divided between the other three categories.

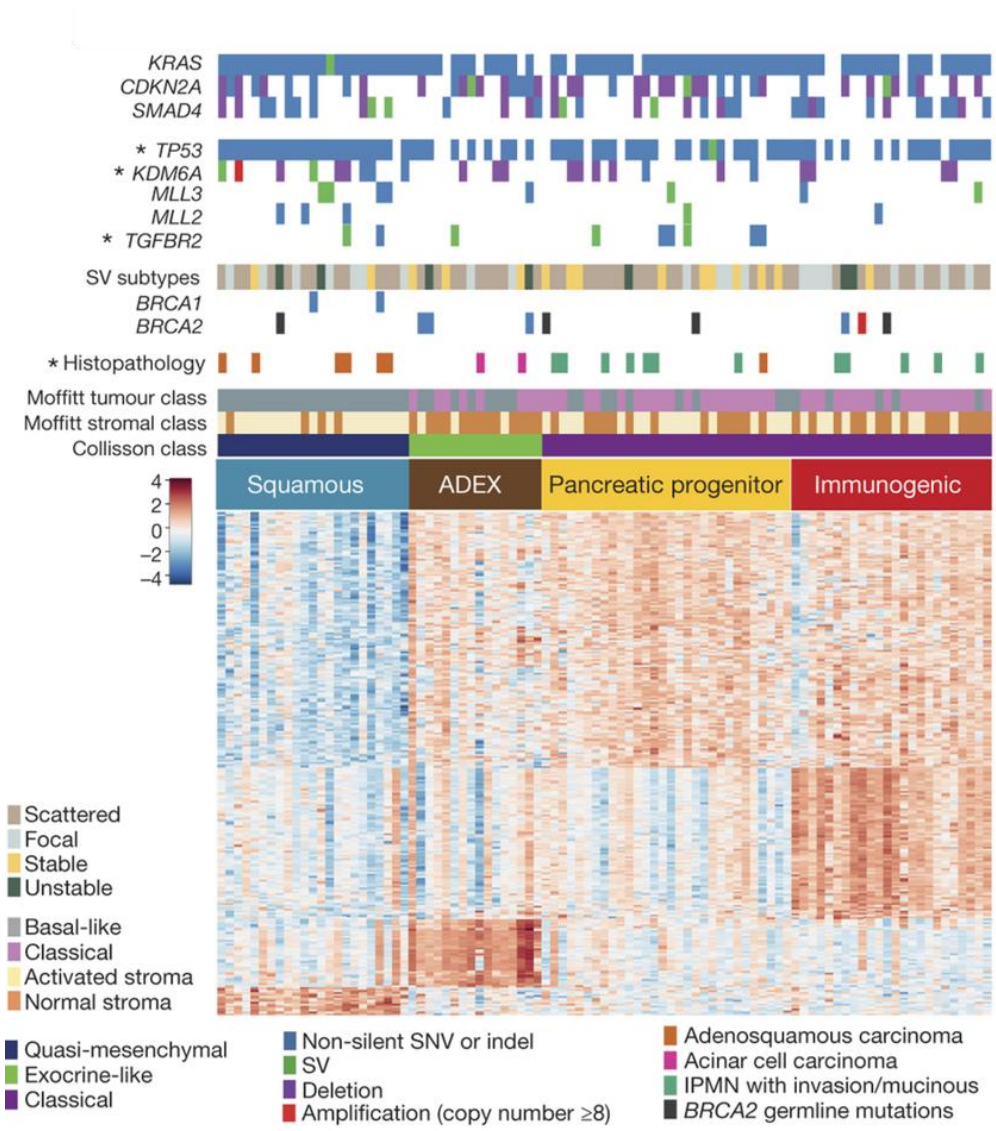

Figure 1.3 Comparison of transcriptomic sub-grouping of PDAC

This summary figure shows how the four sub-groups identified in the Bailey analysis overlapped with previously published transcriptomic sub-groups. In all three sets of data, there is one tumour sub-group that isolates out and is associated with poor survival. The gene expression data were also matched with histopathological and genetic mutation data, however no clear correlation was identified (Bailey et al., 2016)

A further classification of PDAC based on genetic mutations within the tumour has identified sub-groups linked to response to specific therapies (Waddell et al., 2015). The four sub-groups that arose from the whole genome sequencing and copy number variation analysis were named stable, locally rearranged, scattered and unstable. The unstable chromosomal phenotype frequently had mutations within the *BRCA* genes and showed more sensitivity to DNA damaging drugs, such as platinum-based compounds. These patients may also be responsive to poly (ADP-ribose) polymerase (PARP) inhibitor therapies, which can be used as a targeted synthetic lethality approach to tumour treatment (Fogelman et al., 2011).

1.3 PDAC stroma

1.3.1 Stromal composition

PDAC is characterised by a desmoplastic stroma that surrounds the tumour cells (Merika et al., 2012). There are many different cells that can be found within the stroma of PDAC tumours, including fibroblasts, immune cells, endothelial cells and stellate cells, embedded within an abundance of extracellular matrix proteins and polysaccharides, such as collagen, laminin, hyaluronic acid (HA) and fibronectin (Figure 1.4). This stroma creates a hypoxic environment that protects the cancer cells from chemotherapy treatment (Olive et al., 2009). It also means that angiogenesis inhibitors have little effect against pancreatic tumours. The stroma surrounding the tumour is often very stiff and has been shown to help promote tumour development (Nielsen et al., 2016). The most abundant protein found within the desmoplastic stroma is collagen, in particular collagen 1 (Linder et al., 2001). Cross-linking of collagen fibres by the amine oxidase LOX or tissue transglutaminase 2 (TG2) increases the stiffness of PDAC tumours. Expression of LOX is increased under hypoxic conditions and is a mediator of metastasis (Cox et al., 2013). TG2 is induced by TGF-β and can stimulate cancer-associated fibroblasts (CAFs) to produce more collagen (Lee et al., 2015). Additionally, HA is an important glycosaminoglycan present within PDAC stroma. This can bind non-covalently to proteoglycans and retain water to increase the stiffness of the stroma. The stiff stroma disrupts adherens junctions and can trigger cells to lose polarity, leading to increased cell proliferation and tumour progression. Additionally, the desmoplastic stroma has been shown to increase MMP secretion and therefore allow cells to remodel the ECM and metastasise (Haage and Schneider, 2014, Weniger et al., 2018).

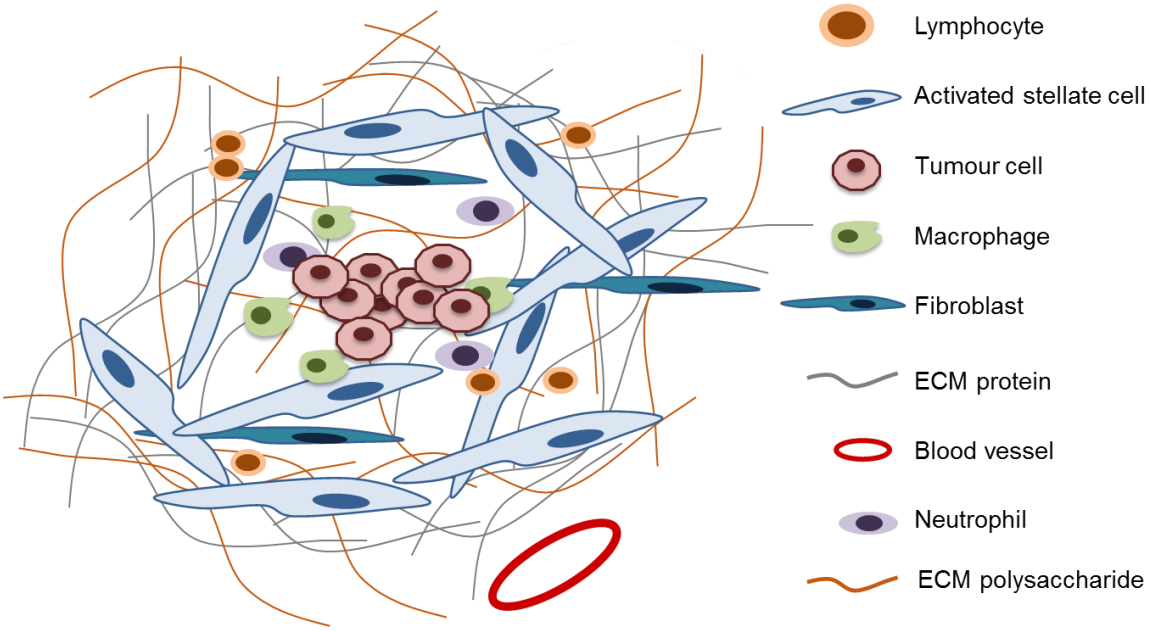

Figure 1.4 Desmoplastic stroma in PDAC

The stroma makes up a large volume of PDAC tumours. Many cells found within the stroma can contribute to tumour progression and invasion, such as activated pancreatic stellate cells, inflammatory immune cells and cancer associated fibroblasts. The stroma is very stiff due to the high levels of ECM proteins and polysaccharides that are laid down by activated stellate cells and fibroblasts. PDAC tumours are hypoxic and do not contain many blood vessels (Chu et al., 2007).

1.3.2 Pancreatic stellate cells

Within the stroma of PDAC, one of the key supporting elements is the stellate cell. The origin of stellate cells is proposed to be local mesenchymal cells in developing organs. They were first described in the liver by Karl van Kuppfer in 1876 and were distinguished by their storage of vitamin A in droplets within the cytoplasm (Geerts, 2001). Since this discovery, stellate cells have been identified in other organs, such as the kidney, intestine and lung (Omary et al., 2007). The first description of vitamin A storing cells within the pancreas was in 1982 in vitamin A loaded mice (Watari et al., 1982). The role of stellate cells has been most widely studied in the liver and pancreas.

Pancreatic stellate cells (PSCs) make up less than 5 % of cells in a healthy pancreas and exist in a quiescent state, with a round cell body and long cytoplasmic processes. However, during pancreatic injury, PSCs become activated, begin proliferating and lose their vitamin A stores (McCarroll et al., 2006). These cells are characterised by the expression of glial fibrillary acidic protein (GFAP), desmin, vimentin and alpha-smooth muscle actin (α-SMA) when activated. The storage of vitamins in lipid droplets in quiescent stellate cells can also be observed using lipid dyes, such as Oil Red O or BODIPY (Bynigeri et al., 2017).

It has been shown that activated stellate cells are critical for the development of PDAC. These cells are involved in cross-talk with the tumour cells via growth factors and cytokines to promote inflammation, extra-cellular matrix (ECM) degradation and tumour metastasis (Apte et al., 2013). Stellate cells promote tumour cell proliferation and invasion, whilst the tumour cells also increase stellate cell activation (Figure 1.5) (Apte and Wilson, 2012). Activated stellate cells release matrix metalloproteinases,

which can digest the surrounding ECM. They may also induce epithelial to mesenchymal transition (EMT) in tumour cells, rendering them with a metastatic potential (Kikuta et al., 2010). This suggests a key role of stellate cells in PDAC tumour invasion and metastasis.

Due to their importance in fibrosis and tumour development, PSCs have been isolated and maintained in cell culture. This process was first described in 1998 using density gradient centrifugation of cells from a rat pancreas and has been replicated with human PSCs (Apte et al., 1998, Bachem et al., 1998). Immortalisation of PSCs using SV40 large T antigen or human telomerase allows them to be studied extensively in the laboratory. PSCs become activated when grown in plastic tissue culture flasks and studies have shown that immortalised PSC lines have a similar phenotype and gene expression profile to activated PSCs (Jaster et al., 2005, Jesnowski et al., 2005, Masamune et al., 2003, Sparmann et al., 2004). This makes immortalised stellate cell lines an invaluable tool for PDAC research (Feig et al., 2012).

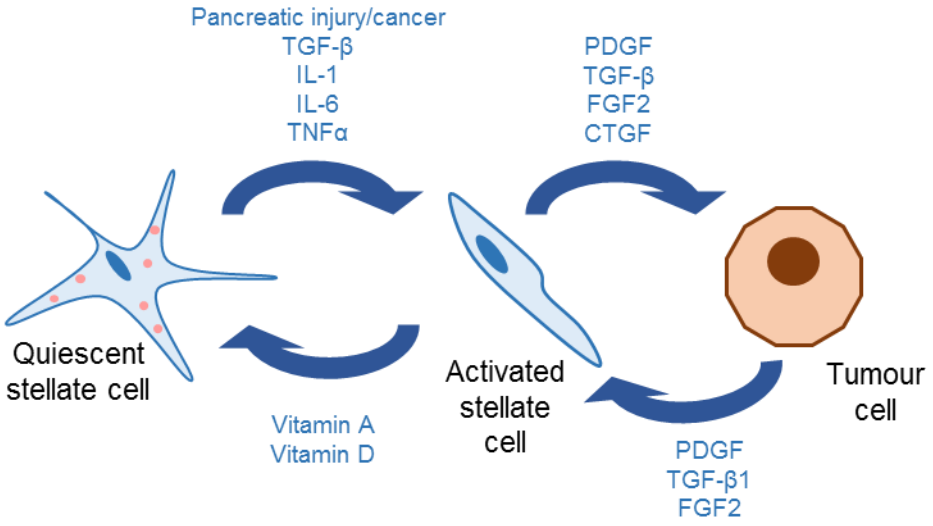

Figure 1.5 Interaction of stellate cells and cancer cells

Pancreatic stellate cells become activated in response to tissue injury and inflammation. This activation causes the cells to lose their vitamin-filled lipid droplets and express myofibroblast markers. Activated stellate cells in tumours can promote tumour cell proliferation through growth factor secretions, such as FGF2. Tumour cells can also promote stellate cell activation through growth factors, such as TGF-β. Activated stellate cells can be returned to their quiescent state through treatment with ATRA or vitamin D derivatives (Habisch et al., 2010). There is increasing evidence for heterogeneity within activated PSCs which may interact with cancer cells in different ways (Neuzillet et al., 2019).

1.3.3 Pancreatic stellate cell heterogeneity

Most attempts to determine subtypes of PDAC have based analysis on properties of the cancer cells (Section 1.2.4). However, a large component of these tumours is the desmoplastic stroma and therefore it may be necessary to consider heterogeneity in this compartment. Recently, there has been a growing interest in the classification of different subtypes of cancer-associated fibroblasts (CAFs), which are considered to be mostly activated PSCs in PDAC tumours. Two spatially distinct types of CAFs have been reported to be present within tumours: αSMA-positive myofibroblastic CAFs and αSMA-negative/IL-6-positive inflammatory CAFs (Ohlund et al., 2017). Another proposed classification is based on the expression of fibroblast activation protein (FAP) (pro-tumour) and αSMA (anti-tumour), determined by ablating either the FAP- or αSMA-positive CAF population (Kalluri, 2016).

A different study has classified CAFs into four subtypes (A-D) using transcriptomic analysis of cells isolated from patient tumour samples. CAF heterogeneity was observed both within the same tumour and between different patients. Subtype A was distinguished by expression of periostin at the invasive front: high expression correlated with aggressive tumours and therefore worse patient prognosis in this group. Myosin-11 was identified as a marker of subtype B and podoplanin expression was a feature of subtype C. There was no clear marker for subtype D CAFs; however platelet-derived growth factor receptor α (PDGFRα) was reported as a pan-CAF marker. In this study, αSMA expression did not associate with any specific CAF subtype. In patient samples, it appeared that periostin expression was at the invasive edge and the centre of PDAC tumours, whereas expression of myosin-11 and podoplanin was found only in the centre of the tumours. CAFs in subtype C have an immunogenic profile, which correlated with a better prognosis than other subtypes.

Moreover, CAF subtypes D and A were associated with worse overall patient survival in the ICGC and Beaujon patient cohorts respectively (Neuzillet et al., 2019).

1.4 Targeting the stroma

1.4.1 Overview

Since the desmoplastic stroma plays a vital role in PDAC development, targeting both the stromal and tumour cells may provide a therapeutic advantage to patients. Stromal modulating agents have been explored within the setting of PDAC alongside immune targeted therapies.

1.4.2 Hyaluronic acid

One key component of the ECM is hyaluronic acid (HA), a glycosaminoglycan that has been associated with tumour development and progression (Provenzano et al., 2012, Toole, 2004). HA is synthesised as a large polysaccharide by hyaluronan synthases (HAS1, 2 and 3) at the plasma membrane, where it is secreted directly into the ECM. HA can be cleaved by hyaluronidases, mainly HYAL1 and 2 (Toole, 2004). In normal tissues HA levels are closely regulated, however in tumours this balance is disrupted and there is a build-up of HA in the ECM. It has been shown that the presence of low-molecular-weight HA (25-75 kDa), rather than high-molecular-weight HA (400-600 kDa) within the PDAC stroma is linked to tumour progression (Cheng et al., 2016, Karbownik and Nowak, 2013, Schmaus et al., 2014). Due to the large accumulation of HA within PDAC stroma and the resulting increase in tumorigenesis (Kultti et al., 2014), HA has gathered interest as a potential therapeutic target. There are three strategies for targeting HA in tumours: blocking the synthesis, interrupting the signalling or depleting from within the stroma. An example of a drug that can block

the synthesis of HA is 4-methylumbelliferone (4-MU). 4-MU competitively binds to UDP-glucuronosyltransferase (UGT) and downregulates HAS2 and 3. UDP-glucuronic acid is used in many different pathways, not just HA biosynthesis. It is synthesised in the cytosol to be used in the production of glycosaminoglycans, and can be translocated into the Golgi apparatus for the biosynthesis of heparan sulphate and chondroitin. UGT is also responsible for adding glucuronic acid to xenobiotics to eliminate them, meaning that it is responsible for the inactivation of many drugs (Kultti et al., 2009). 4-MU has been shown in pre-clinical studies to increase the effects of gemcitabine in combination therapy (Nakazawa et al., 2006). To effect HA signalling, potential therapies could target binding partners, such as CD44 and receptor for hyaluronan-mediated motility (RHAMM) (Sato et al., 2016). The most advanced method of targeting HA within PDAC tumours is through depletion within the stromal compartment. PEGPH20 is an enzyme that has been shown to deplete HA within the stroma and increase the effectiveness of gemcitabine in the KPC mouse model (Jacobetz et al., 2013). The success of this therapy in pre-clinical models has translated into clinical trials in metastatic PDAC patients, in combination with gemcitabine and nab-paclitaxel. Phase I and II trials demonstrated a significant increase in progression-free survival in patients with high HA expression within their tumours (8.6 months compared to 4.5 months in the control arm) (Hingorani et al., 2013, Hingorani et al., 2015, Hingorani et al., 2016). Due to the success in phase II trials, a phase III trial has been launched in PDAC patients (NCT02715804).

1.4.3 Wnt signalling

The Wnt pathway is strongly associated with tumour growth and invasion in PDAC, making it an attractive drug target. Restoration of PSC quiescence leads to increased secretion of frizzled-related protein 4 and, therefore, a decrease in Wnt-β-catenin signalling in cancer cells (Froeling et al., 2011). An antibody against the frizzled

receptor, OMP-18R5 (vantictumab) has shown anti-tumour effects against PDAC cancer in pre-clinical models and is now in clinical trials in combination with gemcitabine and nab-paclitaxel (NCT02005315) (Zhang et al., 2013)(Zhang et al., 2013)(Zhang et al., 2013)(Zhang et al., 2013)(Zhang et al., 2013). Furthermore, a recombinant protein that competes with the frizzled receptor for ligand binding (OMP-54 F28) is in clinical trials in combination with gemcitabine and nab-paclitaxel in PDAC patients (NCT02050178).

1.4.4 Hedgehog signalling

Hedgehog signalling has been strongly associated with PDAC progression. $Kras^{G12D}$ mutations and NF-κB expression have been linked with increased expression of sonic hedgehog in pancreatic tumours (Bailey et al., 2008, Ling et al., 2012). These pre-clinical data suggest that overexpression of sonic hedgehog in cancer cells causes an activation of the hedgehog signalling pathway in stromal cells, creating a pro-tumour microenvironment. However, studies where Shh was knocked out in PDAC cells, or signalling activity was depleted in the stroma, showed a more aggressive phenotype (Bailey et al., 2009, Feldmann et al., 2008). The classical understanding of the role of stroma within PDAC is that it is protective for the tumour cells and supports a pro-tumoural response. However, in recent studies in the KPC mouse model, the stromal compartment of PDAC tumours was decreased following depletion of Shh. Surprisingly, the tumours with Shh deleted in the stroma displayed a more aggressive tumour phenotype, suggesting that the stroma may also have a tumour suppressive role (Rhim et al., 2014). In fact, in a phase I/II clinical trial of the Shh inhibitor (IPI-926) and gemcitabine versus gemcitabine treatment alone in metastatic PDAC, patients receiving the combination treatment had worse outcomes, triggering early termination of the trial (NCT01130142). This indicates that many aspects

relating to the role of the stroma and the contribution of hedgehog signalling to PDAC development and progression are still not understood.

1.4.5 Immune therapies

Immune cells are present within pancreatic tumours, providing new hope for patients with the development of immunotherapy treatments. However, these treatments have not translated to improved outcomes in the clinic (Inman et al., 2014). This could be due to an inflammatory immune cell phenotype and, therefore, a tumour supportive, rather than tumour suppressive, role of immune cells. One of the main risk factors for the development of PDAC is pancreatitis and chronic inflammation within the pancreas. This could recruit inflammatory immune cells and trigger a wound-healing response, activating stellate cells (Bazhin et al., 2014). Another explanation for the disappointing results of immune therapy in PDAC treatment could be that the immune cells are physically separated from the tumour cells by other stromal cells and a stiff ECM. This could prevent an effective immune response from being triggered, particularly in advanced disease (Inman et al., 2014, Kotteas et al., 2016).

1.4.6 Targeting stellate cells

In PDAC patients, there is a reduction in pancreatic and bile acid secretions, causing a deficiency of fat soluble vitamins, such as vitamin A and D. The tumour-activated PSCs cannot be de-activated as their vitamin A stores cannot be replenished. Treatment with All-Trans Retinoic Acid (ATRA) has been found to return activated stellate cells to their quiescent state and induce storage of vitamin A within lipid droplets (McCarroll et al., 2006). Retinoic acid treatment of mice with chronic pancreatitis (induced by repetitive cerulein injection) and cultured PSCs *in vitro* caused down-regulation of Wnt 2 and β-catenin. The treated mice also showed

reduced fibrosis following treatment (Xiao et al., 2015). ATRA treatment in 3D organotypic models and KPC mice also reduced paracrine Wnt signalling, causing decreased cancer cell proliferation and invasion (Froeling et al., 2011). Another study using calcipotriol (a vitamin D receptor ligand) induced a quiescent state within pancreatic stellate cells through transcriptional reprogramming. The reversion of stellate cells to a quiescent state increased the level of gemcitabine within the tumour and increased survival in the KPC mouse model (Sherman et al., 2014). Returning stellate cells to this inactivated state may decrease the fibrotic reaction surrounding the cancer cells and may allow more chemotherapy treatment to reach the tumour, potentially increasing patient response. A combination therapy of gemcitabine and ATRA can decrease tumour cell proliferation and tumour invasion in 3D organotypic models and decrease tumour volume in KPC mice (Carapuça et al., 2016).

These studies suggest a combination therapy approach targeting the stroma alongside cancer cells could be beneficial to patients. Moreover, understanding the critical cross-talk mechanisms within PDAC tumours may present new therapeutic targets that can be interrogated in the clinic.

During PDAC progression, many developmental pathways become activated, which could provide key insights into stromal-cancer cross-talk (Rhim and Stanger, 2010). One of the critical pathways in pancreas development that has also been associated with PDAC is the FGF signalling pathway, which I have examined in this project (Gittes, 2009, Kang et al., 2019b). FGF signalling and its role in cancer development will now be discussed in detail.

1.5 Fibroblast Growth Factor Signalling

1.5.1 FGF signalling overview

The Fibroblast Growth Factor signalling pathway is a key regulator of cell growth, development, cell to cell contact and differentiation. It is made up of a family of 18 secreted growth factors and four signalling receptor tyrosine kinases (FGFR1-4). There is also a fifth FGF receptor (FGFR5), which can bind to FGF ligands but has no tyrosine kinase activity. This may dimerise with the other receptors to negatively control FGF signalling (Regeenes et al., 2018, Trueb, 2011, Wiedemann and Trueb, 2000). The FGF pathway is tightly governed to control cell differentiation and ensure tissue homeostasis. Disruption to FGF signalling has been associated with many different diseases, including cancer, (Carter et al., 2015, Clayton et al., 2017, Tanner and Grose, 2016, Turner and Grose, 2010).

The FGF family can be separated into seven sub-groups relating to their function. There are five canonical secreted FGF subfamilies that all act by binding to the FGFRs with the co-factor heparan sulphate (HSPG) to trigger paracrine signalling: The FGF1 subfamily (FGF1 and 2), the FGF4 subfamily (FGF4, 5 and 6), the FGF7 subfamily (FGF3, 7, 10 and 22), the FGF8 subfamily (FGF8, 17 and 18) and the FGF9 subfamily (FGF9, 16 and 20) (Ornitz and Itoh, 2015). Another subfamily are the endocrine FGFs (FGF15/19 subfamily made up of FGF15/19, 21 and 23). These require Klotho as a co-factor for binding and have been reported to regulate hepatocyte and adipocyte metabolism, as well as bile acid synthesis (Potthoff et al., 2012, Smith et al., 2014). The final group are the intracellular FGFs (FGF11 subfamily made up of FGF11, 12, 13 and 14). These are not secreted and do no interact with FGFRs but instead bind to the carboxy tail of voltage gated sodium channels to regulate neuronal and myocardial excitation (Goldfarb, 2005).

HSPG can contribute to FGF signalling pathway activation and cells lacking HSPG can only stimulate a transient activation of the MAPK pathway and therefore cannot stimulate DNA synthesis (Delehedde et al., 2000, Delehedde et al., 2002). HSPGs are made up of a carbohydrate chain of sulphated disaccharides and glucuronic acid linked to N-acteylglucosamine, which is covalently bound to a core protein (Matsuo and Kimura-Yoshida, 2013). The average HS chain is between 50-200 disaccharides units in length and can be modified by sulphotransferase enzymes (Esko and Selleck, 2002, Kim et al., 2011). HSPGs can interact with both FGF ligands and FGFRs to regulate the activation of FGF signalling. The length and sulphation of the HS chain, as well as cleavage of the core protein can affect binding and therefore activation. The presence of different HSPG saccharides can dictate specificity of ligand-receptor interactions (Guimond and Turnbull, 1999). Longer chains and increased sulphation can increase FGF signalling (Escobar Galvis et al., 2007, Ornitz et al., 1992, Patel et al., 2008).

1.5.2 FGF Receptors

FGFR1-4 are made up of three immunoglobulin-like (Ig) domains, a single transmembrane region and an intracellular tyrosine kinase domain. Ligands bind at the second and third Ig loops, alongside heparan sulphate proteoglycans (HSPG), which stabilise the interaction between the ligand and receptor. The receptors can have tissue- or cell-specific expression and differences in ligand binding specificity arise due to alternative splicing of the third Ig domain. Three common variants of these receptors are IIIa, IIIb and IIIc (Figure 1.6). Fibroblast growth factor receptor IIIa is a secreted, truncated form of the receptor, which has no transmembrane region or signalling capacity. It is involved in mesoderm induction and expressed in embryogenesis and in the brain (Gong, 2014). FGFR IIIb isoforms use exon 8, are generally expressed in epithelial cells and bind ligands in the FGF7 subfamily,

whereas FGFR IIIc isoforms use exon 9, are expressed by mesenchymal cells and bind ligands in the FGF4 and 8 subfamilies (Kelleher et al., 2013). This helps to regulate reciprocal signalling between cell types within tissues.

Receptor N-glycosylation can lead to ligand- and HSPG-binding specificity. Removal of N-glycans from FGFR1-IIIc derived from Chinese Hamster Ovary cells caused an increase in binding to FGF2 and HSPG. Mass spectrometry analysis has demonstrated that the majority of N-glycans on FGFR1 are bi- and tri-antennary core-fucosylated complex structures with one, two or three sialic acids. *In silico* modelling suggests that these N-glycans can be positioned to block FGF/HSPG binding to the receptor and therefore control activation of FGF signalling (Duchesne et al., 2006). In fact, mutations in N-glycosylated sites of FGFRs can result in impaired protein folding, changing the affinity for FGF ligand binding and causing developmental skeletal disorders and craniosynostosis syndromes (Raivio et al., 2009). Studies in *Caenorhabditis elegans* (*C. elegans*) demonstrated that removal of N-glycosylation sites caused phenotypes associated with FGFR over-activation, indicating the importance of glycosylation in the regulation of FGF signalling (Polanska et al., 2009).

In cancer cells, changes in the expression of FGFR isoforms have been linked to tumorigenesis (Liu et al., 2007). Both the b and c isoforms of the receptor can either have three Ig-like domains (FGFR b/c alpha) or only two Ig-like domains (FGFR b/c beta). In the beta form of the receptor, the first Ig domain is deleted by splicing, giving a higher affinity for ligand binding with FGF1 and FGF2. Splicing of the first Ig domain has been found in PDAC, as well as breast cancer and glioblastoma (Bruno et al., 2004).

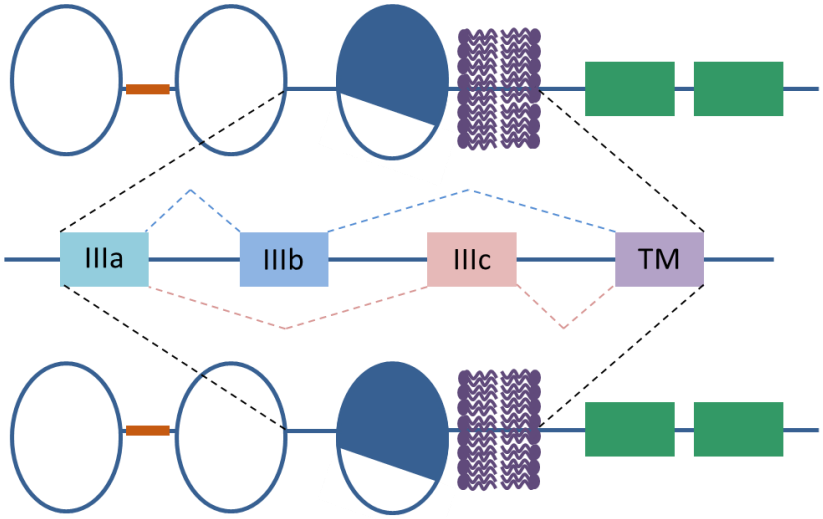

Figure 1.6 Alternative splicing of FGFR isoforms

Alternative splicing of the IgIII domain in FGF receptors can lead to the expression of different isoforms. HSPG co-factor will bind below the acid box (orange box) to stabilise ligand binding. The invariant exon (IIIa) is spliced to either the IIIb or IIIc exon, both of which then splice to the transmembrane (TM) exon (blue filled in area). This alternative splicing leads to ligand binding specificity due to the tertiary structure of the receptor. The b isoform is usually expressed by epithelial cells whilst the c isoform is expressed by mesenchymal cells. Both b and c isoforms can have either two or three Ig-like domains. Isoform expression can change during tumour development (Section 1.5.2) (Turner and Grose, 2010).

1.5.3 FGF signalling pathway

Upon ligand binding, FGFRs dimerise, causing a conformational shift and activating the intracellular tyrosine kinase domain (Goetz and Mohammadi, 2013). This triggers transphosphorylation of key tyrosine residues, activating the receptor and providing docking sites for adaptor proteins inside the cell. Adaptor proteins bind to the phosphotyrosine residues by Src homology 2 (SH2) or phosphotyrosine-binding (PTB) domains (Eswarakumar et al., 2005). The main FGFR adaptor protein is FGFR substrate 2 (FRS2), which is bound to the plasma membrane of the cell and binds to the juxtamembrane region of FGFRs via a PTB domain. The activated FGFR phosphorylates FRS2, which consequently recruits Son of Sevenless (SOS), SH2-containing protein tyrosine phosphatase (SHP2) and growth factor receptor-bound 2 (GRB2), triggering activation of RAS, RAF and the MAPK signalling pathway (Gotoh, 2008). Another protein that can be recruited to GRB2 is GRB2-associated binding protein 1 (GAB1). This can then activate the phosphoinositide 3-kinase (PI3K)-Akt pathway (Altomare and Testa, 2005).

Independently of FRS2 binding and activation, other adaptor proteins can be recruited to activated FGFRs through SH2 domains, such as phospholipase Cγ (PLCγ). Activated PLCγ can then hydrolyse phosphatidylinositol-4,5-bisphosphate (PIP_2) to inositol-1,4,5-triphosphate (IP_3) and diacylglycerol (DAG), subsequently activating protein kinase C (PKC) (Peters et al., 1992). Another pathway activated through FGF signalling is the Janus kinase/signal transducer and activator of transcription (JAK/STAT) pathway (Hart et al., 2000). This is particularly activated upon mutations within FGF receptors, such as FGFR3 (Hart et al., 2000). A predominance of JAK/STAT signalling has been shown downstream of chondrocytes overexpressing FGFR3 (Krejci et al., 2008, Li et al., 2010). It has also been suggested that this could

be due to intracellular activation of mutant FGFR3 and JAK/STAT signalling from the endoplasmic reticulum (Lievens et al., 2004).

Ligand binding specificity of FGFRs can be controlled by the concentration of ligand available to FGFRs, as well as the relative availability of HSPG co-receptors. Gradients of FGFs are important for regulating the development of the ventral foregut into the liver and lung, as well as limb outgrowth (Cohn et al., 1995, Serls et al., 2005). Cells exposed to high levels of FGF2 (100 ng/ml) have little effect on stimulating FGFR1 signalling, with only a transient early peak of MAPK activation and inefficient phosphorylation of FRS2. Whereas, cells stimulated with an optimal dose of FGF2 (300 pg/ml) exhibit a sustained activation of FRS2 and downstream signalling pathways (Zhu et al., 2010). This mimics results seen in *frs2* null mice, where FGF1 can only activate GRB2, triggering transient activation of the MAPK pathway and no cell proliferation. This phenotype can be rescued by re-expressing FRS2 in these cells, restoring their ability to respond to FGF1 and fully activate downstream signalling pathways (Hadari et al., 2001).

Negative feedback mechanisms can regulate FGF signalling. Receptors will be internalised into the cell and then either degraded or recycled back to the membrane. The Casitas B-lineage lymphoma (CBL) protein can trigger ubiquitination of FGFR and FRS2, causing degradation (Thien and Langdon, 2001). Additionally, downstream signalling can be inhibited by negative regulators, such as sprouty (SPRY), similar expression to FGF (SEF), Shp2 and Dual-specificity phosphatase 6 (DUSP6) (Ekerot et al., 2008, Fürthauer et al., 2002, Hacohen et al., 1998). These negative regulators either de-phosphorylate the activated proteins or prevent further binding and activation of downstream signals (Figure 1.7) (Katoh and Nakagama, 2014, Ornitz and Itoh, 2015, Turner and Grose, 2010).

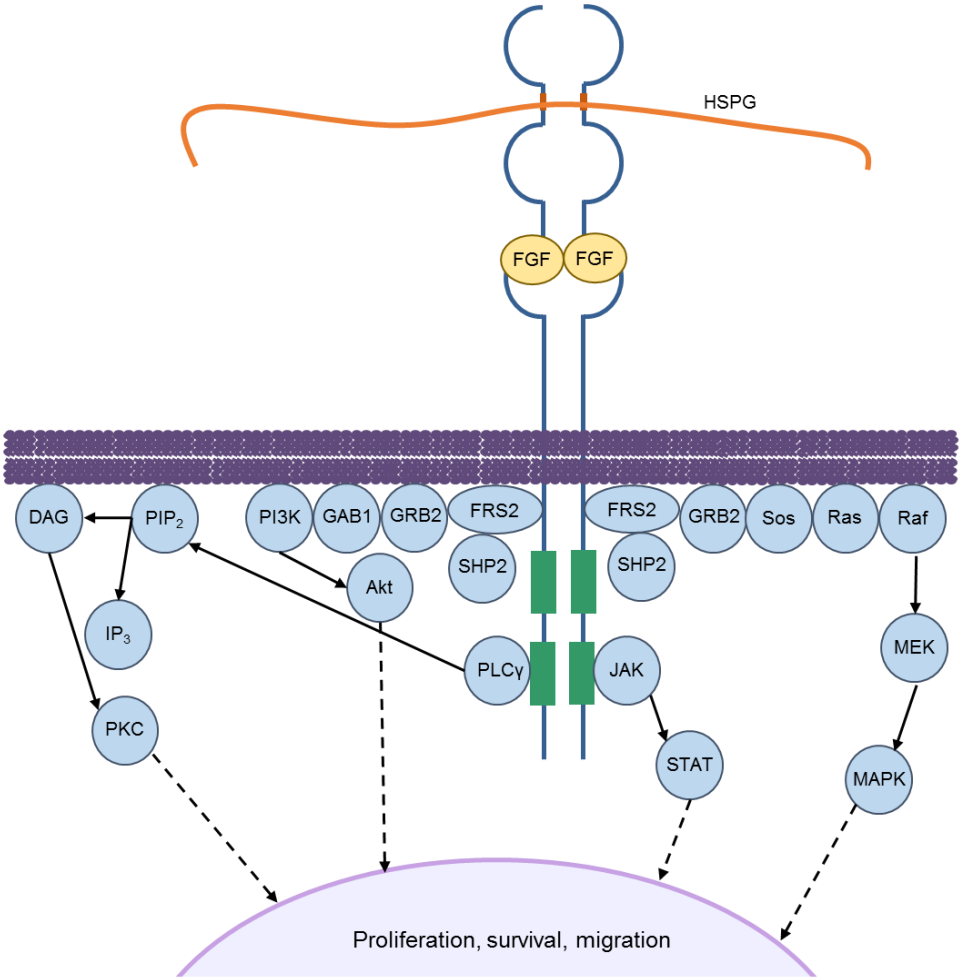

Figure 1.7 FGF signalling pathway

FGF receptors bind to relevant FGF ligands and heparan sulphate (HSPG) to become activated. This triggers receptor dimerization and transphosphorylation of kinase domains. Downstream signalling is initiated by FRS2 binding to the juxtamembrane region, activating the MAPK and PI3K-Akt pathways. FGF receptor tyrosine kinase phosphorylation also activates the PLCγ-PKC and JAK/STAT pathways. These signalling pathways lead to cell proliferation, survival and migration (Section 1.5.3) (Turner and Grose, 2010).

In addition to canonical pathways, FGF signalling can promote cell adhesion and proliferation through interaction with integrins. FGF1 has been reported to bind to $\alpha_v\beta_3$ integrin at a different site to the FGFR binding domain, suggesting formation of an FGFR-FGF-integrin complex (Mori et al., 2008b). Mutations in the integrin binding site of FGF1 interrupt its ability to stimulate DNA synthesis, cell proliferation and migration, suggesting that integrin interactions are critical for activation of FGF1-driven signalling (Mori et al., 2008a, Mori and Takada, 2013, Yamaji et al., 2010). Substrate-bound FGF2 can promote endothelial cell adhesion through interaction with $\alpha_v\beta_3$ integrin and mutations in the integrin binding site of FGF2 causes decreased activation of signalling and DNA synthesis (Mori et al., 2017, Rusnati et al., 1997). Activation of FGFR1 at these FGF2-$\alpha_v\beta_3$ cell adhesion contacts can trigger endothelial cell proliferation and migration, highlighting cross-talk between FGFR1 and $\alpha_v\beta_3$ integrin (Tanghetti et al., 2002).

Tissue cohesion and cell migration can be mediated through the action of cadherins. In particular neuronal cadherin (N-cadherin) is responsible cell migration and neurite outgrowth (Bixby and Zhang, 1990, Derycke and Bracke, 2004). Two main pathways have been associated with this: direct binding of cadherins to the actomyosin cytoskeleton to drive movement and activation of FGFR signalling (Bard et al., 2008, Williams et al., 1994). FGF signalling has been linked to N-cadherin expression in many different cell types, including stem cells, osteogenic cells and ovarian cells to promote survival and differentiation (Debiais et al., 2001, Takehara et al., 2015, Trolice et al., 1997). In breast cancer, prostate cancer and melanoma cells, N-cadherin can stabilise FGFR at the plasma membrane, leading to sustained activation of signalling and promoting cell proliferation (Suyama et al., 2002). It has also been shown that FGFR1 can stabilise N-cadherin at the cell membrane by decreasing its internalisation (Nguyen et al., 2019). Furthermore, in pancreatic cancer xenografts,

inhibition of FGFR signalling causes a decrease in N-cadherin expression and invasion (Taeger et al., 2011). It has been shown that N-cadherin and FGFR1 can interact directly through their extracellular domains, forming stable cadherin junctions and anchoring N-cadherin to actin. This indicates that cell migration may depend on a balance between FGFR1 mediated N-cadherin adhesion and actin interaction (Nguyen et al., 2019).

1.5.4 FGF signalling in cancer

FGF signalling is dysregulated in many different cancers, usually causing uncontrolled activation of the pathway. Recent reports suggest that FGF signalling is disrupted in more than 7 % of cancers (Figure 1.8) (Helsten et al., 2016).

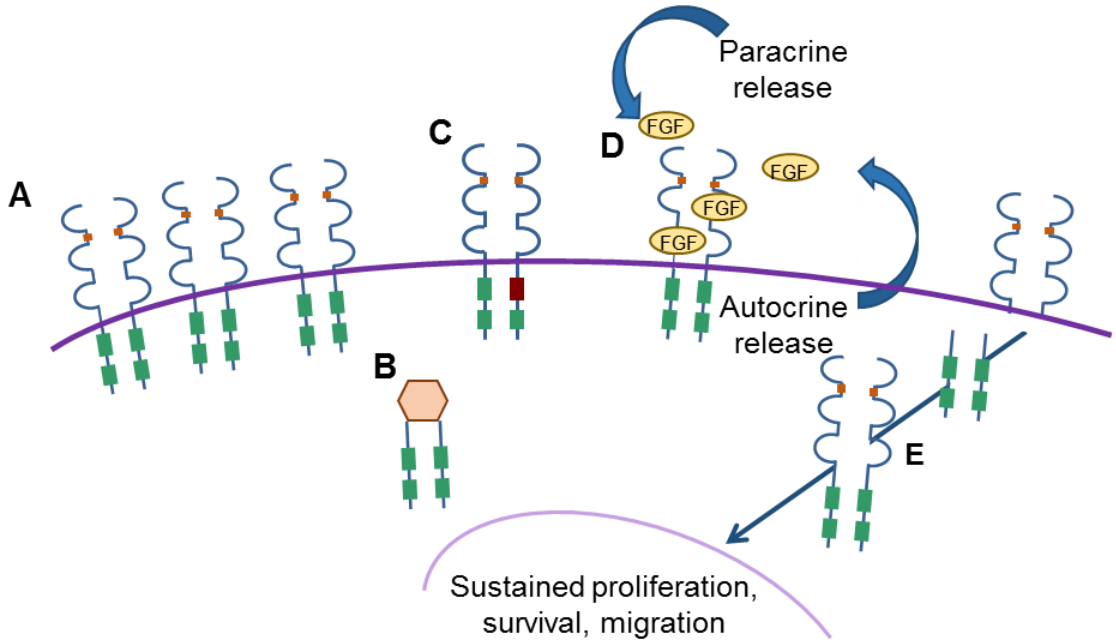

Figure 1.8 FGF signalling pathway alterations in cancer

The FGF signalling pathway can become altered in many ways in cancer to cause sustained cell proliferation and survival: ***A.*** *Overexpression of FGF receptors cause ligand independent activation, e.g. FGFR2 in gastric cancer.* ***B.*** *Receptor translocations can occur also leading to ligand independent activation of signalling, e.g. FGFR fusion with TACC in bladder cancer.* ***C.*** *Activating mutations within the FGF receptors cause constitutive activation even in absence of the ligand, e.g. FGFR2 in endometrial cancer.* ***D.*** *Paracrine or autocrine overexpression of FGF ligands can lead to increased FGF signalling, e.g. FGF1 in ovarian cancer.* ***E.*** *Sub-cellular translocation of either the full length or a cleaved version of the receptor can occur, for example to the nucleus where it could act as a transcription factor, e.g. FGFR1 in pancreatic or breast cancer (Turner and Grose, 2010).*

1.5.4.1 FGFR amplification

FGF receptor amplification can lead to ligand-independent signalling, increased response to ligands or reduced receptor recycling, which in turn increases the activity of the pathway. *FGFR2* is amplified in about 10 % of gastric cancers and is associated with a poor prognosis (Kunii et al., 2008, Matsumoto et al., 2012). Overexpression of FGFR2 has also been reported in about 4 % of triple-negative breast cancers (Turner et al., 2010). Amplification of *FGFR1* occurs in approximately 10-15 % of breast cancers, 75-80 % of head and neck squamous cell carcinomas, 5 % of small cell lung carcinomas and 20 % of non-small cell lung carcinomas, as well as in some cases of prostate, bladder and ovarian cancers, and osteo- and rhabdomyo-sarcomas (Elbauomy Elsheikh et al., 2007, Guagnano et al., 2012, Hamaguchi et al., 1995, Jang et al., 2012, Koole et al., 2016a, Lee et al., 2014, Missiaglia et al., 2009, Peifer et al., 2012, Reis-Filho et al., 2006, Tomlinson et al., 2009, Weiss et al., 2010). Overexpression of FGFR3 has been reported in about 50 % of oral squamous cell carcinomas, as well as some cases of non-small cell lung cancer and bladder cancer (Baldia et al., 2016, Koole et al., 2016b, Theelen et al., 2016). FGFR4 overexpression has been detected in 50 % of hepatocellular carcinomas and is linked to increased tumour invasion (Guagnano et al., 2012, Ho et al., 2009). Melanoma cell lines have increased levels of FGFR2 and 4 (Metzner et al., 2011).

1.5.4.2 FGFR mutation

Another common method of FGF signalling disruption is through activating mutations. This either causes constitutive receptor activation or increased affinity for ligand binding. For example, around 50 % of bladder cancers have a mutation in the *FGFR3* gene (Cappellen et al., 1999). This is associated with non-muscle invasive disease in these patients. The majority of these mutations cause constitutive dimerization and activation of the receptor by formation of a disulphide bridge. However, mutations can

also occur in the transmembrane domain and the kinase domains in these tumours (Pouessel et al., 2016, van Rhijn et al., 2001). Mutations in *FGFR3* also occur in other tumour types, such as spermatocytic seminomas, prostate cancer, cervical cancer, melanoma and multiple myeloma (Goriely et al., 2009, Hafner et al., 2006, Hernandez et al., 2009, Wu et al., 2000). *FGFR2* mutations are present in around 12 % of endometrial carcinomas, which cause increased affinity for ligand binding and autocrine signalling (Dutt et al., 2008, Pollock et al., 2007). An amino acid substitution in FGFR4 in breast cancer cells allows the receptor to form ligand-independent dimers, which triggers constitutive activation of signalling in the tumour cells (Roidl et al., 2010).

1.5.4.3 Paracrine/autocrine signalling

Paracrine or autocrine action of FGF ligands can also cause uncontrolled FGF signalling in cancer. Increased levels of FGFs in plasma of cancer patients suggests that high levels are produced by cells present in the tumour, or that ligands are released from the ECM during cancer progression (Poon et al., 2001). High levels of FGF2-FGFR1 signalling occur in melanoma and a similar FGF2 autocrine loop has been reported in non-small cell lung cancer (Marek et al., 2009, Wang and Becker, 1997). Moreover, amplification of *FGF1* in ovarian cancer is associated with poor survival and increased angiogenesis in tumours (Birrer et al., 2007). Additionally, in prostate cancer, there are increased levels of FGF2 and FGF6, which could indicate a paracrine signalling loop (Giri et al., 1999, Ropiquet et al., 2000). Increased ligand levels from cells or ECM within the tumour could cause over-activation of the FGF pathway.

1.5.4.4 Fusion proteins

Chromosomal translocations can also lead to the expression of FGFR fusion proteins in cancer. FGFR fusion with transforming acidic coiled-coil (TACC) proteins can occur in bladder cancer and glioblastoma, as well as FGFR1 fusion with FGFR1 oncogene partner 1 and 2 (FOP1/2) in lung cancer and leukaemia (Gu et al., 2006, Mano et al., 2007, Singh et al., 2012, Williams et al., 2013). An FGFR2-PPHLN1 fusion has been reported in 16 % of intrahepatic cholangiocarcinoma cases with a poor patient prognosis (Sia et al., 2015). Other FGFR fusion proteins have been discovered in cases of breast, lung and prostate cancer (Wu et al., 2013). These translocations can alter downstream signalling of the FGF pathway in tumours due to loss of specific tyrosine residues or the FRS2 binding site (Jackson et al., 2010, Williams et al., 2013). Moreover, translocations can lead to altered subcellular localisation due to the loss of the transmembrane region in the fusion proteins (Mano et al., 2007, Olsen et al., 2006, Sohal et al., 2001).

1.5.4.5 Sub-cellular localisation

Another method of deregulation of FGF signalling is sub-cellular translocation of the receptors. In lung cancer, full length FGFR1 has been reported to localise to the outer membrane of the mitochondria. Moreover, a FOP2-FGFR1 fusion protein has been found in the intermembrane space of mitochondria in lung cancer cells. Translocation of FGFR1 to the mitochondria can modify metabolism within the cancer cells. FGFR1 can phosphorylate and therefore activate pyruvate dehydrogenase kinase 1 (PDHK1), leading to a decrease in pyruvate dehydrogenase complex (PDC) activity and therefore promoting generation of energy by glycolysis (the Warburg effect) (Hitosugi et al., 2011).

Both FGF ligands and receptors can localise to the nucleus, where they are thought to control gene expression either through direct DNA binding or through interactions with other DNA binding molecules (Chen and Hung, 2015). Nuclear translocation of FGF1 has been associated with DNA synthesis, whilst nuclear FGF2 has been linked with glioma cell proliferation (Lin et al., 1996, Wang et al., 2015). Nuclear FGFR1 is important in neuronal differentiation and appears to be linked with invasion in breast cancer and PDAC (Chioni and Grose, 2012, Coleman et al., 2014b, Stachowiak et al., 2007, Stachowiak and Stachowiak, 2016).

1.5.4.6 FGFR1-mediated invasion

FGFR1 expression has been linked with invasion in many cancers. In breast cancer cells, the upregulation of FGF2 expression has been shown in response to GPER. This leads to an FGF2/FGFR1 paracrine signalling cross-talk between cancer cells and CAFs, triggering expression of CTGF and invasion (Santolla et al., 2019). Additionally, TGF-β mediated EMT in breast cancer cells has been shown to increase expression of the FOXC1 transcription factor, which in turn promotes isoform switching to FGFR1 IIIc, resulting in increased invasion (Hopkins et al., 2017). FGFR1 expression has been negatively correlated with the tumour suppressor miR-133b in osteosarcoma and was related to advanced clinical tumour stage and increased invasion (Gao et al., 2018). Moreover, in colorectal cancer, expression of Crumbs3 has been correlated with increased cell migration and invasion, which has been attributed to its intracellular interaction with FGFR1 (Iioka et al., 2019). Furthermore, in high grade gliomas FGFR1 inhibition demonstrated significant anti-migratory effects in 3D *in vitro* models (Egbivwie et al., 2019). This indicates the importance of FGFR1 in cell migration and invasion, providing a potential novel therapeutic target in the clinic for many cancers.

1.5.5 FGF signalling in PDAC

During PDAC progression, many developmental pathways are activated, including FGF signalling (Rhim and Stanger, 2010). The FGF signalling pathway is deregulated in cancer, either by mutations, overexpression, activation or translocation of receptors, as well as increased ligand expression (Turner and Grose, 2010). Cancers driven by FGF signalling can be treated with targeted therapies, such as tyrosine kinase inhibitors (Table 6.1). This highlights the notion that targeting FGF signalling is a viable clinical option, with therapies already being used in patients.

1.5.5.1 FGF ligands

In PDAC, FGF signalling is increasingly recognised as one of the critical pathways involved in cross-talk between cancer and stellate cells within the tumour (Kang et al., 2019b). FGF1 and FGF2 can be overexpressed by cancer cells and have been correlated with advanced tumour stage (Yamanaka et al., 1993). High levels of FGF2, VEGF and FGF13 have also been correlated with shorter patient survival and increased liver metastasis (Kuwahara et al., 2003, Missiaglia et al., 2010). It was shown that FGF2 overexpression led to increased cell proliferation and invasion in cancer cells (Yamazaki et al., 1997). Antibodies against either FGF2 or FGF receptors caused a 50% reduction in cell proliferation or reduced cell invasion in PDAC cancer cells in rudimentary single cell type 2D cultures, respectively, suggesting FGF signalling could be a good therapeutic target (Hasegawa et al., 1994, Leung et al., 1994). Interestingly, it has also been demonstrated that secretion of FGF2 can lead to increased cancer cell adhesion and inhibition of invasion of cancer cells (El-Hariry et al., 2001a, El-Hariry et al., 2001b, Escaffit et al., 2000).

Other FGF ligands, including FGF5, FGF7 and FGF10, have been reported to be overexpressed in PDAC leading to increased cell proliferation and invasion (Kornmann et al., 1997, Kornmann et al., 2001, Niu et al., 2007, Nomura et al., 2008). In particular, FGF7 and FGF10 are reported to signal from the stroma to the cancer cells. FGF7 can activate nuclear factor kappa B (NF-κB) and induce the expression of VEGF, MMP-9 and urokinase-type plasminogen activator (Niu et al., 2007). A study looking at the pre- and post-chemotherapy serum profiles of PDAC patients demonstrated that FGF10 was differentially expressed in response to gemcitabine and erlotinib, indicating that changes in FGF10 levels could be used as a predictive biomarker of chemotherapy response in patients (Torres et al., 2014). Furthermore, stimulation of PDAC cancer cells with FGF ligands, such as FGF1, 2, 7 and 10, triggered changes in expression of key pancreatic development genes, such as *SRY-related HMG-box gene 9* (*SOX9*), *hepatocyte nuclear factor 3-beta* (*HNF3b*), *hairy and enhancer of split-1* (*HES1*), *GATA-4* and *GATA-6* (Gnatenko et al., 2018).

Moreover, FGF signalling has been associated with increased expression of inducible nitric oxide synthase (iNOS), indicating that oxidative stress may play a role in FGF-mediated PDAC progression (Vickers et al., 1999). To support this, there is evidence that FGF signalling can regulate response to oxidative stress as in keratinocytes (Marchese et al., 1995, Pentland, 1994). In particular, expression of glutathione peroxidase 1 (GPX1) has been shown to be a downstream target of activated FGF signalling in wound healing (Frank et al., 1997, Munz et al., 1997). As well as overexpression of FGF ligands, it has been reported that the levels of FGF-binding proteins (FGF-BP) are increased in PDAC patients (Tassi et al., 2006). This could be an indicator of early initiation of PDAC lesions.

1.5.5.2 FGF receptors

FGF receptors, such as FGFR1, are also overexpressed within PDAC and can be associated with patient survival (Kobrin et al., 1993, Ohta et al., 1995). Overexpression of FGFR4 has been linked with cancer cell adhesion to ECM proteins, such as laminin and fibronectin, decreasing cell migration and increasing patient survival (Motoda et al., 2011). Inhibition of FGFR4 prevented matrix adhesion through neural cell-adhesion molecule (N-CAM), suggesting that this could be a key pathway regulating pancreatic cell migration and invasion (Cavallaro et al., 2001). In contrast, FGFR2 overexpression has been linked with shorter patient survival in PDAC (Nomura et al., 2008). Downregulation or inhibition of FGFR2 can reduce tumour cell survival and migration, as well as tumour development *in vivo* (Matsuda et al., 2014).

Alternative splicing and isoform expression can alter the role of FGF receptors in PDAC. For example, FGFR1α has been linked with decreased cancer cell proliferation and increased anti-tumour responses, whereas expression of FGFR1β increased resistance to chemotherapy treatment in xenograft models, consistent with an inhibitory role for the first Ig-loop, which is absent in FGFR1β (Vickers et al., 2002). The third membrane proximal Ig-loop is also important: expression of the IIIc isoform of FGFR2 has been associated with increased cell proliferation and liver metastasis (Ishiwata et al., 2012). Contrastingly, expression of the FGFR1 IIIb isoform has been shown to decrease tumour growth in mouse models (Liu et al., 2007). Additionally, it has been reported that the overexpression of FGFR1 IIIb in PDAC cells induces the expression of secreted protein acidic and rich in cysteine (SPARC), which regulates cell-cell interactions and decreases tumour progression (Chen et al., 2010). FGFR IIIb isoforms are usually expressed on epithelial cells, whilst FGFR IIIc isoforms are expressed by mesenchymal cells (Turner and Grose, 2010). Changes in isoform

expression in cancer cells have been linked with tumorigenesis (Liu et al., 2007). The expression of FGFR1 isoforms on PDAC cells can be modulated by the stroma, with PSCs inducing cancer cells to switch to the mesenchymal FGFR1-IIIc isoform (Kornmann et al., 2001, Tian et al., 2012).

1.5.6 Targeting FGF signalling

Due to the frequency of FGF signalling disruption in cancer, it is a popular therapeutic target. Many of the strategies to disrupt this pathway are designed to prevent ligand-dependent activation of signalling, such as small-molecule tyrosine kinase inhibitors (TKIs), antibodies to prevent ligand binding, antagonistic peptide mimics or ligand traps. TKIs have been the main focus of FGF therapies, with some clinical success; however, drug resistance often develops (Babina and Turner, 2017, Camidge et al., 2014, Katoh, 2019).

Phase I and II clinical trials of FGFR inhibitors, such as dovitinib, lucitanib, ponatinib, nintedanib and pazopanib are ongoing in a variety of solid tumours. For example, a phase Ib trial determined that dovitinib is safe to give to PDAC patients, alongside gemcitabine and capecitabine. Dovitinib is a multi-kinase inhibitor and FGF23 changes in the plasma can be used as an indicator of FGFR modulation. The major toxicities caused by adding dovitinib to standard chemotherapy were neutropenia and thrombocytopenia (Ma et al., 2019). Addition of FGFR inhibitors to chemotherapy treatment of PDAC could lead to enhanced overall survival and improved patient prognosis. Using FGF23 as a serum biomarker to assess the effectiveness of treatment is also an important aspect for future studies. *FGFR1* is upregulated in about 5 % of pancreatic tumours and this has been related to an increase in overall survival and improved patient prognosis (Haq et al., 2018). This reveals a clear clinical

sub-group of PDAC patients that may respond to FGFR inhibitors in the clinic, however this analysis did not provide information on isoform switching, which will be critical for determining patient outcomes. Sensitivity to FGFR inhibition has also been demonstrated in a subset of cell lines and primary explant cultures *in vitro*, supporting that this is a viable clinical option in some patients (Zhang et al., 2014a). Despite an increase in overall survival, the prognosis of all PDAC patients is poor; therefore any options to effectively target sub-groups of patients, such as FGFR inhibitors, should be explored.

The nuclear role of FGFRs has been shown to be very important in cancer. Therefore another approach to targeting the FGF pathway could be to prevent nuclear translocation. For example, targeting granzyme B could prevent FGFR1 cleavage and translocation to the nucleus in breast cancer (Chioni and Grose, 2012). Furthermore, inhibiting importin-β reduces the nuclear translocation of FGFR1 and therefore decreases cell proliferation (Mahipal and Malafa, 2016, Reilly and Maher, 2001). Therapies that focus on preventing the nuclear translocation of the receptor rather than traditional TKIs may help to avoid the development of resistance in patients (Porębska et al., 2018).

1.6 Nuclear receptor signalling

1.6.1 Nuclear receptor tyrosine kinase signalling

Nuclear signalling by several transmembrane receptors has been reported, such as insulin (Sun et al., 2003), vascular endothelial growth factor (Carpenter and Liao, 2013), epidermal growth factor (EGF) (Carpenter and Liao, 2013), nerve growth factor (Bryant and Stow, 2005), FGF (Stachowiak et al., 1996, Maher, 1996) and interleukin receptors (de Oca B et al., 2010). These receptors are usually considered to be located within the plasma membrane. Upon binding to their target ligand, intracellular activation occurs, for example through tyrosine kinase transphosphorylation. This activates an intracellular signalling cascade, which can cause cell effects such as proliferation, growth and invasion. However, discovery of these receptors within the nucleus suggests that there is a less well-understood non-canonical mechanism of action within these pathways. Membrane-bound receptors are known to be taken into endosomes upon activation and then either degraded or recycled back to the plasma membrane. However, it is now understood that some of these receptors can translocate into the nucleus instead. Other methods of nuclear translocation of these proteins could be alternative splicing to create nuclear receptor tyrosine kinase (RTK) fragments, binding to nuclear chaperones or by retro-translocation from the endoplasmic reticulum (Bryant and Stow, 2005, Wiley and Burke, 2001). Once in the nucleus, RTKs can act as kinases or as transcriptional regulators and are related with a poor prognosis in cancers.

One of the most well documented receptor translocations is for the epidermal growth factor receptor family. Nuclear full-length ErbB1-4 have all been reported, whilst ErbB-4 can also be cleaved to produce an intracellular domain, which can translocate to the nucleus (Wang and Hung, 2009). Nuclear ErbB1 (EGFR) correlates with highly

proliferating cells (Lin et al., 2001, Marti et al., 1991). Moreover, nuclear ErbB2-4 have been detected in the frontal cortex of monkeys, suggesting they play a role in brain development (Thompson et al., 2007). This nuclear localisation of ErbB proteins was also found in primary human umbilical venous endothelial cells (HUVEC) and arterial endothelial cells (HUAEC) (Bueter et al., 2006). EGFR is associated with chromatin at specific DNA sequences, alongside other transcription factors, suggesting it plays a role in transcriptional regulation. *Cyclin D1*, *iNOS*, *Aurora A* and *B-MYB* have emerged as potential targets for EGFR within the nucleus (Hanada et al., 2006, Hung et al., 2008, Lin et al., 2001, Lo et al., 2005). *COX-2* has been reported as a target for nuclear ErbB2 (Wang et al., 2004), and ErbB4 has been reported to increase expression of *β-casein* and decrease expression of the tumour suppressor gene *ETO-2* (Linggi and Carpenter, 2006, Williams et al., 2004). Nuclear ErbB4 can activate oestrogen receptor α (ER-α) and render breast cancer cells sensitive to tamoxifen treatment (Naresh et al., 2008).

It has also been reported that ErbB1, -2 and -4 can continue to act as tyrosine kinases within the nucleus. For example, $p34^{Cdc2}$ can be phosphorylated by nuclear ErbB2, delaying M-phase entry and causing drug resistance in breast cancer (Tan et al., 2002). Moreover, ErbB4 can inhibit mouse double minute 2 (MDM2), increasing p53 and p21 expression (Arasada and Carpenter, 2005). It has also been reported that EGFR can phosphorylate proliferating cell nuclear antigen (PCNA), which led to increased DNA synthesis and repair (Wang et al., 2006).

Nuclear expression of EGFR in oropharyngeal squamous cell carcinoma was associated with recurrence and a decrease in progression-free survival (Psyrri et al., 2008). Moreover, a high level of phosphorylated-EGFR in the nucleus, but not elsewhere in the cell, correlated with a more aggressive disease stage and poorer

patient prognosis in oesophageal cancer (Hoshino et al., 2007). A constitutively active form of EGFR (EGFRvIII) has also been described in the nucleus of prostate, breast and brain tumour cells (de la Iglesia et al., 2008, Edwards et al., 2006, Ge et al., 2002). In hormone-refractory prostate cancer this nuclear translocation was associated with a decreased overall survival, whilst in glioblastoma it is reported to induce glial transformation by binding to STAT3 and upregulating iNOS (de la Iglesia et al., 2008, Edwards et al., 2006). Blocking nuclear translocation of EGFR by inhibiting receptor activation or treatment with vitamin D has been shown to decrease tumour growth and re-sensitise cells to other therapeutic agents, highlighting the clinical significance of the nuclear role of this receptor (Cordero et al., 2002, Kim et al., 2009, Wang and Hung, 2009).

1.6.2 FGF signalling within the nucleus

Nuclear translocation of FGFRs can occur through a number of mechanisms. One example is retrotranslocation of full length FGFRs from the ER/Golgi into the nucleus (Stachowiak and Stachowiak, 2016). FGFRs may be released into the cytosol by the sec61 channel in a similar manner to ER-associated protein degradation (ERAD) (Stachowiak et al., 2007). The cytosolic FGFRs may then bind with other proteins, such as FGF2 or ribosomal S6-kinase 1 (RSK1), which can target localisation to the nucleus (Coleman et al., 2014a, Dunham-Ems et al., 2006, Hu et al., 2004). Importin β has also been shown to be involved in nuclear translocation of FGFRs in fibroblasts. This caused increased expression of *c-Jun,* resulting in cell proliferation (Reilly and Maher, 2001). Another method of nuclear translocation of full length FGFRs is through internalisation from the plasma membrane. Instead of being degraded or recycled, the endosomal FGFRs are targeted to the nucleus using retrograde vesicular transport (Bryant et al., 2005, Maher, 1996, Spooner and Lord, 2015).

Another purported mechanism of nuclear FGFR signalling is through proteolytic cleavage creating intracellular fragments, which can then be transported into the nucleus. For example after FGFR3 binding to FGF1, it has been reported that the extracellular and intramembrane domains of the receptor can be cleaved off by γ-secretase and other proteases, releasing a soluble intracellular fragment. This can then be transported into the nucleus (Degnin et al., 2011). Moreover, nuclear FGFR signalling has been described in breast cancer through Granzyme B mediated cleavage of the intracellular portion of the receptor. It was found that this truncated form of FGFR1 was binding to the DNA and controlling the expression of target genes. Three target genes had increased expression, *keratin associated protein 5-6 (KRTAP5-6)*, s*tratifin (SFN)* and *serine protease 27 (PRSS27)*, whilst the expression of *glutamate ionotropic receptor NMDA type subunit associated protein 1 (GRINA)* and e*pstein barr virus induced 3 (EBI3)* was decreased. The respective changes in expression of these target genes all caused an increase in cell migration and invasion in breast cancer cells (Chioni and Grose, 2012).

In head and neck squamous cell carcinoma (HNSCC) samples, nuclear FGFR1 correlates with poorly differentiated cells, invasion and poor survival. Treatment with the FGFR inhibitor, PD173074, decreased growth and invasion in HNSCC cell lines, associated with a decrease in the expression of matrix metalloproteinases (MMPs) and Snail1 and 2. Therefore nuclear FGFR1 has been associated with the induction of EMT in HNSCC, which can be reversed using the inhibitor PD173074 though the transcription factor AP-1 (Nguyen et al., 2013).

Nuclear localisation of FGFR1 regulates gene expression to determine cell proliferation and differentiation. In neural progenitor cells, FGFR1 is translocated into the nucleus by importin β due to signals from neurotransmitters, hormonal or growth

factor receptors. Once in the nucleus, FGFR1 works with cyclic AMP responsive element-binding protein (CBP) to activate transcription and regulation of a multitude of developmental and differentiation genes. This has been termed integrative nuclear fibroblast growth factor receptor 1 signalling (INFS) (Peng et al., 2002, Stachowiak et al., 2007). Nuclear FGFR1 has been shown to be necessary for neuronal differentiation through binding to cAMP-response elements (CREs) and activator protein-1 (AP-1) sites, affecting expression of many active neuronal genes (Bharali et al., 2005, Fang et al., 2005, Stachowiak et al., 2009). Three different states of nuclear FGFR1 have been described: fast mobile, slower mobile (chromatin-bound) or immobile (associated with the nuclear matrix). When transcription is activated, FGFR1 is released from the immobile nuclear-matrix bound and fast mobile populations to increase the levels bound to chromatin (Dunham-Ems et al., 2009). Furthermore, within embryonic stem cells there is an accumulation of nuclear FGFR1 in response to retinoic acid. Nuclear FGFR1 forms complexes with retinoic acid receptors (RARs), retinoid acid receptors (RXRs) and Nurs to activate response elements and induce neuronal differentiation in these cells (Baron et al., 2012, Lee et al., 2012, Lee et al., 2013, Terranova et al., 2015). This suggests that nuclear FGFR1 could be a global regulator of neuronal cell differentiation during development (Terranova et al., 2015).

1.6.3 Nuclear FGFR1 signalling in PDAC

It has been shown previously that nuclear translocation of full length FGFR1 occurs within stellate cells situated at the invasive front of tumours in patients. This was also confirmed using 3D models within the laboratory. Invading stellate cells showed FGFR1 and FGF2 within nuclear speckles and co-localised with SC35, indicating that these proteins may be involved in gene transcription (Figure 1.9). Furthermore, treatment with an FGFR selective inhibitor (PD173074) can decrease the nuclear

translocation of FGFR1 in stellate cells and prevent invasion into 3D organotypic gels (Figure 1.9) (Coleman et al., 2014b), suggesting that FGFR1 could be a good therapeutic target in PDAC patients. To determine the role and importance of nuclear FGF signalling within pancreatic stellate cells, it is necessary to validate target genes that are under transcriptional control of FGFR1. This may lead to the discovery of new therapeutic targets that can provide improved treatment for PDAC patients.

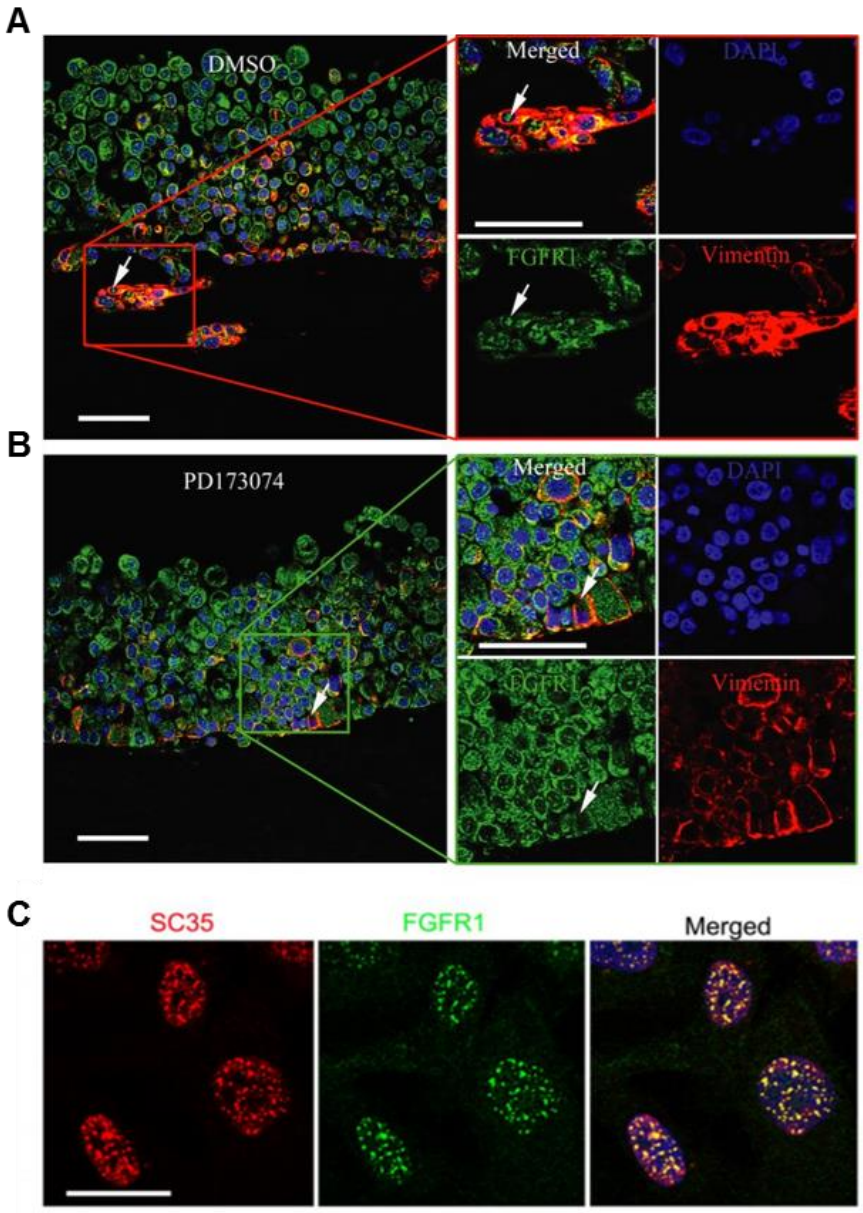

Figure 1.9 Nuclear FGFR1 within PSCs

Organotypic gels showing PS1 cells highlighted by positive vimentin staining (red) and stained for FGFR1 (green). The organotypics were treated with either the FGFR inhibitor PD173074 or DMSO vehicle control on alternate days until the gels were harvested on day 14. Scale bar = 100 µm. ***A.*** *PS1 cells have started invading into the gel at 14 days. The highlighted area shows positive nuclear FGFR1 staining within the invading PSCs.* ***B.*** *Following treatment with PD173074, there is a decrease in nuclear FGFR1 localisation within the stellate cells, as well as a decrease in invasion.* ***C.*** *Immunofluorescence staining shows the co-localisation of nuclear FGFR1 with SC35 in stellate cells. This suggests that FGFR1 may have a transcriptional role in the nucleus of stellate cells. Scale bar = 20 µm (Coleman et al., 2014b).*

1.7 Aims and Objectives

PDAC is a disease that has a poor patient prognosis and requires the development of new therapeutic targets. The stroma has a significant role in the development of PDAC tumours and can modulate the response to standard chemotherapy, with pancreatic stellate cells playing a key role in tumour progression and invasion. However, targeting the stroma in patients is complicated and so far has yielded limited success in the clinic (Section 1.4). This highlights the importance in developing our understanding of stromal-cancer cross-talk and translating this into effective treatment options for patients.

Invasion and metastasis are responsible for the poor survival of PDAC patients, meaning that understanding this process is critical. Nuclear translocation of FGFR1 (nFGFR1) occurs in stellate cells that are present at the invasive edge of these desmoplastic tumours. Inhibition of FGFR1 can prevent receptor translocation and decrease stellate cell invasion. Furthermore, nFGFR1 localises in speckles with SC35, indicating it may contribute to transcriptional control (Section 1.6). Therefore, as nFGFR1 appears to be a major regulator of cellular cross-talk mediated invasion in PDAC, it is pertinent to develop further understanding of its activity.

The overall aim of this project is to understand the novel role of nFGFR1 and use this to develop therapeutic strategies to decrease stellate cell invasion and tumour metastasis.

The main objectives of my PhD project are:

- To investigate the specificity of targeting FGFR1 in PSCs to disrupt stromal-cancer cross-talk and its consequent effects
- To identify mechanisms of FGFR1-mediated changes in PSCs
- To build on existing and developing PDAC therapies by including FGFR1 targeting

Chapter 2: Materials and Methods

2.1 Cell Lines and culture reagents

2.1.1 Cell Lines

The PDAC cell lines, AsPC-1, MIA PaCa-2, PANC-1 and COLO 357, and the stellate cell line, PS1, have been used in this project (Chen et al., 1982, Lieber et al., 1975, Morgan et al., 1980, Wu et al., 1977, Yunis et al., 1977). All cell lines have been submitted for short tandem repeat (STR) profiling (Appendix 1) and tested for mycoplasma every six months. The PS1 cell line was isolated and immortalised previously by expression of ectopic human telomerase reverse transcriptase (hTERT) (Li et al., 2009). HEK293T (Human embryonic kidney) cells were used to generate lentiviral particles. The primary cancer-associated stellate cell lines M1245 and M1090T (sub-type A) were used to confirm the validity of PSC FGFR1 expression in PDAC. These cell lines were isolated using the outgrowth method and confirmed to be of stellate cell origin by expression of key PSC markers and reversion to quiescence with ATRA treatment and Oil Red O staining (Section 2.3.2) (Neuzillet et al., 2019). PS1 cells with inducible expression of an FGFR1-HaloTag construct have been generated (referred to as PS1-HT). Three PS1 cell lines with inducible shRNA-mediated knockdown of FGFR1 have also been generated in this project (referred to as shRNA1, shRNA2 and shRNA3). Stable cell lines expressing fluorescently labelled histone subunits were also generated using lentiviral constructs. Stellate cell lines were labelled with H2B-GFP and PDAC cancer cell lines were labelled with H2B-RFP.

2.1.2 Cell Culture

AsPC-1 and COLO 357 cancer cells were cultured in RPMI-1640 medium (R8758, Sigma-Aldrich) supplemented with 10 % (v/v) foetal bovine serum (FBS) (F9665, Sigma). PS1, PS1-HT, shRNA1, shRNA2 and shRNA3 cells were cultured in 45 % (v/v) Dulbecco's modified Eagle's medium (DMEM) (D6429, Sigma), 45 % (v/v) Ham's

F-12 (N 6658, Sigma-Aldrich), 10 % (v/v) FBS and occasionally supplemented with 1 µg/ml puromycin as a selection agent (P9620, Sigma-Aldrich). M1090T, M1245, HEK293T, MIA PaCa-2 and PANC-1 cells were cultured in DMEM plus 10% FBS. All cell lines were incubated at 37ºC and 5 % humidified CO_2.

To passage the cells, the growth medium was removed from the flasks without disturbing the cell layer. Trypsin-EDTA 10X (59418C, Sigma-Aldrich) was added to the flask and incubated at 37ºC until all the cells detached. The trypsin-EDTA action was inhibited by adding appropriate medium (with FBS). The cell suspension was centrifuged at 240 x g for 3 minutes to form a pellet of cells and then the cells were re-suspended in fresh medium. The cells were counted using a haemocytometer and seeded as necessary into new flasks.

For storage, cell pellets were resuspended in FBS plus 10 % (v/v) dimethyl sulfoxide (DMSO) (D/4120/PB08, Fisher Scientific) and 1 ml aliquots were placed into cyrovials. These were frozen slowly to -80ºC and then transferred to liquid nitrogen for long-term storage. Upon cell recovery, cyrovials were thawed at 37ºC in a water bath and transferred into a falcon tube containing standard medium. The cell suspension was then centrifuged at 240 x g for 3 minutes to remove DMSO in the supernatant and cells were re-suspended in standard medium ready for culture.

2.1.3 Stimulation assay

Cells were seeded in standard medium at a relevant density and incubated at 37ºC. After 24 hours, medium was removed and cells were serum-starved in FBS-free medium overnight. Following this, cells were stimulated for 15 minutes with 100 ng/ml recombinant FGF2 (100-18C, Peprotech) plus 300 ng/ml heparin sodium salt (H3393,

Sigma-Aldrich), compared to relevant unstimulated controls, then harvested as appropriate.

2.2 Cell survival assays

2.2.1 MTS Assays

Cells were seeded into the middle 60 wells of a 96 well plate (Figure 2.1) at an optimal density of 2 x 10^3 and 1.5 x 10^3 cells per well for cancer and stellate cell lines, respectively. 200 µl of phosphate buffered saline (PBS) was added to the outside wells to prevent dehydration within the plate during incubation. The cells were seeded in relevant medium at a volume of 90 µl per well and incubated at 37°C and 5 % CO_2 for 24 hours.

Serial dilutions of AZD4547 (S2801, Selleckchem) were prepared to treat the cell cultures after 24 hours. In total, 17 drug solutions were added to the 96 well plates (10 µl per well) to give a final drug concentration ranging from 0.122 nM to 100 µM. Background absorbance was removed from the analysis using a positive control (Staurosporine 1 µM) (S5921, Sigma-Aldrich) and the results were normalised to negative vehicle control samples. There were three repeats of each drug concentration on each 96 well plate. The plates were then incubated at 37°C for 72 hours.

To analyse the level of cell survival at each dilution, 20 µl of MTS reagent (3-(4,5-dimethylthiazol-2-yl)-5-(3-carboxymethoxyphenyl)-2-(4-sulfophenyl)-2H-tetrazolium) (G3581, Promega) was added. This was left at 37°C for two hours for AsPC-1 cells or four hours for PS1 cells. MTS is a tetrazolium dye that is metabolised by the

mitochondria in viable cells into a brown formazan product. After incubation, the intensity of the colour in each well was measured by the absorbance at 492 nm, using a 96-well microplate reader (Infinite® F50, Magellan software). These values were adjusted to allow for the background absorbance and normalised to the control wells, providing a Cell Viability Index. Non-linear regression was used to draw dose response curves and determine the GI_{50} value on GraphPad Prism® (GraphPad).

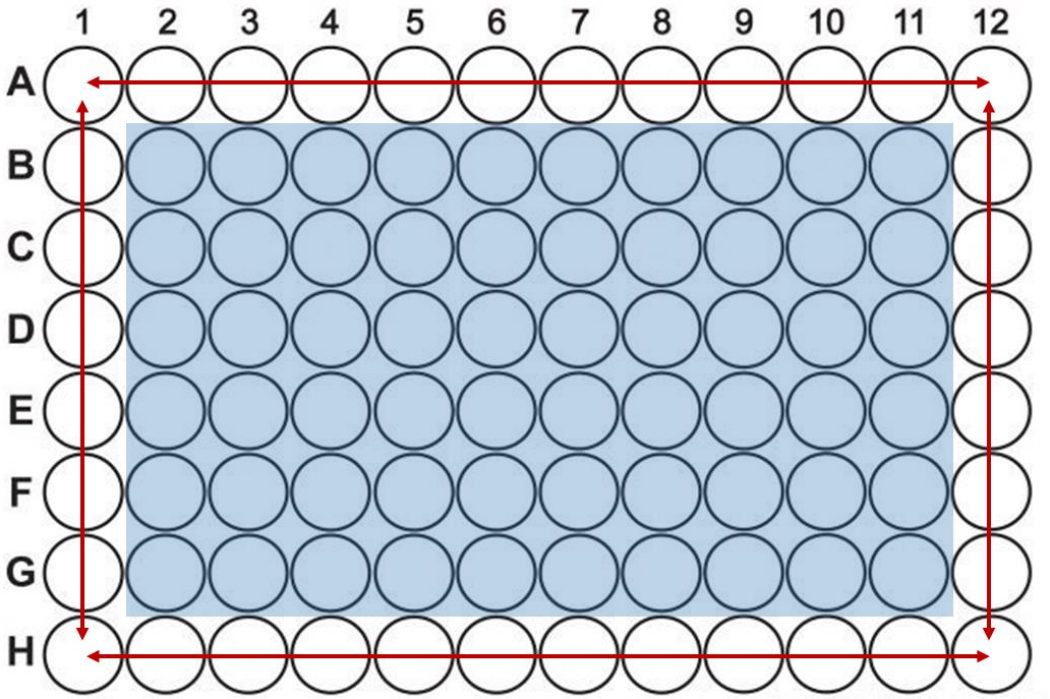

Figure 2.1 MTS assay plate layout

MTS cell viability assays were performed in 96 well plates. PBS was placed in the outer wells (shown by red arrows) to reduce edge effect and prevent dehydration within the plate during the experiment. All drug treatments were given to cells seeded within the middle 60 wells (shown by the blue box).

2.2.2 Flow Cytometry

Cell proliferation assays of PS1 and AsPC-1 proliferation in response to increasing concentrations of AZD4547 in mono- and co-culture conditions were carried out using CellTracker dyes and Flow Cytometry analysis. Cells were labelled with 5 µM green CellTracker dye (AsPC-1) (C2925, Life Technologies) or red CellTracker dye (PS1) (C34553, Life Technologies) for 45 minutes in serum free medium. The cells were then seeded in 60 mm dishes in either monoculture or co-culture conditions at an optimal density of 1.5 x 10^5 and 2 x 10^5 cells for PS1 and AsPC-1 monoculture, respectively. In co-culture conditions, 2 x 10^5 cells were plated in total in a 2:1 ratio of PS1 cells to AsPC-1 cells (Kadaba et al., 2013). After 24 hours, the cells were treated with either vehicle control or increasing concentrations of AZD4547, in the range of 0.5-50 µM. These plates were then incubated at 37^{o}C for 48 hours.

To analyse the effect of increasing drug concentration on proliferation, the cells were detached from the dishes with trypsin-EDTA 10X. After neutralising the trypsin and centrifuging, the cell pellet was re-suspended in PBS plus 2 % (v/v) FBS and transferred into a polystyrene round bottom tube for flow cytometry analysis. The cell solutions were then analysed on a BD LSRFortessa™ machine (Becton Dickinson). After gating to exclude debris and doublets, the AsPC-1 and PS1 fluorescent populations were recorded. When cells divide, the CellTracker dye will be passed to both daughter cells, decreasing the staining intensity in each cell by half and therefore demonstrating the level of proliferation in a sample. Geometric mean (average fluorescence intensity per cell) was calculated for each cell line and normalised to vehicle controls. This was used to determine changes in cell proliferation with increasing drug concentrations. The differences in proliferation between mono- and co-culture were analysed in GraphPad Prism®.

2.3 Immunostaining

2.3.1 Immunocytochemistry

Cells were seeded onto coverslips and grown until confluent. They were then fixed in 10 % (v/v) formalin (4 % formaldehyde) (BAF-0010-01A, CellPath) for 10 minutes and blocked in 0.1 % (w/v) saponin (S4521, Sigma-Aldrich), 6 % (w/v) bovine serum albumin (BSA) (A8022, Sigma-Aldrich) in PBS for 15 minutes. The relevant antibodies were then added according to the dilutions and incubation times in Table 2.3 in 6 % (w/v) BSA in PBS. Between primary and secondary antibodies, the coverslips were washed three times in PBS-0.05 % (v/v) Tween-20 (A1389, Pancreac Applichem) (PBST). After the final antibody incubation, the samples were washed three times in PBST and once in distilled water. The nuclei were counterstained and samples were mounted with Pro-Long® Gold Antifade mountant with DAPI (4,6-diamidino-2-phenylindole) (P36931, Life Technologies). The samples were viewed using the Confocal 710 or Confocal 510 microscope (Carl Zeiss MicroImaging LLC).

2.3.2 Oil Red O staining

Cells were seeded onto coverslips and treated daily with either ATRA (1 µM) (R2625, Sigma-Aldrich) or 0.1 % (v/v) ethanol (E/0650DF/17, Fisher Scientific) vehicle control. The coverslips were fixed in formalin for 10 minutes and then stained with Oil Red O (O-0625, 5 mg/ml, Sigma-Aldrich) for one hour. The Oil Red O stain was freshly diluted in water (3:2) and filtered on the day of use. The cells were then counterstained with Mayer's haematoxylin (MHS16, Sigma) and mounted. Images were taken using the Axiophot microscope and Axiovision Rel 4.8 software (Carl Zeiss MicroImaging LLC).

2.3.3 Immunofluorescence

Formalin fixed, paraffin embedded sections were dewaxed using xylene (X/0250/17, Fisher Scientific) and rehydrated by passing through graded alcohols (100 %, 80 %, 70 %, 50 % (all v/v) and distilled water), finally ending in PBS/Tween. Heat induced epitope retrieval (HIER), to unmask antigens, was performed by boiling sections in 10 mM citrate buffer pH 6.0 (S/3280/60, Fisher Scientific) for 11 minutes (20 minutes for Ki67 staining). Samples were blocked with 0.05 % goat serum (v/v) (R2283, Sigma) in ABC buffer, 2 % (w/v) BSA, 0.02 % (w/v) fish gelatin (G-7765, Sigma) and 10 % (v/v) FBS in PBS, for 1 hour at room temperature. Primary antibodies were diluted in ABC buffer and incubation was performed according to Table 2.3. After washing the primary antibodies, the slides were incubated with relevant secondary antibodies (Table 2.3) diluted in PBS for 1 hour at room temperature in the dark. The samples were viewed using the Confocal 510, 710 or 880 microscopes (Carl Zeiss MicroImaging LLC).

2.3.4 Immunohistochemistry

Formalin fixed, paraffin embedded sections were dewaxed and rehydrated as described above, including an extra incubation in methanol plus 3 % (v/v) hydrogen peroxide (231-765-0, Fisher Scientific) to block endogenous peroxidases. IHC was carried out using the Vectastain kit (PK-6101, Vector) and samples were blocked according to manufacturer's instructions, briefly samples were incubated with 1.5 % (v/v) goat serum in PBS for 15 minutes. Antigen retrieval, primary antibody dilution and incubation were performed according to Table 2.3. After washing off the primary antibodies, the slides were incubated with relevant secondary biotinylated antibodies (50 µl in 1.5 % (v/v) goat serum in PBS) and an avidin-biotin layer (100 µl avidin and 100 µl biotinylated HRP in 1.5 % (v/v) goat serum in PBS) to amplify the staining

signal, according to manufacturer's instructions. After washing, the samples were incubated with 3,3'-diaminobenzidine (DAB) (SK-4100, Vector) to view the positive staining. After washing off excess DAB, the slides were counter-stained with Mayer's haematoxylin, dehydrated through graded alcohols and mounted with a coverslip using DPX, which is a mix of distyrene, plasticiser and xylene (360294H, VWR). H&E staining was performed by the BCI Pathology Core Services and all slides were viewed using the Pannoramic scanner (3DHISTECH).

2.3.5 IN Cell analysis

PS1 cells were seeded into a 96 well plate at a density of 6,000 cells per well. After 24 hours, the cells were treated with increasing concentrations of AZD4547 (0.25-1 µM) or vehicle control and then after another 24 hours the plates were processed for imaging. Cells were fixed in formalin for 10 minutes, before being stained for FGFR1 using the same conditions as Section 2.3.1. The cells were counterstained with DAPI (D9542, Sigma-Aldrich) for ten minutes at room temperature in the dark. Nuclear staining was analysed using the IN Cell 2200 high-throughput microscope (GE Healthcare Life Sciences) and the number of nuclear foci in each well was quantified using the IN Cell Investigator Software (GE Healthcare Life Sciences).

2.4 Western Blotting

2.4.1 Protein isolation

Cells were lysed using lysis buffer (50 mM Tris-HCl pH 7.5 (T3253, Sigma), 150 mM sodium chloride (NaCl, 7647-14-5, Sigma-Aldrich), 1 mM EDTA (D/0450/50, Fisher Scientific), 1 % (v/v) Triton-X-100 (A16046, Alfa Aesar)) with protease and phosphatase inhibitors (539131 and 524625, Millipore) and scraping with a cell

scraper. The lysate was centrifuged for 10 minutes at 20,000 x g at 4°C to pellet cell debris (some membrane proteins may be sequestered in the pellet). The protein in the supernatant was quantified using Bio-Rad DC Protein Assay (solution A 500-0113, solution B 500-0114 and solution S 500-0115), according to manufacturer's instructions. Briefly add 20 µl reagent S to 1 ml reagent A to make the working solution. Place 25 µl of this solution into each well then add 5 µl of the relevant protein standard or sample. Finally add 200 µl of reagent B and incubate the plate for 5 minutes at room temperature. After incubation, the intensity of the colour in each well was measured by the absorbance at 620 nm, using a 96-well microplate reader (Infinite® F50, Magellan software). Equal amounts of protein were prepared with sample buffer (60 mM Tris-HCl pH 6.8, 2 % (v/v) sodium dodecyl sulphate (SDS, BP1311, Fisher Scientific), 10 % (v/v) glycerol (49782, Sigma-Aldrich), 0.5 M dithiothreitol (DTT) (D0632, Sigma-Aldrich), 0.01 % (v/v) bromophenol blue (B5525, Sigma-Aldrich) final concentration).

2.4.2 Western blotting

The prepared lysate samples were boiled for 5 minutes to denature the proteins and separated on either 7.5 % (v/v) or 10 % (v/v) sodium dodecyl sulphate polyacrylamide gel electrophoresis (SDS-PAGE) gels. The gels were run at 140V for 1.5 hours and then transferred onto a nitrocellulose membrane (1060000, GE Healthcare) in a Bio-Rad semi-dry transfer tank at 20V for 1 hour, or using a BioRad wet transfer tank at 120V for 1 hour. Ponceau S solution (P7170, Sigma) was used to confirm efficient protein transfer and then the membranes were blocked in 5 % (v/v) milk (70166, Sigma) in Tris-buffered saline (20-6400-10, Severn Biotech Ltd)-0.1 % (v/v) Tween-20 (TBST) for at least 30 minutes.

2.4.3 Detection and analysis

The membranes were incubated with primary antibodies (Table 2.3) diluted in 3 % (v/v) BSA-TBST at 4ºC overnight, to detect the levels of specific proteins in the samples. After unbound primary antibody was removed from the membrane with TBST, HRP-conjugated secondary antibodies (Table 2.3) were incubated with the membranes for at least one hour at room temperature. Excess secondary antibody was also removed from the membrane using TBST and detection was carried out using Luminata Forte Western HRP substrate (WBLUF0100, Millipore) and the Amersham Imager 600 (GE Healthcare).

2.5 Generation of inducible cell lines

2.5.1 Transient transfection of FGFR1-HaloTag

Cells were seeded into dishes to achieve 50 % confluency after 24 hours. An FGFR1-HaloTag construct (FHC10532, Kazusa DNA Research Institute) was then transiently transfected into these cells using 1 µg of plasmid DNA in 50 µl of OptiMEM (31985062, ThermoFisher Scientific) and 3 µl of FuGENE HD transfection reagent (E2311, Promega). This solution was incubated at room temperature for ten minutes and then added to the cells in 1 ml of fresh medium (plus FBS). Confirmation of transfection was carried out by tetramethyl rhodamine (TMR) (G825A, Promega) labelling 48 hours later. Successful transfection was also confirmed using Western Blot analysis (as described in 2.4).

2.5.2 Gateway cloning of FGFR1-HaloTag

The gateway cloning system (12535-027, Invitrogen) was used to generate an inducible FGFR1-HT construct (Figure 2.2) (Reece-Hoyes and Walhout, 2018).

Primers were designed to amplify FGFR1-HT from the pFC14K HaloTag vector (9PIG966, Promega) with attB sites (see Table 2.1 and Figure 2.3), using Phusion polymerase (F530S, ThermoFisher). Confirmation of successful PCR was determined by a positive band at ~3,200 bases on an agarose gel and direct sequencing (SourceBioScience). After effective PCR of the FGFR1-HT construct, this was put into a pDONR/zeo plasmid (12535-035, Invitrogen) using the BP clonase recombination reaction (11789-013, Invitrogen). Heat shock transformation of TOP10 cells (C4040-03, Invitrogen) was then carried out using the product of the BP clonase reaction. The TOP10 cells were grown on zeocin (46-0509, Invitrogen) agar plates overnight to produce colonies.

After antibiotic selection, clones were selected and amplified in overnight cultures. Plasmid DNA was removed from these cells using the peqGOLD plasmid miniprep kit (732-2780, VWR), according to manufacturer's instructions. Briefly, the culture was pelleted by centrifuging at 5,000 x g for 10 minutes and the supernatant was discarded. The pellet was lysed by vortexing in 250 µl of solution I, then adding 250 µl of solution II and mixing gently. Neutralisation of the solution with 350 µl of solution III was performed and then this was loaded onto a PerfectBind DNA column. The column was centrifuged at 10,000 x g for 1 minute to allow the DNA to bind and the flow-through was discarded. Three washes were performed by adding wash buffer to the column and centrifuging at 10,000 x g for 1 minute, discarding the flow-through. The column was dried to remove all the ethanol by centrifuging at 10,000 x g for 2 minutes. The DNA was eluted by adding 50 µl of elution buffer and centrifuging at 5,000 x g for 1 minute.

Following miniprep extraction and restriction digest with BsrG1 (R0575S, New England Biolabs), clone 4 (which expressed the FGFR1-HT construct) was selected

to move forwards into the LR clonase reaction (11791-019, Invitrogen). This reaction transferred the construct into the pInducer21 plasmid (46948, Addgene). Transformation of this product into one shot Stbl3 *Escherichia coli* (C737303, ThermoFisher) was carried out and the cells were grown on agar plates containing ampicillin (11593027, ThermoFisher) overnight. Again clones were selected and amplified in overnight cultures. After miniprep of plasmid DNA and restriction digest with BsrG1 to isolate the construct, one clone was selected to be sequenced using the sequencing primers in Table 2.1 and Figure 2.4 by Source Bioscience. Following confirmation of successful cloning, this construct was used to generate lentiviral particles (pInducer21-FGFR1-HT).

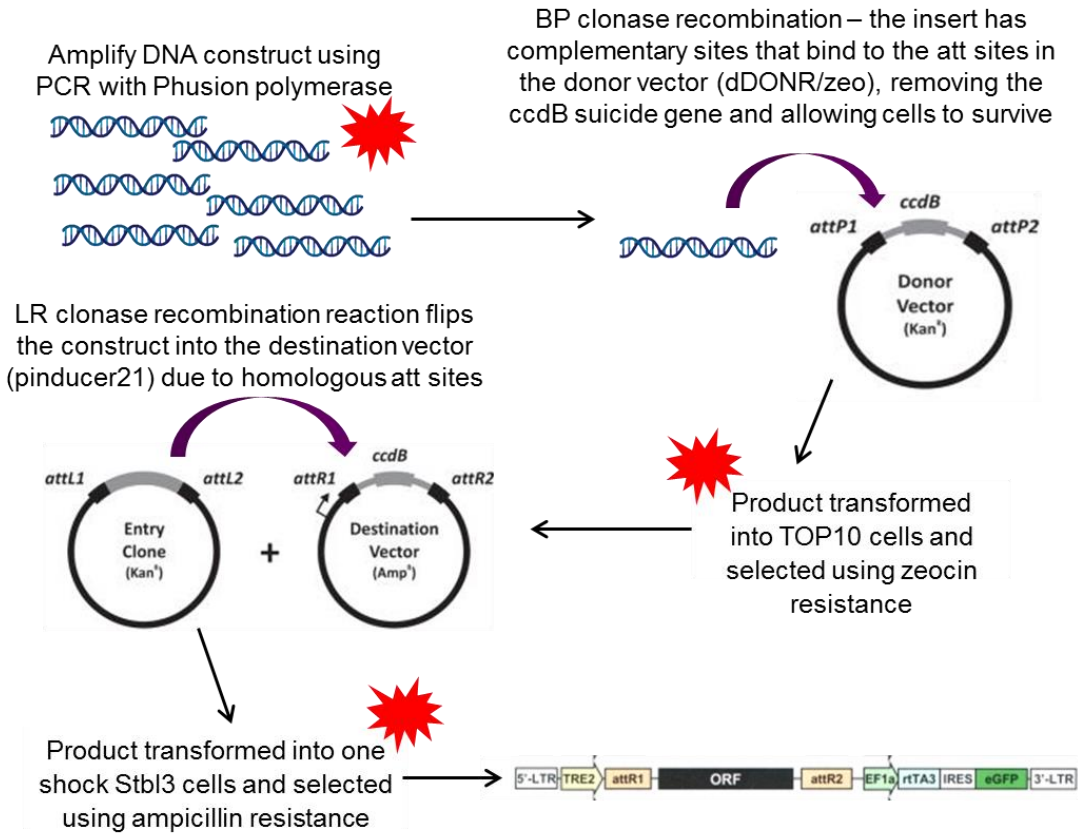

Figure 2.2 Gateway cloning process

Summary of the process to produce a pinducer21 plasmid expressing the FGFR1-HT construct to use for lentiviral production. Primers were designed to amplify the construct with attB sites on either end. This allowed homologous recombination reactions to transfer the construct into the donor vector and finally into the destination vector. At each point with the red star, confirmation of the presence of the construct was carried out by running the product on an agarose gel. The final pinducer21 construct has GFP expression as a selection marker and doxycycline inducible expression of FGFR1-HT (Reece-Hoyes and Walhout, 2018).

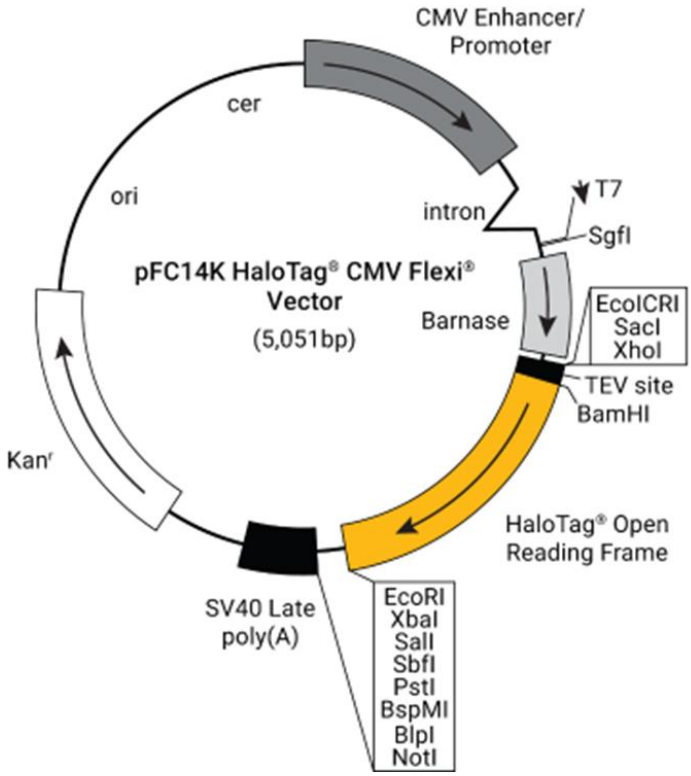

Figure 2.3 pFC14K HaloTag CMV Flexi Vector plasmid map

FGFR1-HaloTag construct was isolated from a purchased pFC14K HaloTag plasmid

2.5.3 FGFR1 shRNA generation

Three validated shRNA constructs were created with Age1 (R0552S, New England BioLabs) and EcoR1 (R0101, New England BioLabs) restriction sites on the 5' end of the sequence (TRCN0000312516, TRCN0000312574 and TRCN0000312572, Sigma-Aldrich). The oligonucleotides were annealed by diluting in annealing buffer (0.1 M NaCl and 10 mM Tris-HCl pH 7.4 final concentration) and placing the solution in a boiling water bath, which was allowed to cool to 30^{o}C over 2-3 hours. The oligonucleotide mixture was then diluted 1:400 in 0.5X annealing buffer.

The tet-pLKO-neo plasmid (21916, Addgene) (Figure 2.4) was used as the lentiviral vector for shRNA expression. Firstly, the plasmid was digested with Age1 and EcoR1 in a sequential restriction digest (Age1 plus NEB buffer 1 (B7001S, New England BioLabs) at 37^{o}C for 1 hour then EcoR1 plus NEB buffer 3 (B7003S, New England BioLabs) at 37^{o}C for 1 hour). The product of this digest was run on a gel to separate the backbone and the stuffer fragments. The backbone was cut from the gel and purified using Monarch® DNA Gel Extraction Kit (T1020S, New England BioLabs) according to manufacturer's instructions. Briefly, the gel was dissolved by adding 4 volumes of gel dissolving buffer and incubating at 50^{o}C for 10 minutes with vortexing. The solution was then added to the DNA column and centrifuged at 10,000 x g for 1 minute to allow the DNA to bind, the flow-through was discarded. Two washes were performed by adding DNA wash buffer to the column and centrifuging at 10,000 x g for 1 minute, discarding the flow-through. The DNA was retrieved in a fresh 1.5 ml collection tube by adding DNA elution buffer to the column and centrifuging at 10,000 x g for 1 minute.

Ligation of the oligonucleotides and pLKO backbone was carried out in ligase buffer (B0202S, New England BioLabs) using T4 DNA ligase (M0202S, New England BioLabs) overnight at 4ºC. One shot Stbl3 cells (C737303, ThermoFisher) were transformed using this plasmid and grown overnight on agar plates containing ampicillin (11593027, ThermoFisher). Clones were isolated, amplified in overnight cultures and screened to check for successful uptake of the tet-pLKO-neo plasmid by digest with Xho1 (R0146S, New England BioLabs). One clone of each shRNA was selected to generate lentiviral particles.

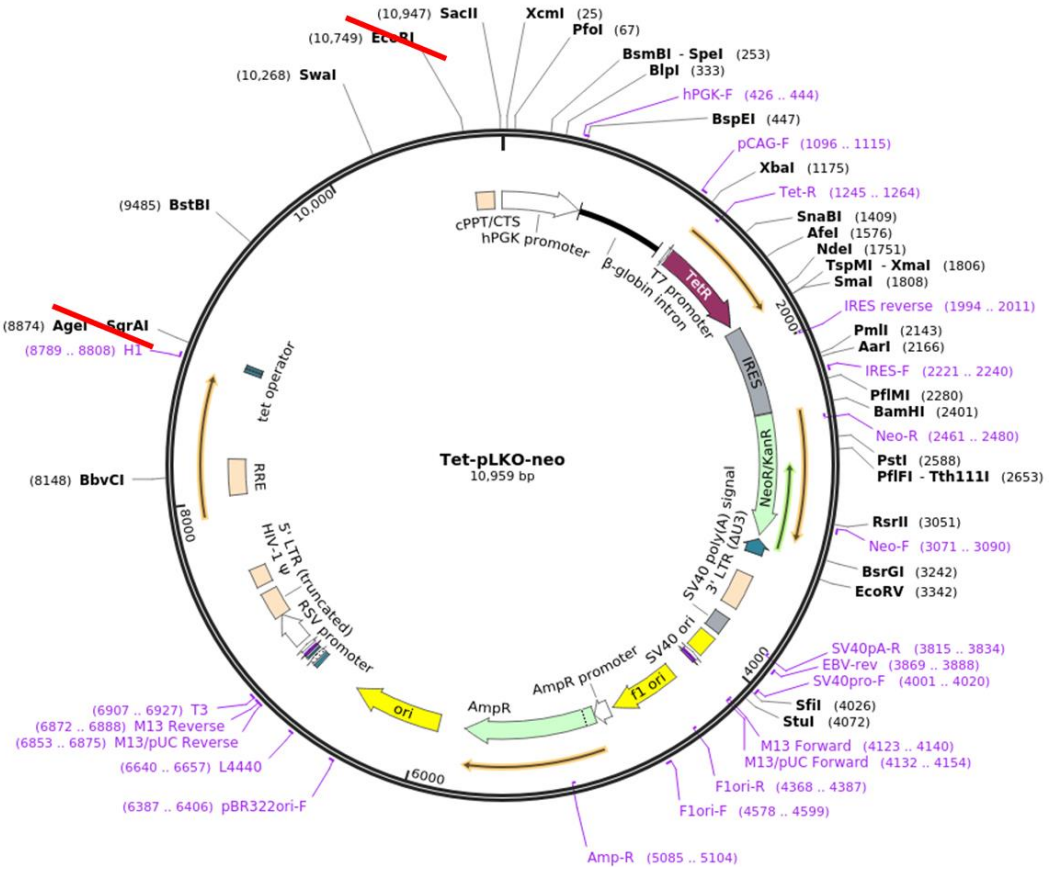

Figure 2.4 Tet-pLKO-neo plasmid map

The tet-pLKO-neo plasmid was used as a lentiviral vector for creating the PS1 FGFR1 shRNA cell lines in this project. The red lines indicate where sequential digest was used to linearise the plasmid, remove the stuffer and insert the relevant shRNA construct.

2.5.4 Lentiviral production and infection

HEK293T cells were seeded into a 60 mm dish to reach 90 % confluency after 24 hours. The following day 5 µg of pinducer21-FGFR1-HT plasmid (46948, Addgene), H2B-RFP (26001, Addgene), H2B-GFP (25999, Addgene) or tet-pLKO-neo (FGFR1 shRNA containing) plasmid, 1.75 µg pMD2.G (1259, Addgene) and 3.25 µg CMVR8.74 (12263, Addgene) was prepared in 470 µl optiMEM with 30 µl FuGENE transfection reagent. This mixture was incubated at room temperature for 10 minutes and then added to the HEK293T cells in 5 ml of fresh medium (plus FBS). After 24 hours, the medium was replaced with fresh DMEM. The viral supernatant was collected 24 hours later, pelleted for cell debris and stored at -80^{o}C.

To infect PS1 cells, the cells were seeded into a six well plate to reach 30 % confluency the next day. Viral supernatant was then added to the PS1 cells and incubated for 24 hours. After this, fresh medium was placed on the cells and infection efficiency was confirmed. Cells were selected for successful transduction by sorting on the expression of GFP or RFP (PS1-HT and H2B labelling) using the BD FACS Aria II or Aria Fusion cell sorters (BD Biosciences) or treatment with 600 µg/ml neomycin (shRNA).

2.5.5 RNA extraction and qPCR analysis

RNA was extracted using the RNeasy Mini Kit (74104, QIAGEN), according to manufacturer's instructions. Briefly, cells were lysed by adding 350 µl of RLT buffer and vortexing. Next, 350 µl of 70 % (v/v) ethanol was added to the lysate and this was loaded into an RNeasy spin column, centrifuged at 8,000 x g for 15 seconds and the flow-through was discarded. The RNA was washed three times by adding wash buffer into the column and centrifuging at 8,000 x g for 15 seconds. The column was

dried to remove all the ethanol by centrifuging at 10,000 x g for 1 minute. RNA was eluted into a 1.5 ml collection tube by adding 30 µl of RNase-free water to the column and centrifuging at 8,000 x g for 1 minute. The RNA was quantified following extraction using a nanodrop ND-1000 spectrophotometer. Reverse transcription was carried out to convert 1 µg of RNA into cDNA using Superscript II reverse transcriptase kit (18064014, Invitrogen) with deoxynucleotide triphosphates (dNTPs) (BIO-39036 – 39039, Bioline) and random hexamer primer mix (RHP-108G, Bioline) according to manufacturer's instructions. Briefly, sample RNA, random hexamer primer mix and 10 mM dNTP mix were heated to 65^{o}C for 5 minutes before being chilled on ice. Next, first strand buffer and 0.1 M DTT were added and the solution was incubated at room temperature for 2 minutes. Following this incubation, the Superscript II RT enzyme was added to the mix and this was incubated at 25^{o}C for 10 minutes, 42^{o}C for 50 minutes and then 70^{o}C for 15 minutes. The cDNA was subjected to quantitative polymerase chain reaction (qPCR) analysis using SensiFAST SYBR® HI-ROX kit (BIO-92005, Bioline), according to manufacturer's instructions, using relevant primers (Table 2.1) and the StepOnePlus Real Time PCR system (ThermoFisher Scientific). Briefly, each well had 9 µl of mastermix (0.3 µM relevant forward and reverse primers and 5 µl SYBR-green diluted in RNase-free water) plus 1 µl of cDNA or water control. The plate was then heated to 95^{o}C for 10 minutes, before entering 40 cycles of 95^{o}C for 30 seconds (denaturation), 60^{o}C for 30 seconds (annealing) and 72^{o}C for 30 seconds (extension). The plate was then incubated at 95^{o}C for 15 seconds, 60^{o}C for 1 minute and 95^{o}C for a further 15 seconds to end the reaction.

Table 2.1 Primer and oligonucleotide sequences

Target	Sequence – Forward	Sequence – Reverse
FGFR1b	TTA-ATA-GCT-CGG-ATG-CGG-AG	ACG-CAG-ACT-GGT-TAG-CTT-CA
FGFR1c	TGC-TGG-AGT-TAA-TAC-CAC-CG	CCA-GAA-CGG-TCA-ACC-ATG-CA
HPRT-1	GAC-CAG-TCA-ACA-GGG-GAC-AT	CCT-GAC-CAA-GGA-AAG-CAA-AG
B2M	AGT-TAA-GTG-GGA-TCG-AGA-C	GCA-AGC-AAG-CAG-AAT-TTG-G
FGFR1-HT	GGG-GAC-AAG-TTT-GTA-CAA-AAA-AGC-AGG-CTT-CAT-GTG-GAG-CTG-GAA-GTG-CC	GGG-GAC-CAC-TTT-GTA-CAA-GAA-AGC-TGG-GTC-TTA-ACC-GGA-AAT-CTC-CAG-AGT
FGFR1-HT sequencing 1	CCA-TCC-TGC-AAG-C	
FGFR1-HT sequencing 2	GCA-GAC-AGG-TAA-C	
FGFR1-HT sequencing 3	GGA-GCA-GCT-CTC	
FGFR1-HT sequencing 4	GTA-CCT-GGA-CC	
FGFR1-HT sequencing 5	GGA-GTT-CAT-CC	
FGFR1 shRNA1	CCG-GGA-TGG-CAC-CCG-AGG-CAT-TAT-TCT-CGA-GAA-TAA-TGC-CTC-GGG-TGC-CAT-CTT-TTT	AAT-TAA-AAA-GAT-GGC-ACC-CGA-GGC-ATT-ATT-CTC-GAG-AAT-AAT-GCC-TCG-GGT-GCC-ATC
FGFR1 shRNA2	CCG-GTG-CCA-CCT-GGA-GCA-TCA-TAA-TCT-CGA-GAT-TAT-GAT-GCT-CCA-GGT-GGC-ATT-TTT	AAT-TAA-AAA-TGC-CAC-CTG-GAG-CAT-CAT-AAT-CTC-GAG-ATT-ATG-ATG-CTC-CAG-GTG-GCA
FGFR1 shRNA3	CCG-GCC-ACA-GAA-TTG-GAG-GCT-ACA-ACT-CGA-GTT-GTA-GCC-TCC-AAT-TCT-GTG-GTT-TTT	AAT-TAA-AAA-CCA-CAG-AAT-TGG-AGG-CTA-CAA-CTC-GAG-TTG-TAG-CCT-CCA-ATT-CTG-TGG

2.6 3D assays

2.6.1 Mini-organotypic

Cells were grown in the 3D mini-organotypic model to assess effects on invasion. For this assay, Transwell™ inserts (3413, Costar) were coated with collagen I (354249, BD Biosciences) diluted in PBS (1:100) for 1 hour at 37ºC. The collagen coat was carefully removed by pipetting and replaced with organotypic gel mix (2.25 volumes collagen I (2 mg/ml final concentration), 1.75 volumes matrigel (354234, BD Biosciences), 1 volume 10X DMEM (E15-843, PAA Laboratories), 1 volume relevant cell culture medium and 1 volume FBS). The pH of the gel was adjusted with 1 M sodium hydroxide (124260010, Acros Organics) to neutralise the acidic collagen, allowing cells to grow. The gels were left at 37ºC for 2 hours to set, then 350 µl of relevant medium was placed underneath the Transwell insert, creating an air-liquid interface.

Cells were then seeded on top of the gel in either mono or co-culture with 100,000 cells per gel. In co-culture conditions, a 2:1 ratio of stellate cells to cancer cells was used (Coetzee et al., 2019, Kadaba et al., 2013). The cells were left for 24 hours to attach to the gel before treatments were added into the medium below the Transwell insert. For this study, organotypic gels were treated with either 1 µM AZD4547 daily or on alternate days, 2 µM PD173074 (P2499, Sigma-Aldrich) on alternate days, 1 µM ATRA daily (R2625, Sigma), 100 nM gemcitabine (Fresenius Kabi Oncology PLC 38 mg/ml) weekly or 1 µg/ml doxycycline on alternate days (Figure 2.5).

After 7 days, the gels were incubated with 1 mM BrDU (550891, BD Biosciences) (plus or minus drug) for 2 hours at 37ºC. The Transwells were then gently washed once in PBS and fixed in 10 % (v/v) formalin for 24 hours. The formalin was replaced

by 70 % (v/v) ethanol and the gels were cut in half and embedded in paraffin wax. H&E, immunofluorescence and immunohistochemistry were carried out on sections prepared from these gels as described previously (Section 2.3). Embedding and sectioning of these gels was performed by the Pathology department at Barts Cancer Institute. Invasion and total cell layer area on top of the gels was quantified from H&E sections using the Pannoramic Viewer software (3DHISTECH). Cells invading into the gels were counted individually using the manual cell counter tool and the cell layer thickness was calculated from 4-6 distance measurements made per gel. Proliferation was measured by immunofluorescence staining for Ki67 and counting the number of positive nuclei as a percentage of the total cell nuclei in at least five fields of view from each gel (the whole gel layer was imaged). Apoptosis was measured by staining for cleaved caspase 3 and counting the number of positive nuclei as a percentage of the total cell nuclei for each gel. Median and Interquartile range was used to summarise the data and the Kruskal-Wallis statistical test with Dunn's multiple comparison was performed.

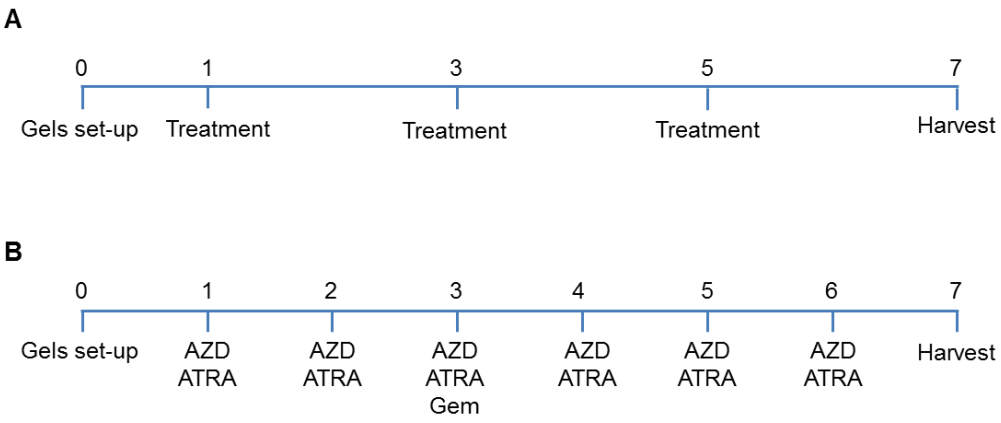

Figure 2.5 Experimental timelines for organotypic cultures

*Organotypic gels were made and cells seeded on top on day 0. The gels were then maintained in culture for 7 days before fixing in formalin and harvesting. On the day of harvesting, some gels were treated with BrDU for 2 hours before fixing to assess proliferation. Gels were treated with AZD4547 or doxycycline every other day (**A**) by refreshing the medium beneath the gels. For the combination therapy protocol, AZD4547 and ATRA treatment were given daily, whilst gemcitabine treatment was only given once, to match patient protocols in the clinic (**B**).*

2.6.2 Spheroid

A second 3D PDAC model was used in this project. In the spheroid model, cells were seeded into a 2.5 % (v/v) methylcellulose (M0512, Sigma) droplet. This droplet was suspended from the lid of a 150 mm dish, allowing cells to form a sphere inside. 1,000 cells were seeded per droplet in either mono- or co-culture, with the same 2:1 co-culture ratio as previously described (Kadaba et al., 2013).

Twenty-four hours later, a 96 well plate was pre-coated with organotypic gel mixture (10.5 volumes high concentration collagen (354249, Corning®, 2 mg/ml final concentration), 7 volumes matrigel, 1 volume HEPES (H7006, Sigma) and 21.5 volumes relevant cell culture medium plus sodium hydroxide to neutralise the pH). The coating prevented spheres from touching the plastic at the base of the well. Once the pre-coating had set, the spheres were gently collected using a cut pipette tip, washed and suspended in organotypic mixture. These were seeded into the 96 well plate (50 µl of gel with an average of 6 spheres per well) and the gels were left to set. Medium containing any relevant drug treatments was placed on top of the gels and the cultures were incubated for 2-5 days.

At the end of the assay the gels were imaged using an Axiovert 135 (Carl Zeiss MicroImaging LLC) and quantified using ImageJ (National Institutes of Health). Quantification was performed by drawing around the whole spheroid to obtain the total area, as well as around the central sphere to get the sphere area. The central sphere area was then subtracted from the total area to obtain the invasive area, including the protrusions leaving the central spheroid. Median and Interquartile range was used to summarise the data and the Mann-Whitney U statistical test was performed. Stellate cell lines labelled with H2B-GFP and PDAC cancer cell lines

labelled with H2B-RFP were used to determine which cells were leading the invasion out of the sphere. Z-stack images were taken of the whole spheroid using the Confocal 710 microscope.

2.7 Chromatin Immunoprecipitation

2.7.1 Chromatin Isolation

To perform chromatin immunoprecipitation (ChIP), chromatin must be isolated from the cell of interest, fragmented to an optimal length, immunoprecipitation performed with a suitable antibody and then the immunoprecipitated DNA extracted. To give an unbiased analysis of genome binding by FGFR1, cross-linked ChIP (XChIP) with random sonication induced chromatin shearing was used.

2.7.2 Active Motif optimisation

ChIP assays were initially optimised using the ChIP-IT High Sensitivity kit (53040, Active Motif), according to manufacturer's instructions. Briefly, Complete Cell Fixation Solution was prepared by adding 180 µl of Fixation Buffer, 1.57 ml of sterile water and 750 µl of 37 % (v/v) formaldehyde. This was then added to the plates (1/10 of the growth medium volume) and incubated at room temperature for required fixation time, gently shaking. The fixation reaction was stopped by adding 1/20 medium volume of Stop Solution and incubating at room temperature for 5 minutes. The cells were then removed from the plate by scraping and collected into a tube on ice. The cells were pelleted by centrifugation at 1,250 x g at 4^{o}C for 3 minutes. The supernatant was then discarded and the pellet was washed twice in ice-cold PBS wash buffer (21.25 ml sterile water, 2.5 ml 10X PBS and 1.25 ml Detergent). Following the final wash, the pellet was re-suspended in 5 ml Chromatin Prep Buffer (supplemented with 5 µl PIC

and 5 µl 100 mM PMSF) and incubated on ice for 10 minutes. The cells were then lysed using a needle and syringe. The chromatin was pelleted by centrifugation at 1,250 x g at 4ºC for 3 minutes. The pellet was then re-suspended in 500 µl ChIP Buffer (supplemented with 5 µl PIC and 5 µl 100 mM PMSF), incubated on ice for 10 minutes and sonicated. The first step was testing different fixation times (either 5 or 10 minutes) and number of sonication cycles (10, 15 or 20). A Bioruptor sonicator (Diagenode) was used for the sonication of samples throughout ChIP optimisation using an optimal 30 seconds ON 30 seconds OFF sonication cycle setting.

2.7.3 Millipore optimisation

A further ChIP kit was used for optimisation, the EZ-ChIP kit (17-295, Merck Millipore), according to manufacturer's instructions. Briefly, to prepare the cells, 14 confluent T-175 flasks were used to collect chromatin, with 1 confluent T-175 flask of MFE-296 cells as a positive control. The samples were fixed in 1 % (v/v) formaldehyde at 37ºC for 10 minutes, then 1 M glycine (1/10) was added to stop the fixation reaction at 4ºC. The samples were then washed twice with ice cold PBS and harvested by scraping in PBS (plus PIC). The cells were pelleted by centrifuging at 8,000 x g at 4ºC for 3 minutes and the supernatant was discarded. The cells were lysed by incubation with SDS Lysis Buffer on ice for 10 minutes and sonicated for 10 cycles (30 seconds ON, 30 seconds OFF). The input DNA was then extracted (Section 2.7.4.4) and run on a 1 % (w/v) agarose (16500, Invitrogen) gel to confirm chromatin fragmentation.

2.7.4 ChIP-seq

2.7.4.1 Culture conditions

Cells were seeded into 10 x 150 mm dishes per condition to achieve confluency at time of harvest (~20 million cells). After 24 hours, cells were treated with AZD4547,

doxycycline to induce FGFR1 knockdown, or relevant vehicle controls. Cells treated with FGFR inhibitors were harvested 24 hours after treatment and shRNA cells were harvested after 48 hours of knockdown.

2.7.4.2 Chromatin harvesting and fragmentation

At the time of harvesting, medium was removed and the cells were incubated at room temperature on a rocker for 5 minutes with fixing solution: 1 % (v/v) formaldehyde (28908, Thermofisher) in relevant cell culture medium plus protease inhibitor cocktail (05 056 489 001, Roche). This reaction was then quenched by 5 minutes incubation with 1.25 M glycine solution pH 6.0 (G/0800/60, Fisher Scientific) at a final concentration of 125mM, at room temperature on a rocker. The cells were then washed twice in ice cold PBS and collected by scraping with PBS plus protease inhibitor cocktail. Once all the dishes had been harvested, the cells were pelleted, the supernatant was discarded and the pellet was snap frozen and stored at -80^{o}C.

Chromatin was harvested by thawing cell pellets on ice for 30 minutes. Lysis buffer (1 % (v/v) SDS, 50 mM Tris-HCl pH 8.0, 10 mM EDTA plus protease inhibitor cocktail) was then added to the pellet and it was broken up using a syringe and 27 gauge needle – whilst being careful not to introduce bubbles. Cells were lysed on ice for 30 minutes. The chromatin was then sonicated using a Bioruptor pico sonicator (Diagenode) in 15 ml TPX tubes with beads (C01020031, diagenode) to enhance the fragmentation. The samples were originally sonicated for 10 cycles (30 seconds ON and 30 seconds OFF), the fragmentation was then examined by taking a small sample, extracting the DNA and running on 1 % (w/v) agarose gel. If further fragmentation was required, five more sonication cycles were performed.

2.7.4.3 Immunoprecipitation

Once the fragmentation of the samples was satisfactory, as judged by a diffuse band of 100-300 bp following agarose gel electrophoresis, the samples were subjected to immunoprecipitation with an FGFR1 antibody (ab10646, Abcam). Briefly, chromatin samples were diluted in 1:4 ratio with dilution buffer plus protease inhibitor cocktail (Table 2.2), giving a final concentration of 0.2 % (v/v) SDS. The diluted chromatin was then incubated with dynabeads (10003D, Life Sciences, resuspended in working buffer, Table 2.2) rotating at 4^{o}C for 2 hours to pre-clear any non-specific binding.

Following pre-clearing with dynabeads, 10 % of each sample was taken to be used as an input. The rest of the sample was incubated with 4 µg of FGFR1 antibody at 4^{o}C rotating overnight. To prevent non-specific binding 0.5 % (w/v) BSA and 0.1 µg/µl tRNA (10 109 541 001, Roche Diagnostics) were added. Meanwhile, dynabeads were blocked overnight at 4^{o}C with 0.5 % (w/v) BSA.

The next day, the blocked dynabeads were incubated with the chromatin-antibody solution at 4^{o}C, rotating for 2 hours. After this incubation, the bound dynabeads were subjected to a series of washes (low salt immune complex, high salt immune complex, LiCl immune complex and TE buffer, Table 2.2) before eluting in elution buffer (Table 2.2) at room temperature.

2.7.4.4 DNA extraction

The enriched chromatin samples were then incubated with RNase A (EN0531, Thermo Scientific) and proteinase K (P8107S, New England BioLabs) overnight to remove protein-DNA cross-links. The DNA was then extracted from the sample using phenol-chloroform (77617, Sigma) and ethanol precipitation, following a standard

protocol. Qubit and Tapestation™ analysis confirmed DNA quality and fragmentation before the samples were submitted for sequencing at Oxford Genomics Centre.

2.7.4.5 ChIP-seq analysis

Sequencing hits were analysed by aligning to the reference genome (hs37d5). Reads were mapped using MACS2 and peaks were called using diffBind. Initial analysis of FGFR1 binding was performed by examining the enriched peaks in control samples compared to the relevant input background control. Known blacklist regions, such as satellite regions, were removed from the analysis. The enriched peaks could then be compared between samples to highlight the most reliable hits. Search Tool for the Retrieval of Interacting Genes/Proteins (STRING) was used to analyse interactions between common enriched peaks across the samples.

Table 2.2 Chromatin Immunoprecipitation buffers

Buffer	Recipe
Immunoprecipitation Lysis Buffer	2 % (v/v) Triton 1 % (v/v) SDS 100 mM NaCl 10 mM Tris-HCl pH 8.0 1 mM EDTA Protease Inhibitor Cocktail
Dilution Buffer	50 mM HEPES pH 8.0 140 mM NaCl 1 mM EDTA 0.75 % (v/v) Triton 0.1 % (v/v) sodium deoxycholate (D5670, Sigma) Protease Inhibitor Cocktail
Working Buffer	1 x Immunoprecipitation Lysis Buffer 4 x Dilution Buffer Protease Inhibitor Cocktail
Low Salt Immune Complex Wash Buffer	1 % (v/v) Triton 150 mM NaCl 20 mM Tris-HCl pH 8.0 0.1 % (v/v) SDS 2 mM EDTA
High Salt Immune Complex Wash Buffer	1 % (v/v) Triton 500 mM NaCl 20 mM Tris-HCl pH 8.0 0.1 % (v/v) SDS 2 mM EDTA
LiCl Immune Complex Wash Buffer	0.25 M LiCl 1 % (v/v) sodium deoxycholate 10 mM Tris-HCl pH 8.0 1 % (v/v) NP40 1 mM EDTA
TE buffer	10 mM Tris-HCl pH 8.0 1 mM EDTA
Elution Buffer	0.1 M Sodium bicarbonate ($NaHCO_3$, 25080094, ThermoFisher Scientific) 1 % (v/v) SDS

2.8 Sub-cellular Mass Spectrometry

2.8.1 Culture conditions and fractionation

Cells were seeded into 30 x 150 mm dishes to achieve confluence at time of harvest (~60 million cells). After 24 hours, the plates were either placed in serum free medium overnight or treated with 1 μM AZD4547, doxycycline to induce FGFR1 knockdown or relevant vehicle control. The cells were harvested 24 hours after AZD4547 treatment and 48 hours after FGFR1 knockdown by washing with ice-cold PBS and then scraping off the dishes in PBS plus protease inhibitors. In the serum starved condition, cells were stimulated according to Section 2.1.3 and harvested as described above.

Once the cells had been collected, sub-cellular fractionation was carried out using the Minute™ Plasma Membrane Protein Isolation and Fraction kit (SM-005, Invent Biotechnologies) according to manufacturer's protocol. Briefly, cells were collected by centrifuging at 500 x g for 5 minutes, the pellet was washed once with cold PBS and re-suspended in 500 μl of buffer A. The cell suspension was incubated on ice for 10 minutes and then the tube was vortexed vigorously for 30 seconds. The cell suspension was transferred to the filter cartridge and centrifuged at 16,000 x g for 30 seconds. The cell suspension in the collection tube was then transferred back onto the same filter and centrifuged again to increase the yield. Then the filter was discarded and the pellet was re-suspended in the collection tube by vortexing for 10 seconds. This was centrifuged at 700 x g for 1 minute to collect the intact nuclei. The supernatant was then transferred into a fresh 1.5 ml tube and centrifuged at 16,000 x g for 30 minutes at 4°C. The supernatant was removed and kept as the cytosol fraction. Then the pellet was re-suspended in 200 μl of buffer B by vortexing. This was centrifuged at 7,800 x g for 1 hour at 4°C, the pellet contained the intracellular

membrane-bound organelles. The supernatant was then transferred into a fresh 2 ml tube and 1.6 ml cold PBS was added. This was mixed by inverting the tube a few times and then centrifuged at 16,000 x g for 1 hour at 4^{o}C. The supernatant was discarded and the pellet was kept as the plasma membrane fraction. The efficiency of sub-fractionation was confirmed by looking for the enrichment of relevant peptides in each fraction (Figure 5.17). Each fraction was re-suspended in SDS lysis buffer (2 % (v/v) SDS, 100 mM Tris-HCl pH 7.5).

2.8.2 Peptide isolation and preparation

The protein concentration in each fraction was quantified using Bio-Rad DC Protein Assay, according to manufacturer's instructions (Section 2.4.1), and 25 µg was taken forward to carry out Mass Spectrometry analysis. DTT was added to each sample at a final concentration of 100 mM and the tubes were incubated at 95^{o}C for 10 mins. Following this, 7 x volumes of urea buffer (UA, 8 M urea plus 100 mM Tris HCl pH 8.5) was added to all the samples and this was mixed gently. The samples were then transferred into vivacon 500 filters (VN01H21, Sartorius) and centrifuged at 14,000 x g for 20 minutes. Following this another 400 µl of UA buffer was added to the samples and they were centrifuged again (14,000 x g for 20 mins). Flow through was discarded.

Following this, 0.05 M iodoacetamide (IAA, 786-228, G Biosciences) dissolved in UA buffer was added to each sample. These were incubated in the dark for 30 mins. The sample was concentrated by centrifuging at 14,000 x g for 10 minutes. Next, three washes with UA buffer were carried out with centrifuging at 14,000 x g for 20 minutes and the flow-through was discarded. After this, three washes with 100 mM triethylammonium bicarbonate (TEAB, 90114, Thermo Scientific) were performed on

each filter, centrifuging the samples at 14,000 x g for 10 minutes and the flow-through was discarded. The filters were then placed into collection tubes and 100 µl of 100 mM TEAB buffer was added. Next, 2.5 µg (2.5 µl) of trypsin (T6567, Sigma) was added to the filters and they were incubated overnight at 37^{o}C, shaking.

The following day, acetonitrile (271004, Sigma-Aldrich) was added to each tube and incubated with vortexing for 5 minutes. The relevant TMT label (90061, ThermoFisher Scientific) was incubated with each fraction for 1 hour at 25^{o}C, shaking. The peptides were eluted by centrifuging at 14,000 x g for 10 minutes. A further two washes and centrifugations with TEAB buffer were carried out to ensure all the peptides were eluted fully. In the final elution, 30 % (v/v) acetonitrile was added to the filters before centrifuging at 14,000 x g for 10 minutes. All the eluates from each fraction were combined and vacuum dried overnight.

2.8.3 Mass Spectrometry analysis

The number of peptides detected was increased by fractionating the samples using Pierce™ high pH Reverse-Phase Peptide Fractionation Kit (84868, Thermo Scientific), according to the manufacturer's protocol. Briefly, the spin column was centrifuged at 5,000 x g for 2 minutes to remove the solution and pack the resin material, the flow-through was discarded. Next, the column was conditioned by centrifuging at 5,000 x g for 2 minutes with acetonitrile twice and 0.1 % (v/v) trimethylamine (TEA) twice. The peptide solution dissolved in 0.1 % (v/v) TEA was then added to the column and centrifuged at 3,000 x g for 2 minutes. The eluate was kept as the flow-through fraction. The column was then placed into a new collection tube and the sample was centrifuged again with water, the eluate was kept as the wash fraction. The TMT-labelled samples were then subjected to a further wash step

to remove unbound TMT reagent by centrifuging with 5 % acetonitrile in 0.1 % (v/v) TEA. The 8 peptide fractions were then collected in new collection tubes by centrifugation with increasing percentages of acetonitrile (10 %, 12.5 %, 15 %, 17.5 %, 20 %, 22.5 %, 25 % and 50 %) (all v/v) in 0.1 % (v/v) TEA. Samples were vacuum dried overnight and then analysed by Liquid Chromatography Mass Spectrometry (Dr Faraz Mardakheh). Quantitative peptide identification was performed using MaxQuant software. The log2fold change was then used to highlight the most up- or down-regulated peptides upon AZD4547 treatment in the whole cell lysate samples. For the sub-cellular analysis, the percentage change of each peptide within the nuclear compartment between the two conditions was calculated to demonstrate the most increased or decreased nuclear peptides. STRING was used to analyse potential interactions between the significantly changed peptides upon AZD4547 treatment in both the whole cell lysate and nuclear compartment. This was a pilot experiment and will be repeated in future (Section 5.4).

2.9 Murine experiments

2.9.1 Cell preparation

MIA PaCa-2 cancer and PS1 stellate cells were amplified in tissue culture ahead of *in vivo* pilot experiments. MIA PaCa-2 cells were prepared for injection in either mono- or co-culture with PS1 cells in a ratio of 1:2 respectively. On the day of injection various cell numbers were prepared in both mono- and co-culture in either PBS or PBS plus 50 % (v/v) matrigel: 1 x 10^6 MIA PaCa-2 + 2 x 10^6 PS1; 2 x 10^6 MIA PaCa-2 + 4 x 10^6 PS1; 4 x 10^6 MIA PaCa-2 + 8 x 10^6 PS1 or 5 x 10^6 MIA PaCa-2 + 10 x 10^6 PS1. Cells were kept on ice before being transferred to the animal house for injection. PS1 cells in mono-culture were injected into mice as a control to demonstrate that these cells cannot induce tumour formation alone.

2.9.2 *In vivo* injections and tumour monitoring

Female nude mice were purchased from Charles River and maintained within the BSU at Charterhouse Square. Mice were left for at least one week to acclimatise before any procedures were carried out. Cell preparations were injected subcutaneously into each flank of the mice (two tumours per mouse). Each mouse either had two tumours consisting of cancer cells in either monoculture or co-culture with stellate cells. Mice were weighed twice a week and tumour size was measured using callipers three times a week, starting from 7 days post injection. AZD4547 treatment (12.5 mg/kg AZD4547 in a 2.5 % (v/v) solution of Tween-80/PEG300) was given to mice by oral gavage daily, following a five days on, two days off protocol. All procedures were completed according to Home Office guidelines under the project license of Professor Kairbaan Hodivala-Dilke (PF220CE02). No tumours were allowed to breach the limit of 1.44 cm^3. Any animals showing signs of pain, ill health or with a weight loss of 20 % body weight were euthanised.

2.9.3 Tumour harvesting

At the end of each pilot experiment, mice were euthanised by cervical dislocation and any tumours were removed. These were either fixed in formalin for 24 hours, washed in ethanol and paraffin embedded or snap frozen in liquid nitrogen. The pancreata of 3 mice from the co-culture cohort of each experiment were also harvested. Half of each pancreas was formalin fixed and paraffin embedded, whilst the other half was snap frozen. The lungs and kidney of these mice were also snap frozen in liquid nitrogen.

Table 2.3 Antibodies used in the project

Antibody	Species	Incubation conditions	Dilution for IF/IHC	Dilution for WB
α-SMA (F3777, Sigma)	Mouse	1h RT (dark)	1:500	
Vimentin (HPA001762, Sigma)	Rabbit	1h RT	1:100	
Vimentin (M0725, DAKO)	Mouse	O/N 4ºC	1:200	
Desmin (D1033, Sigma)	Mouse	1h RT	1:100	
GFAP (G3893, Sigma)	Mouse	1h RT	1:500	
FGFR1 (ab10646, Abcam)	Rabbit	1h RT	1:100	
HaloTag (G9211, Promega)	Mouse	O/N 4ºC		1:2000
FGFR1 (9740, Cell Signalling)	Rabbit	O/N 4ºC		1:500
Fibronectin (sc-73601, Santa Cruz)	Mouse	O/N 4ºC		1:1000
GAPDH (MAB374, Millipore)	Mouse	O/N 4ºC		1:2000
HSC70 (SC-7298, Santa Cruz)	Mouse	O/N 4ºC		1:1000
PHLDA1 (HPA019000-100UL, Sigma-Aldrich)	Rabbit	O/N 4ºC		1:1000
Ki67 (DAKO M7240)	Mouse	O/N 4ºC	1:100	
Cytokeratin 8/18 (ab194130, Abcam)	Guinea-pig	O/N 4ºC	1:100	
E-Cadherin (ab1416, Abcam)	Mouse	O/N 4ºC	1:100	
Cleaved caspase 3 (D175, Cell Signaling)	Rabbit	1h RT	1:400	
Pan-cytokeratin (Z0662, DAKO)	Rabbit	1h RT	1:200	
Anti-Mouse-HRP (P0447, DAKO)	Goat	1h RT		1:5000
Anti-Rabbit-HRP (P0448, DAKO)	Goat	1h RT		1:5000
Anti-Mouse 488/546 (A11017, A11003, Invitrogen)	Goat	1h RT (dark)	1:500	
Anti-Rabbit 488/546 (A11034, A11035, Invitrogen)	Goat	1h RT (dark)	1:500	
Mouse IgG (X0931, DAKO)	Mouse	1h RT	1:10	
Rabbit IgG (ab172730, Abcam)	Rabbit	1h RT	1:100	

RT = room temperature

Chapter 3 Results I: Targeting FGF signalling in pancreatic stellate cells

3.1 Introduction

FGF signalling is an important developmental pathway that can become activated in cancer to drive tumour progression (Helsten et al., 2016, Turner and Grose, 2010). One of the ways that FGF signalling can drive tumour progression is by nuclear translocation of the FGF receptors or ligands. Nuclear translocation of the FGF2 ligand has been associated with glioma progression (Wang et al., 2015). On the other hand nuclear translocation of the receptor, FGFR1, in either cancer or stromal cells is related to tumour progression and invasion in breast and pancreatic neoplasms (Chioni and Grose, 2012, Coleman et al., 2014b). It has also been shown that nuclear translocation of FGFR1 plays a role in transcriptional regulation of neurons in physiology (Lee et al., 2013, Terranova et al., 2015).

FGF signalling has been linked with PDAC development and progression for some time, though the exact mechanism has remained elusive. For example, increased expression of FGF1 and FGF2 has been correlated with a more advanced PDAC stage in patient tumours (Yamanaka et al., 1993). FGF2 expression was also linked with shorter overall survival and increased hyperplasia (Kuniyasu et al., 2001). In contrast to this, there is evidence that overexpression of FGFR1 in PDAC tumours is correlated with lower grade tumours and therefore better patient prognosis (Haq et al., 2018). The conflicting effects of FGF signalling on PDAC development could be due to different isoform expression. It has been reported that PDAC tumours and cancer cell lines switch to expression of the FGFR1 and 2 IIIc isoforms, promoting autocrine signalling through the MAPK pathway and driving cell proliferation and migration (Ishiwata et al., 2012, Kornmann et al., 2002). This makes FGF signalling an interesting though complex target to explore in PDAC tumours.

We have shown that nuclear FGFR1 can be found in myofibroblast cells at the invasive edge of PDAC tumours (Coleman et al., 2014b). By blocking nuclear FGFR1 signalling in 3D models, the invasion of cancer and stellate cells can be reduced. This indicates that FGF signalling may mediate a critical cross-talk mechanism between different cellular compartments of PDAC tumours. To assess the role of FGF signalling in PDAC progression, I first investigated the importance of nuclear FGFR1 in pancreatic stellate cells and possible therapeutic strategies to target receptor translocation.

3.2 FGF expression in PDAC cancer cell lines

To investigate the effect of disrupting FGF signalling cross-talk, I needed to assess the importance of this pathway in PDAC. The pancreatic expression database (PED) (Marzec et al., 2018) is a repository of published data relating to pancreatic cancer. One of the key features of this database is that it allows interrogation of gene expression in PDAC cell lines. I searched the database for the relative expression of all the FGF receptors and some relevant FGF ligands (Table 3.1, Figure 3.1 and 3.2).

The data from all the cancer cell lines included in the PED analysis showed a variable expression of the FGFs and FGFRs, with no clear link between expression and site of cell line isolation, for example from a primary tumour or a metastatic site. FGFR1 was the receptor with maximal expression in the highest number of PDAC cell lines. These data support the concept that expression of FGF signalling components may not be enough to explain the complex role this pathway plays in PDAC development and progression. Additionally PED does not provide information on the specific receptor isoforms expressed, which could be critical for the effect of FGF signalling

within these cells. I used a range of PDAC cell lines in this project, isolated from either primary tumours or metastatic sites, with variable expression of FGFs and FGFRs.

Table 3.1 FGF/FGFR expression in PDAC cell lines

Cell Line	Source	FGFR1	FGF2
MIA PaCa-2	Primary	↓	↑↑
PANC-1	Primary	↑	↑
AsPC-1	Ascites	↑	↑↑
COLO 357	Metastasis (lymph node)	↓	↑↑

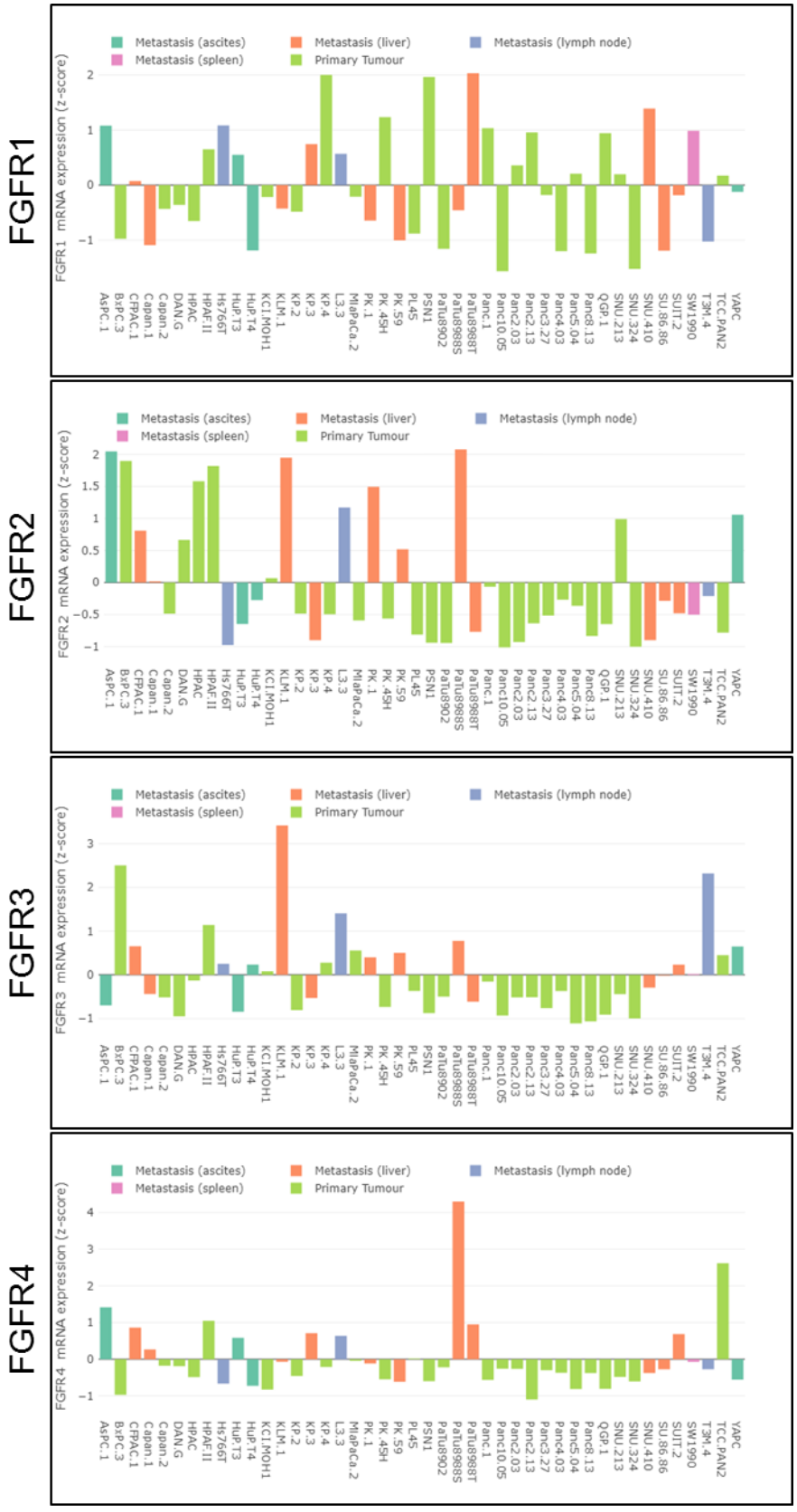

Figure 3.1 FGFR expression in PDAC cell lines

The relative expression of FGFR1-4 in a range of PDAC cell lines is shown compared to the average, taken from PED. The colour of the bars relates to the site that the cell line was generated from, either a primary or metastatic (ascites, spleen, liver or lymph node) tumour. There is variable expression of all four FGFRs across the cell lines.

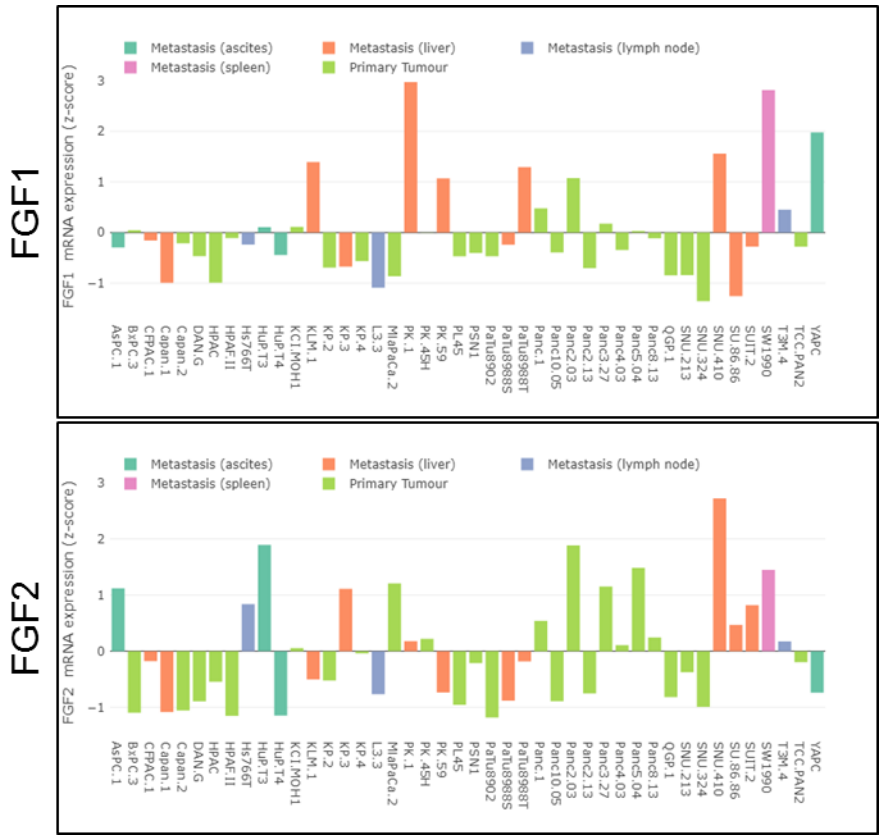

Figure 3.2 FGF expression in PDAC cell lines

The relative expression of FGF1 and FGF2 in a range of PDAC cell lines is shown compared to the average, taken from PED. The colour of the bars relates to the site that the cell line was generated from, either a primary or metastatic (ascites, spleen, liver or lymph node) tumour. There is variable expression of both FGFs across the cell lines.

3.3 Stellate cell line characterisation

3.3.1 Immunostaining

The PS1 stellate cell line was used in this project. These cells were isolated from a healthy donated pancreas and immortalised by expression of ectopic hTERT (Li et al., 2009). To confirm that these cells retained their phenotype in culture, immunofluorescence for stellate cell markers was carried out. PS1 cells were confirmed to stain positive for four different stellate cell markers (Apte et al., 1998): GFAP, α-SMA vimentin and desmin (Figure 3.3).

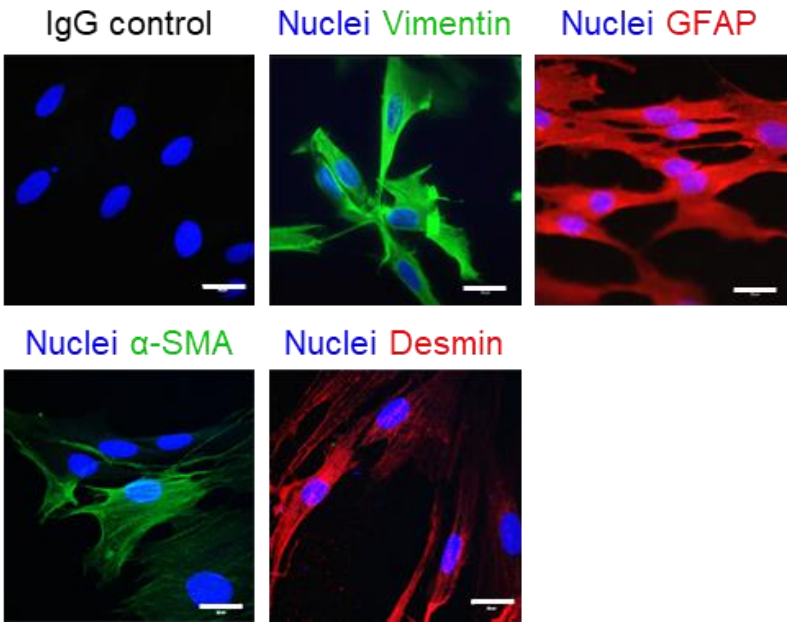

Figure 3.3 Immunocytochemistry staining for PS1 characterisation

PS1 cells grown on coverslips were fixed and stained for four different stellate cell markers: vimentin, GFAP, α-SMA and desmin (Section 2.3.1). The images are representative of three biological replicates and show positive staining for all the markers, with an unstained negative control. Scale bar = 20 µm.

3.3.2 Oil Red O

A feature of stellate cells is that upon treatment with vitamin A, the cells will become quiescent, stop proliferating and store the vitamin in lipid droplets within the cell. PS1 cells were treated daily with either ATRA or ethanol vehicle control. After fixing, Oil Red O staining was carried out to identify the induction of storage of vitamin A in lipid droplets following treatment with ATRA (Bachem et al., 1998, Froeling et al., 2011). Nuclei were counterstained with haematoxylin (Figure 3.4).

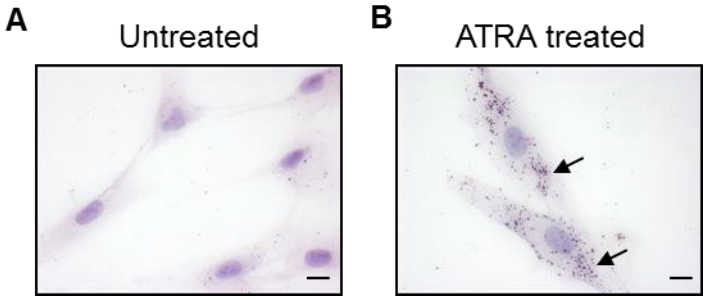

Figure 3.4 Oil Red O staining of lipid droplets in PS1 cells

*PS1 cells grown on coverslips and treated daily with either ethanol vehicle control (**A**) or ATRA (**B**). The cells were fixed and stained for lipid droplets using Oil Red O (Section 2.3.2). The ATRA treated cells showed a greater number of lipid droplets than the untreated controls (shown by the arrows). These slides were counter stained with haematoxylin and are representative of three biological replicates. Scale bar = 10 µm.*

3.4 Drug response assays

To assess the effect of interrupting FGF signalling cross-talk in PDAC, I used FGFR tyrosine kinase inhibitors. Several ATP-mimetic FGFR inhibitors are available and previous work in the laboratory had been carried out using PD173074 (Coleman et al., 2014b). PD173074 can only be used as a laboratory tool compound due to its toxicity. Therefore I decided to use an ATP-mimetic FGFR inhibitor that is currently in clinical trials: AZD4547 (Gavine et al., 2012) (Figure 3.5). AZD4547 is active against FGFR1-4 and VEGFR2 (Table 6.2).

3.4.1 AZD4547

Initial phase 1 trials of AZD4547 were carried out in advanced solid malignancies to determine tolerability and safety (NCT01213160, NCT00979134). Following this a number of phase 2/3 trials were initiated to target tumours with FGFR mutations, gene amplifications and fusions. Specifically, AZD4547 has been used in clinical trials to target recurrent gliomas expressing *FGFR-TACC* gene fusion (NCT02824133) and FGFR1/2 amplified gastric, oesophageal, breast or squamous lung cancers (NCT01795768, NCT02965378). It has also been tested in combination with docetaxel in NSCLC (NCT01824901). In oestrogen receptor positive breast cancer, AZD4547 has been trialled in combination with anastrozole/letrozole in patients that have progressed (RADICAL, NCT01791985) and in combination with fulvestrant in patients with *FGFR1* polysomy or gene amplification (GLOW, NCT01202591). In gastric and gastro-oesophageal cancer, AZD4547 treatment has been compared with paclitaxel in patients with *FGFR2* polysomy or gene amplification (SHINE, NCT01457846). This drug has now been included in many trials with multiple targeted therapies using a biomarker driven approach to recruit patients to relevant treatment arms. For example, the BISCAY (NCT02546661) phase 1b trial in patients with

muscle invasive bladder cancer, the Lung-MAP second line therapy trial in patients with recurrent stage IV squamous cell lung cancer (NCT02154490), the MATCH (NCT02465060) screening trial in patients with advanced refractory solid tumours, lymphomas or multiple myeloma and the national lung matrix trial in patients with NSCLC (NCT02664935). There are also two trials using genetic analysis as a decision tool in patients with metastatic disease to decide on treatment with relevant therapies including AZD4547, SAFIR02_Breast (NCT02299999) and SAFIR02_Lung (NCT02117167).

Following all these clinical trials using AZD4547 to target FGFR driven tumours in patients, we decided to use this inhibitor to target cross-talk in PDAC tumours.

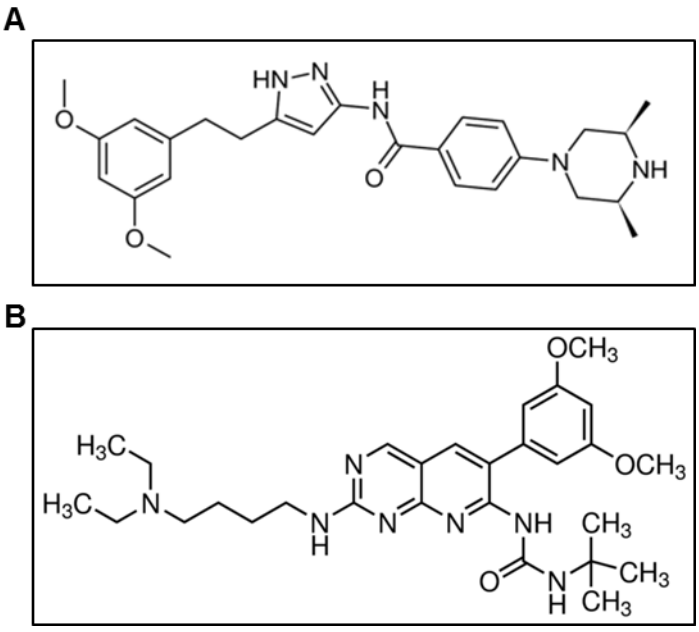

Figure 3.5 Structure of FGFR inhibitors

*Structure of the FGFR inhibitors AZD4547 (**A**) and PD173074 (**B**) (Gavine et al., 2012, Mohammadi et al., 1998).*

3.4.2 Cell viability

Cell viability was determined using standard MTS assays. The growth inhibition to 50 % viability (GI_{50}) of the FGFR inhibitor AZD4547, for PS1, AsPC-1, MIA PaCa-2, COLO 357 and PANC-1 cell lines in 2D culture was calculated (Figure 3.6).

Non-linear regression shows that all cell lines were insensitive to FGFR inhibition in 2D culture. The lowest GI_{50} value was 6 µM (MIA PaCa-2). Therefore, selecting a dose below 6 µM for future experiments would ensure that cell viability is not impacted by treatment. In future experiments a dose of 1 µM AZD4547 was used, which has been previously established in endometrial cancer models in the laboratory (Fearon et al., 2018). This was a suitable concentration as it was above the active dose but below the toxic dose.

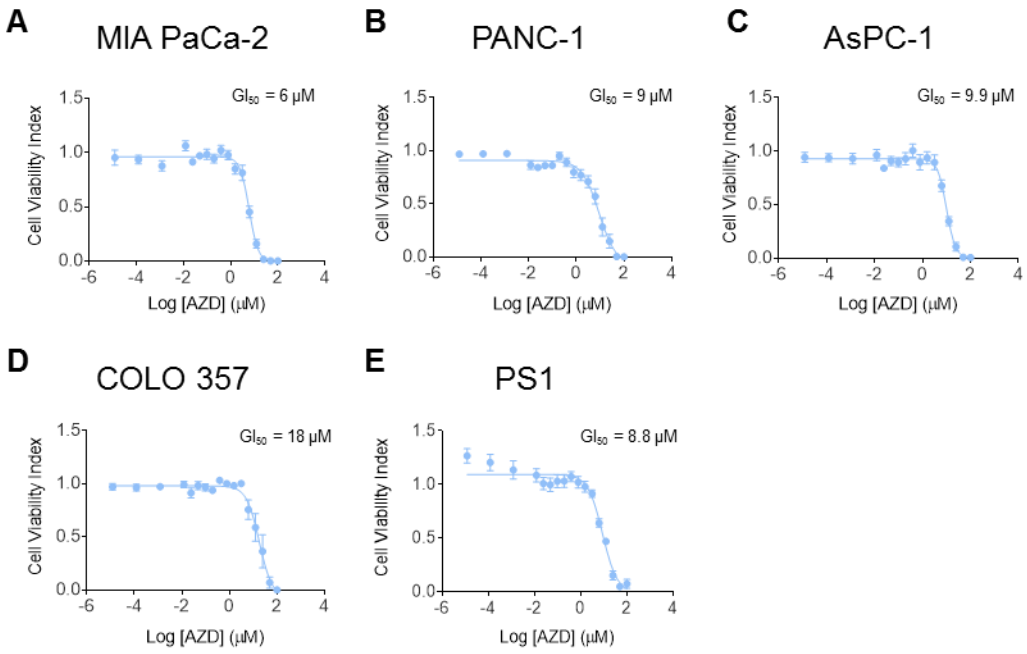

Figure 3.6 MTS assay dose response following AZD4547 treatment

*MTS cell viability assays were used to calculate a Cell Viability Index (absorbance in each well adjusted for background and normalised to control wells, Section 2.2.1). Linear regression was then used to determine a GI_{50} value of 6 µM (**A**), 9 µM (**B**), 9.9 µM (**C**), 18 µM (**D**) and 8.8 µM (**E**) for AZD4547 with the MIA PaCa-2, PANC-1, AsPC-1, COLO 357 and PS1 cell lines respectively. These values provide a starting value to use for drug treatment moving into co-culture and 3D models. The concentration of AZD4547 used should be below the GI_{50} value for all cell lines to ensure cell viability is not affected. The data points on the graph represent the mean cell viability from three technical repeats for each plate, with at least three biological replicates plotted for each cell line.*

3.4.3 Mono- and co-culture proliferation

CellTracker dyes were used to analyse PS1 and AsPC-1 proliferation in response to increasing concentrations of AZD4547 in mono- and co-culture conditions (Figure 3.7). There was no difference between the response of either cell line to drug in mono or co-culture at 1 µM in 2D cultures (Two-way ANOVA analysis).

1 µM AZD4547 will not decrease cell proliferation and, therefore, should be effective at selectively studying cross-talk between the cells.

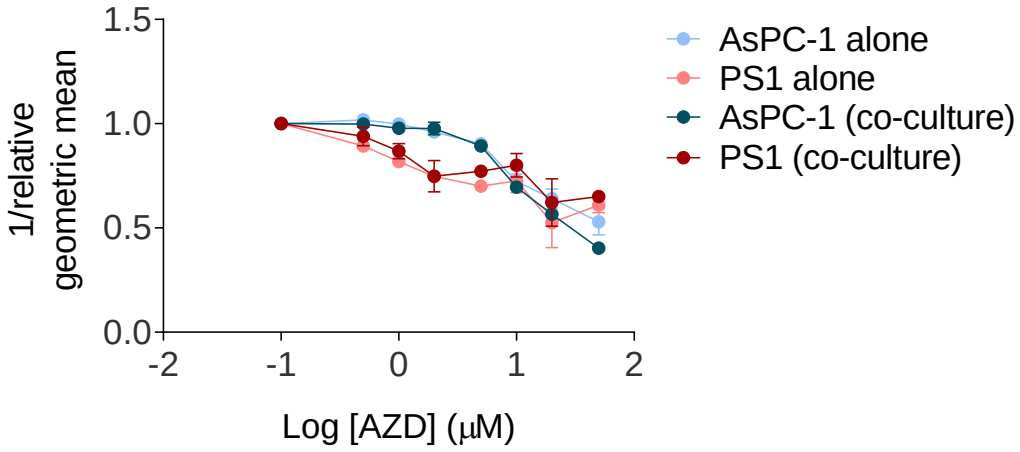

Figure 3.7. Flow Cytometry analysis of AZD4547 dose response

Flow Cytometry analysis assays showed that as the drug concentration increased, the proliferation of the cells decreased (measured by an increasing geometric mean indicating greater fluorescence intensity per cell and therefore less cell division, Section 2.2.2). The graph shows the change in cell proliferation of both cell lines in mono- or co-culture to AZD4547 treatment. The average geometric mean value from three biological replicates was calculated (relative geometric mean) and 1/relative geometric mean has been plotted with standard error of the mean (SEM). Two-way ANOVA analysis was carried out to analyse the data. There was no significant difference in response to AZD4547 treatment of each cell line in mono- or co-culture.

3.5 Nuclear FGFR1

3.5.1 Localisation of FGFR1 in stellate cells

Previous studies in our laboratory have demonstrated that FGFR1 can translocate to the nucleus in pancreatic stellate cells. I stained PS1 stellate cells, alongside primary cancer-associated stellate cells (M1090T and M1245, Section 2.1.1), for FGFR1 localisation following culture on coverslips (Figure 3.8). The primary cells have previously been confirmed to be stellate cells by expression of PSC markers and reversion to quiescence upon ATRA treatment (Neuzillet et al., 2019). The FGFR1 staining showed heterogeneity between different cells within each population, highlighting a sub-population of cells expressing nuclear FGFR1 speckles.

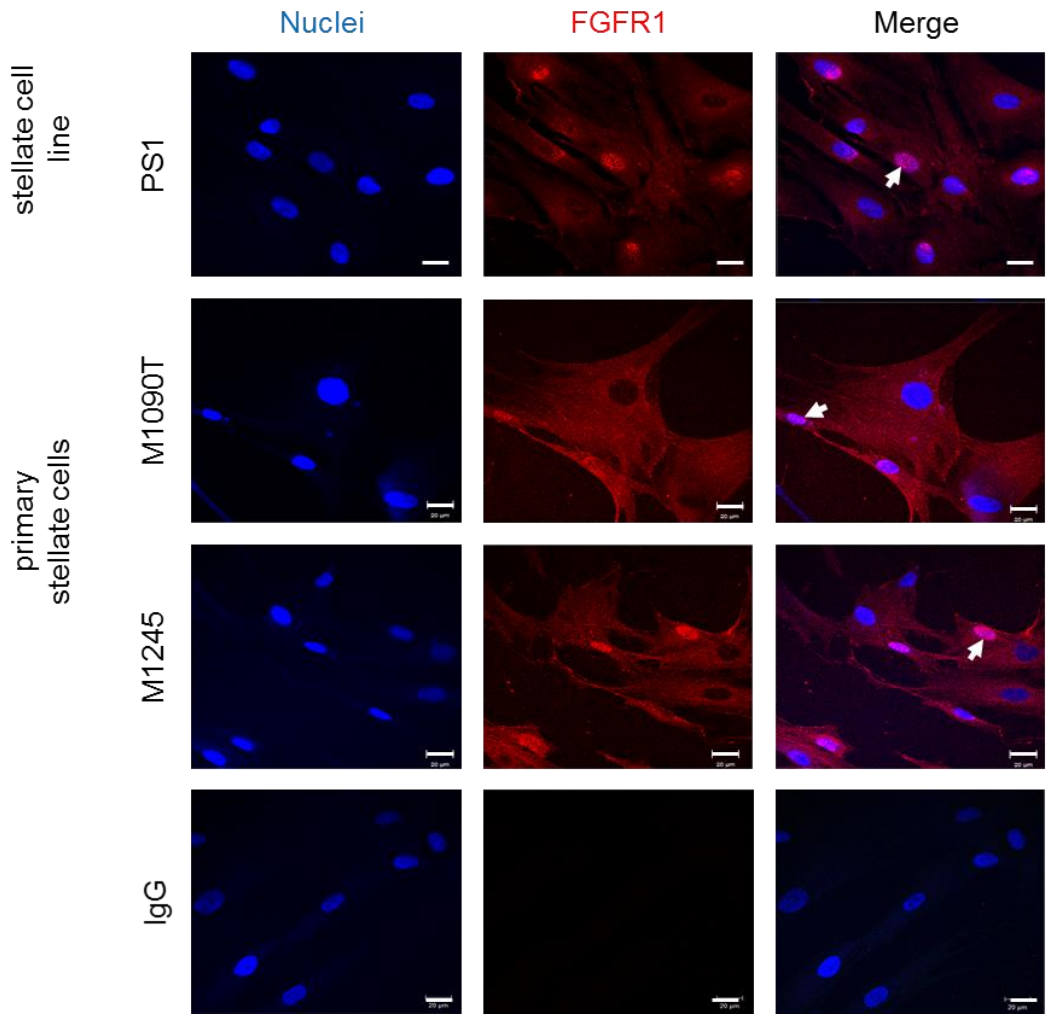

Figure 3.8 Nuclear FGFR1 speckles in pancreatic stellate cells

The PS1 stellate cell line and primary cancer associated stellate cells (M1090T and M1245) were cultured on coverslips, fixed and stained for FGFR1 (ab10646, Abcam, performed according to Section 2.3.1). PS1, M1090T and M1245 all showed a sub-population of cells with nuclear FGFR1 speckles (highlighted by the arrows). These images are representative of three technical repeats. Scale bar = 20 µm.

3.5.2 Nuclear localisation following FGFR inhibition

The IN Cell 2200 high-throughput microscope was used to analyse the effect of FGFR inhibition with AZD4547 on FGFR1 nuclear localisation. One-way ANOVA analysis was performed on the levels of nuclear foci with increasing AZD4547 concentration (Figure 3.9).

AZD4547 treatment, up to 1 µM at least, in 2D monoculture did not reduce the levels of nuclear FGFR1 in PS1 cells. This is in contrast to previous work showing a decrease in nuclear FGFR1 following treatment with 2 µM of FGFR inhibitor PD173074 for 48 hours (Coleman et al., 2014b). This difference could be due to experimental conditions, such as drug concentration and length of treatment. Moreover, FGFR signalling cross-talk interruption with AZD4547 should ideally be tested with both cell types (PSCs and cancer cells) in co-culture. It was difficult to test the effect of cross-talk within this assay as the two cell types (PSCs and cancer cells) could not be reliably distinguished following staining, preventing the automated quantification using the IN Cell Investigator Software from being performed on the PSC compartment only.

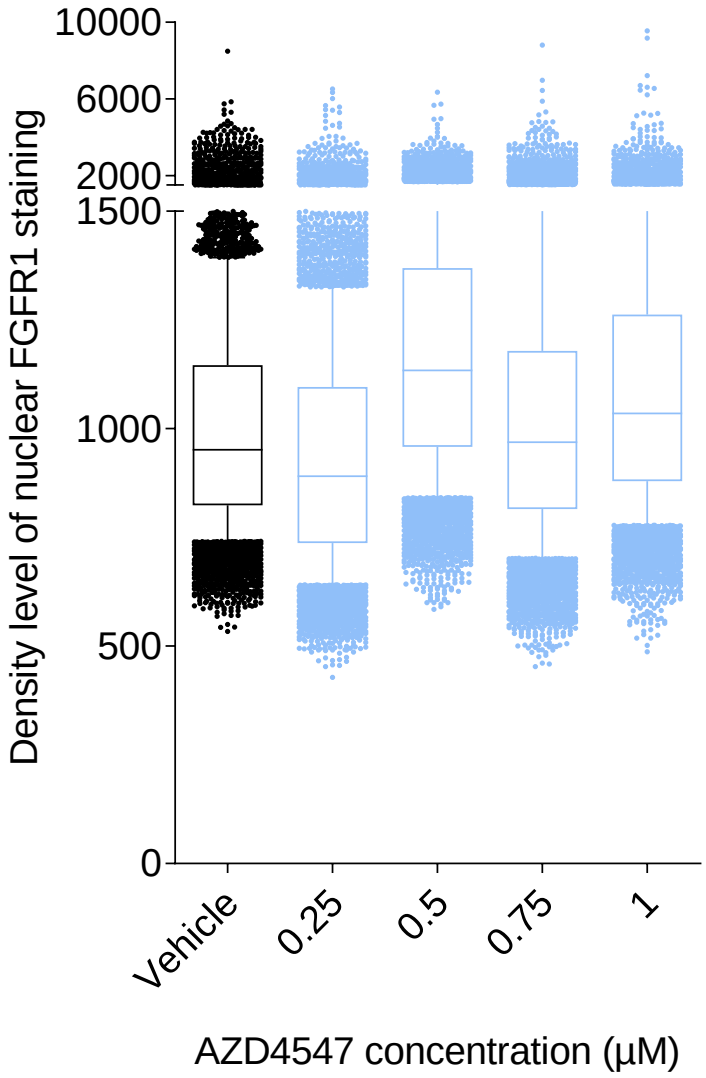

Figure 3.9 Nuclear FGFR1 following AZD4547 treatment

PS1 cells seeded in a 96-well plate and treated with increasing concentrations of AZD4547 for 24 hours were fixed, stained for FGFR1 and analysed using the IN Cell 2200 high-throughput microscope (Section 2.3.5). The nuclear density of FGFR1 staining in PS1 cells did not decrease following treatment with increasing doses of the FGFR inhibitor AZD4547 in medium containing 10 % (v/v) FBS. This suggests that AZD4547 treatment does not decrease levels of nuclear FGFR1 in 24 hours in stellate cells grown on plastic in 2D mono-culture conditions. One-way ANOVA analysis was used to compare the FGFR1 nuclear foci intensity. This data is from three biological replicates.

3.6 Discussion

PDAC cell lines with a range of FGF and FGFR expression were used to investigate the role of FGF mediated cross-talk in pancreatic cancer. The PS1 stellate cell line was characterised and confirmed to have nuclear FGFR1, making it a suitable cell line to use in this study. Cancer-associated primary stellate cells also had nuclear FGFR1 staining, demonstrating that PS1 cell line is representative of stellate cells in PDAC patients. The 2D drug assays showed that only high concentrations of AZD4547 are toxic to PDAC cancer cell lines and the PS1 cell line. This finding showed that it was appropriate to use a concentration of 1 μM AZD4547 for FGFR1 mediated cross-talk inhibition without affecting cell viability (Fearon et al., 2018).

Treating cells in co-culture with 1 μM AZD4547 did not appear to affect proliferation of either cell type, which may be because FGF signalling cross-talk plays a role in invasion rather than proliferation in PDAC (Coleman et al., 2014b). Moreover, treatment of stellate cells in 2D with increasing concentrations of AZD4547 did not reduce the levels of nuclear FGFR1, in contrast to previously published data using another FGFR inhibitor, PD173074 (Coleman et al., 2014b). This could be due either to experimental differences or to the primary role of nuclear FGFR1 in mediating cross-talk led invasion in PSCs. Therefore the most appropriate assays to test the effect of AZD4547 treatment would be 3D co-culture PDAC models (Coetzee et al., 2019).

Chapter 4 Results II: Interrupting FGF-mediated cross-talk in PDAC

4.1 Introduction

It is widely accepted that, whilst necessary, traditional 2D cell culture is not representative of human tumours (Kapałczyńska et al., 2018). This may be part of the reason that many promising therapies in the laboratory end up failing in patients. The use of 3D *in vitro* models in cancer research is increasing as these provide an alternative to 2D cell culture or expensive *in vivo* models (Bardeesy and DePinho, 2002, Pérez–Mancera et al., 2012).

4.1.1 Epithelial Organoids

Many different PDAC 3D models have now been developed, allowing the complex cellular and ECM interactions to be studied (Baker et al., 2016, Coetzee et al., 2019, Moreira et al., 2018). Organoids can be grown from patient-derived tumour resections or biopsy tissue (Figure 4.1). One method implants patient tumour cells into matrigel domes, supplemented with a wide range of growth factors to mimic the signals from the desmoplastic stroma (Boj et al., 2015). This technique has successfully recapitulated PDAC-like structures in the laboratory and organoids can be frozen and thawed, making it a useful research tool. Another method uses patient-derived PDAC tissue to grow organoids on top of a matrigel layer. The cultures still require many additional growth factors to support the survival of the cancer cells (Huang et al., 2015). Pancreatic organoids have also been grown on top of a collagen gel, in an air-liquid interface model, from minced pancreatic tumour tissue (Li et al., 2014, Ootani et al., 2009). Organoids offer the potential to screen different targeted therapies for patients to allow for more effective and personalised treatment. This could be very useful in the clinic, however only in the patients who survive long enough to allow the cultures to be established and therapies to be screened. Furthermore, the need for primary patient tissue to establish organoids for research is a limiting factor. Only 10-

15 % of PDAC patients are eligible for surgery at the point of diagnosis (Ryan et al., 2014) and therefore it can be difficult to routinely obtain patient-derived tissue. Another method of culturing primary epithelial-based organoids is by inducing differentiation of pluripotent stem cells into pancreatic exocrine or endocrine cells in culture (Greggio et al., 2013, Huang et al., 2015, Scavuzzo et al., 2017, Sugiyama et al., 2013). These cultures can recapitulate pancreatic structures and are useful in investigating the development and progression of PDAC. Whilst useful, the scarce availability of patient tissue and absence of fibroblasts and PSCs make organoids impractical and non-informative for studying stroma-cancer cross-talk.

4.1.2 Co-culture

Other types of organoids use co-culture of cancer cells with stromal cells to reduce the number of growth factors needed in the culture media, reducing the complexity and the cost. A simple method is to include fibroblasts in the cultures alongside cancer cells, the fibroblasts can then provide many of the growth factors needed for cancer cell survival (Walsh et al., 2016). Furthermore, multi-cellular organoids have been developed by using tissue fragments from tumour resection, ascites or rapid autopsy and implanting them in matrigel domes. This makes a more complex tumour model and can allow the interactions between the cancer cells and the tumour microenvironment to be studied (Tsai et al., 2018).

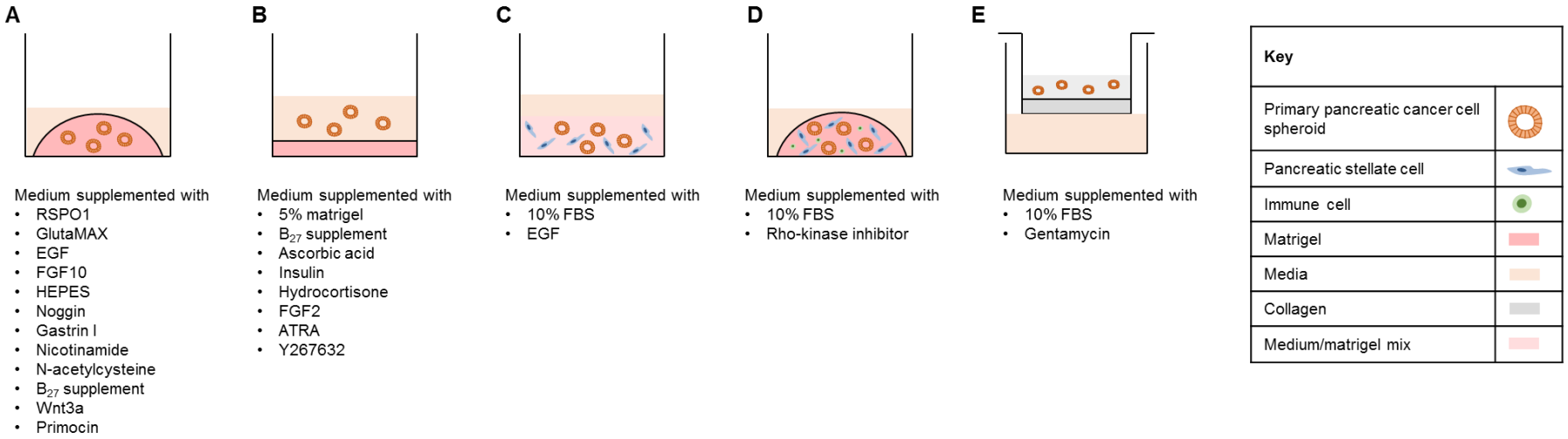

Figure 4.1 Pancreatic cancer organoid methods

*Pancreatic tumours from a human or murine pancreas are broken down into their cellular components. The cancer cells can then be embedded into a pure matrigel dome (**A**) with growth factors added to the medium on top to stimulate cell growth. Another method is to culture these primary cells in medium on top of a matrigel layer (**B**). The medium must also be supplemented with many growth factors to stimulate cellular survival and growth. Alternatively cancer cell spheroids can be co-cultured with stromal cells in a gel made up of 50% matrigel and 50% medium, drugs can be added to medium on top of the gel (**C**). To make the organoid model more complex, immune cells can be added to stellate cells and cancer cell spheroids in a matrigel dome. Medium can be added to the top of this dome but fewer growth factors are needed due to the presence of stromal cells in the gels (**D**). Another method to culture cancer spheroids is to place them into collagen in a Transwell insert. This gel can then be fed with medium from below to create an air-liquid interface (**E**) (Coetzee et al., 2019).*

4.1.3 Other 3D cultures

Other 3D PDAC models have been developed. For example, microfluidics can be used to grow PDAC cells on a collagen coated HepaChip® chamber. These cultures are quick to establish and can be adjusted to reflect the perfusion rates of tumours, which could make them useful for screening personalised therapies for patients (Beer et al., 2017b). Furthermore, different concentrations of Oligomer (type 1 collagen) can be used, along with matrigel, to create ECM gels with varying levels of stiffness to effectively model PDAC tumours in the laboratory (Puls et al., 2017). In order to faithfully reproduce all of the cellular interactions within PDAC tumours, tumour slice models have been developed. In this model, slices of fresh PDAC resections are placed onto collagen coated membranes, which are then supplemented with medium containing FBS, glutaMAX, $NaHCO_3$, HEPES, L-cysteine and antibiotics. The tumour slices can be maintained for up to 6 days in culture (Jiang et al., 2017, Vaira et al., 2010).

All of these models vary in complexity and could offer invaluable tools for both studying PDAC development and screening potential therapies. However, they can be costly and time consuming to establish. Hence, for this project, I used two distinct 3D methods (mini-organotypics and spheroids) to study the effect of FGF signalling cross-talk between cancer cells and stellate cells in PDAC. These were useful models to easily investigate the effect of targeting FGF cross-talk on PDAC invasion, however none of these experiments were performed under hypoxic conditions and still lack the full complexity of the desmoplastic stroma. This may be an important factor to consider in future when translating these results into PDAC tumours.

4.2 FGFR inhibition

4.2.1 FGFR inhibitors in mini-organotypics

To assess the role of FGF signalling cross-talk, 3D mini-organotypic co-cultures were treated with FGFR inhibitors and the effect on invasion was analysed. The mini-organotypic model is a well-established 3D model in our laboratory, adapted from large organotypic models (Coleman et al., 2014c). Briefly, organotypic gels made up of a collagen/matrigel mix are placed into a 24 well plate (for large cultures) or Transwell inserts (for mini-cultures) and left to polymerise. Cells are then seeded in co-culture on top of the gel in a 2:1 PSC to PDAC cell ratio (Kadaba et al., 2013). The mini-organotypic model can then be fed with medium from below (day 0) to create an air-liquid interface model. After 24 hours the large cultures are raised on top of pre-coated nylon membrane placed onto a metal grid. These can then be fed with medium from below to create an air-liquid interface (day 0). Relevant drugs can be added to the cultures through the medium. Following incubation for 7 days in mini-organotypics or up to 24 days in large organotypics, invasion can be studied or cultures can be stained for relevant markers (Figure 4.2 and Section 2.7.1). Mini-organotypics are quick and use fewer cells, and therefore, are useful for primary cell culture, whereas large organotypics can be maintained for longer, allowing treatment effects on more established cultures to be analysed.

Three PDAC cancer cell lines (MIA PaCa-2, COLO 357 and PANC-1) were cultured in mini-organotypics either alone or with PS1 stellate cells and treated with two FGFR inhibitors, PD173074 and AZD4547, or vehicle control. These three PDAC cell lines had a varying expression of FGFR1 and FGF2 (Table 3.1 and Figures 3.1 and 3.2). MIA PaCa-2 and PANC-1 cells were both isolated from primary PDAC tumours, whereas COLO 357 cells were isolated from a lymph node metastasis (Appendix 1).

MIA PaCa-2 cells were isolated from a 65-year-old male with a tumour in the body and tail of the pancreas. This tumour did not express CEA and contained *KRAS*, *TP53*, *INK4A* mutations (Yunis et al., 1977). PANC-1 cells were isolated from a 56-year-old male with a tumour in the head of the pancreas and a metastasis in the peripancreatic lymph node. The tumour did not express CEA and also contained *KRAS*, *TP53*, *INK4A* mutations (Lieber et al., 1975). COLO 357 cells were isolated from a lymph node metastasis in a 77-year-old female. The tumour expressed CEA and contained *KRAS*, *SMAD4* mutations (Morgan et al., 1980). All three cell lines were classified as the quasi-mesenchymal sub-type (Section 1.2.8) (Collisson et al., 2011). FGFR inhibition had no effect on PDAC cell mini-organotypic mono-cultures (Figure 4.3), but caused a significant decrease in the number of cells invading into the gels after 7 days of mini-organotypic co-culture (Figure 4.4). This is consistent with previous independent work showing that treatment with PD173074 can reduce invasion in large organotypic cultures (Coleman et al., 2014b).

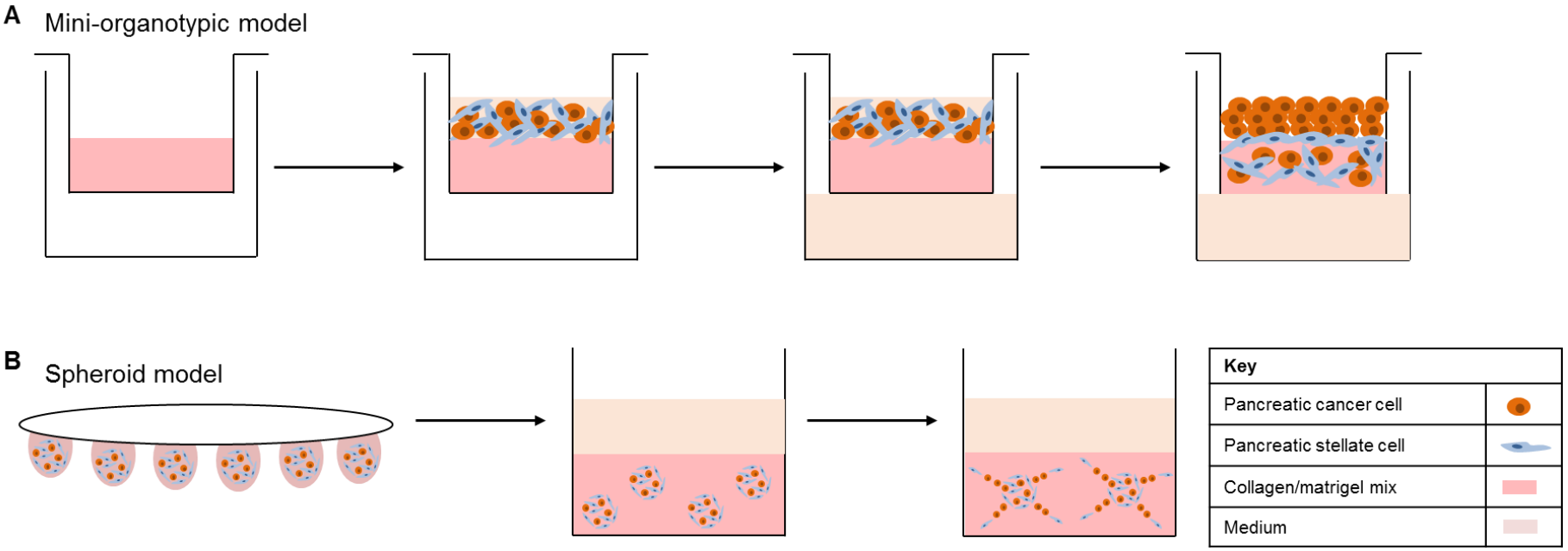

Figure 4.2 Pancreatic cancer 3D *in vitro* models

***A**. Mini-organotypic model - a mix of collagen and matrigel is set to form the organotypic gel within a Transwell insert. Cells can then be seeded in co-culture on top of the gel and fed with medium from below, creating an air-liquid interface. At the end of the experiment, the gels can be harvested and analysed (Coetzee et al., 2019). **B.** Spheroid model - cancer and stellate cells are seeded in a 1:2 ratio in a methylcellulose hanging drop for 24 hours, allowing them to form spheres. These are then embedded in organotypic gels and fed with medium from above. This allows multi-directional invasion, which can be observed over time of incubation.*

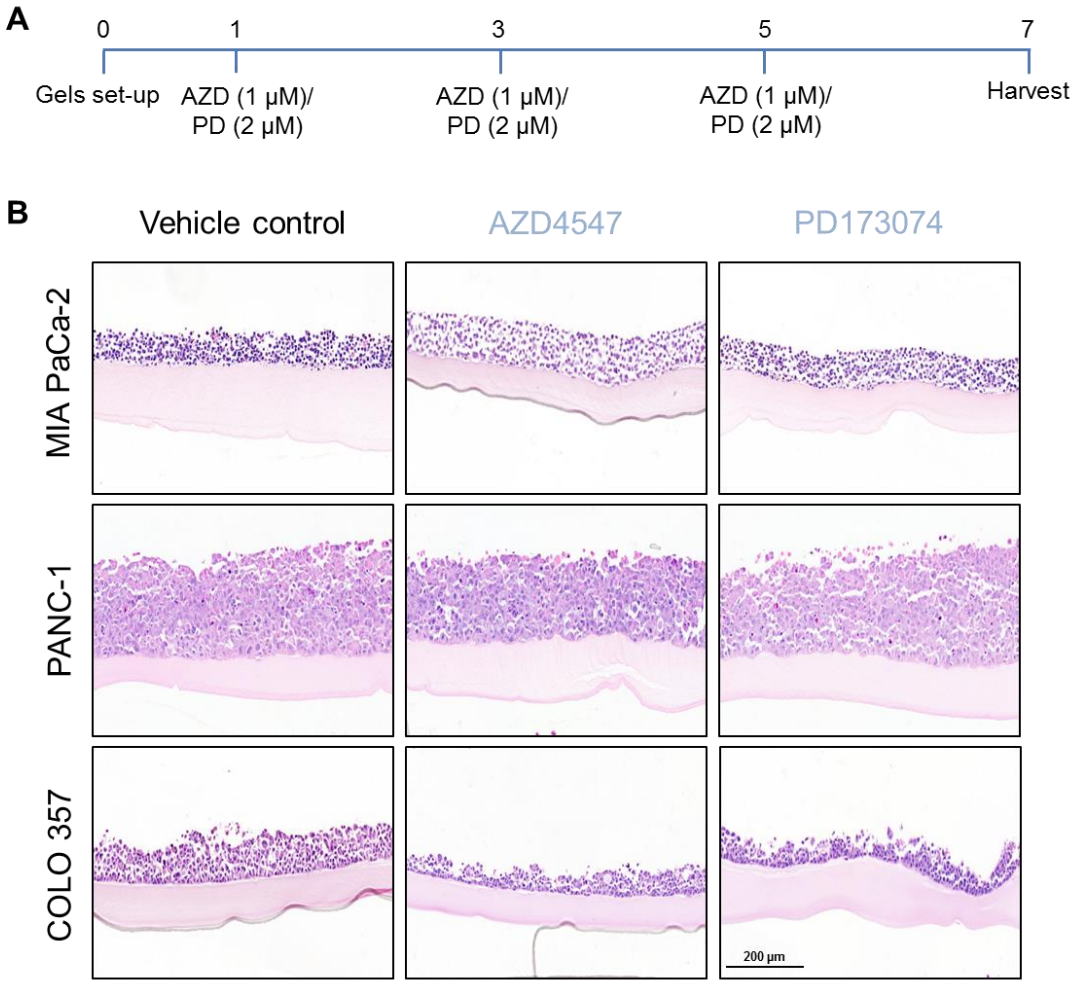

Figure 4.3 FGFR inhibition has no effect 3D PDAC mini-organotypic models

A. *Three PDAC cell lines (MIA PaCa-2, PANC-1 and COLO 357) were grown for 7 days in mini-organotypic models. Treatment with FGFR inhibitors AZD4547 (AZD, 1 μM) or PD173074 (PD, 2 μM) or vehicle control was given every other day (Section 2.6.1).* ***B.*** *No change in invasion or cell survival were observed when the cultures were treated with AZD or PD. These images are representative of at least three biological replicates. Scale bar = 200 μm.*

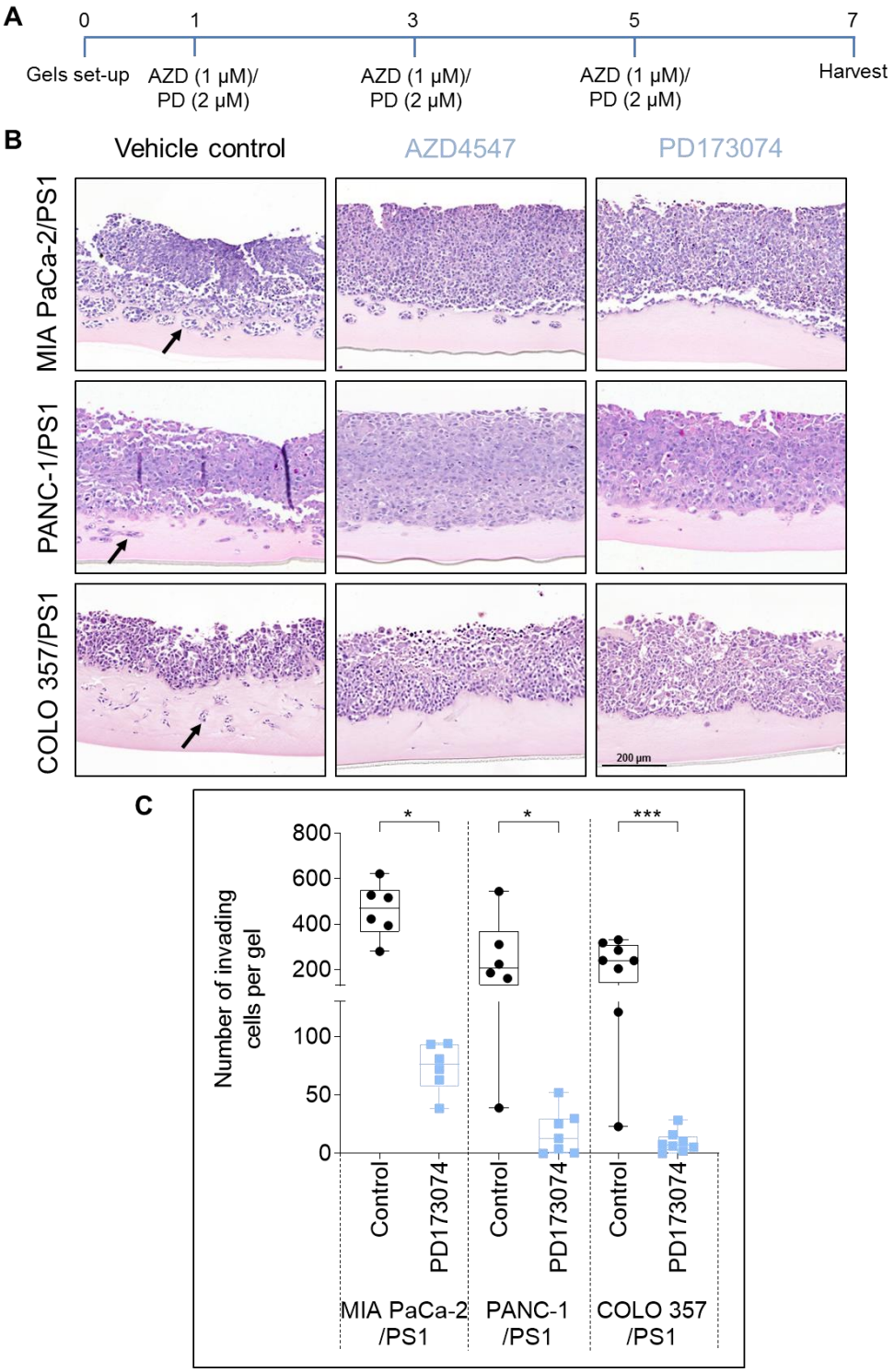

Figure 4.4 FGFR inhibition reduces invasion in 3D co-culture mini-organotypic models

A. *Three PDAC cell lines (MIA PaCa-2, PANC-1 and COLO 357) were grown for 7 days in mini-organotypic models in co-culture with PSCs (PS1). Treatment with FGFR inhibitors AZD4547 (AZD, 1 μM) or PD173074 (PD, 2 μM) or vehicle control was given every other day (Section 2.6.1).* ***B.*** *Under vehicle conditions, cellular invasion into the gels can be seen (shown by the arrows). However, when the cultures were treated with AZD or PD, the invasion was significantly reduced. Scale bar = 200 μm.* ***C.*** *Quantification of the number of invading cells in each gel (points), the median (middle line) and inter-quartile range (box) for each condition is shown in the graph. This was analysed by Kruskal-Wallis test with Dunn's multiple comparison of at least three biological replicates *p<0.05, **p<0.01, ***p<0.001.*

4.2.2 FGFR inhibitors in a spheroid model

Another approach developed within our laboratory is a hanging drop spheroid model (Figure 4.2 and Section 2.7.2). This model allows multi-directional invasion to be studied, as well as reducing the number of cells needed for each condition (as required for patient-derived primary cells). Briefly, cells are seeded in methylcellulose hanging drops and incubated for 24 hours to allow spheres to form. The cells are seeded in the same 2:1 ratio of PSCs to cancer cells as used in the organotypic cultures (Kadaba et al., 2013). The spheres are then harvested from the hanging drops and placed into organotypic gels for 2-5 days with an average of six spheres per gel. Treatments are added in medium placed on top of the gels. Gels can be imaged during incubation to monitor invasion, as well as being fixed and stained for specific markers.

Treatment of co-cultures with the FGFR inhibitor AZD4547 significantly decreased invasion, replicating results from the mini-organotypic model (Figure 4.5). In the spheroid model, cells transduced with a fluorescent nuclear H2B construct were used (stellate cells with H2B-GFP and cancer cells with H2B-RFP). Reconstructed Z-stack images of these spheres demonstrate that there is often a leading stellate cell at the tip of each invasive protrusion, highlighting these cells as potential drivers of invasion in PDAC (Figure 4.6).

All the work in this model has been carried out in collaboration with Dr Ed Carter, a post-doctoral researcher in our group, to independently confirm the role of FGF-mediated invasion.

The invasion of each PDAC cell line in 3D co-culture models may be different (Figure 4.6). Cancer cells can invade either in cohorts or single cells. Studies have shown the PANC-1 cells often invade as single cells, rather than as cohorts, which could explain the phenotype seen in the spheroid cultures (Stahle et al., 2003). Both MIA PaCa-2 and PANC-1 cells are classified as invasive cell lines, however there have been conflicting reports as to which line is more invasive (Duxbury et al., 2004, Ellenrieder et al., 2001, Takada et al., 2002). COLO 357 cells are regarded as poorly invasive cancer cells (Huang et al., 2012).

Each PDAC cell line appears to display a different invasive phenotype when placed in co-culture with PS1 cells in 3D *in vitro* models. In the spheroid cultures, both MIA PaCa-2 and PANC-1 cells follow PSCs out of the central sphere, whereas COLO 357 cells mostly remain tightly packed within the central sphere (Figure 4.6). Additionally, in the mini-organotypic model, the more invasive MIA PaCa-2 and PANC-1 cells seem to have more collective invasion into the gels in the H&E sections (Figure 4.4), whereas the COLO 357 cells appear to invade as smaller cohorts or single cells. The difference in invasive phenotype could be due to both MIA PaCa-2 and PANC-1 cells being poorly differentiated and expressing mesenchymal markers, such as vimentin, whereas COLO 357 cells are well differentiated and express many epithelial markers, such as E-cadherin and β-catenin (Deer et al., 2010, Huang et al., 2012). However, the total number of invading cells or the invasive area in each model is not decreased in COLO 357 cultures, compared to the other two PDAC cell lines (Figure 4.4C and Figure 4.5C). To fully investigate any differences in invasion of the PDAC cell lines in both models, it will be important to quantify invasion of each cell type alone. This can be done from imaging of the labelled cells in the spheroid model (as in Figure 4.6) using light sheet microscopy and high-throughput quantification of each cell type in the invasive zone from Z stack images (Veelken et al., 2017, Lu et al., 2019).

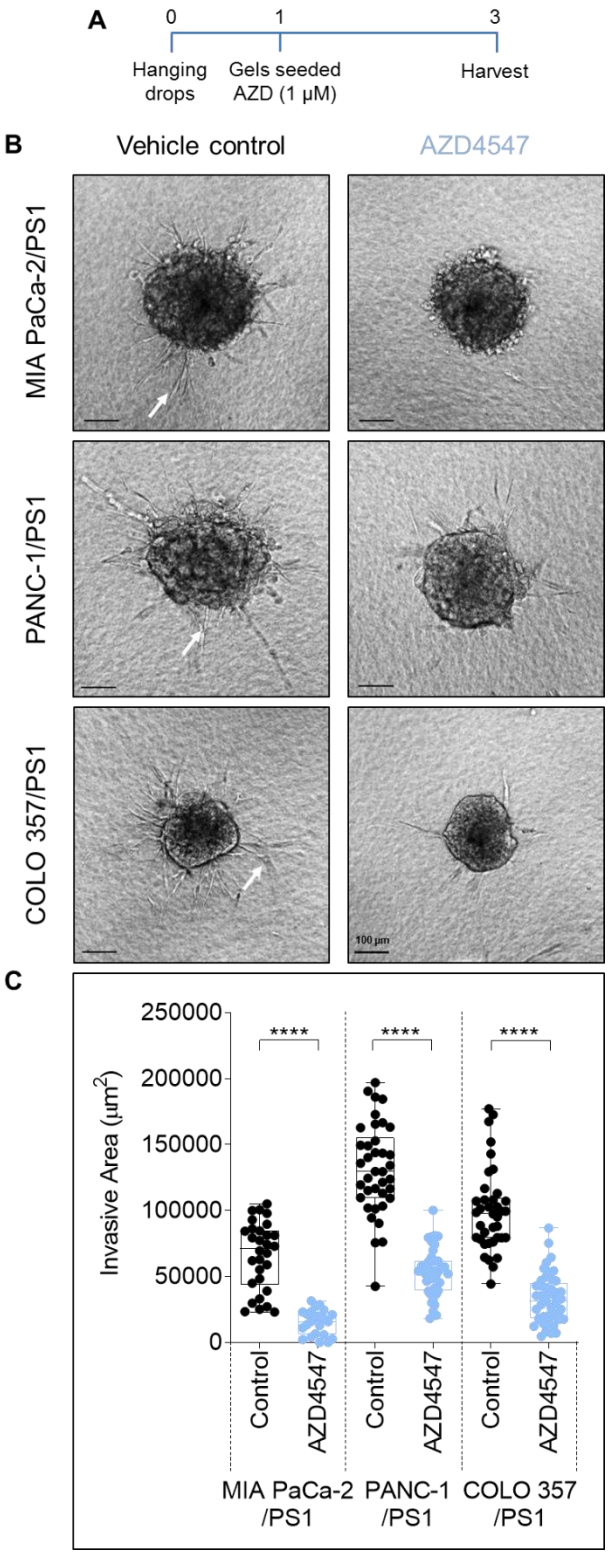

Figure 4.5 FGFR inhibition reduces invasion in 3D co-culture spheroid models

A. *Three PDAC cell lines (MIA PaCa-2, PANC-1 and COLO 357) were grown in spheroid models in co-culture with PS1 stellate cells and were treated with the FGFR inhibitor AZD4547 (AZD, 1 µM) or vehicle control (Section 2.6.2).* ***B.*** *In control spheres cellular invasion into the gels can be seen (shown by the arrows). However, in AZD treated spheres, the invasion was significantly reduced. Scale bar = 100 µm.* ***C.*** *Quantification of the number of invading cells in each gel (points), the median (middle line) and inter-quartile range (box) for each condition is shown in the graph. This was analysed by Mann-Whitney U test of at least three biological replicates ****p<0.0001.*

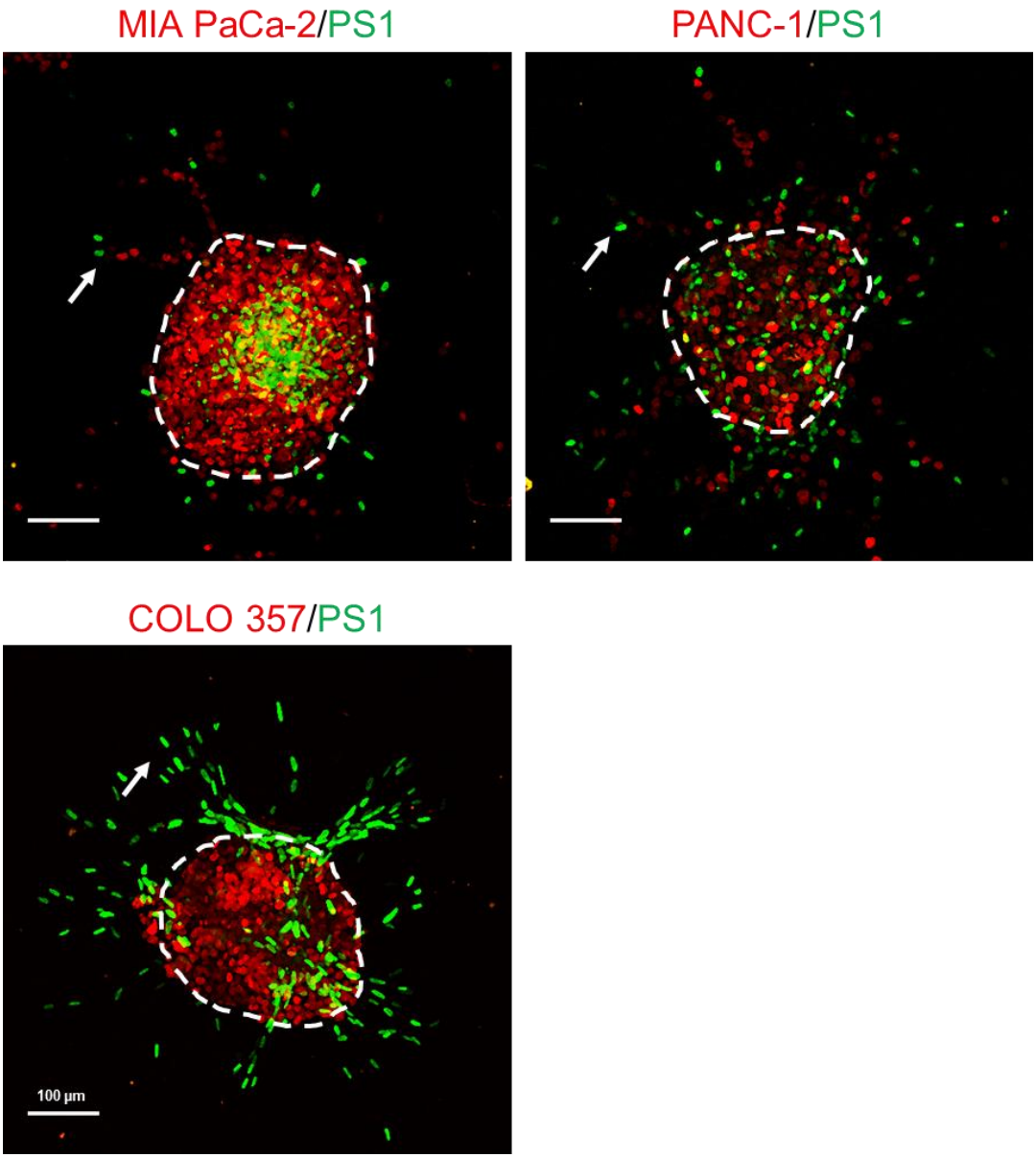

Figure 4.6 Stellate cells lead invasion

Three PDAC cell lines (MIA PaCa-2, PANC-1 and COLO 357) labelled with H2B-RFP were grown in spheroid models in co-culture with PS1 stellate cells labelled with H2B-GFP. Representative Z-stack reconstructions show that at the end of every protrusion leaving the central sphere (shown by dashed white line), a stellate cell is leading the invasion (shown by arrows). These images are representative of at least three biological replicates. Scale bar = 100 µm.

4.3 FGFR1 staining

Immunofluorescent staining for FGFR1 was performed on sections from mini-organotypic gels, to determine the subcellular localisation of FGFR1 in invading cells. Nuclear FGFR1 was visible in invading cells (Figure 4.7), supporting the hypothesis that nuclear translocation of the receptor plays a role in triggering stellate cell-led invasion.

Further analysis will be conducted in the future to strengthen and support these findings. The labelled PSC and PDAC cell lines will be used in the spheroid model, which can then be stained for FGFR1 to demonstrate clearly whether the invading stellate cells have nuclear translocation of the receptor, and if this can be reduced with AZD4547 treatment. This will also show which cell type is invading and live imaging could illuminate the process of stellate-cell led invasion out of the spheres. These images could be viewed and quantified using 4-colour IN Cell high throughput analysis.

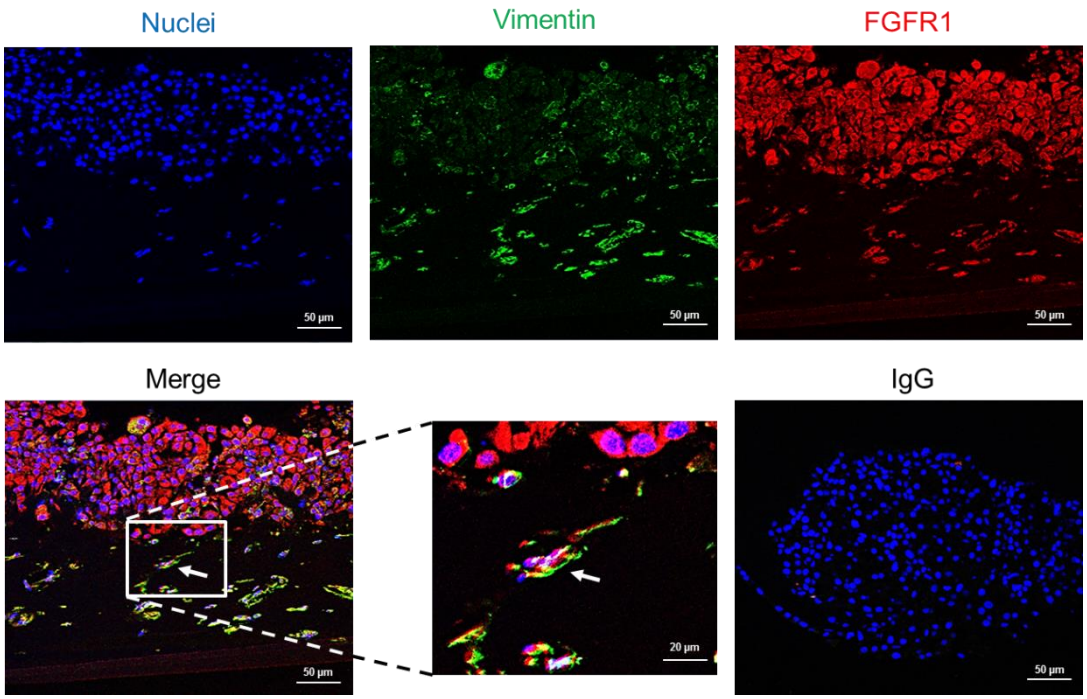

Figure 4.7 Nuclear FGFR1 is present in invading stellate cells

Representative immunofluorescence staining of three biological replicates of co-culture mini-organotypic models of COLO 357 and PS1 cells (day 7) demonstrates that stellate cells invading into the gel, highlighted by positive green vimentin staining, have nuclear FGFR1, shown in red (arrows) (Section 2.3.3). The zoomed in image shows FGFR1 staining localised to the nucleus in invading vimentin positive cells.

4.4 FGFR1 knockdown

To confirm that the reduction in invasion upon FGF inhibition with AZD4547 treatment is due to FGFR1 specifically within the stellate cell compartment, three stable FGFR1 shRNA cell lines were generated (as described in Section 2.6.3). The use of stable doxycycline-inducible shRNA cell lines allowed for efficient FGFR1 knockdown over time in longer term models, as well as more consistent knockdown compared to siRNA transfection of PS1 cells.

Knockdown of FGFR1 within all three cell lines upon treatment with doxycycline was confirmed at protein and RNA level (Figure 4.8). It was also confirmed that FGFR1 knockdown did not affect the proliferation rate of the PS1 cells (data not shown).

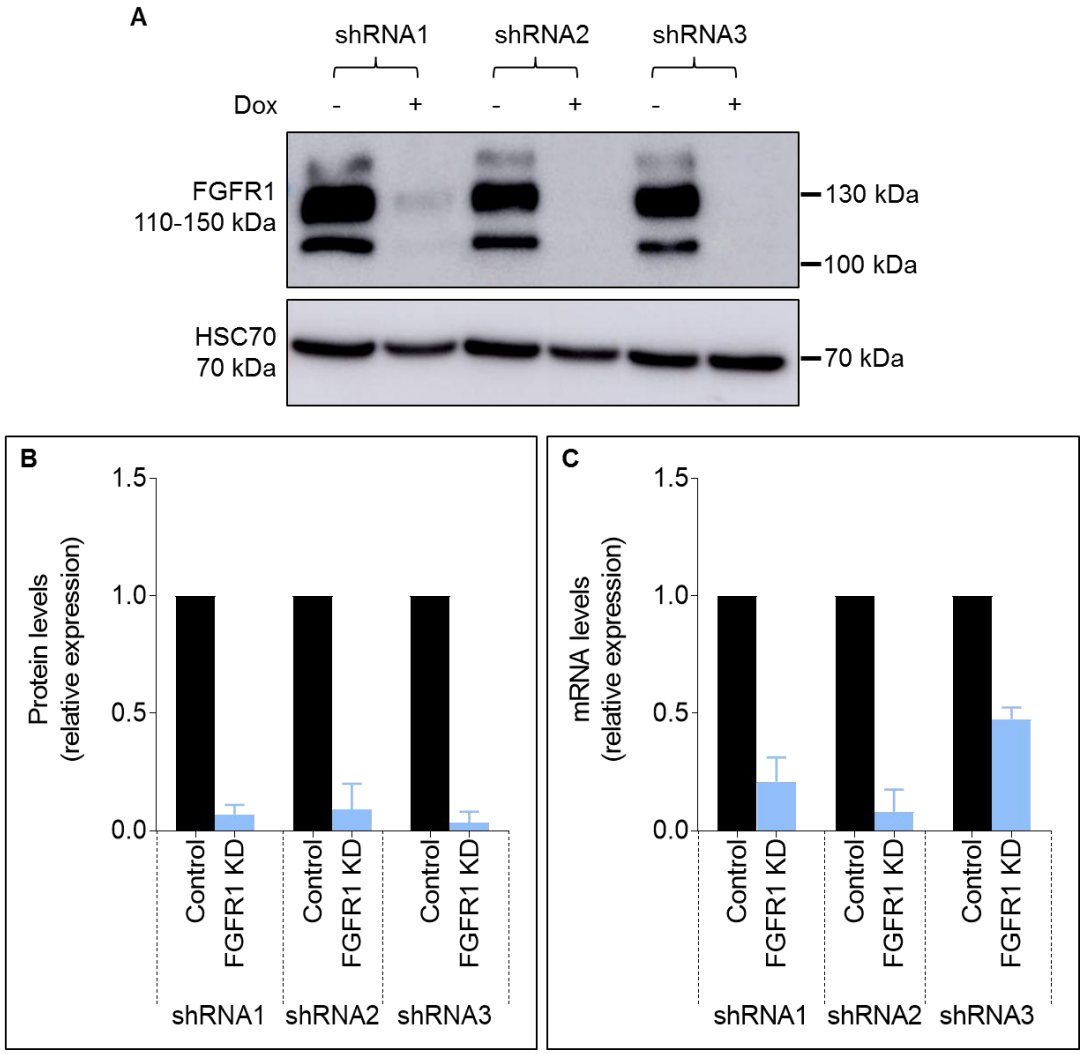

Figure 4.8 FGFR1 knockdown in PS1 shRNA inducible cell lines

*Three doxycycline-inducible FGFR1 shRNA PS1 stellate cell lines were generated. Efficient knockdown of FGFR1 following treatment with doxycycline for 48 hours was confirmed for all three cells lines by protein (**A** and **B**) and RNA (**C**) levels, compared to relevant housekeeping controls (HSC70 for Western blot and B2M and HPRT-1 for qPCR, Sections 2.4 and 2.5). This data is from three biological repeats, graphs show mean and standard deviation of quantification, relative to control.*

4.4.1 FGFR1 knockdown in mini-organotypics

The three stable FGFR1 shRNA cell lines were then placed into mini-organotypic models with MIA PaCa-2 cells and invasion was quantified after seven days of culture with or without doxycycline treatment (Figure 4.9).

Knockdown of FGFR1 reproduced the reduction in invasion seen with AZD4547 treatment, suggesting that FGFR1 is a key mediator of stellate cell-led invasion. This reduction was statistically significant for two out of the three shRNA cell lines.

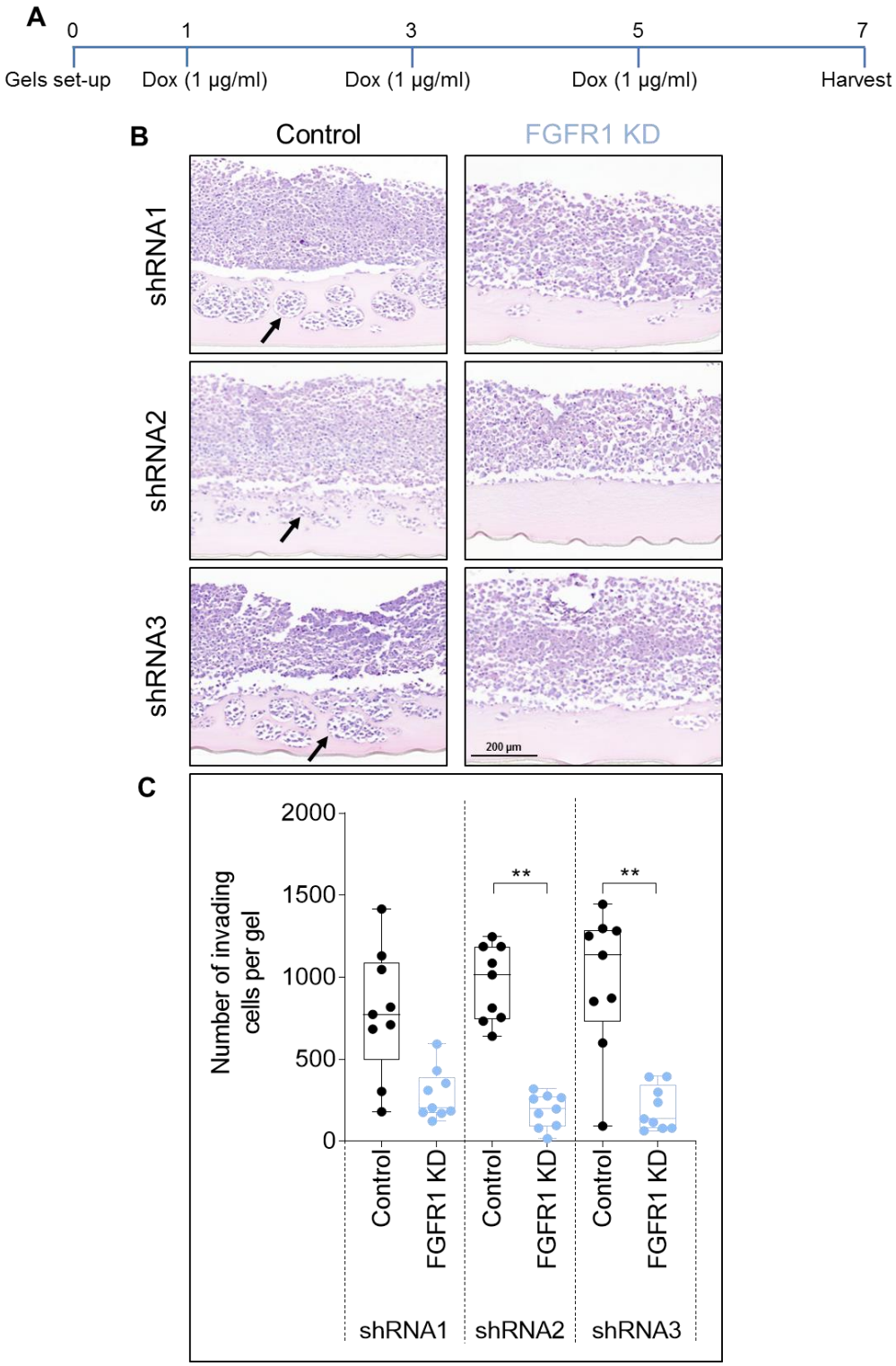

Figure 4.9 FGFR1 knockdown in stellate cells reduces invasion in co-culture mini-organotypic models

A. *MIA PaCa-2 cancer cells were grown for 7 days in mini-organotypic models in co-culture with three inducible PS1 shRNA cell lines. Cultures were treated with doxycycline (dox, 1 µg/ml) every other day to induce FGFR1 knockdown (Section2.6.1).* ***B.*** *Under control conditions, cellular invasion into the gels can be seen (shown by the arrows). However, upon FGFR1 knockdown in PSCs, the invasion was significantly reduced. Scale bar = 200 µm* ***C.*** *Quantification of the number of invading cells in each gel (points), the median (middle line) and inter-quartile range (box) for each condition is shown in the graph. This was analysed by Mann-Whitney U test of at least three biological replicates ** p<0.01.*

4.4.2 FGFR1 knockdown in spheroids

Having shown that knockdown of FGFR1 in the stellate cell compartment recapitulates the reduction of invasion seen with FGFR inhibition, the result was confirmed in our spheroid model using the shRNA2 and shRNA3 PS1 cells (Figure 4.10). Both the shRNA2 and shRNA3 cell lines demonstrated a significant reduction in multi-directional invasion following stellate cell specific knockdown of FGFR1.

These findings highlight the key role that stellate cells play in leading invasion in PDAC and confirm that FGFR1, specifically, is an important mediator of this invasive phenotype.

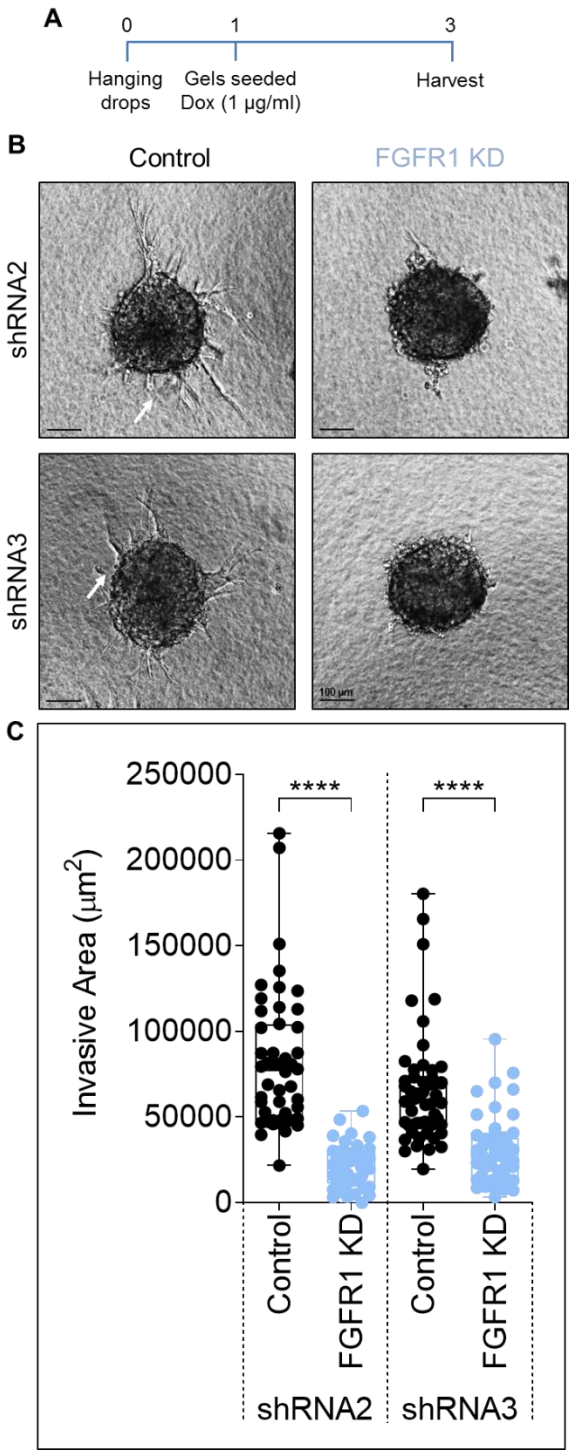

Figure 4.10 FGFR1 knockdown in stellate cells reduces invasion in co-culture spheroid models

A. *MIA PaCa-2 cancer cells were grown in spheroid models in co-culture with two inducible PS1 shRNA cell lines. Cultures were treated with doxycycline (dox, 1 µg/ml) every other day to induce FGFR1 knockdown (Section 2.6.2).* ***B.*** *Under control conditions, cellular invasion into the gels can be seen (shown by the arrows). However, upon FGFR1 knockdown in PSCs, the invasion was significantly reduced. Scale bar = 100 µm.* ***C.*** *Quantification of the number of invading cells in each gel (points), the median (middle line) and inter-quartile range (box) for each condition is shown in the graph. This was analysed by Mann-Whitney U test of at least three biological replicates **** p<0.0001.*

4.5 Combination therapy

PDAC stroma plays a vital role in tumour progression, demonstrated by the effective reduction in invasion when interrupting FGF-mediated cellular cross-talk in co-culture models. Co-targeting the tumour and the stroma has become a popular strategy for improving therapeutic options in PDAC patients. Therapies targeting the ECM (e.g. hyaluronic acid), key paracrine signalling pathways (e.g. Wnt and hedgehog signalling) and immune cells (e.g. immune checkpoint blockade inhibitors) have all been investigated and translated into clinical trials (Doherty et al., 2018, Gong et al., 2018, Jacobetz et al., 2013, Kabacaoglu et al., 2018, Merika et al., 2012, Olive et al., 2009, Richards et al., 2012, Thompson et al., 2010). By decreasing the desmoplastic stromal reaction and hypoxia within the tumours, chemotherapy may be given to patients with increased effect, improving prognosis. However, targeting the stroma is more complex than first thought, as shown when one promising avenue targeting hedgehog signalling or depleting activated PSCs gave disappointing results. In pre-clinical studies and a clinical trial, tumours treated with anti-stromal therapies appeared to be more aggressive and patients survived longer on the control treatment arm, leading to early termination of the trial (Bailey et al., 2009, Feldmann et al., 2008, Rhim et al., 2014).

In particular, targeting the activated stellate cells to return them to a quiescent phenotype has been an area of interest. Treatment of activated stellate cells with a metabolite of vitamin A (ATRA) can return them to their quiescent phenotype and induce vitamin storage within lipid droplets. Therefore, combination therapy regimens of gemcitabine and ATRA were tested in 3D *in vitro* assays and KPC mice. This study demonstrated that co-targeting the two cell types resulted in decreased cancer cell proliferation, stellate cell activation and increased apoptosis, compared to either

treatment given alone (Carapuça et al., 2016). This study has been translated into a phase 1b clinical trial in PDAC patients (NCT03307148).

Following the success of combining treatments to target both the stellate and cancer cell compartments of PDAC tumours, I hypothesised that adding AZD4547 in combination with these therapies, thereby targeting cellular cross-talk and inhibiting stellate cell-led invasion, might augment the efficacy of ATRA/gemcitabine combination treatment. Therefore, these three different drugs were tested in mono- and combination therapy in the 3D mini-organotypic model (Figure 4.11). The dose of gemcitabine and ATRA were used according to previous optimisation in 3D *in vitro* models within the laboratory (Carapuça et al., 2016, Neuzillet et al., 2019).

4.5.1 Effects on invasion

AZD4547 was most effective at reducing invasion into gels, both alone and in combination with ATRA and/or gemcitabine. However, measuring the cell layer thickness on top of the gel, AZD4547 treatment alone did not appear to impact on cell proliferation, unless in combination with ATRA or in the triple therapy gels (Figure 4.11). Cell layer thickness was measured at four representative points across each gel using the Pannoramic Viewer software (Section 2.6.1).

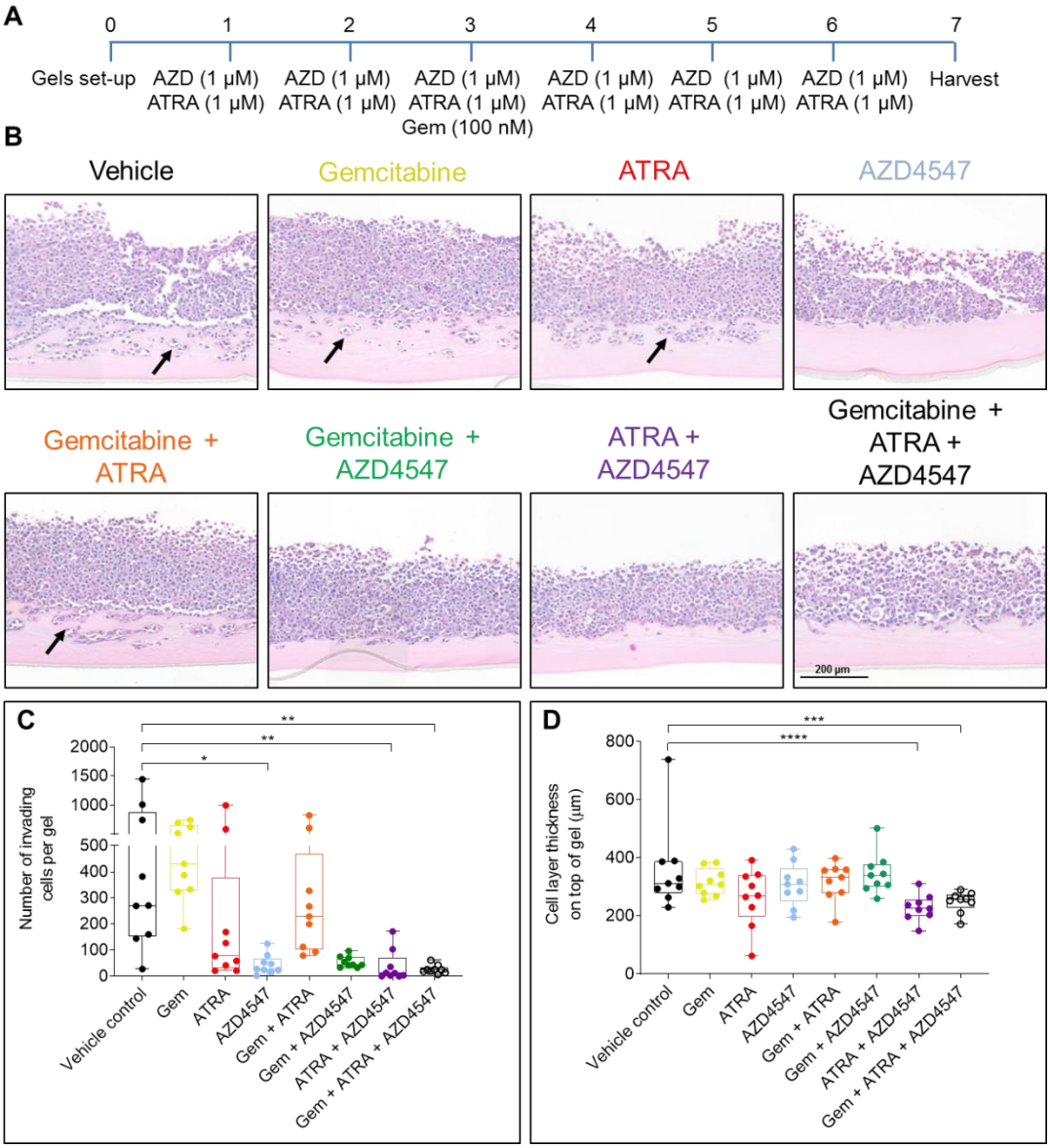

Figure 4.11 FGFR inhibition reduces invasion in co-culture mini-organotypic models alone and in combination therapy

A. *MIA PaCa-2 cancer cells were grown in co-culture with PS1 stellate cells in mini-organotypics for 7 days and treated with AZD4547 (AZD, 1 μM), ATRA (1 μM) and gemcitabine (Gem, 100 nM) either alone or in combination with relevant controls. AZD and ATRA treatment was given daily, whilst Gem treatment was given weekly (once) (Section 2.6.1).* ***B.*** *Cellular invasion into the gels can be seen (shown by the arrows). However, when the cultures were treated with AZD4547 invasion was reduced. Scale bar = 200 μm. Quantification of the number of invading cells in each gel (points,* ***C****) or the cell layer thickness on top of the gel (points,* ***D****), with the median (middle line) and inter-quartile range (box) for each condition is shown in the graph. AZD4547 either alone or in combination with ATRA or gemcitabine plus ATRA significantly reduced invasion. Whereas AZD4547 alone did not affect the cell layer thickness on top of the gel, this was only reduced AZD4547 treatment was combined with ATRA or gemcitabine plus ATRA. Quantification was analysed by Kruskal-Wallis test with Dunn's multiple comparison of three biological replicates *p<0.05, **p<0.01, ***p<0.001, ****p<0.0001.*

4.5.2 Effects on cell survival

To determine the cellular effect of all three drugs, sections were stained for Ki67 and cleaved caspase 3 as markers of proliferation and apoptosis, respectively (Figures 4.12 and 4.13). The percentage of Ki67 positive nuclei did not appear to change between the different treatments, indicating no change in the rate of proliferation. The percentage of cleaved caspase 3 positive nuclei seemed to increase in the gemcitabine plus AZD4547, ATRA plus AZD4547 and triple therapy combinations, indicating a potential change in apoptosis, however, not with statistical significance. This could be because the total cell number has decreased in the cultures treated with the triple combination; therefore, the percentage of proliferating cells remains the same. Furthermore, these cultures may have been too short to determine the true effect of combining gemcitabine, ATRA and AZD4547.

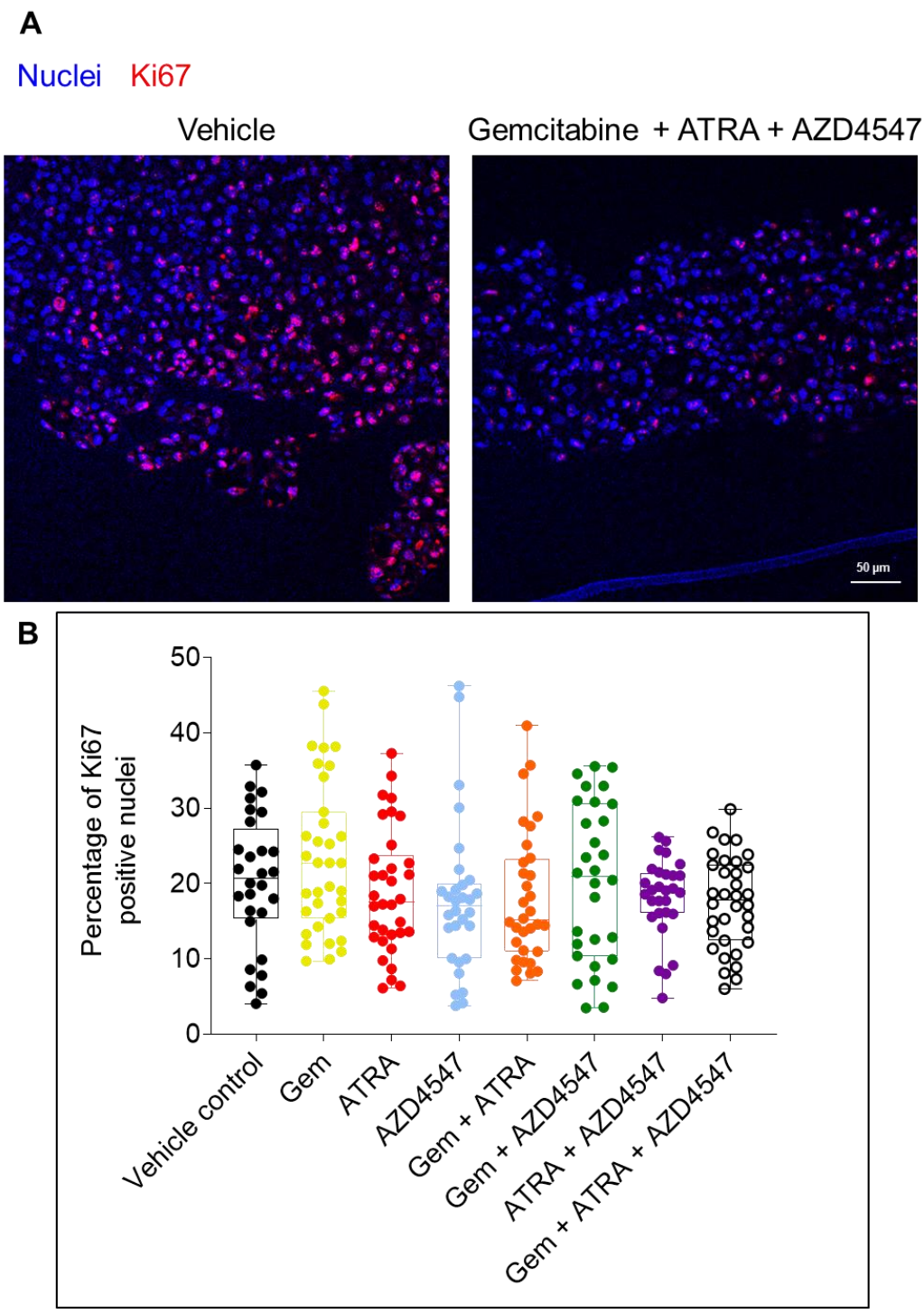

Figure 4.12 Proliferation rate is unchanged upon treatment with gemcitabine, ATRA and AZD4547 in combination

All of the sections of the mini-organotypic co-cultures treated with combination therapies were stained for Ki67 as a marker of proliferation (Section 2.3.3). ***A.*** *Representative staining from a control and treated section.* ***B.*** *The number of positive Ki67 nuclei was calculated as a percentage of the total nuclei in the section. For each treatment, the whole gel was imaged and at least 5 fields of view from the centre of the gel were quantified. Quantification was analysed using by Kruskal-Wallis test with Dunn's multiple comparison of three biological replicates. Scale bar = 50 µm.*

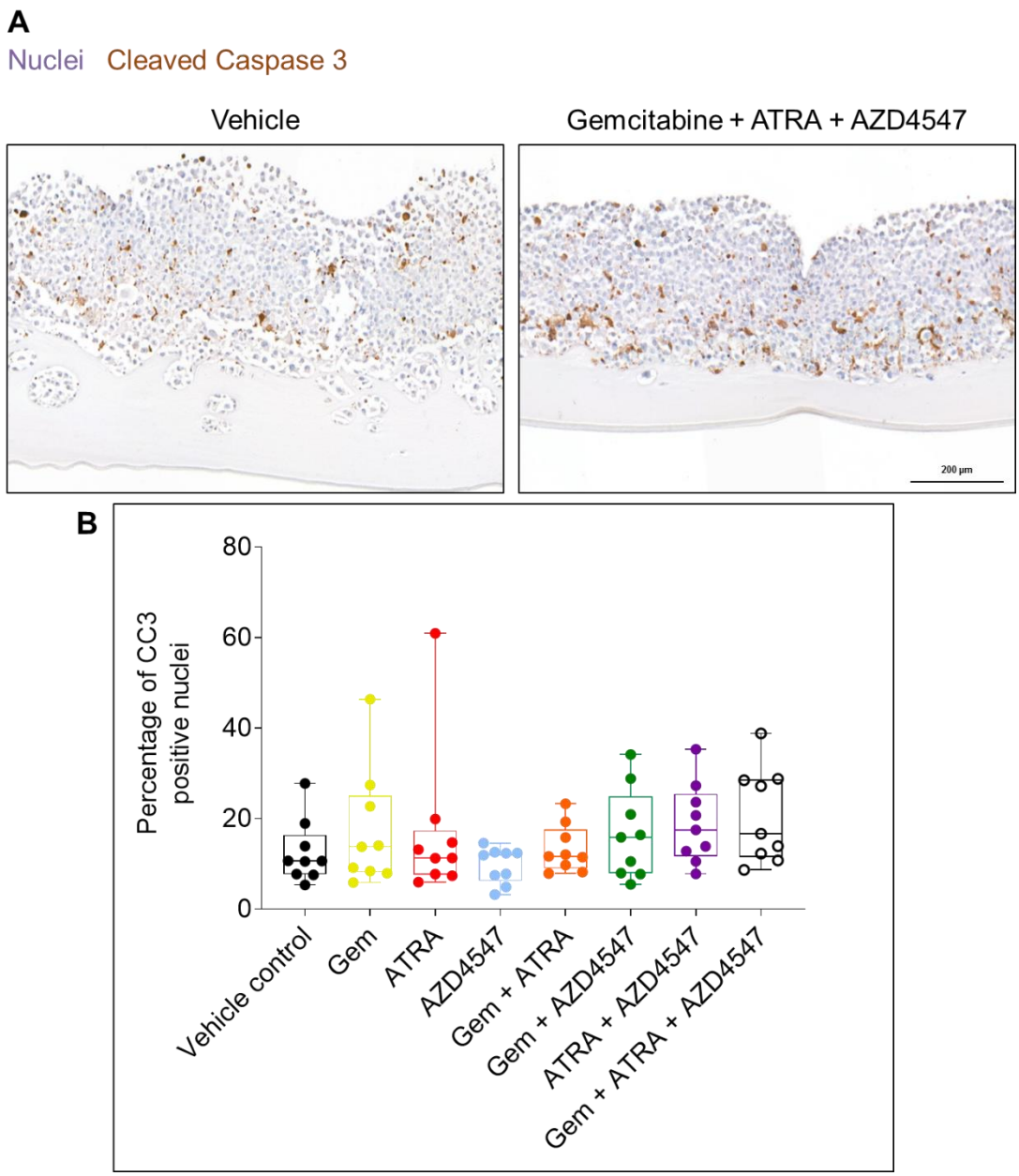

Figure 4.13 Apoptosis is increased upon treatment with gemcitabine, ATRA and AZD4547 in combination

All of the sections of the mini-organotypic co-cultures treated with combination therapies were stained for cleaved caspase 3 as a marker of apoptosis (Section 2.3.4). ***A.*** *Representative staining from a control and treated section.* ***B.*** *The number of positive cleaved caspase 3 nuclei was calculated as a percentage of the total nuclei in the whole section. Quantification was analysed by Kruskal-Wallis test with Dunn's multiple comparison of three biological replicates. Scale bar = 200 µm.*

4.6 Combination treatments *in vivo*

Building on the triple combination therapy data in 3D mini-organotypic models, this combination was tested in a mouse model. *In vivo* testing allowed examination of the effect of the three drugs in a more complex system, to investigate whether this may be a viable clinical approach.

4.6.1 Pilot experiments

Pilot experiments to determine the response to AZD4547 *in vivo* were performed using subcutaneous nude (nu/nu, *Foxn1*^{nu}) mice models. Nude mice lack a thymus and, therefore, have no T cell immunity, making them useful for tumour xenograft experiments (Szadvari et al., 2016). MIA PaCa-2 cells were injected in mono- or co-culture with PS1 cells, whilst another group of mice was injected with PS1 cells alone as a control. Three pilot experiments were carried out, with different cell numbers used to find the optimal tumour growth. Short experiments of 21 days post-injection were designed, to ensure that the human stellate cells were not replaced by murine stromal cells recruited to the tumours.

Unfortunately, in the first two pilot experiments the tumours failed to grow significantly in any of the mice (Figures 4.14 and 4.15). In these two experiments five mice were included in each group, with three mice in the PS1-only control group. Cells were injected subcutaneously in PBS into each flank, therefore there were two tumours per mouse. There was no difference in tumour growth whether mice were injected with cancer cells alone or in combination with stellate cells. During the first experiment, mice were treated with 12.5 mg/kg AZD4547 or vehicle control by oral gavage from day 7 post injection. Due to the limited growth of all the tumours in the first experiment, mice were only planned to be randomised for treatment once their tumours reached

a minimum size of 100 mm^3 in the second pilot experiment. As no tumours reached this size limit, no treatment was given.

Following the failure of the first two pilot experiments, a third was performed. In this experiment, cells were injected in mono- or co-culture at two different cell densities (four mice in total). One flank was injected using cells re-suspended in PBS alone and the other with cells in PBS plus matrigel. Mice were weighed twice a week and any tumours were measured (using callipers) three times a week. Two mice in this experiment grew tumours (Figure 4.16). It appeared that the presence of stellate cells may have slowed tumour growth in these models. However, due to the limited number of mice included in the experiment, it is difficult to conclude anything definitive. At the end of the experiment, tumours were harvested and stained with H&E. This showed large necrotic areas within the tumours and presence of cells which could be identified as innate immune infiltrate (Figure 4.17). These findings support the notion that this model will not reach the tumour volume required within the experimental time frame.

4.6.2 NSG mice

These pilot *in vivo* experiments demonstrated that nude mice could not reliably establish MIA PaCa-2 xenograft tumours, especially within the 21 day optimal time frame. Therefore a collaboration was developed with Professor Yaohe Wang's group based at Zhengzhou University in China. This group are currently using MIA PaCa-2 based subcutaneous and orthotopic xenograft models in non-obese diabetic (NOD) severe combined immunodeficiency (scid) gamma (NSG, NOD.Cg-*Prkdc*^{scid} *Il2rg*^{tm1Wjl}/SzJ) mice in their research. These mice were developed in the Jackson laboratory and lack T cells, B cells and natural killer cells. This makes them highly immunodeficient and they have many defects in innate immunity, increasing

the chance of successful engraftment of human cell lines (Ishikawa et al., 2005, Shultz et al., 2005). Other groups have also demonstrated that MIA PaCa-2 cells can be successfully grown orthotopically and subcutaneously in NSG mice, highlighting that this is a suitable model (Almawash et al., 2018, Lim et al., 2019, Pal et al., 2018, Shannon et al., 2015). Pilot experiments are ongoing in these mice, MIA PaCa-2 cells have been injected alone and in combination with PS1 cells and tumour growth is being monitored. If during this pilot experiment tumours have established within the 21 day time frame in the mice, this model will be used to test the three drugs (gemcitabine, ATRA and AZD4547) in combination.

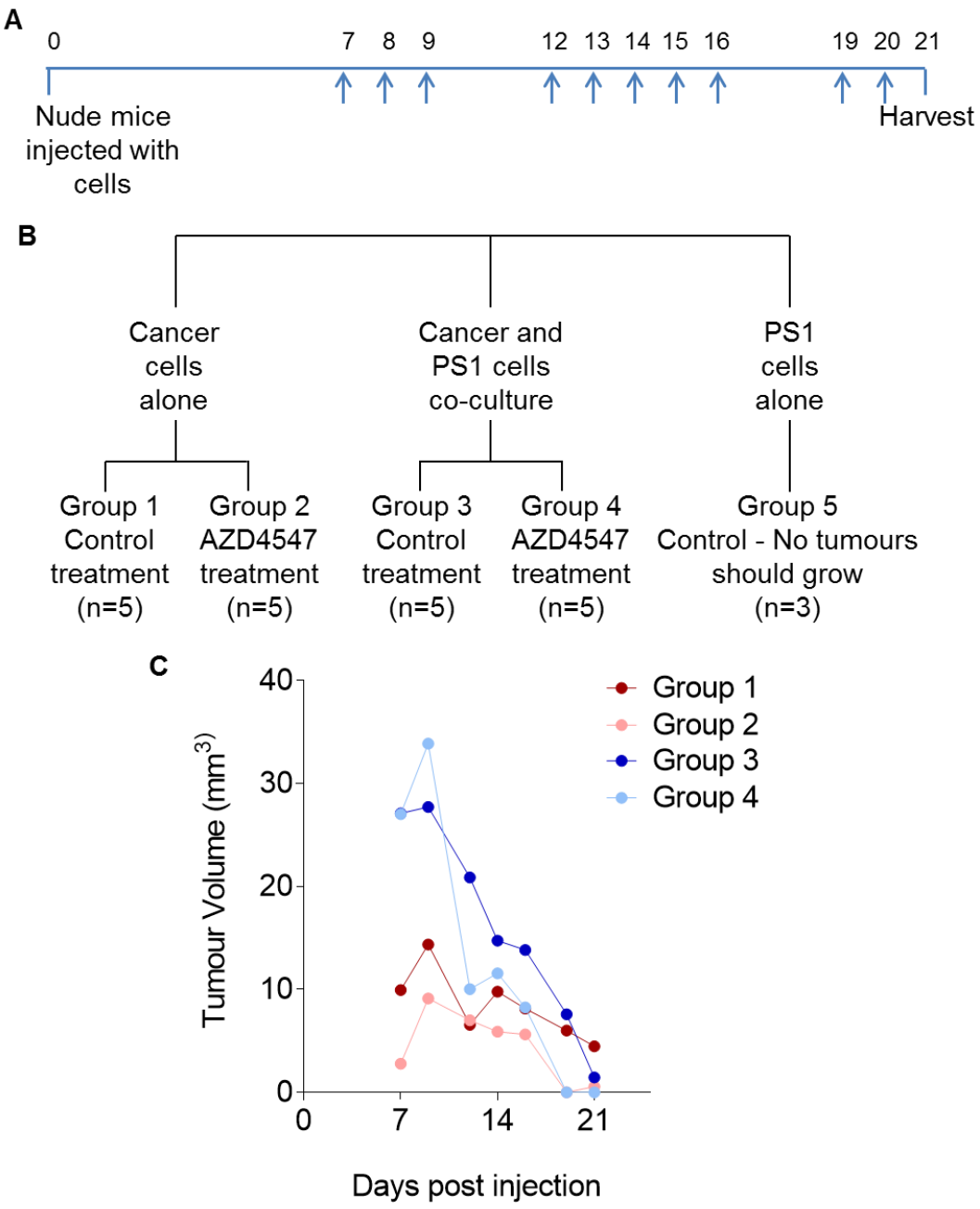

Figure 4.14 MIA PaCa-2 xenograft tumours in nude mice

A. *Nude mice were injected subcutaneously into each flank and tumours were left for 7 days to form. Mice were then either treated with AZD4547 or control by oral gavage daily, following a 5 day on, 2 day off protocol. Mice were euthanised and tumours were harvested on day 21 (Section 2.9).* ***B.*** *5 mice were injected with either 1 x 10^6 MIA PaCa-2 cells alone (group 1 and 2) or in co-culture with 2 x 10^6 PS1 cells (group 3 and 4). A control group of 3 mice was injected with PS1 cells alone (group 5), which confirmed these cells do not form tumours.* ***C.*** *Tumours were measured three times a week from day 7 to day 21. There appeared to be initial tumour formation on day 7 in all the groups, although the MIA PaCa-2 alone tumours (groups 1 and 2) were very small. As the experiment progressed, the tumours shrank in all the groups, irrespective of treatment or initial cells injected. At day 21, any remaining tumours were very small, all below 10 mm^3.*

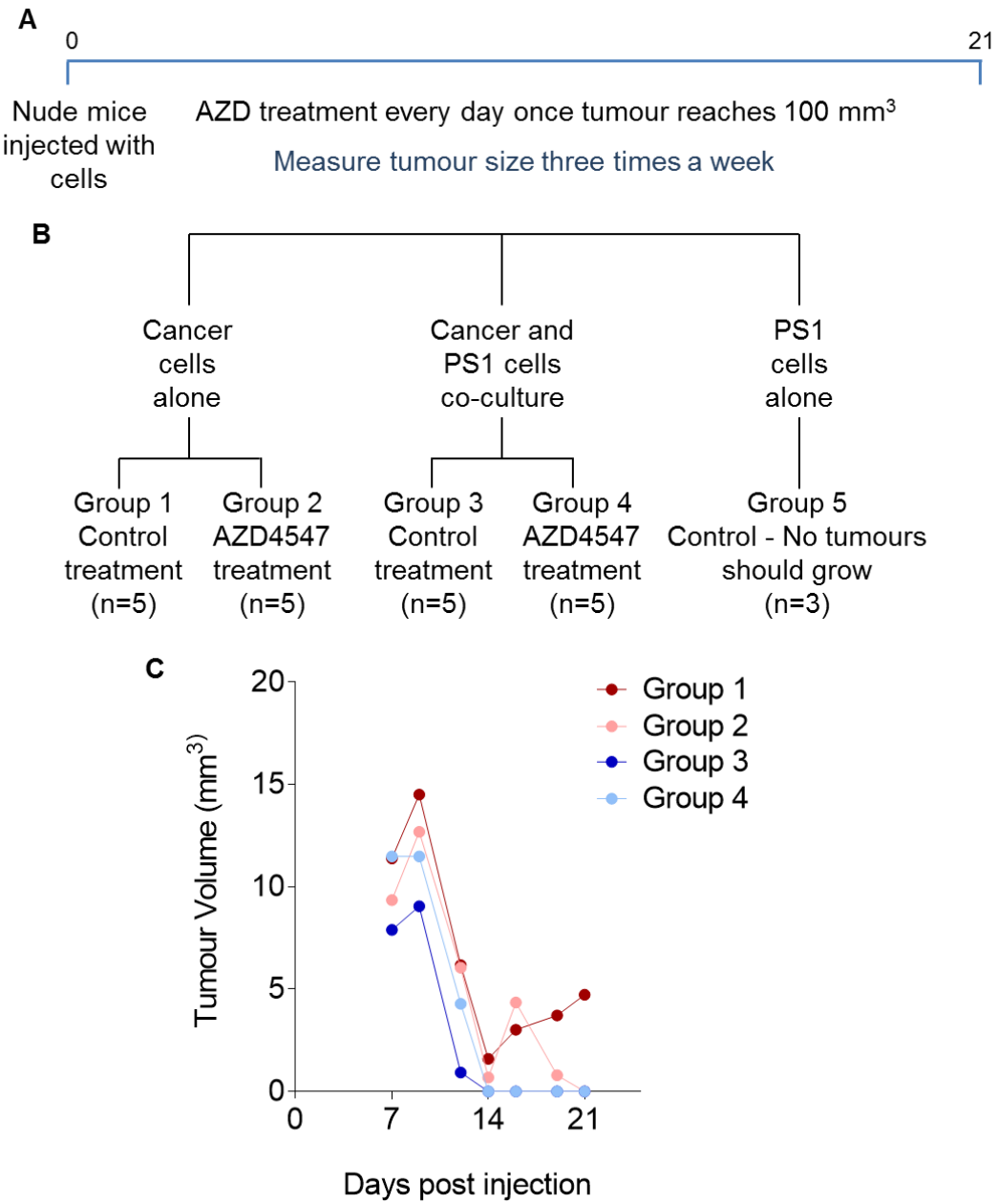

Figure 4.15 MIA PaCa-2 xenograft tumours do not grow in 21 days

A. *Nude mice were injected subcutaneously into each flank and tumours were left to form. Tumour size was measured three times a week from 7 days post injection and mice were either recruited to AZD4547 or control treatment groups once their tumours reached 100 mm^3. Mice were euthanised and tumours were harvested on day 21 (Section 2.9).* ***B.*** *5 mice were injected with either 5 x 10^6 MIA PaCa-2 cells alone (group 1 and 2) or in co-culture with 10 x 10^6 PS1 cells (group 3 and 4). A control group of 3 mice was injected with PS1 cells alone (group 5), which confirmed these cells do not form tumours.* ***C.*** *Tumours were measured three times a week from day 7 to day 21. All of the growths measured during this time were even smaller than the first experiment, indicating that in all the conditions the tumours did not grow. No mice were treated with either AZD4547 or control as no tumours grew to the required size of 100 mm^3.*

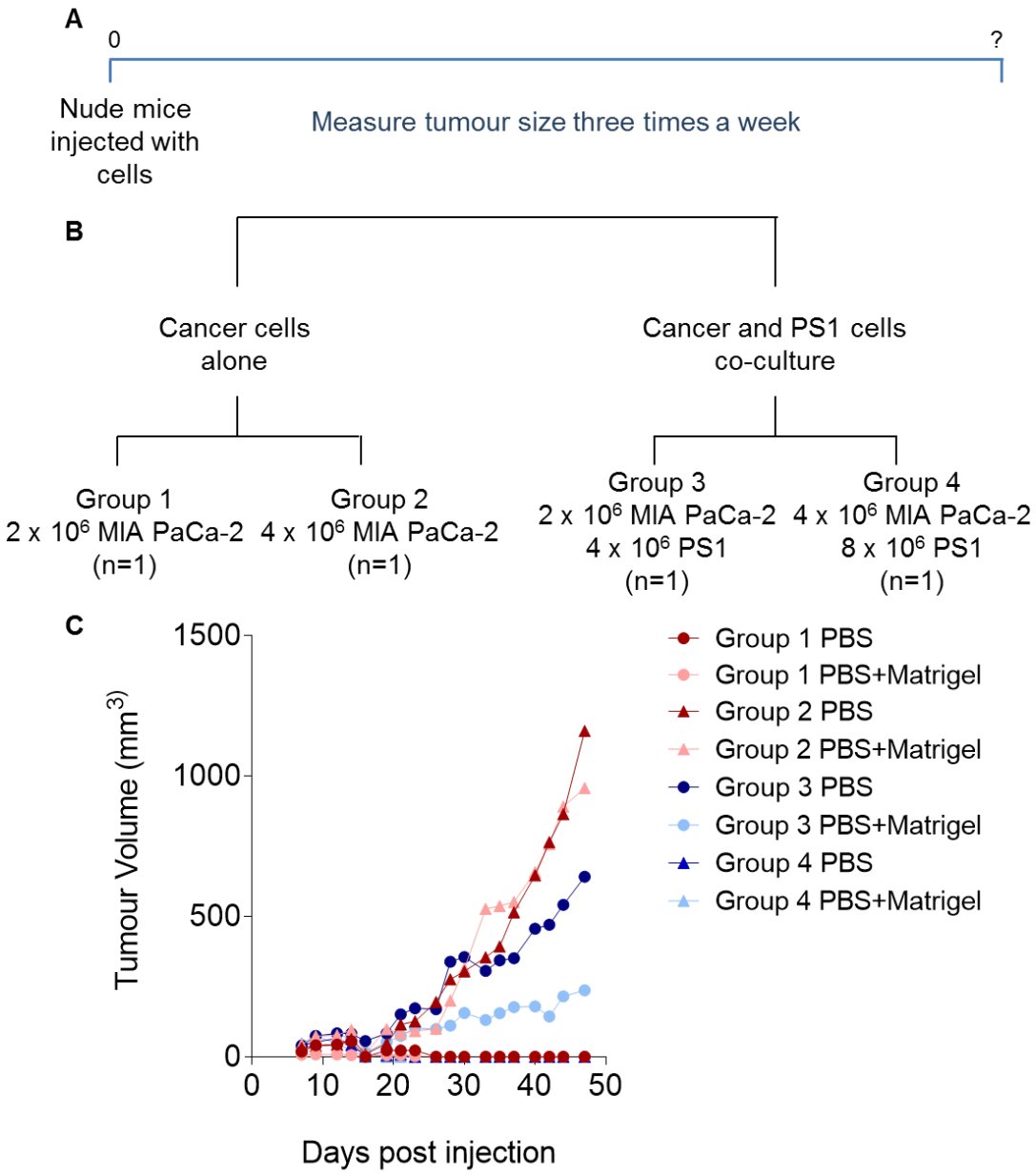

Figure 4.16 Optimising MIA PaCa-2 subcutaneous xenograft tumour conditions in nude mice

A. *Nude mice were injected subcutaneously into each flank and tumours were left to form. One flank was injected with cells resuspended in PBS, and the other with cells resuspended in PBS + matrigel. Tumour size was measured three times a week from 7 days post injection until mice were euthanised and tumours were harvested on day 47 (Section 2.9).* ***B.*** *One mouse was injected with either 2 x 10^6 or 4 x 10^6 MIA PaCa-2 cells alone (group 1 and 2 respectively) or in co-culture with 4 x 10^6 or 8 x 10^6 PS1 cells (group 3 and 4 respectively).* ***C.*** *Tumours were measured three times a week from day 7 to day 47.Tumours grew in two of the mice (group 2 and 3) and these began to increase in volume from day 20. The group 2 mouse had tumours that reached a significant size by the end of the experiment, with no difference between cells injected in PBS or PBS + matrigel. The group 3 mouse demonstrated significant growth in the PBS tumour, compared to the PBS + matrigel tumour.*

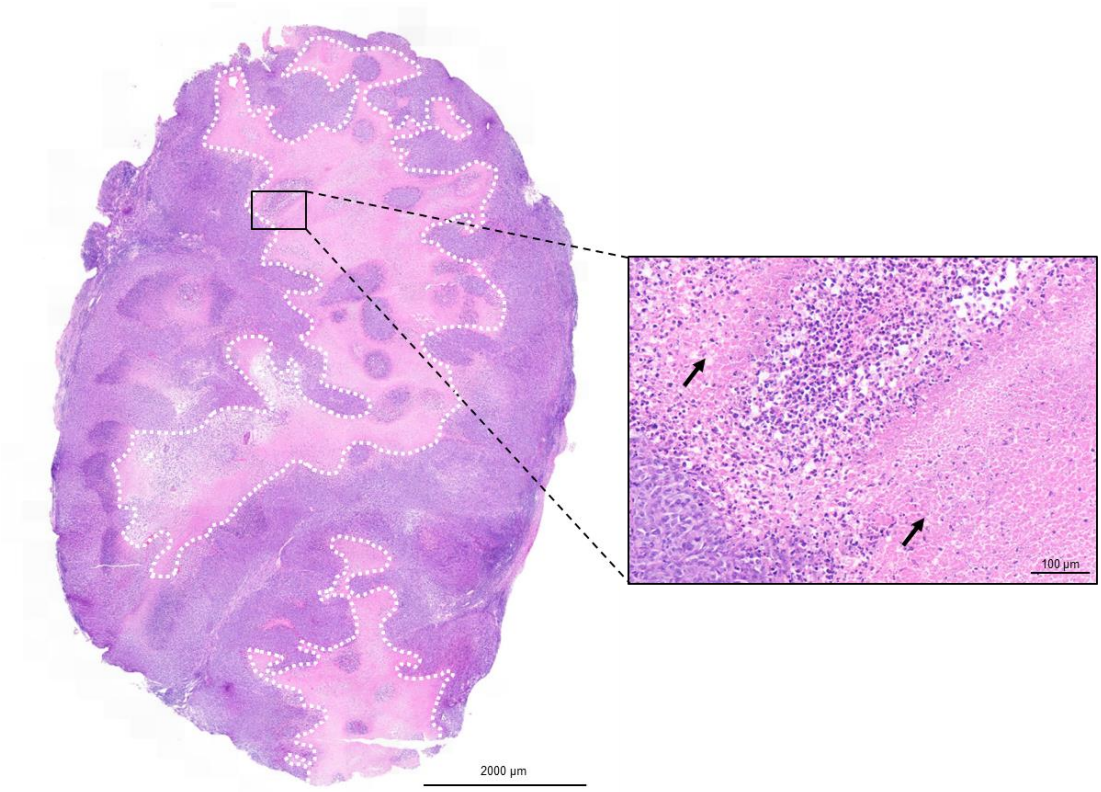

Figure 4.17 Necrotic MIA PaCa-2 subcutaneous xenograft tumours infiltrated with immune cells

H&E image of injected co-culture tumour from the group 3 mouse. Much of the tumour is necrotic (enclosed in the white dashed line). In the zoomed-in section, infiltrating immune cells can be identified at the edge of the tumour tissue and within the necrotic regions (black arrows).

4.7 Discussion

Nuclear FGFR1 (nFGFR1) has been found in myofibroblast cells at the invasive edge of PDAC tumours, compared to reduced nuclear localisation of the receptor within the centre of the tumour (Coleman et al., 2014b). This indicates that nFGFR1 may play a role in PDAC progression and invasion. Previous work has shown that treatment with FGFR inhibitors can reduce invasion in 3D models, supporting a role for FGF signalling in PDAC invasion (Coleman et al., 2014b). During this project, I used two different and distinct 3D *in vitro* co-culture models to investigate the effect of targeting FGF signalling. I also used a clinically relevant FGFR inhibitor AZD4547 (Gavine et al., 2012) to examine the effects on invasion in these models. Treatment with AZD4547 in the mini-organotypic model reduced invasion, at a dose which does not inhibit proliferation in 2D cultures, supporting data demonstrating the same effect when treating PDAC co-cultures with a laboratory tool compound FGFR inhibitor, PD173074, (Coleman et al., 2014b). This result was also confirmed when examining multi-directional invasion using a novel spheroid model. At the end of each invasive protrusion in the spheroid model, a stellate cell can be found leading the way. This supports previous work showing that pancreatic stellate cells can act to indirectly increase cancer cell proliferation and invasion (Liu et al., 2019). It has also been shown that stellate cells can be found within the metastatic niche of PDAC patients, suggesting that PSCs leave the tumour and travel to distant sites with the cancer cells. PSCs may be responsible for re-modelling tissue to form suitable metastatic sites (Apte and Wilson, 2012, Apte et al., 2013, Hwang et al., 2012, Thomas and Radhakrishnan, 2019, Vonlaufen et al., 2008a, Xu et al., 2010).

To ensure that the reduction in invasion was due to FGFR1 within the stellate cell compartment specifically, inducible FGFR1 shRNA PS1 cell lines were used. In both 3D models, PS1-specific knockdown of FGFR1 reproduced the reduction in invasion

seen with AZD4547 treatment. This confirms that FGFR1 signalling within PSCs plays a significant role in PDAC invasion, and is targeted effectively by AZD4547 treatment.

AZD4547 is effective at reducing PSC-led invasion in PDAC models, however, to improve patient prognosis in the clinic this will need to be combined with other therapies. Co-targeting the cancer and stromal cells together in PDAC can lead to improved treatment outcomes (Carapuça et al., 2016). Based on this previous work using ATRA and gemcitabine in combination, AZD4547 was added to these regimens. This work confirmed that inhibiting stromal-cancer cross-talk with AZD4547 caused the biggest effect on invasion. However, combining AZD4547 with ATRA (returning the stellate cells to a quiescent phenotype) and gemcitabine (to target the cancer cells) led to decreased cell number shown by cell layer thickness on top of the gel, indicating superior anti-tumour effects over either drug alone. There appeared to be no significant changes in the percentage of Ki67 or cleaved caspase 3 positive nuclei between the different treatment conditions. Whilst this could be due to the total number of cells surviving at the end of the treatment being reduced in the triple combination treatment and, therefore, there was no change in the relative percentage of proliferating cells, it may be due to inhibition of cross-talk rather than proliferation or apoptosis. It is plausible that the surviving cells may be resistant to gemcitabine treatment. These cultures were also only maintained for a short time (7 days), with one snapshot quantification at the end of the culture, in contrast to previous work with gemcitabine and ATRA treatments in large 3D organotypic models, which were performed in cultures maintained for up to 24 days (Carapuça et al., 2016). Furthermore dynamic quantification over time may give more reliable results. Subsequent *in vivo* testing of the triple combination will confirm if this is a viable therapeutic option for translation into patients in the clinic.

Chapter 5 Results III: Role of FGFR1 in pancreatic stellate cells

5.1 Introduction

Nuclear FGFR1 has been shown to regulate cell growth and differentiation through altering gene expression in neuronal cells (Section 1.6) (Stachowiak et al., 2007, Stachowiak and Stachowiak, 2016). Previous studies in our laboratory also showed FGFR1 organising into nuclear speckles and co-localising with SC35 in PS1 cells (Coleman et al., 2014b). This suggests that nFGFR1 could act as a transcription factor or part of a transcription complex within pancreatic stellate cells. ChIP-seq is a recognised method to identify genes regulated by specific transcription factors (Johnson et al., 2007). This was adopted to determine nFGFR1 target genes, to examine how this novel signalling method may be influencing PDAC invasion and metastasis in patients.

5.2 HaloTag

One of the requirements for successful ChIP is to have a specific and sensitive antibody against the protein of interest (Kidder et al., 2011). Many commercial antibodies are not ChIP-grade. They must bind to the protein of interest with sufficient efficacy to pull down enough DNA to analyse, whilst also ensuring that there is no non-specific binding to proteins with a similar structure, which could compromise the validity of the results. Monoclonal or polyclonal antibodies can be used in ChIP, but either must be validated for the protein within the cells of interest (Landt et al., 2012). Monoclonal antibodies only recognise one specific epitope of the protein, which may not be available due to DNA binding and formaldehyde cross-linking. Polyclonal antibodies can be raised against a whole protein, making it more likely that there will be positive binding. However, there is a limited amount of antibody-containing serum that can be produced for each batch of polyclonal antibody. Each new batch must be re-validated to ensure it is suitable for the ChIP assay (Wardle and Tan, 2015).

Many FGFR1 antibodies are not ChIP-grade and, therefore, are not suitable to use in this assay. A possible way to overcome this problem is to use a tagged version of FGFR1. HaloTag technology was therefore explored to circumvent the need for a ChIP-grade antibody.

HaloTag is a modified bacterial haloalkane dehalogenase. It is a useful tag to use in biological assays as it can bind covalently to synthetic ligands in a quick, specific and irreversible way. This means that expression can be tracked inside a cell using fluorescent ligands, such as TMR (Figure 5.1). Furthermore, Halo-ChIP can be performed, where HaloTag expressed in cells can bind to a chloroalkane linker on beads to allow effective pull-down for ChIP without the need for an antibody (Los et al., 2008).

A construct of FGFR1 with C-terminally linked HaloTag (FGFR1-HT, Figure 2.4) was purchased in the pCK14 plasmid (FHC10532, Kazusa DNA Research Institute). This was then used to express a tagged version of FGFR1 in cells.

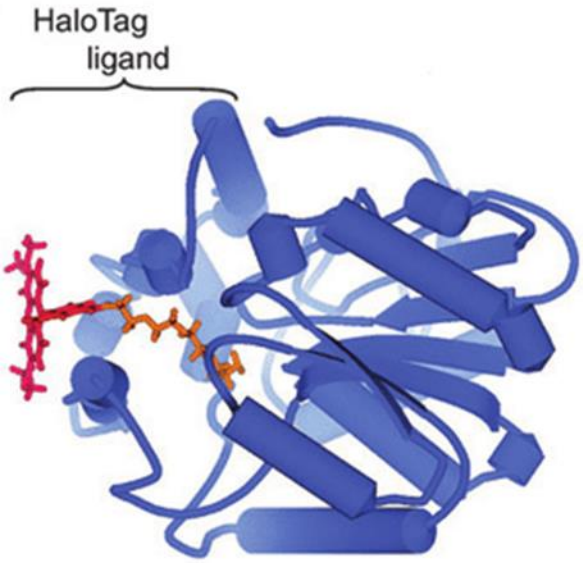

Figure 5.1 HaloTag binding to TMR

The HaloTag protein binds to the fluorescent ligand TMR. This interaction is irreversible and allows HaloTag expression to be viewed by immunofluorescence or live imaging (Los et al., 2008, Marchesan and Prato, 2015)

5.2.1 Transient transfection

HEK293T and PS1 cells were transiently transfected with the FGFR1-HT, and fluorescent TMR ligand was added to determine successful transfection (Figure 5.2). Wherever HaloTag is expressed, TMR will bind and can be detected by fluorescence imaging.

HEK293T cells showed successful transfection of the FGFR1-HT construct, albeit with a low efficiency. PS1 cells showed an even lower level of successful transfection with the construct. Therefore, due to the low transfection efficiency and the large number of cells required for ChIP analysis, transient transfection would not give sufficient expression of FGFR1-HT for determination of the nuclear targets. This approach was, hence, abandoned.

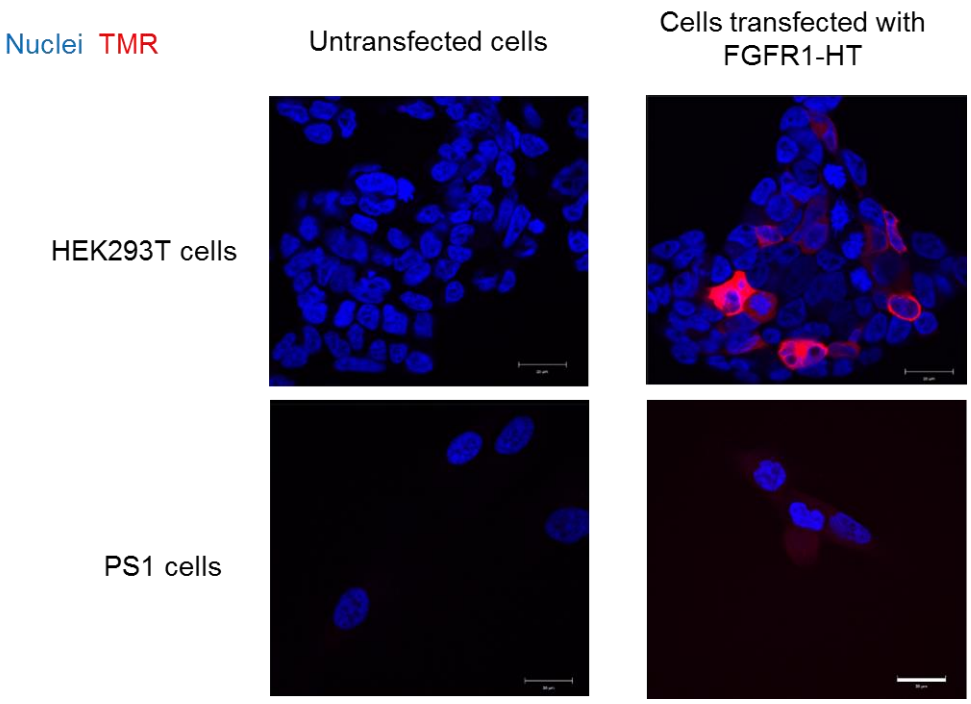

Figure 5.2 Transient transfection of FGFR1-HT

HEK293T and PS1 cells were transiently transfected with the FGFR1-HT construct (Section 2.5.1). Successful transfection was determined using the fluorescent TMR ligand, which covalently binds to HaloTag directly. HEK293T cells demonstrated a low level of positive transfection, whereas no transfection was seen in the PS1 cells. The nuclei in the cells were co-stained with DAPI. This is representative data from two biological repeats. Scale bar = 20 µm.

5.2.2 HaloTag cloning

Due to the limited success of transient transfection, PS1 cells with stable inducible expression of FGFR1-HT were created to isolate a sufficient amount of chromatin to perform successful Halo-ChIP. Primers were designed to amplify the FGFR1-HT construct to use for cloning (Table 2.1). Two template plasmids were used for PCR amplification of FGFR1-HT and confirmation of amplification was demonstrated by a band at ~3,200 bp after agarose gel electrophoresis (Figure 5.3).

The pCK14 plasmid gave a product the correct size (~3,200 bp). Plasmid template only, with no Phusion polymerase enzyme, and water only with no plasmid DNA were used as negative controls. The product from this PCR was used in gateway cloning to create a lentiviral plasmid (see method 2.6.2). During this protocol, clones expressing the construct were selected after the BP and LR clonase recombination reactions to use in further steps. Construct expression was determined after restriction digest with BsrG1, giving two bands on an agarose gel at ~1,500 bp (Figure 5.4).

After the BP recombination reaction, colony 4 was selected as it showed two bands at ~1,500 bp following restriction digest, indicating successful transformation with the FGFR1-HT construct. This was used in the LR recombination reaction. Successful cloning into the pinducer21 plasmid was confirmed in clone 4 and this was used to generate lentiviral particles (Figure 5.4).

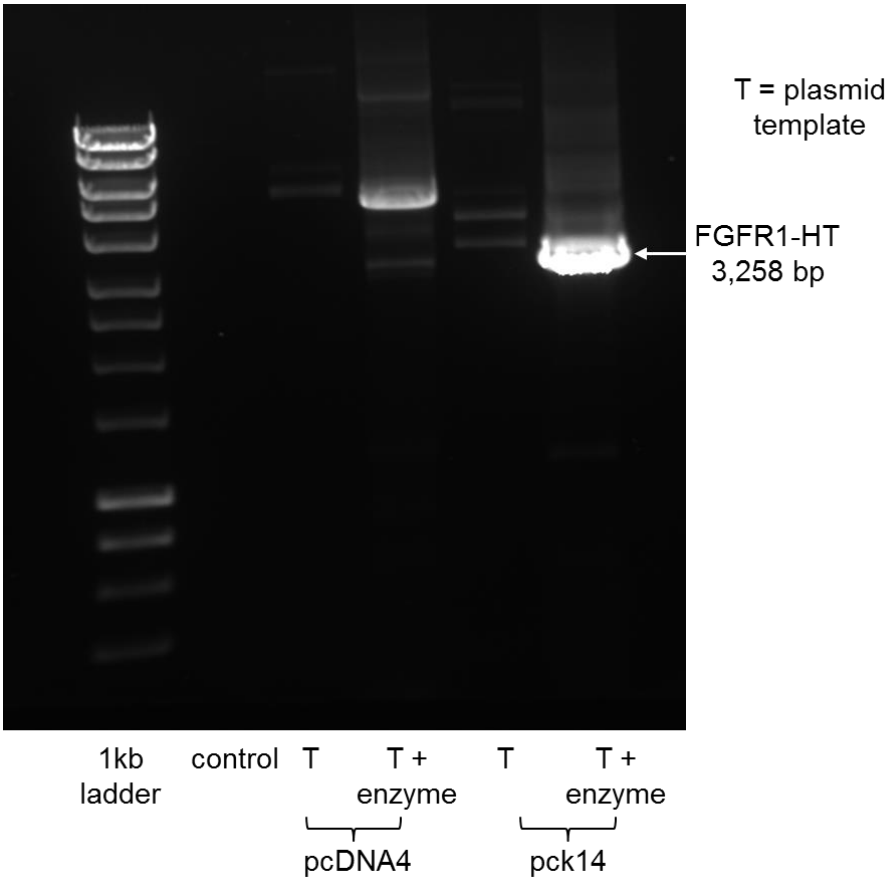

Figure 5.3 Amplification of FGFR1-HT for cloning

PCR was used to amplify the FGFR1-HT construct to use in gateway cloning. Successful PCR was confirmed by running the products on an agarose gel. The construct size was 3,258 bp, as seen in the last lane of the gel and this was performed once (Section 2.5.2).

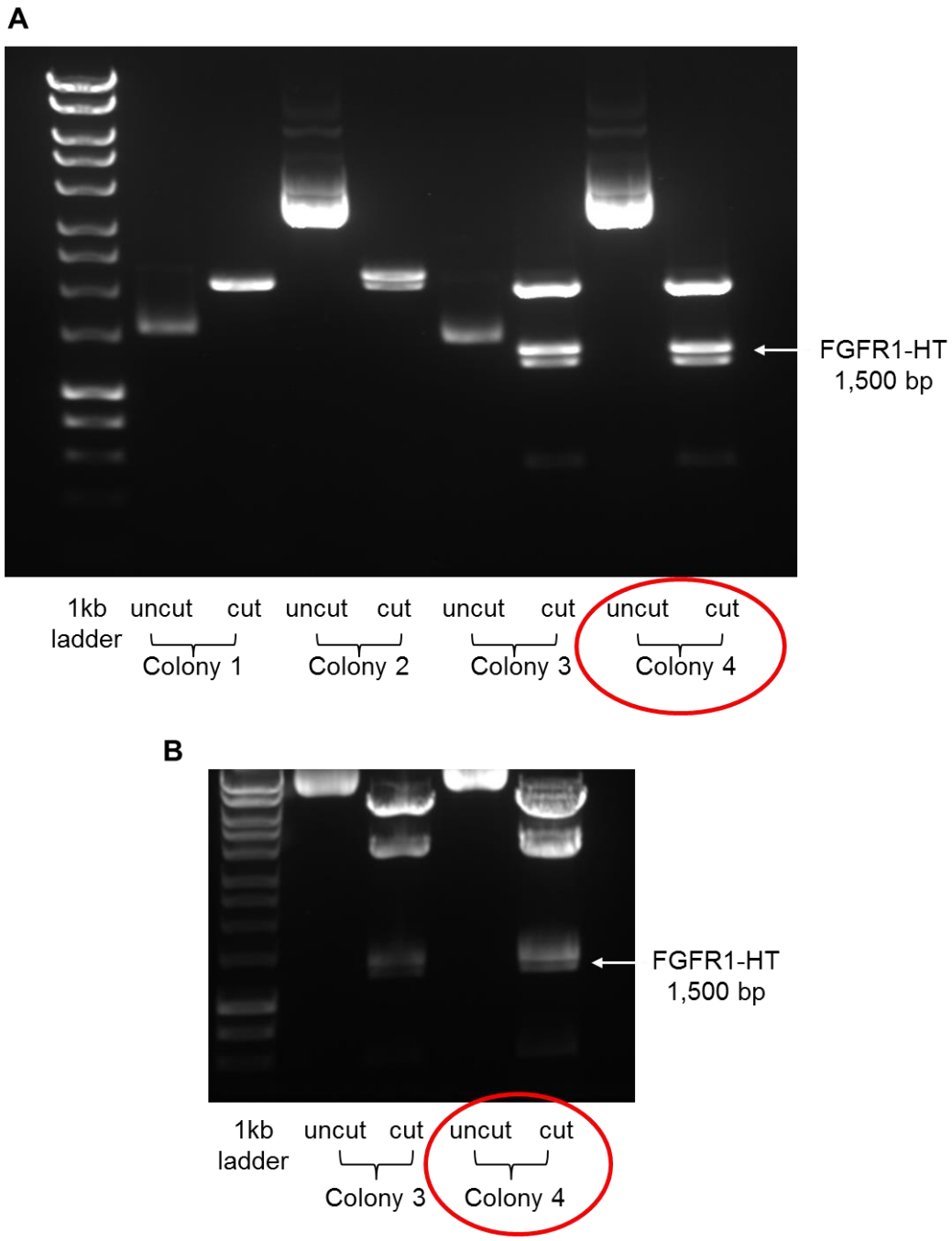

Figure 5.4 Gateway cloning reactions

*During the gateway cloning protocols, bacterial clones harbouring the construct were selected following restriction digest of miniprep DNA with BsrG1 and identification of the FGFR1-HT construct on an agarose gel. BsrG1 cuts in the middle of the construct, giving two bands of around 1,500 bp. Clones were selected after BP (**A**) and LR (**B**) recombination reactions and then sequenced before creating lentivirus (this was performed once, Section 2.5.2 and 2.5.3).*

5.2.3 Lentiviral production

Following gateway cloning of the FGFR1-HT construct into a pinducer21 plasmid, lentiviral particles were made and PS1 cells were infected (see method 2.6.4). Expression of the construct within cells was confirmed by TMR staining following doxycycline (dox) treatment (Figure 5.5). Different concentrations of dox were added to the cells and lysates were taken to check for the expression of the HaloTag protein, as well as the overexpression of FGFR1. A non-doxycycline treated control was included as well as a non-infected PS1 sample as a negative control (Figure 5.6).

These results showed that the PS1 cells transduced with the FGFR1-HT construct and positively selected based on green fluorescent protein (GFP) expression (PS1-HT) could successfully express a tagged FGFR1 construct, induced by the addition of doxycycline.

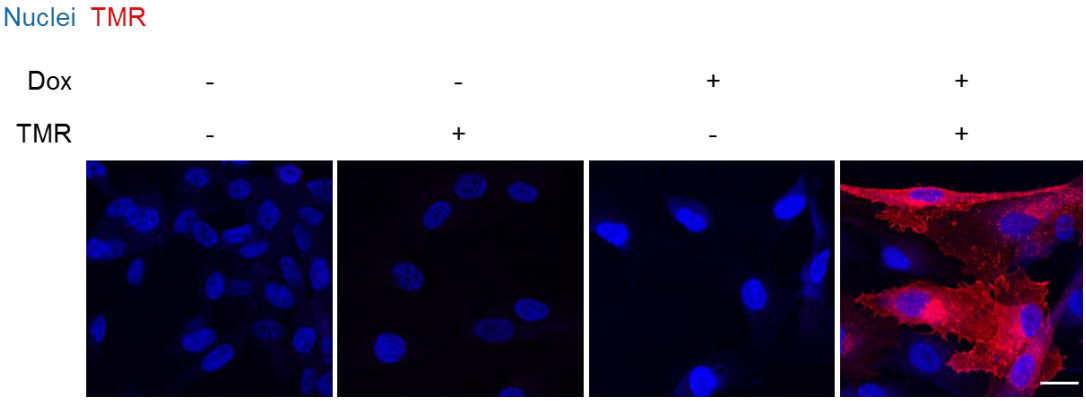

Figure 5.5 Inducible FGFR1-HT expression

Doxycycline (dox) induction of expression of the FGFR1-HT construct was used to check the efficiency of PS1 infection and the generation of the PS1-HT cells. PS1-HT cells were treated with doxycycline or control conditions, 48 hours later the TMR ligand was used to detect HaloTag expression. TMR ligand binding in red demonstrates successful integration and expression of HaloTag within these cells. This is representative data from three biological replicates. Scale bar = 20 µm.

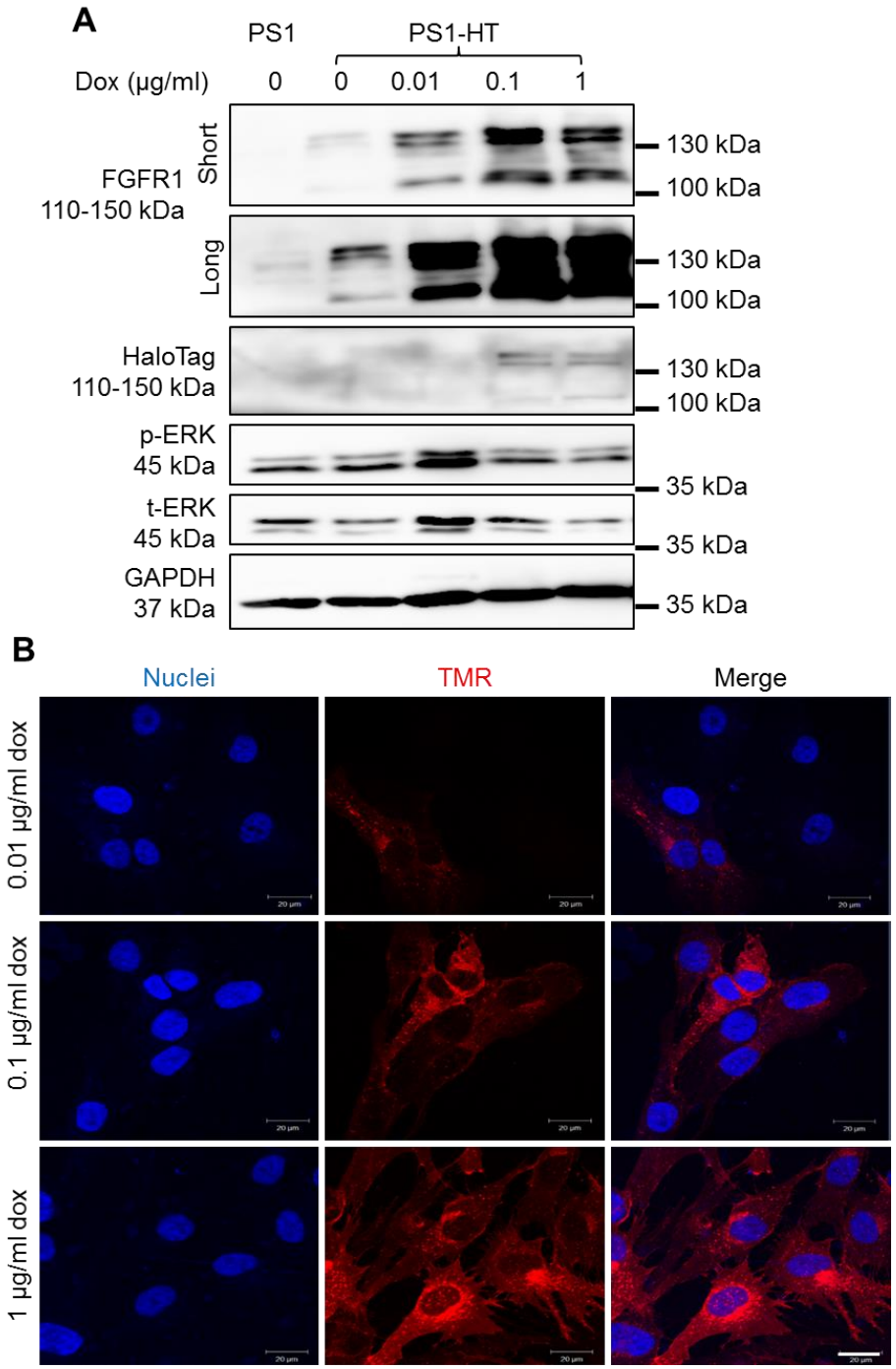

Figure 5.6 Increasing FGFR1-HT expression with increasing concentrations of doxycycline

*PS1-HT cells were treated with increasing concentrations of doxycycline for 48 hours and FGFR1-HT expression was analysed by Western blot (**A**) and immunofluorescent staining (**B**) (Sections 2.3.3 and 2.4). FGFR1 expression was analysed by a long and short Western blot exposure to show both endogenous and exogenous protein. Increasing concentrations of doxycycline (dox) demonstrated increasing expression of FGFR1 and HaloTag. The levels of p-ERK in doxycycline treated cells did not increase with increasing dox concentrations, suggesting that overexpression of FGFR1 was not causing ligand-independent activation of the receptor and downstream signalling pathways. This is data from one biological replicate. Scale bar = 20 µm*

5.2.4 PS1-HT validation

To ensure that the newly generated PS1-HT cells still behaved as a typical stellate cell, immunofluorescence staining for the four stellate cell markers (GFAP, α-SMA, desmin and vimentin) was performed (Figure 5.7). The PS1-HT cells expressed all four of the stellate cell markers. To further confirm that these cells were behaving as PSCs, they were treated daily with ATRA or ethanol vehicle control. After fixing the cells, Oil Red O staining identified the formation of lipid droplets following the ATRA treatment (Figure 5.7).

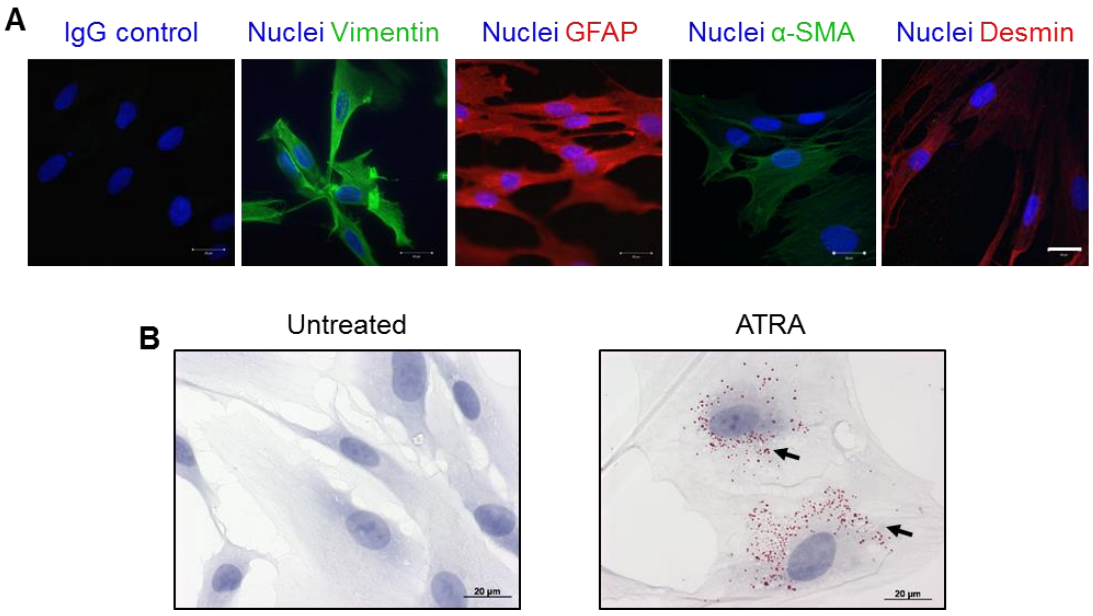

Figure 5.7 PSC characterisation of PS1-HT cells

A. *PS1-HT cells grown on coverslips were fixed and stained for four different stellate cell markers: vimentin, GFAP, α-SMA and desmin (Section 2.3.1). The pictures show positive staining for all the markers, with an unstained negative control. Scale bar = 20 µm.* ***B.*** *PS1-HT cells grown on coverslips were treated daily with either ATRA or ethanol vehicle control. The cells were fixed and stained for lipid droplets using Oil Red O (Section 2.3.2). The ATRA treated cells showed a greater number of lipid droplets than the untreated controls (shown by the arrows). These slides were counter-stained with haematoxylin. These images are representative of at least three technical replicates. Scale bar = 10 µm.*

5.2.5 PS1-HT signalling

To use the dox-inducible PS1-HT cells for Halo-ChIP, I needed to confirm that the exogenous FGFR1-HT construct still behaved and signalled in the same way as endogenous FGFR1.

FGFR1-HT within PS1-HT cells was labelled and tracked using live imaging of TMR ligand on the spinning disk confocal microscope (Figure 5.8). The TMR ligand can be used to accurately follow the FGFR1-HT construct in live PS1 cells. The staining showed that the construct appeared to be localised in vesicles in the cytoplasm, without reaching the plasma membrane or the nucleus.

PS1 cells were treated with FGF2 and immunofluorescence was used to observe the co-localisation of FGFR1 and HaloTag within the cells. When FGFR1-HT expression was induced in the PS1 cells with doxycycline, the presence of the construct was seen by TMR binding. However, the majority of the tagged protein was located in the peri-nuclear region, rather than at the membrane or within the nucleus. Stimulation of the cells with FGF2 did not affect the localisation of FGFR1-HT, or increase p-ERK levels above those seen in endogenous FGFR1 expressing cells, indicating that this construct may not be able to signal effectively (Figure 5.9).

The results demonstrated that FGFR1-HT did not show significant localisation to the plasma membrane or the nucleus, and stimulation with FGF2 did not increase signalling within the cells treated with doxycycline, despite expressing FGFR1 at a much higher level. Therefore, I decided to change from using Halo-ChIP with the PS1-HT cells and focus on performing ChIP-seq with a recently ChIP-validated anti-FGFR1 antibody instead (Baron et al., 2012, Terranova et al., 2015).

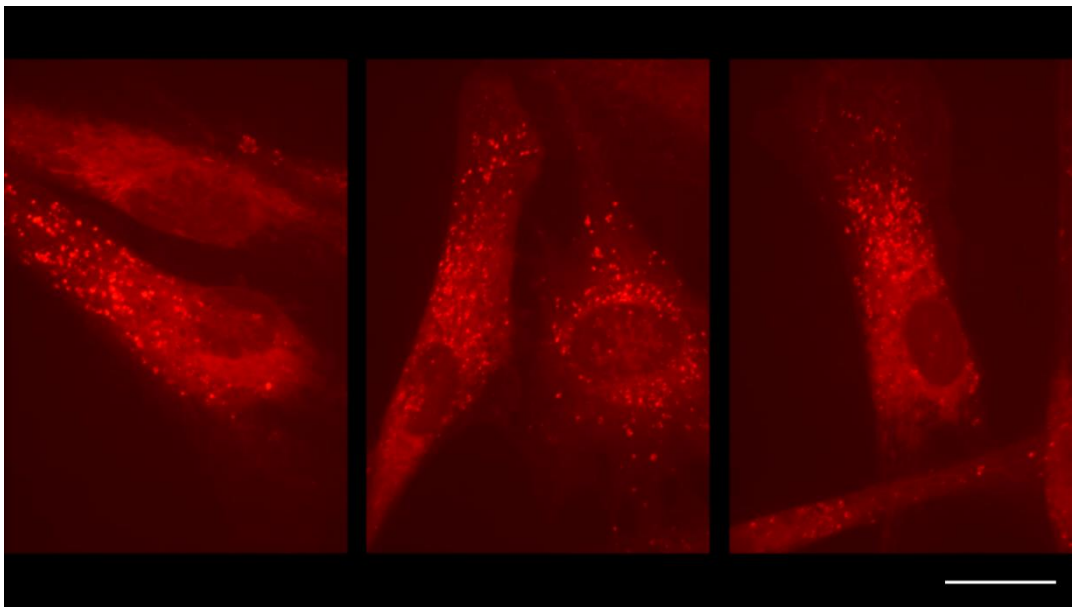

Figure 5.8 Live tracking of FGFR1-HT expression

TMR binding to HaloTag was used to track expression of the FGFR1-HT construct using live imaging of PS1-HT cells. This image taken from the live video shows that FGFR1-HT can be found in vesicles within the stellate cells, however there was no clear staining at the plasma membrane or in the nucleus of the cells. This is representative data from two biological replicates. Scale bar = 20 µm.

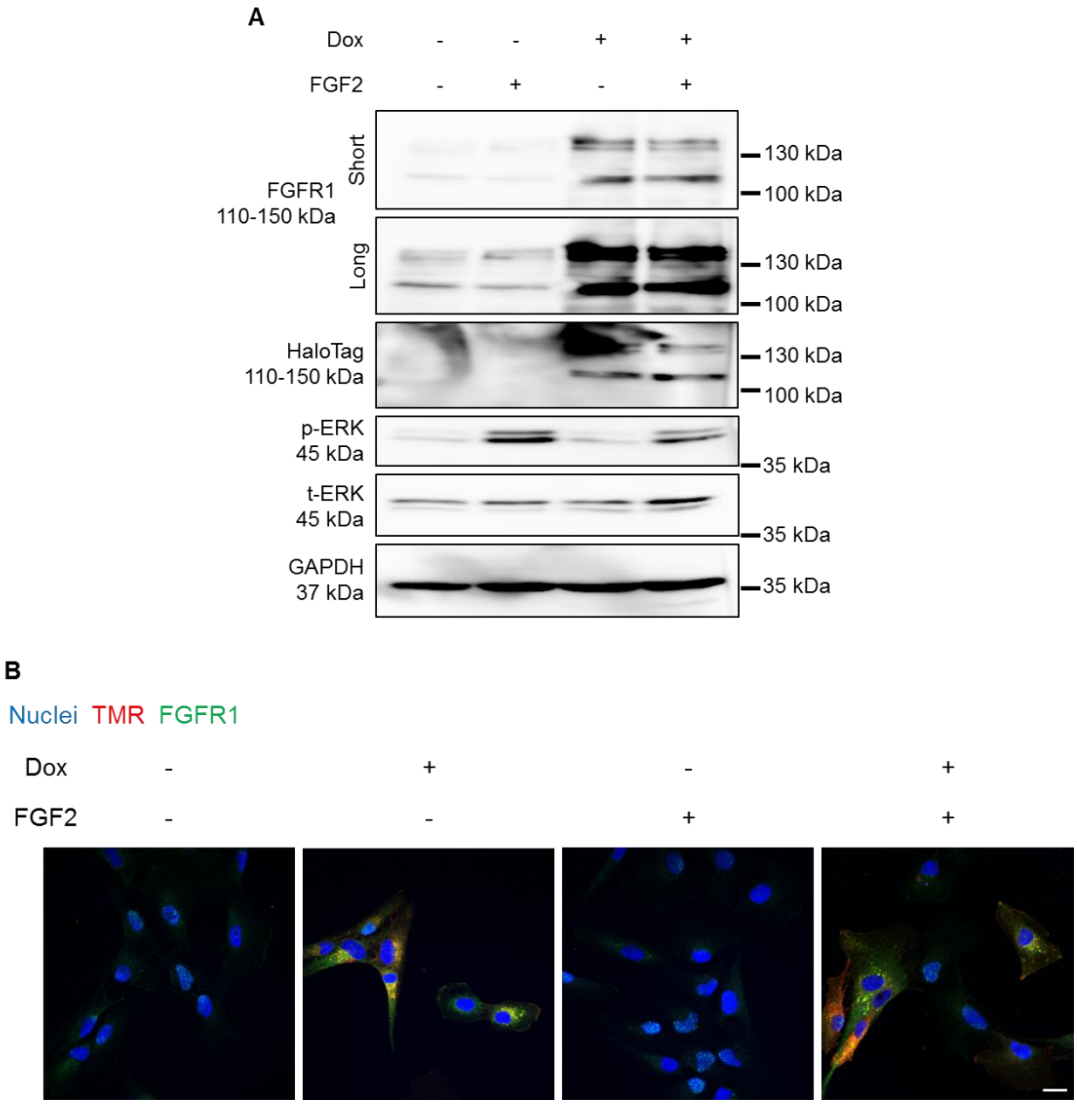

Figure 5.9 Functionality of FGFR1-HT construct

To determine whether FGFR1-HT was signalling and trafficking within the stellate cells as expected, expression was induced and FGF2 stimulation was performed, compared to relevant controls (Section 2.1.3). ***A.*** *Upon doxycycline induction, FGFR1-HT was overexpressed and the HaloTag could be detected. However, there was no significant increase in p-ERK signalling upon 100 ng/ml FGF2 stimulation for 15 minutes in the cells overexpressing the receptor.* ***B.*** *TMR ligand binding confirmed HaloTag co-localisation with FGFR1 in cells treated with doxycycline. However, this was not detected in the nuclei of the cells, even when stimulated with 100 ng/ml FGF2 for 15 minutes. This is data from one biological replicate. Scale bar = 20 µm.*

5.3 Nuclear FGFR1

5.3.1 Introduction

Chromatin immunoprecipitation is a method that can be used to determine where specific proteins are interacting with the DNA or to detect epigenetic regulation of gene expression. This method was originally used to look at protein-DNA interaction in bacteria in the 1980s (Gilmour and Lis, 1984), before moving on to *Drosophila* (Gilmour et al., 1986) and subsequently histone acetylation in chicken nuclei (Hebbes et al., 1988, Solomon et al., 1988). ChIP has now been used to study chromatin remodelling and gene expression in many different cell types.

The role of nuclear FGFR1 has been studied using ChIP in neuronal cells (Stachowiak and Stachowiak, 2016), showing that nFGFR1 regulates a transcriptional programme triggering neuronal cell differentiation and migration. This not only supports the possible role of nFGFR1 in transcriptional regulation but also provides validation for using the ChIP-grade ab10646 FGFR1 antibody in ChIP-seq experiments.

5.3.2 ChIP method optimisation

A key challenge in successful ChIP is efficient chromatin harvesting and processing, and the most effective method must be validated for each different cell type. There are two methods for isolating chromatin: cross-linked ChIP (XChIP) or native ChIP (NChIP) (Table 5.1) (Carey et al., 2009, O'Neill and Turner, 2003, Orlando, 2000). In X-ChIP, formaldehyde is usually used to fix the chromatin. A nucleophilic group on an amino acid or DNA forms a covalent bond with formaldehyde, giving a methylol adduct that can be converted to a Schiff base. This is then stabilised by bonding with

another functional group to form a methylene bridge, which is achieved when quenching with glycine in ChIP assays, or by bonding with another macromolecule that is in close proximity. Due to the small size of formaldehyde, it will form bonds between groups that are ~2Ã apart making it useful to study molecules that are interacting. Formaldehyde is most reactive against available lysine residues (which are common mediators of interactions with DNA) and deoxyguanosine. Reversal of cross-links is usually performed by heating the sample (Hoffman et al., 2015). Given that FGFR1 is a potential transcription factor, XChIP was used to allow random shearing of DNA during sonication, rather than the digestion of linker DNA by micrococcal nucleases in NChIP, reducing bias in the results.

Table 5.1 Methods of chromatin isolation

	Cross-linked (XChIP)	Native ChIP (NChIP)
Process	Cells are fixed with formaldehyde, which cross-links protein to the DNA. The DNA is sheared by sonication into small random fragments. The chromatin must be kept cool throughout the process of sonication to prevent protein denaturation	DNA is sheared using micrococcal nuclease digestion of the linker DNA around nucleosomes. This will give defined small fragments
Useful for	Examining where proteins bind to DNA	Histone modification and epigenetic gene regulation
Advantage	Less bias, as the fragmentation is random during sonication	Can be used for proteins that may be disrupted by the fixing with formaldehyde
Disadvantage	Optimise fixing and sonication for each cell line. Must determine that the fragment sizes are correct following sonication (100-1,000 bp), which takes more time	Results may be biased, as the enzymes will cut the DNA at specific locations on the genome

Three different methods of chromatin isolation were tested. The first was based on an Active Motif kit that was being used by another group within our institute, the second was a Millipore kit that had been used by a previous PhD student and the third was a protocol from another group currently performing ChIP. For each protocol, the time of formaldehyde fixation and the number of sonication cycles needed to be optimised.

5.3.3 Chromatin isolation

For successful ChIP-seq, a large amount of chromatin is required. Therefore these experiments were begun using 20 million cells per condition. PS1 cell fixation was optimal using formaldehyde for 5 minutes at room temperature, followed by sonication at 20 cycles in the bioruptor sonicator or 10 cycles in the bioruptor pico sonicator, 30 seconds ON and 30 seconds OFF (Figures 5.10 and 5.11). If the sonication was not optimal for a sample, it was re-sonicated for 5 more cycles (Figure 5.12). Once sufficient fragmentation of each sample was achieved, the samples were immunoprecipitated using the FGFR1 ChIP-validated antibody and then DNA was extracted. Qubit was used to quantity the DNA (Table 5.2) and samples were sent to Oxford Genomics for library preparation and sequencing.

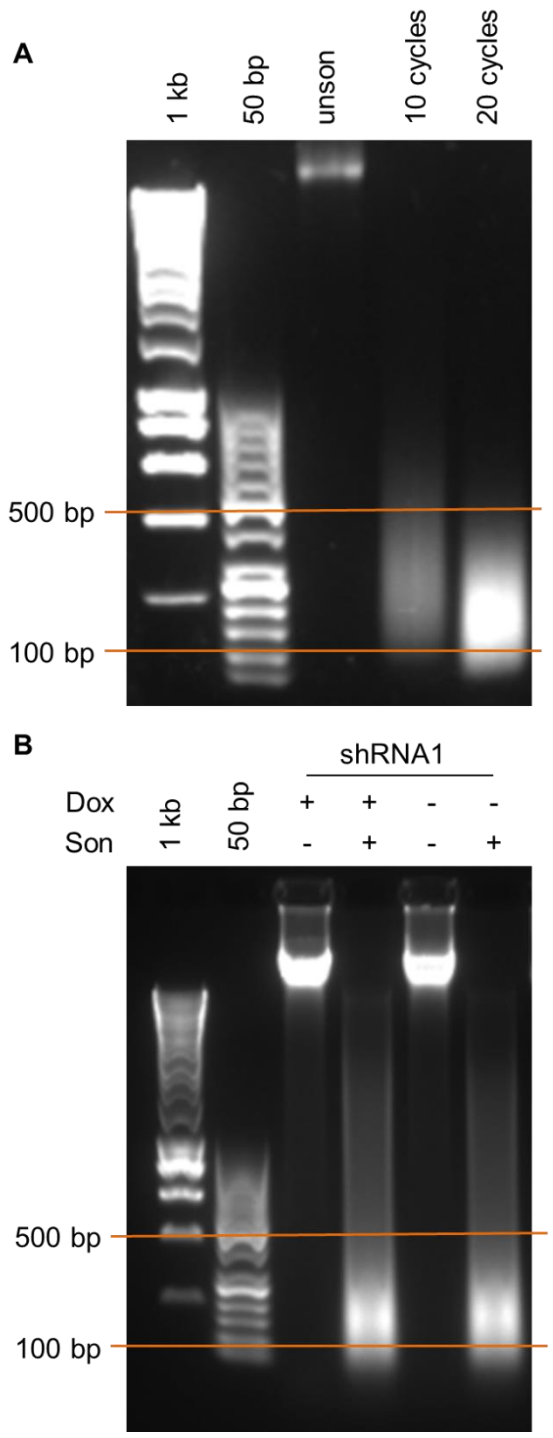

Figure 5.10 PS1 chromatin isolation and sonication optimisation

*Chromatin isolation and sonication (Son) was optimised using two different sonicators. The acceptable range of fragments is 100-500 bp, with 100-300 bp being optimal. The first Bioruptor sonicator demonstrated 20 cycles of 30 seconds ON, 30 seconds OFF as the most efficient conditions, shown by a bright tight band of fragmented chromatin in the desired range (**A**). When using the Bioruptor pico sonicator, 10 cycles was used as a standard initial sonication, giving fragments in the desired range for shRNA1 samples tested (**B**). Unsonicated chromatin for each sample was included as a control. This data is representative of one biological replicate.*

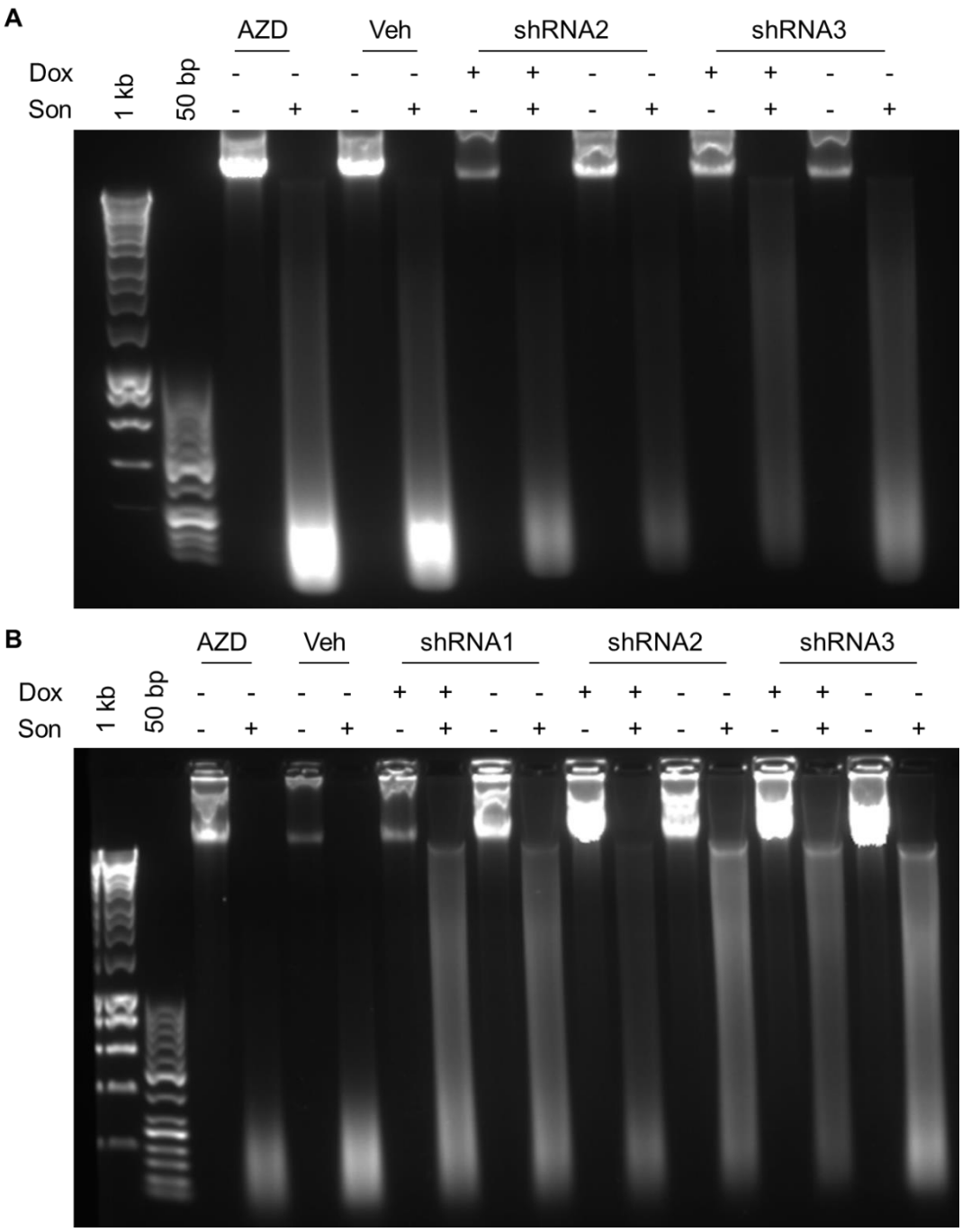

Figure 5.11 ChIP-seq chromatin sonication quality check

*Chromatin shearing following sonication (Son) from samples processed for ChIP-seq, AZD4547 (AZD), vehicle (Veh) or shRNA cells, from two different biological replicates (shown in **A** and **B**). The sonication was not optimal for the shRNA1, shRNA2 and shRNA3 cells in repeat 2 (**B**), therefore these samples were sonicated for another five cycles (Figure 5.12). Unsonicated chromatin for each sample was included as a control.*

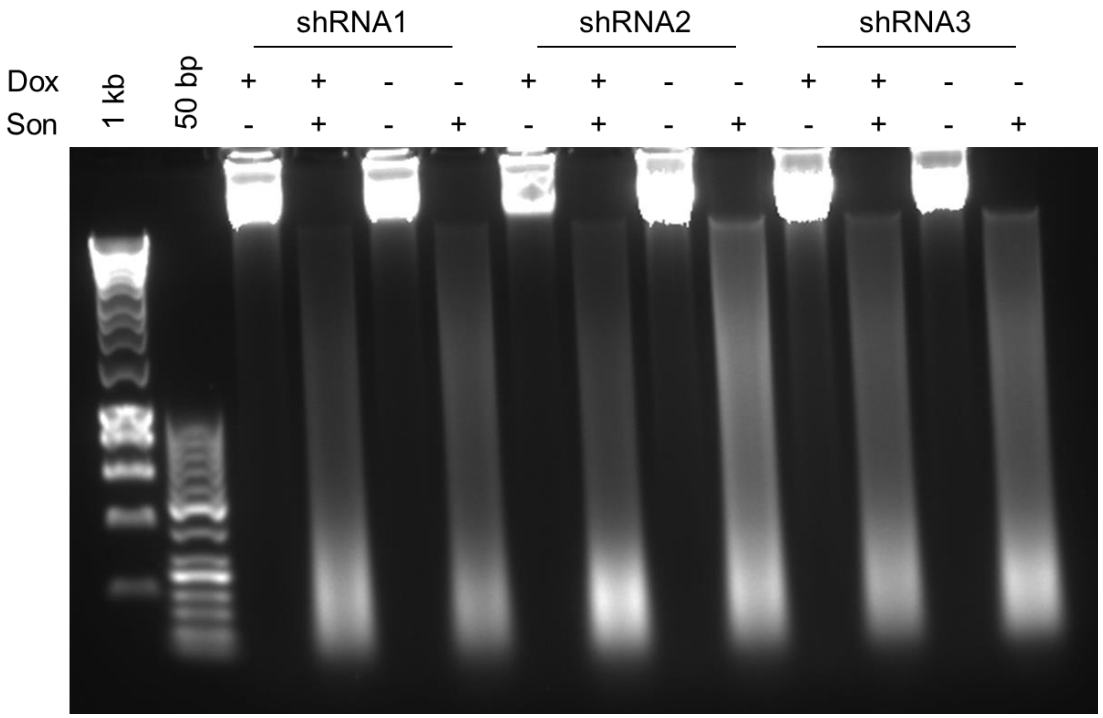

Figure 5.12 ChIP-seq chromatin sonication quality check (15 cycles)

Chromatin shearing following sonication (Son) from samples from the second biological replicate processed for a further 5 cycles (Figure 5.11). Chromatin fragmentation was now producing brighter bands at the required size and therefore these samples were processed for ChIP-seq. Unsonicated chromatin for each sample was included as a control.

Table 5.2 Qubit DNA concentrations of ChIP-seq samples

Sample	DNA concentration (ng/μl)
AZD rep 1	0.124
Vehicle rep 1	too low
shRNA1 + dox rep 1	0.644
shRNA1 - dox rep 1	0.492
shRNA2 + dox rep 1	0.248
shRNA2 - dox rep 1	0.35
shRNA3 + dox rep 1	0.416
shRNA3 - dox rep 1	0.654
AZD rep 2	0.296
Vehicle rep 2	too low
shRNA1 + dox rep 2	0.752
shRNA1 - dox rep 2	0.406
shRNA2 + dox rep 2	0.834
shRNA2 - dox rep 2	0.382
shRNA3 + dox rep 2	3.32
shRNA3 – dox rep 2	0.306

5.3.4 ChIP-seq analysis

Results from the ChIP-seq experiments were analysed bioinformatically in collaboration with two post-doctoral researchers within the Institute, Dr Firat Uyulur and Dr James Heward. The raw sequences were aligned to the human genome (hs37d5), the reads were mapped and peaks were called using the MACS2 programme (Tables 5.3 and 5.4). The peaks were called against a relevant input control sample, where no enrichment using the FGFR1 antibody was performed. Differential peaks were analysed using the diffBind tool (Section 2.7). After looking at the peak enrichment and following data from the 3D models, shRNA1 was eliminated from the analysis due to very limited peaks and no statistically significant reduction in invasion with these cells (Figure 4.8).

Firstly, the number of enriched peaks in the two vehicle samples was analysed to select the most reliable peaks relating to FGFR1 binding (Figure 5.13). Known blacklist regions, such as satellite regions, were removed from the data, giving 143 common peaks between the two samples. These peaks were also related to the control shRNA samples. Most of the samples overlapped with the vehicle peaks, apart from shRNA3 – dox repeat 2. This could be due to the wide difference in the number of peaks called between the samples (Table 5.4).

Comparison of the enriched peaks in the control samples with either the relevant drug-treated or FGFR1 knockdown samples was then performed. Heat maps (Figure 5.14) show that comparing the 143 vehicle overlap peaks with shRNA2 – dox samples indicates many overlapping regions surrounding transcription start sites. However, if these 143 peaks are compared to shRNA2 + dox, where FGFR1 has been knocked down, there are fewer overlapping regions shown by the lighter heat map colours.

This looks similar but slightly less striking if all the peaks found in vehicle repeat 2 are compared to the two shRNA2 samples. There was a stronger correlation in the overlapped vehicle samples compared to the peaks enriched in vehicle repeat 2, suggesting many of these peaks may be background noise.

Peaks enriched in control samples, compared to the relevant knockdown or treatment sample, were also compared. Overlapping enriched peaks from both shRNA2 and shRNA3, with or without doxycycline treatment, were combined with enriched peaks in vehicle samples, compared to relevant AZD4547 treated samples. This combined list of enriched peaks was then analysed using STRING to discover any networks of pathways that may be changing upon FGFR1 binding to DNA. Some networks emerged from this analysis (Figure 5.15) and interesting pathways, such as Hippo signalling, appeared to be changing between conditions (Table 5.5). These results will need to be put into context regarding relevant interactions and pathways related to the phenotype seen with FGFR inhibition or knockdown. Further analysis is ongoing and peaks will be validated by ChIP-PCR with FGFR1 and relevant IgG control antibodies. Hits will also be confirmed by phenotypic assays, such as the siRNA-mediated knockdown in the spheroid assay (Appendix 3.1 and Section 2.6.2) or changes in gene expression of targets in PSCs upon FGFR1 inhibition or knockdown (Section 2.5.5).

Table 5.3 Number of mapped reads

Sample	Number of uniquely mapped reads
Vehicle input	64 million
AZD rep 1	49 million
AZD rep 2	46 million
Vehicle rep 1	20 million
Vehicle rep 2	29 million
shRNA input	78 million
shRNA1 + dox rep 1	46 million
shRNA1 - dox rep 1	60 million
shRNA1 + dox rep 2	56 million
shRNA1 - dox rep 2	52 million
shRNA2 + dox rep 1	64 million
shRNA2 - dox rep 1	40 million
shRNA2 + dox rep 2	43 million
shRNA2 - dox rep 2	15 million
shRNA3 + dox rep 1	55 million
shRNA3 - dox rep 1	18 million
shRNA3 + dox rep 2	47 million
shRNA3 - dox rep 2	49 million

Table 5.4 Number of peaks called

Sample	Number of peaks called (q<0.01)
Vehicle input	39
AZD rep 1	398
AZD rep 2	143
Vehicle rep 1	1640
Vehicle rep 2	112
shRNA input	51
shRNA1 + dox rep 1	29
shRNA1 - dox rep 1	98
shRNA1 + dox rep 2	91
shRNA1 - dox rep 2	14025
shRNA2 + dox rep 1	1763
shRNA2 - dox rep 1	8741
shRNA2 + dox rep 2	9
shRNA2 - dox rep 2	68593
shRNA3 + dox rep 1	2048
shRNA3 - dox rep 1	29
shRNA3 + dox rep 2	39
shRNA3 - dox rep 2	398

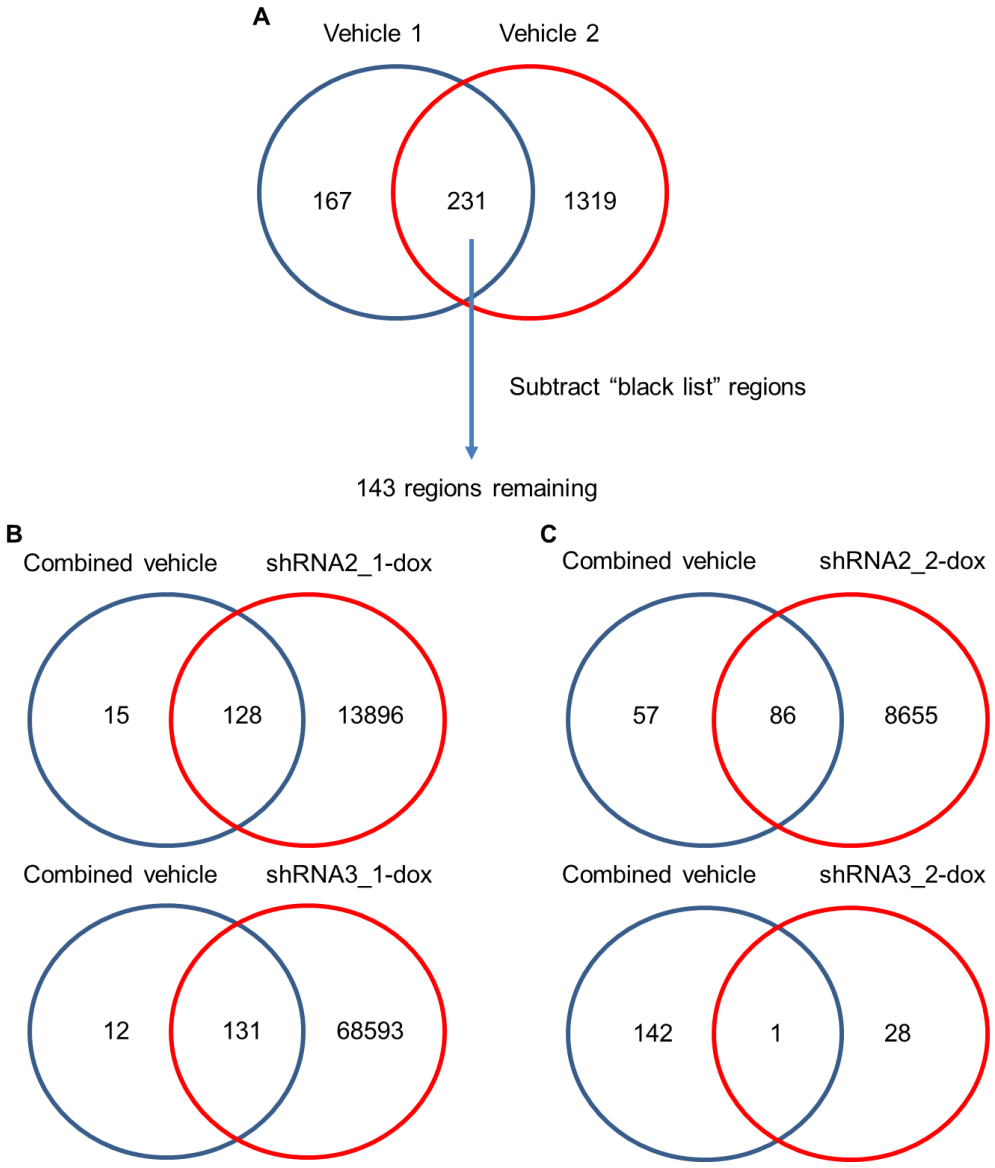

Figure 5.13 Overlap of enriched peaks between control samples

*The enriched peaks in the two biological replicates of the vehicle control samples were compared and had 231 peaks overlapping (**A**). Following this, known blacklist regions were removed, such as satellite regions, leaving 143 common peaks. These were then compared to the enriched peaks in both biological replicates from the shRNA2 (**B**) and shRNA3 (**C**) control samples. Most of the samples had a good overlap of peaks, apart from shRNA3 repeat 2 (shRNA3_2-dox).*

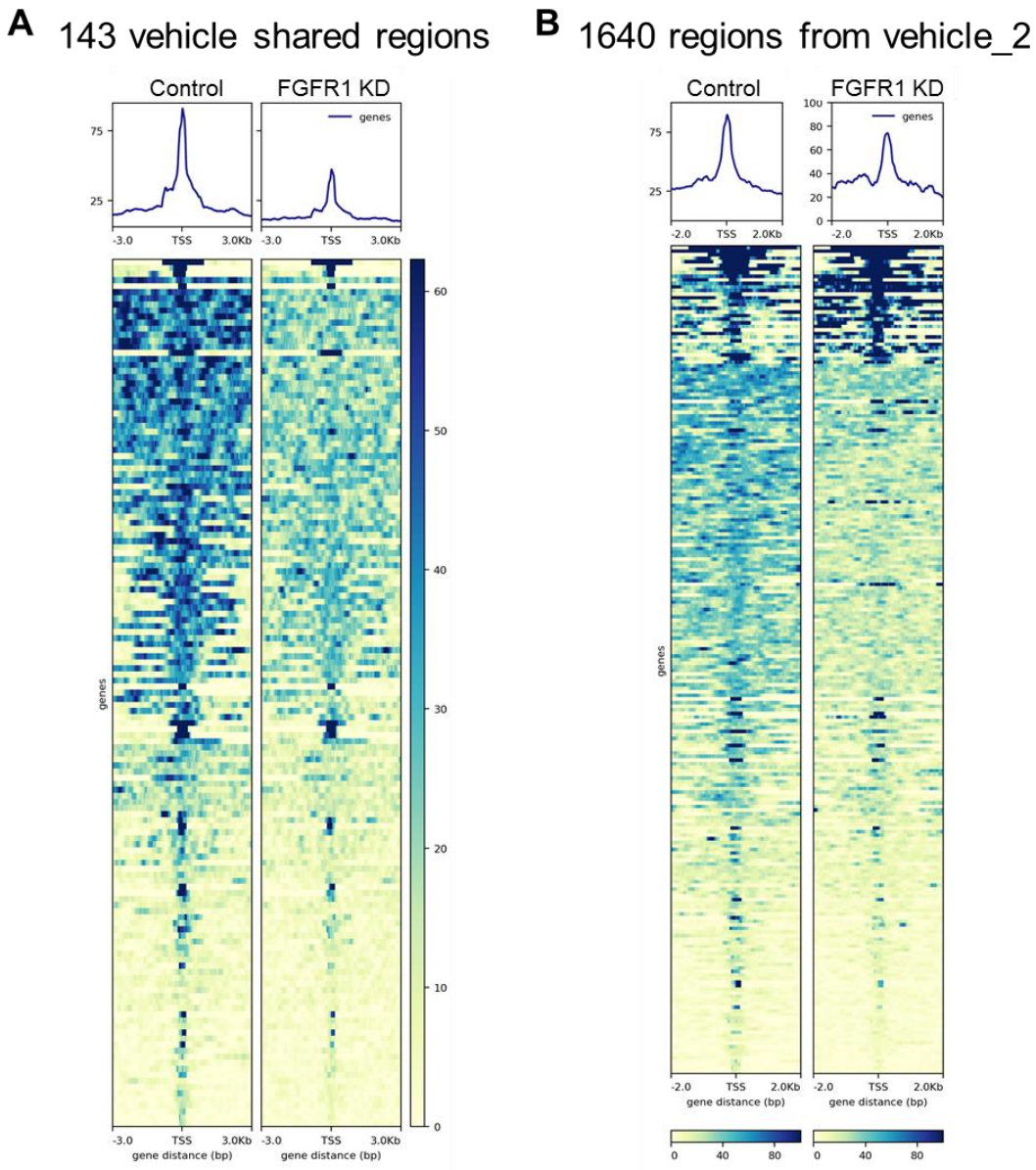

Figure 5.14 Peaks enriched in control samples are consistent

*Heat maps showing the correlation between peaks present in the combined vehicle (**A**) and vehicle repeat 2 (**B**) samples with shRNA2 samples. The left heat map in each set is the shRNA2 control sample, showing a high correlation of peaks in these expected regions, compared to the FGFR1 knockdown sample on the right.*

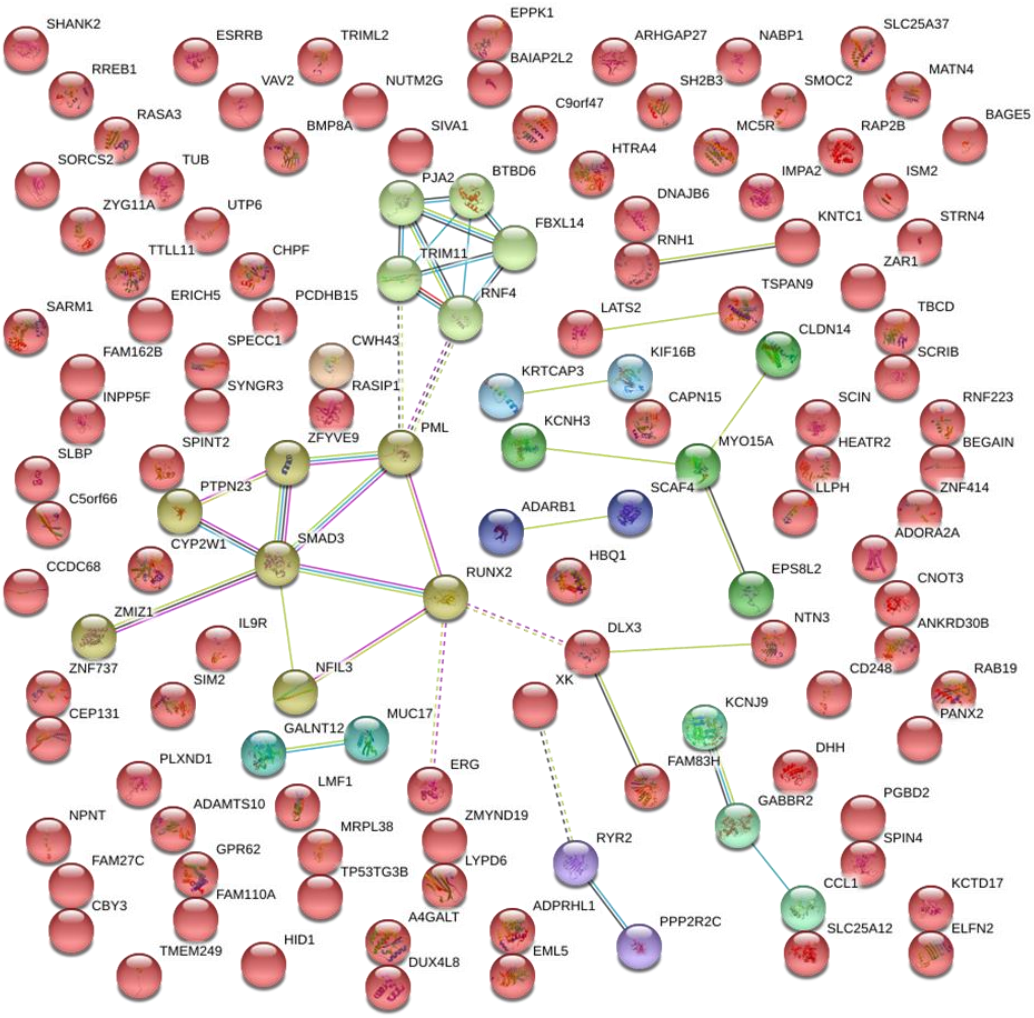

Figure 5.15 Networks of enriched peaks

STRING was used to examine any networks significantly enriched within the peaks from both the shRNA and AZD4547 treated samples in both biological replicates. Many hits were not linked, however a few networks did begin to emerge from this analysis, such as ubiquitination, proteasome and Hippo signalling pathways (Table 5.5).

Table 5.5 Enriched pathways in combined peaks from FGFR inhibitor and FGFR1 knockdown samples

Enriched pathways
Hippo signalling pathway
E3:Ub:substrate
Biochemical Reaction: Transfer of Ub from E2 to substrate and release of E2
Biochemical Reaction: Polyubiquitination of substrate
Catalysis
Complex: Ag-substrate:E3:E2:Ub
Antigen processing: Ubiquitination & Proteasome degradation
Control
Complex Assembly

5.3.5 Future ChIP-seq analysis

The hits identified from the ChIP-seq analysis need to be validated. Firstly, FGFR1 binding to these regions will be confirmed using ChIP-PCR. Functional validation of the top hits and pathways will then be performed using an siRNA-mediated knockdown screen in the co-culture *in vitro* spheroid model (Section 2.7.2).

5.4 PSC FGF signalling flux

To show FGFR1 moving between the sub-cellular compartments within the stellate cells, mass spectrometry was performed. Given that it is difficult to get enough protein from different sub-cellular compartments of stellate cells to analyse on Western blot, as well as inconsistent specificity of antibodies, mass spectrometry can offer a more sensitive approach (Aebersold and Mann, 2003, Diamandis, 2004, Ghaemmaghami et al., 2003). Additionally, mass spectrometry allowed me to analyse all of the different peptides changing within the stellate cells following FGFR inhibition, giving an indication of the role of nFGFR1 and FGFR signalling in general.

5.4.1 Sub-cellular fractionation

Two experimental approaches were tested. Stellate cells were either treated with AZD4547 compared to vehicle control or serum-starved overnight and then stimulated for 15 minutes with FGF2 compared to unstimulated control. The cells were then harvested and fractionated into four different sub-cellular fractions (nucleus, cytoplasm, intracellular organelles and plasma membrane). Each fraction was prepared for mass spectrometry and labelled with a different Tandem Mass Tag (TMT) (Section 2.8).

TMT isobaric mass tags methodology was first described in 2003 (Thompson et al., 2003). Work then progressed to increase the number of labels that could be used within a single experiment. A 6-plex of mass tags was used to analyse protein mixtures within human cerebrospinal fluid samples, validating the method for quantitative proteomic studies (Dayon et al., 2008). These tags have four regions, a mass reporter region (M), a cleavable linker (F), a mass normalisation region (N) and a protein reactive group (R). The structures of the TMT reagents are the same but they contain different combinations of ^{13}C and ^{15}N isotopes in the mass reporter and balancer group to give different isobaric mass tags. This creates a specific reporter ion at m/z 126, 127, 128, 129, 130 and 131 (Figure 5.16). These can be detected during analysis to assign peptides to specific groups within a single experiment (Rauniyar and Yates, 2014).

The samples were run to compare peptide localisation between the conditions, compared to a whole cell lysate of the relevant condition and basal PS1 control sample, which was the same across the four conditions (Section 2.8). The results were run and analysed by Dr Faraz Mardakheh (Barts Cancer Institute). Following analysis, the efficiency of the fractionation was confirmed (Figure 5.17). Sub-cellular fractionation appeared specific, with histone peptides enriched in the nuclear fraction and tetraspanin peptides enriched in the plasma membrane fraction (Figure 5.17).

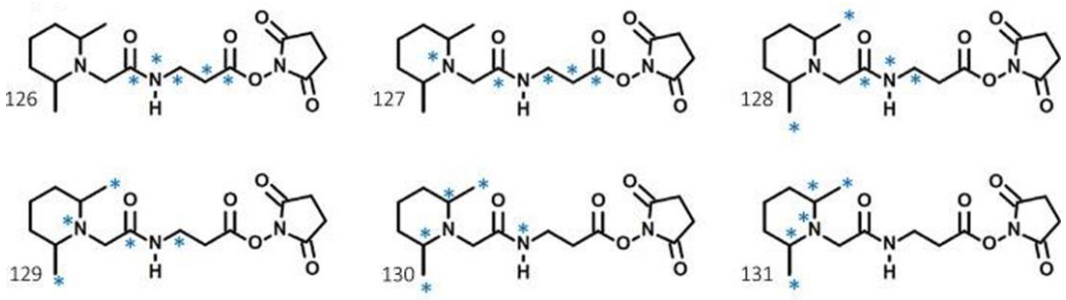

Figure 5.16 Chemical structure of TMT sixplex reagents

TMT tags are isobaric with a different distribution of isotopes between the reporter and balance groups. Blue asterisks show the positions of ^{13}C *and* ^{15}N *isotopes to create the six different tags: 126, 127, 128, 129, 130 and 131* (Rauniyar and Yates, 2014).

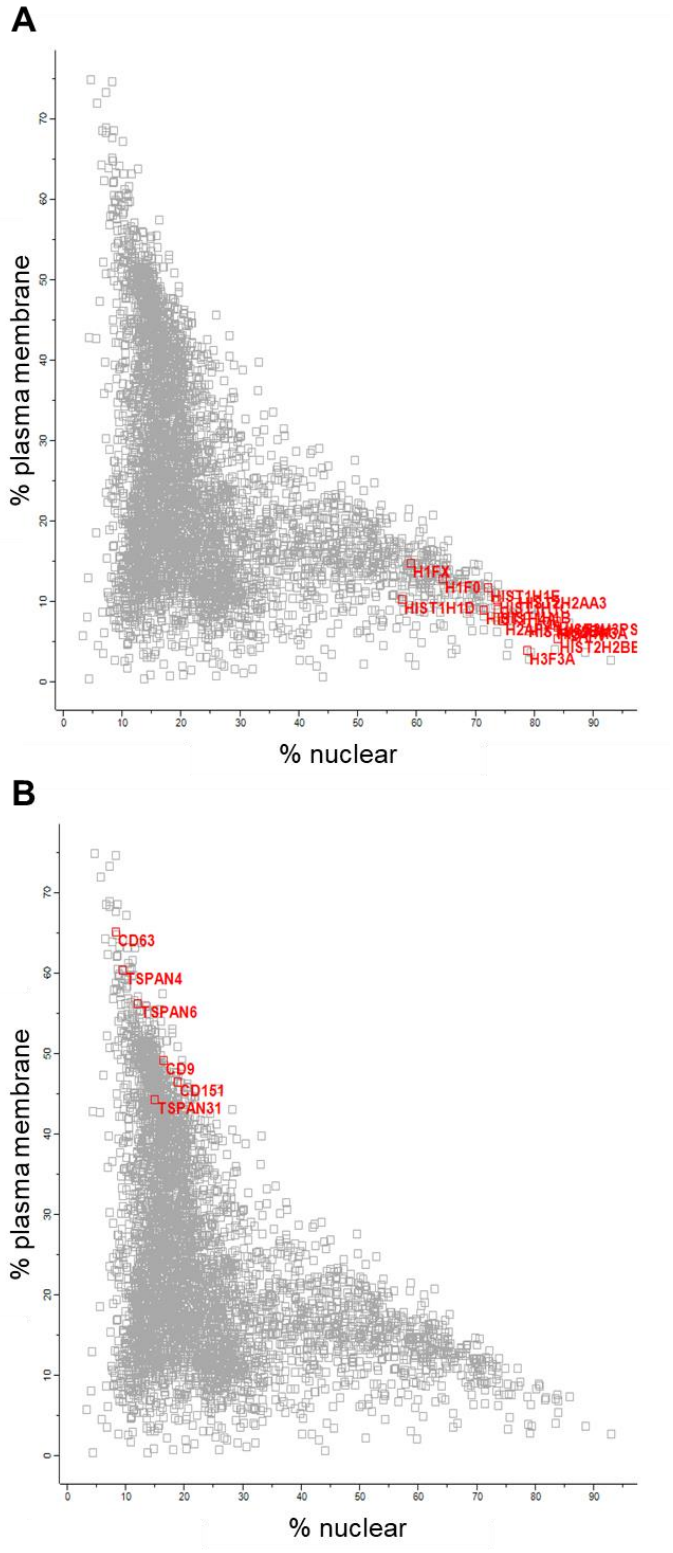

Figure 5.17 Efficient sub-cellular fractionation of PSCs

*The efficiency of sub-cellular fraction of the samples was confirmed by looking for the location of control peptides. Histone peptides were enriched in the nuclear fraction compared to other sub-cellular compartments, such as the plasma membrane (**A**), whereas tetraspanin membrane-bound peptides were enriched in the plasma membrane fraction, compared to other sub-cellular compartments, such as the nucleus (**B**), as expected. This data is from one biological replicate.*

5.4.2 FGFR1 localisation

Unfortunately, following the mass spectrometry analysis, only one peptide of FGFR1 was detected in the vehicle control sample. No FGFR1 peptides were detected in the AZD4547, unstimulated or stimulated samples. This could be due to the abundance of the peptides within the sample. Within the field, there is some controversy over whether the detection level for mass spectrometry is better in label-free or labelled methods, although quantitation of peptides is more reliable in labelled methods (Li et al., 2012, Megger et al., 2014, Patel et al., 2009). The detection level can drop as the number of multiplexed labels is increased. However, a study comparing sixplex and duplex TMT labelling showed that both methods had unique peptides identified from the same original sample (Rauniyar et al., 2013). This highlights the fact that the labelling efficiency and analysis can vary from experiment to experiment, making it harder to reliably identify low abundance peptides. Moreover, these peptides are more likely to be lost due to noise generated in the reporter ion region and from partially modified peptides (Beer et al., 2017a). Even though FGFR1 could not be detected, there was a significant change in total peptide levels and peptide flux upon AZD4547 treatment, which could highlight key mechanisms of invasion related to FGFR signalling in stellate cells.

5.4.3 Total peptide changes

Following analysis of the whole cell lysate samples from each condition, there were no significant changes between the unstimulated and stimulated samples (Figure 5.18). This could be due to the quick timeframe of stimulation before harvesting (only 15 minutes), therefore these samples were discarded from the analysis. Additionally, it has been shown that stimulation with high concentrations of FGF2 (100 ng/ml) can lead to ineffective phosphorylation of FRS2 and only transient activation of

downstream signalling pathways, which could explain the low number of changes between these two samples (Zhu et al., 2010). Excitingly however, there were pathways identified that significantly increased or decreased upon 24 hours of AZD4547 treatment (Table 5.6). The most significant peptide changes were determined using a cut-off value of two log2fold change between the conditions (Figure 5.19). The most significantly altered peptides were also analysed using STRING to form networks (Figure 5.20). These data highlighted some key peptides involved in cell migration and motility or FGF signalling regulation being altered upon AZD4547 treatment. We are currently validating three hits in the laboratory; MARCKSL1, FHOD1 and GPX1.

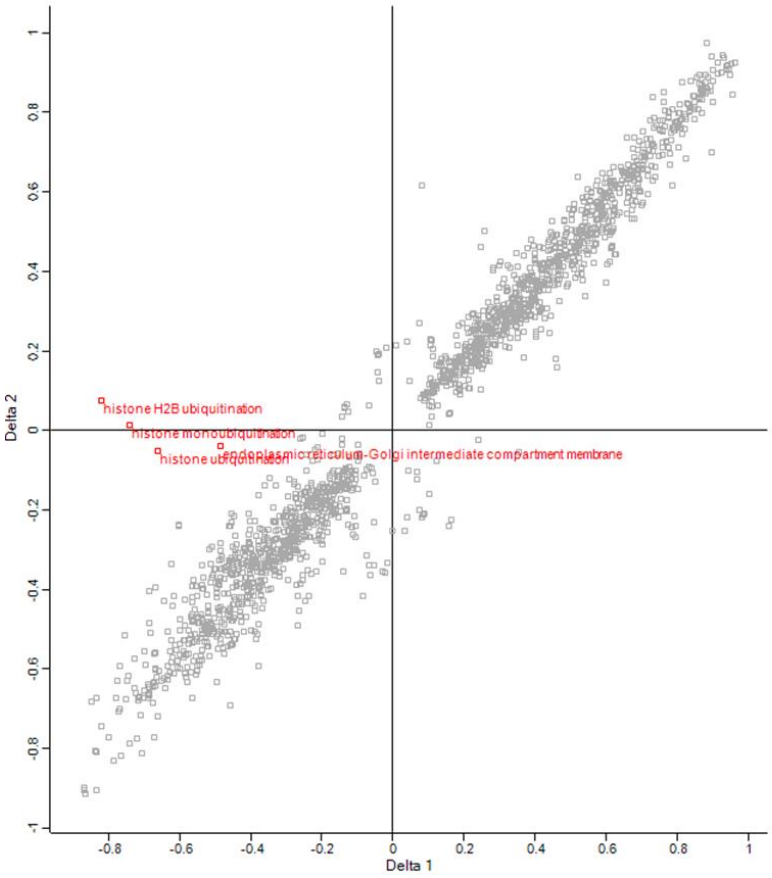

Figure 5.18 Expression of peptides in FGF2 stimulated samples

The expression of peptides between PSCs stimulated with FGF2 was correlated with the control unstimulated sample (Sections 2.1.3 and 2.8). This shows that stimulation with 100 ng/ml FGF2 for 15 minutes was not long enough to see significant proteomic changes. This data is from one biological replicate.

Table 5.6 Enriched pathways in whole cell lysate mass spectrometry data

Enriched pathways	N: Peptides	N: Score	p value
Increased in AZD treated cells			
Cellular macromolecular complex subunit organization	277	0.183377	3.62E-07
Translational termination	77	0.275821	3.35E-05
Viral transcription	76	0.269749	5.54E-05
Translational elongation	83	0.256801	6.15E-05
Protein targeting to ER	99	0.233161	7.35E-05
Ribosome	77	0.250964	0.00016
Nucleus	1098	0.077686	0.000174
Reduced in AZD treated cells			
Leucine-rich repeat	34	-0.36857	0.000211
Membrane	1375	-0.0719	0.000232
Mitochondrion	505	-0.12825	3.40E-06

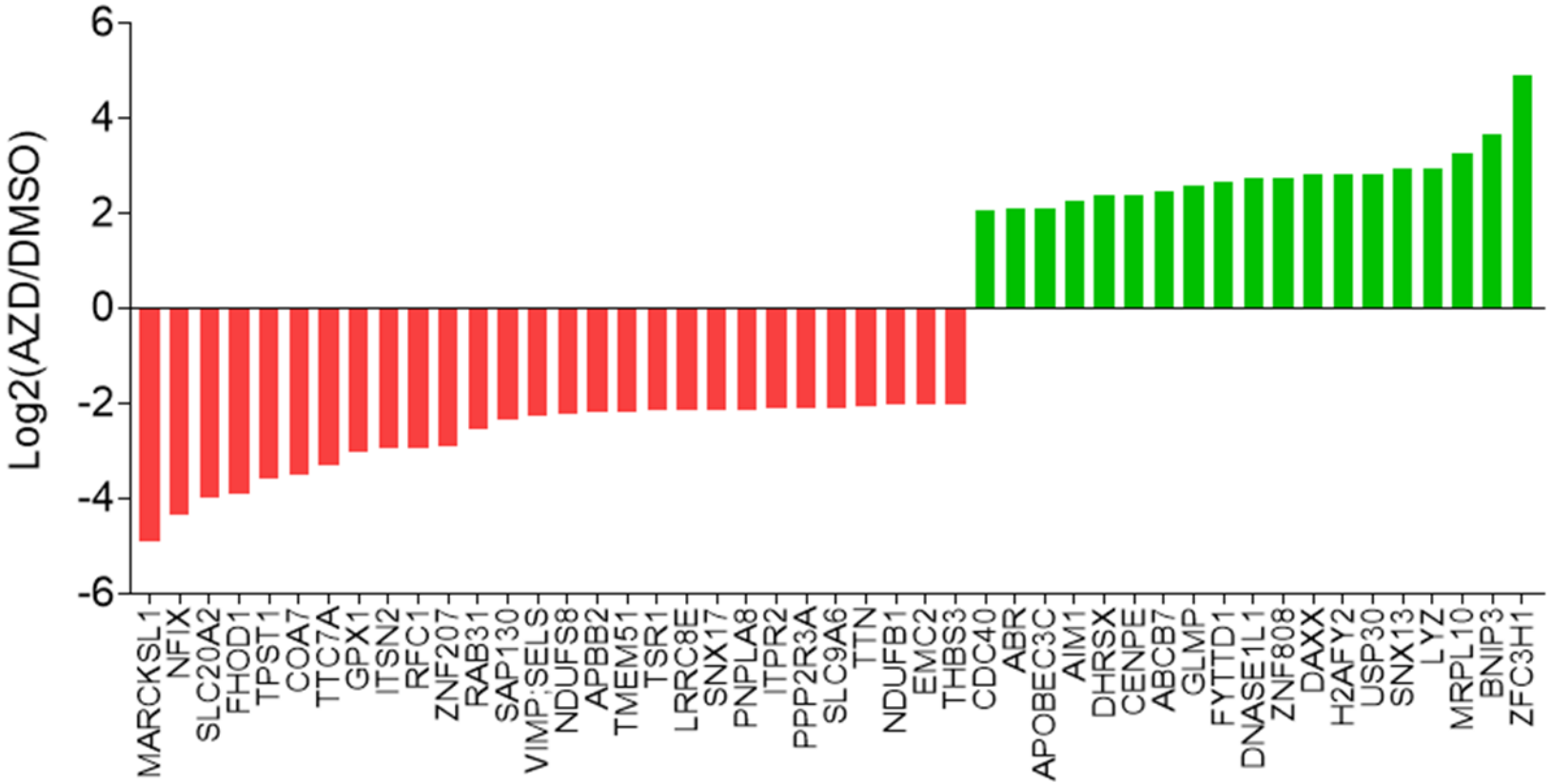

Figure 5.19 Peptides most significantly altered upon AZD4547 treatment

The waterfall plot shows the peptides that were most significantly decreased (red) or increased (green) upon treatment with AZD4547 (one biological replicate, Section 2.8). A cut off value of two log2fold change was used to highlight the most significant peptides. Many of the downregulated peptides are involved in cell migration and motility and many of the increased peptides are involved in transcriptional repression.

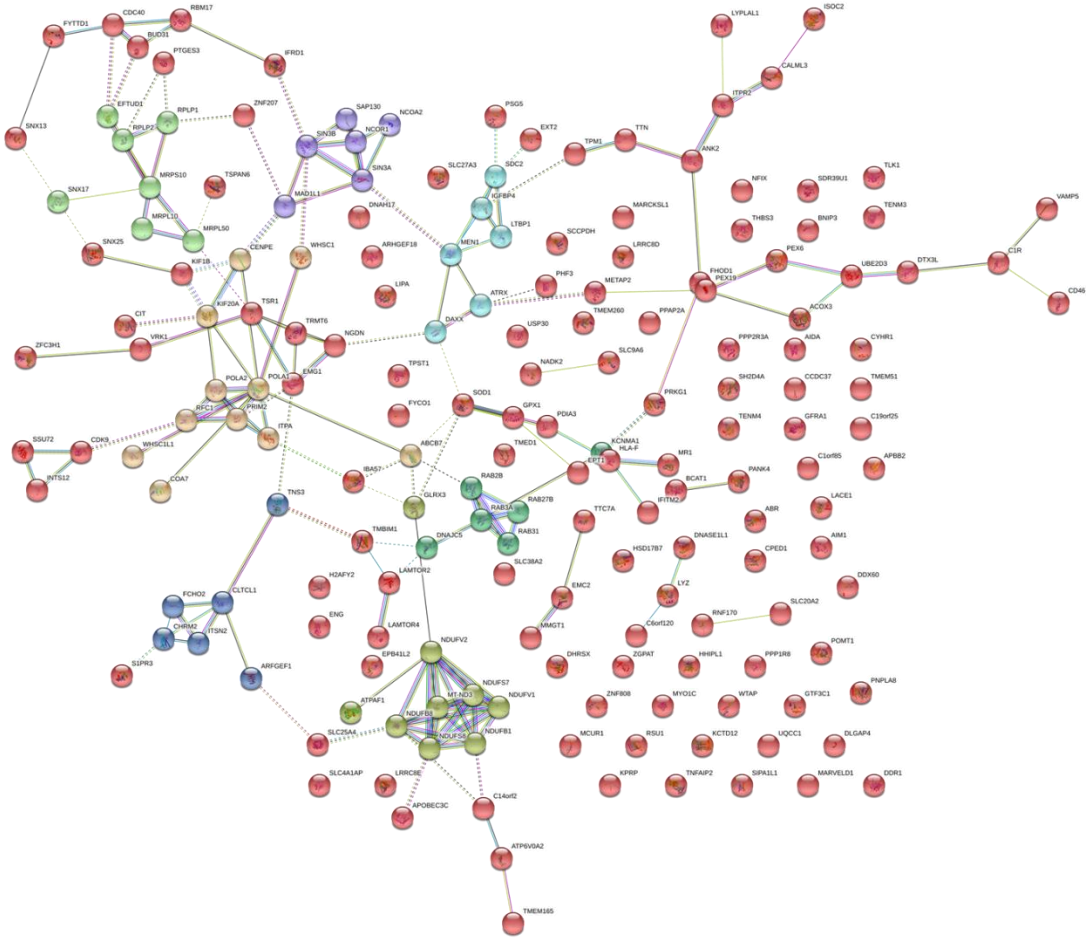

Figure 5.20 Networks of significantly changed total peptides

STRING was used to examine any networks significantly changed in the whole cell lysate between AZD4547 treated PSCs and control. The significant hits (greater than two log2foldchange) were enriched into 8 categories, with red nodes being the mainly unconnected peptides (Table 5.6). Data is from one biological replicate.

5.4.4 Nuclear changes

The sub-cellular fractionation analysis identified peptides moving between cellular compartments upon AZD4547 treatment. For the analysis, all the hits that were significantly changed within the nuclear compartment between the two conditions were examined. The most significantly changed pathways are listed in Table 5.7. The most increased or decreased 20 peptides within the nuclear compartment (Figure 5.21) were then investigated. Within these hits, there were many peptides involved in transcriptional epi-genetic regulation. Network analysis was performed using the significantly changed nuclear peptides (Figure 5.22). One of the interesting top nuclear hits was c-MET, which was present in all fractions but enriched in the nuclear fraction in the control cells, and this nuclear enrichment decreased significantly upon AZD4547 treatment (Figure 5.23).

Table 5.7 Enriched pathways in nuclear fraction of mass spectrometry data

Enriched pathways
Spliceosome
Transcriptional misregulation in cancer
Intron Large Complex
RNA Polymerase II Pre-transcription Events
Hepatocellular carcinoma
Thermogenesis

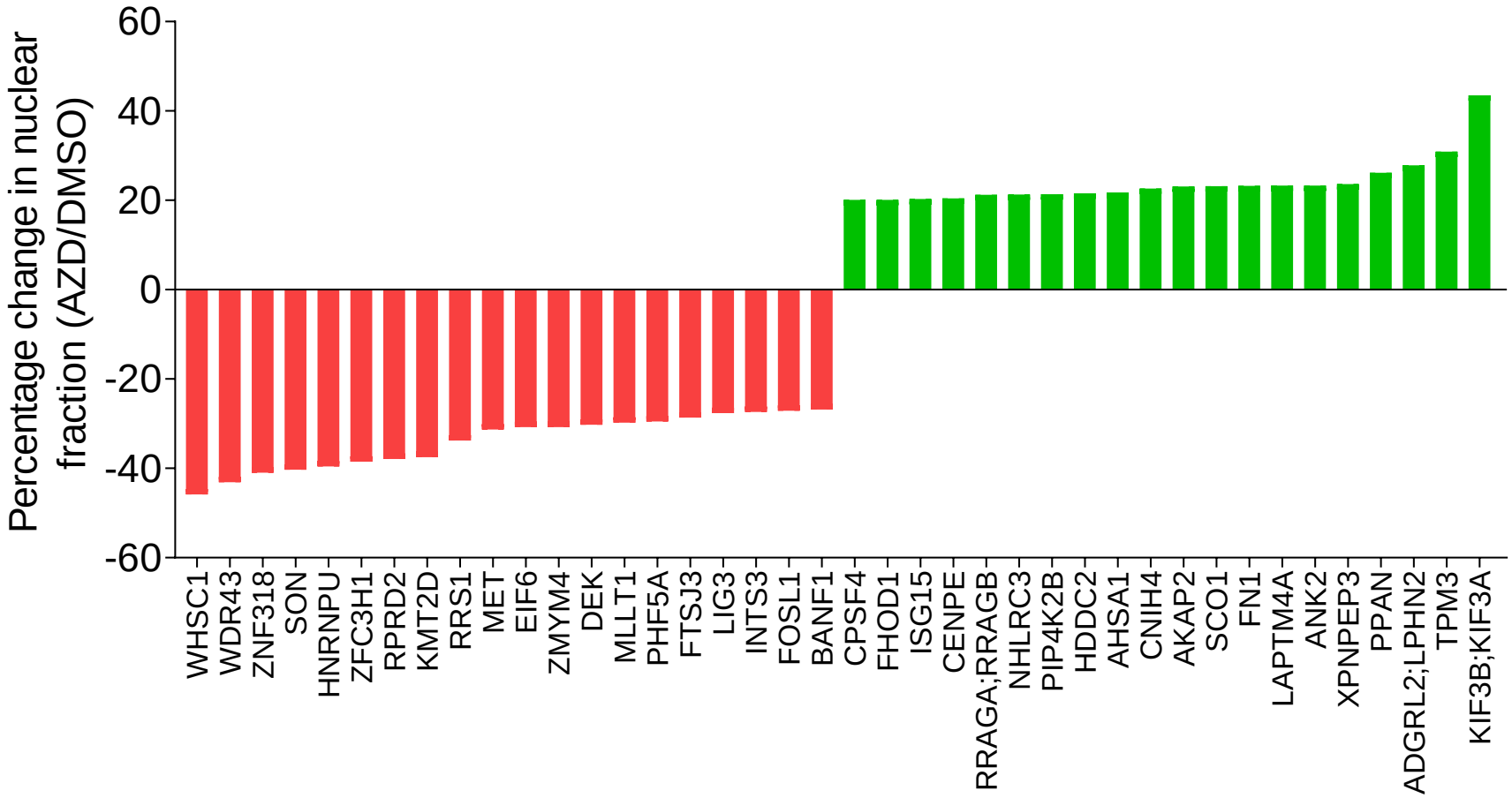

Figure 5.21 Peptides most significantly altered in the nuclear fraction upon AZD4547 treatment

The waterfall plot shows the peptides that were most significantly decreased (red) or increased (green) within the nuclear fraction upon treatment with AZD4547 (one biological replicate, Section 2.8). The top 20 peptides in each direction were included to highlight the most significant peptides.

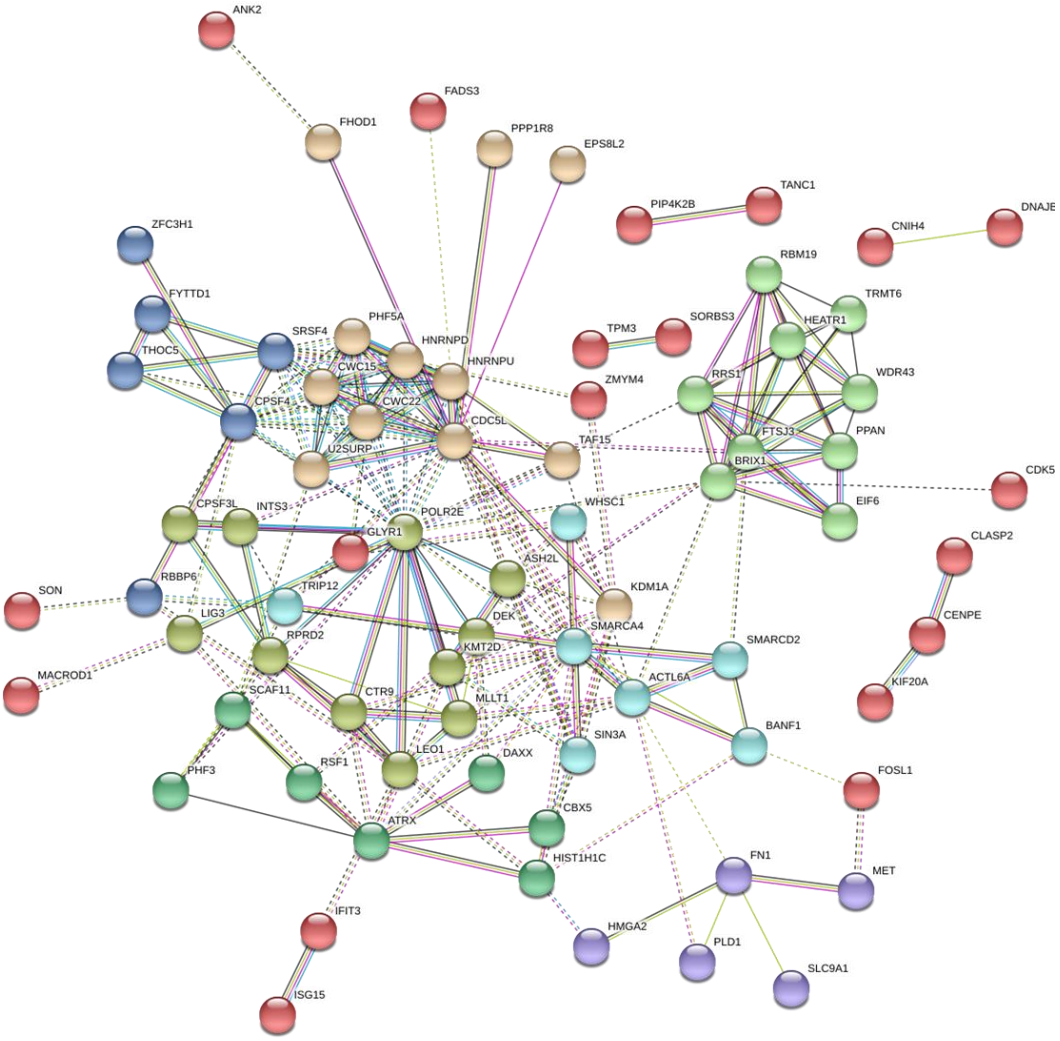

Figure 5.22 Networks of significantly changed nuclear peptides

STRING was used to examine any networks changed in the nuclear fraction between AZD4547 treated PSCs and control. The top 20 increased or decreased hits were enriched into 8 categories (Table 5.7). Data is from one biological replicate.

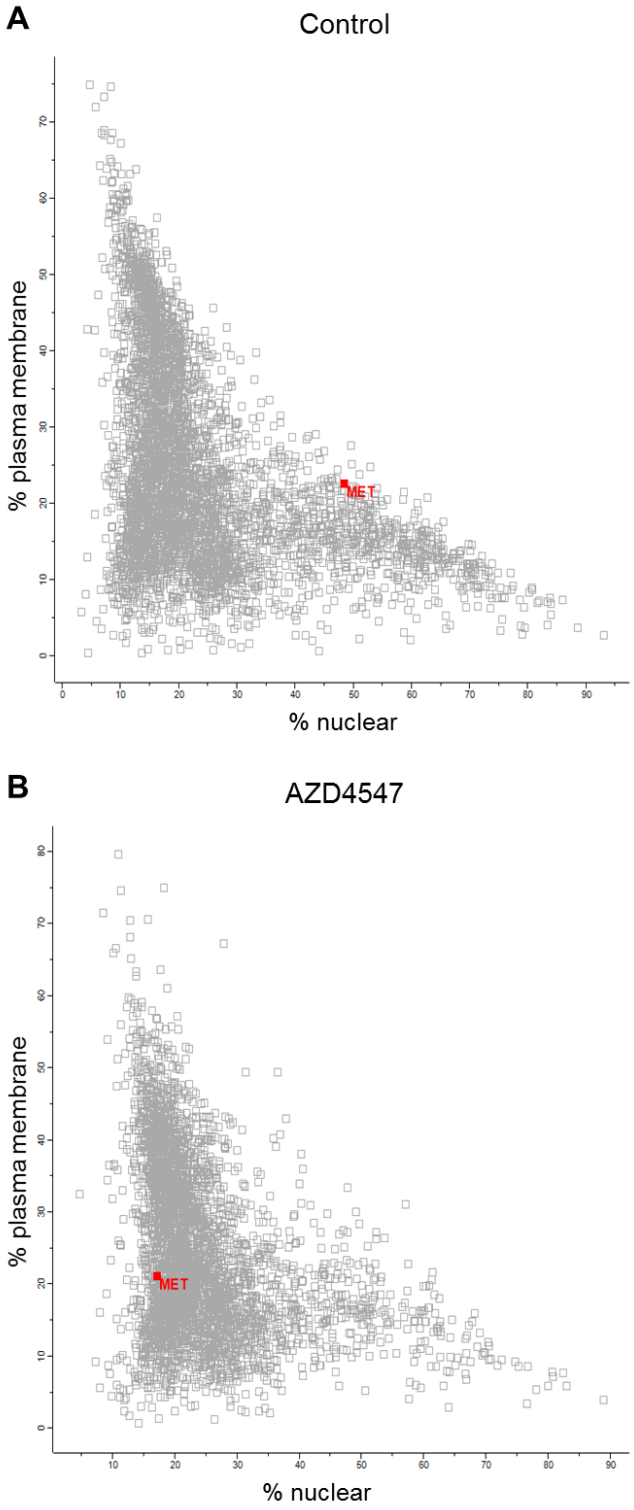

Figure 5.23 c-MET enrichment in the nucleus of PSCs is lost upon AZD4547 treatment

*Analysis of the sub-cellular location of peptides detected by mass spectrometry indicated that c-MET is enriched in the nuclear fraction of control PS1 cells (**A**). However, when these cells are treated with the FGFR inhibitor, AZD4547, c-MET is decreased in the nuclear fraction (**B**). Data is from one biological replicate.*

5.5 Discussion

Nuclear FGFR1 can be found in PSCs in nuclear speckles and co-localising with the splicing factor sc35 (Coleman et al., 2014b). These data, as well as previous findings in other cells, suggests that nFGFR1 can bind to DNA either directly or as part of a complex to trigger transcriptional changes. The novel role of nuclear FGFR1 within pancreatic stellate cells was investigated using chromatin immunoprecipitation.

A tagged version of FGFR1 was created using the HaloTag technology (Los et al., 2008). PS1 cells that had inducible expression of an FGFR1-HT construct were successfully created and overexpression of FGFR1-HT upon doxycycline treatment was confirmed. Using HaloTag allows the construct to be followed using the fluorescent TMR ligand, which is particularly useful in live imaging. Additionally, covalent binding of HaloTag to beads means that ChIP can be performed without the need for an antibody (HaloChIP). This would have been a significant advantage as many FGFR1 antibodies are not specific or sensitive enough for ChIP-seq analysis (Kidder et al., 2011). However, upon validation of the PS1-HT cells, it became apparent that even though the FGFR1-HT construct could be expressed inducibly, it could not translocate correctly between the sub-cellular compartments or signal effectively. Therefore, this was not suitable for use in ChIP-seq experiments.

Instead of using Halo-ChIP, an FGFR1 anitbody that has been used recently for ChIP-seq in neuronal cells was selected to perform this analysis (Stachowiak and Stachowiak, 2016). After optimisation, succesful ChIP-seq was performed on PS1 cells treated with either AZD4547 or subjected to shRNA-mediated FGFR1 knockdown, compared to relevant controls. Initial analysis of the sequencing data demonstrated enrichment of peaks indicating regions where FGFR1 is interacting

either directly or indirectly with DNA in these cells. Peaks overlapped between all the control conditions provide the most reliable peaks to validate. STRING analysis comparing the most significantly enriched peaks between all the conditions gave Hippo signalling and ubiquitination as key pathways mediated by nuclear FGFR1. These will warrant further validation and investigation, especially a potential novel cross-talk mechanism between FGF and Hippo signalling pathways. Interaction between the FGF and Hippo pathways has been previously reported in cancer. For example, in cholangiocarcinoma nuclear YAP can enter into an autocrine signalling loop with FGFR2/FGF5 (Rizvi et al., 2016). In bladder cancer, mutant FGFR3 has been shown to increase TAZ levels and in HER2 positive breast cancer, FGFR4 has been correlated with increased YAP activity (di Martino et al., 2019, Turunen et al., 2019). Furthermore in colorectal cancer, YAP1 has been identified as a downstream target of FGF8 (Liu et al., 2015). Another pathway that will be interesting to investigate is the TGF-β signalling pathway as SMAD3 was a central node for the network analysis in STRING (Figure 5.15)

In tandem, sub-cellular mass spectrometry analysis was performed on PS1 cells to observe the changes in localisation of FGFR1 within these cells. PSCs treated with AZD4547 or stimulated with FGF2 to either reduce or increase FGFR1 nuclear translocation respectively, were compared to relevant controls. Although FGFR1 peptides could not be detected reliably in all of the conditions, there were significant changes in both total and sub-cellular peptides in PS1 cells upon FGFR inhibition with AZD4547. Some of the key peptides decreased upon AZD4547 treatment in the whole cell lysate fraction are now being validated (MARCKSL1, FHOD1 and GPX1), as well as the change in nuclear localisation of c-MET and epi-genetic regulators upon FGFR inhibition. This was a pilot experiment that will need to be optimised and repeated in the future. STRING analyses may be useful to identify networks of

proteins that are changing in response to FGFR inhibition in PSCs over multiple conditions and repeats. These results will help to deconstruct the downstream effects of nuclear translocation of FGFR1 within stellate cells, providing incerased understanding of this novel mechanism of invasion in PDAC.

Chapter 6: Final Discussion

6.1 Introduction

Currently, PDAC is a cancer of high unmet clinical need. Understanding the biology of PDAC's characteristic desmoplastic stroma represents a critical challenge in potentially improving patient outcomes (Sections 1.3 and 1.4). Recent research has demonstrated that activated PSCs are vital for the construction of the dense desmoplastic stroma, as well as tumour progression and invasion, making these cells an attractive therapeutic target. FGF signalling has been identified as a key pathway involved in cross-talk between cancer and stellate cells within the desmoplastic stroma of PDAC tumours (Kang et al., 2019b, Rhim and Stanger, 2010).

Due to the importance of FGF signalling in PDAC development, we previously investigated the role of FGF ligands and receptors in both cancer cells and activated stellate cells. This highlighted that nuclear translocation of FGFR1 occurs within activated PSCs at the invasive edge of PDAC tumours (Section 1.6.3) (Coleman et al., 2014b). Nuclear FGFR1 in PSCs was co-localised with FGF2 and nuclear translocation increased upon FGF2 stimulation. In the novel 3D *in vitro* organotypic models, nuclear translocation of FGFR1 was reduced upon FGFR inhibition with PD173074, leading to decreased invasion. Thus I started exploring the importance of FGF-mediated cross-talk between the tumour and stroma in PDAC invasion in further detail.

The aims of my project were to investigate the specificity of targeting FGFR1 in PSCs to disrupt cellular cross-talk, to identify the mechanisms of FGFR1-mediated changes in PSCs and to explore the utility of FGFR1 targeting to improve current and developing PDAC therapies. I will now put into context my findings in relation to the

explicit aim and the current literature, including clinical trials, in each of the following Sections (6.2, 6.3 and 6.4).

6.2 Targeting FGFR1 in PSCs

6.2.1 FGF signalling mediates PDAC invasion

During this project, the previous findings targeting FGF signalling within PSCs were translated into a clinically relevant model. Two novel 3D *in vitro* co-culture models were used, mini-organotypics and spheroids (Section 2.6), to demonstrate that stellate cell-led invasion is decreased upon treatment with the clinically relevant drug, AZD4547 (Figures 4.2, 4.3 and 4.4). These two models can be used to interrogate invasive phenotypes at both the single cell and multi-cellular level.

6.2.1.1 FGFR inhibition

Recent activity has resulted in development of many FGFR inhibitors (Section 1.5.7) (Table 6.1). AZD4547 was selected since it has specificity against FGFR1-3 (Table 6.2) (Gavine et al., 2012). Furthermore, AZD4547 is currently in clinical trials in patients with gastric, lung, breast and bladder cancers (NCT00979134, NCT01202591, NCT01213160, NCT01457846, NCT01791985, NCT01795768, NCT01824901, NCT02117167, NCT02154490, NCT02299999, NCT02465060, NCT02546661, NCT02664935, NCT02824133 and NCT02965378). The breadth of these clinical trials underscore the clinical relevance of AZD4547 and suggest that it could be adopted to interrupt cellular cross-talk in PDAC patients. Furthermore, it has been shown that AZD4547 treatment can reduce the proliferation and invasion of primary fibroblasts isolated from juvenile nasopharyngeal angiofibromas (Le et al., 2017). Additionally, AZD4547 can reduce FGF21-mediated tumour progression and invasion in papillary thyroid cancer cells (Kang et al., 2019c). In breast cancer *in vitro*

and *in vivo* models, AZD4547 treatment decreases cell proliferation and invasion, as well as the formation of lung metastases (Liu et al., 2014). This indicates that FGFR inhibition with AZD4547 can have an anti-invasive effect.

Table 6.1 The action of FGFR inhibitors in pancreatic cancer

Inhibitor	Targets	Function	References
AZD4547	FGFR1-4 VEGFR2 IGFR	Inhibits downstream signalling, decreases cell survival and induces tumour stasis	(Gavine et al., 2012, Guan et al., 2019, Kang et al., 2019a)
BGJ398	FGFR1-3	Inhibits cancer cell proliferation	(Lehnen et al., 2013)
Dovitinib	FGFR1-4 PDGFRβ VEGFR2	Inhibits tumour growth, motility and metastasis. Increases response to gemcitabine and capecitabine	(Ma et al., 2019, Taeger et al., 2011, Zhang et al., 2014a)
Lanvatinib	FGFR1-4 VEGFR1-3 PDGFRα RET c-KIT	Decreases angiogenesis and inhibits tumour growth	(Yamamoto et al., 2014)
Masitinib	c-KIT FGFR1-4 PDGFR	Decreases inflammation and pain. Increases response to gemcitabine	(Deplanque et al., 2015, Humbert et al., 2010, Mitry et al., 2010, Waheed et al., 2018)
Nintedanib	FGFR1-3 VEGFR1-3 PDGFRα/β	Inhibits tumour growth, cancer cell proliferation, angiogenesis and metastasis. Enhances response to gemcitabine or afatinib	(Awasthi et al., 2015, Bahleda et al., 2015, Bill et al., 2015, Kutluk Cenik et al., 2013)
PD173074	FGFR1-4 VEGFR2	Inhibits angiogenesis and tumour growth. Induces cancer cell apoptosis and reduces cancer stem cells	(Buchler et al., 2007, Greggio et al., 2013, Lai et al., 2018, Memon et al., 2018)
Ponatinib	FGFR1-4 BCR-ABL SRC PDGFRα VEGFR2 AKT ERK1/2	Inhibits cell proliferation, enhanced activity with MEK inhibitor	(Musumeci et al., 2018, Sahu et al., 2017)
SSR128129E	FGFR1-4	Inhibits PDAC cell proliferation and migration	(Bono et al., 2013)

Table 6.2 IC_{50} values of AZD4547 against target receptors

Receptor	IC_{50} value (nM)
FGFR1	0.2
FGFR2	2.5
FGFR3	1.8
FGFR4	165
VEGFR2	24

6.2.1.2 FGFR1 within PSCs facilitates cancer cell invasion

FGFR inhibition within PSCs with the clinically relevant agent AZD4547, at a dose well below the GI_{50} level (Figure 3.6), reduced cancer cell invasion in 3D co-culture *in vitro* models. This supported previous work with the laboratory compound, PD173074, and independently validates the importance of FGF signalling as a key pathway regulating stromal-cancer cross-talk mediated invasion (Coleman et al., 2014b). Stellate cells with inducible FGFR1 shRNA knockdown replicated the results of FGFR pharmacological inhibition (Figures 4.8 and 4.9), confirming that the pro-invasive effect of FGF signalling in PDAC is mediated specifically by FGFR1 expression and activation in the stellate cells. This highlights the notion that targeting FGF signalling with AZD4547 is a viable clinical option for patients with PDAC.

6.2.2 Stellate cell-led invasion

6.2.2.1 Cancer-associated fibroblasts promote invasion

Previous work has suggested that cancer-associated fibroblasts (CAFs) are key mediators of tumour invasion and metastasis (Section 1.3) (Barbazán and Matic Vignjevic, 2019, McCarthy et al., 2018). CAFs can be seen leading invasion, creating tracks to allow collective invasion of cancer cells behind (Gaggioli et al., 2007). This has been attributed to cytokine signalling through GP130-IL6ST and JAK1 activating Rho-kinase dependent signalling and actomyosin contractility within both tumour and stromal cells in oral squamous cell carcinoma (Sanz-Moreno et al., 2011). This was also shown to be a key mechanism allowing migration of individual melanoma cells in an amoeboid mode (Sanz-Moreno et al., 2011). YAP and endoglin/BMP9 have been demonstrated as key signalling mechanisms within CAFs to promote invasion, which can be blocked by ROCK or endoglin inhibition respectively (Calvo et al., 2013, Paauwe et al., 2018). It has also been postulated that apart from cytokine signalling,

CAFs may physically pull cancer cells out of tumours. The physical force exerted by CAFs onto cancer cells is mediated by heterophilic adhesion of N-cadherin (expressed on CAFs) with E-cadherin (expressed on cancer cells). This interaction recruits downstream signalling, such as β-catenin recruitment and polarises the CAFs to move actively away from the cancer cell population (Labernadie et al., 2017). Additionally, CAFs have been shown to drive invasion in cancer cells via integrin signalling between the two cell types (Attieh et al., 2017, Wen et al., 2019), as well as packaging pro-invasive signalling molecules into extracellular vesicles (Dourado et al., 2019). Additionally, integrins and N-cadherin have been shown to bind to FGFs and FGFRs to regulate FGF signalling within cells (Section 1.5.1) (Nguyen et al., 2019, Tanghetti et al., 2002). Whilst a variety of mechanisms have been suggested in different cancers, and this may be context- and disease-specific, it demonstrates the biological importance of CAFs in tumour progression and invasion.

Specifically within PDAC, activated PSCs make up the main proportion of CAFs and have been shown to facilitate tumour progression and invasion (Section 1.3) (Apte et al., 2013). Sex mismatch *in vivo* studies have shown the presence of PSCs at distant metastatic sites, indicating their critical role in PDAC progression, though the signalling mechanism responsible for this has not been elucidated (Apte and Wilson, 2012, Apte et al., 2013, Hwang et al., 2012, Thomas and Radhakrishnan, 2019, Vonlaufen et al., 2008b, Vonlaufen et al., 2008a, Xu et al., 2010, Yuan et al., 2019). In my work I have confirmed the importance of activated PSCs in invasion, particularly in the spheroid model, where a leading stellate cell can be seen at the end of each protrusion, with cancer cells following behind (Figure 4.5).

6.2.2.2 PSCs use multiple mechanisms to trigger PDAC invasion

A number of potential mechanisms of stellate cell-led invasion have been identified, including PSC activation, direct contact with cancer cells or ECM proteins and secretion of paracrine signals, such as FGF-mediated cellular cross-talk (Coleman et al., 2014b). Trefoil factor 1 expression on both PSCs and cancer cells has been shown to induce invasion and metastasis in orthotopic xenograft *in vivo* models (Arumugam et al., 2011). In patient derived organoids, addition of PSCs caused destruction of basement membrane structures and triggered invasion through direct binding of MMP2 with membrane type-1 MMP (Koikawa et al., 2018). Additionally, expression of the co-chaperone protein Bcl2-associated athanogene 3 (BAG3) on PSCs has been shown to promote paracrine invasion of cancer cells through IL-8, MCP1, TGF-β2 and IGFBP2 (Yuan et al., 2019).

Analysis of the secretome of activated PSCs highlighted some key proteins that could be involved in re-modelling PDAC stroma to allow tumour invasion (Wehr et al., 2011). Proteins associated with cell adhesion, migration and cancer invasion were identified, such as members of the urokinase plasminogen activator pathway, annexin A2 (ANXA2) and serpin peptidase inhibitor, clade I (pancpin) member 2 (SERPINI2), as well as transforming growth factor beta induced (TGFBI), ubiquitin carboxyl-terminal esterase L1 (UCHL1) and ezrin (EZR). Furthermore galectin-3-binding protein (LGALS3BP), which is expressed in PDAC metastases, and galectin-1, which can increase both stellate and cancer cell invasion, have been found to be secreted by activated PSCs (Berberat et al., 2001, Wehr et al., 2011, Xue et al., 2011). Furthermore, secretion of ligands such as PDGF, TGF-β, FGF2 and CTGF by activated PSCs has been shown to promote cancer cell proliferation and invasion (Charrier and Brigstock, 2013, Habisch et al., 2010, Mahadevan and Von Hoff, 2007).

Reversal of PSC activation, by ATRA or inhibition of G protein-coupled oestrogen receptor (GPER) by tamoxifen, can decrease actomyosin contractility and, therefore, prevent ECM remodelling and invasion, as well as reducing cancer cell proliferation (Chronopoulos et al., 2016, Cortes et al., 2019, Froeling et al., 2011). This supports the notion that activated stellate cells are the key drivers of invasion in PDAC (Section 1.3). I focused on FGF signalling, as it is critically important in pancreas development (Gittes, 2009, Kim and Hebrok, 2001), and it is generally believed that embryonic signalling mechanisms are hijacked by cancer in an organ-specific manner (Aiello and Stanger, 2016).

Specifically, I have shown that despite using different cancer cell lines, I can universally block FGFR1 in PSCs and the resultant cancer cell invasion. Interestingly, in both 3D *in vitro* models used in this project, the invasive phenotype of the co-cultures was different between the three PDAC cell lines. This was shown very clearly in the spheroid model (Figure 4.5). This could be due to activated PSCs triggering invasion through a number of mechanisms, which may be specific to cancer cell type. Moreover, the three PDAC cell lines have different invasive capacity (Section 4.2.1). PANC-1 and MIA PaCa-2 cells are poorly differentiated and express mesenchymal markers (Deer et al., 2010). Both cell lines have been reported to be invasive and PANC-1 cells can invade as single cells (Ellenrieder et al., 2001, Duxbury et al., 2004, Stahle et al., 2003, Takada et al., 2002). On the other hand, COLO 357 cells express epithelial markers and are regarded as a poorly invasive cell line (Huang et al., 2012). Hence, I explored the potential different mechanisms by which FGFR1 within PSCs may trigger invasion of cancer cells.

6.3 Mechanisms of FGFR1-mediated changes in PSCs

Based on previous observations (Coleman et al., 2014b, Santolla et al., 2019) I had two potential leads for mechanisms of FGFR1 mediated cancer cell invasion, a nuclear FGFR1 role and the intracellular flux related to FGF signalling in PSCs.

6.3.1 Nuclear translocation of FGFR1

Nuclear localisation of FGFR1 can relate to cell migration and invasion (Section 1.6) (Chioni and Grose, 2012, Coleman et al., 2014b, Nguyen et al., 2013, Stachowiak et al., 2007, Stachowiak and Stachowiak, 2016). Upon FGFR inhibition in stellate cells, nuclear FGFR1 is decreased. Whilst this was not replicated using AZD4547 treatment in short term stellate cell mono-culture in 2D (Figure 3.9), it is very evident in 3D models that vimentin positive PS1 cells invading into the gel have nuclear FGFR1 (Figure 4.6). This indicates that nuclear translocation of FGFR1 could be linked with cellular cross-talk and stellate cell-led invasion in a context-specific manner, especially when co-cultures are constructed in a physiological manner with relevant surrounding matrix proteins.

The method of translocation of FGFR1 into the nucleus has not been fully elucidated (Section 1.6.2 and 1.6.3). It was previously confirmed that, in pancreatic stellate cells, this was full-length FGFR1 (Coleman et al., 2014b), unlike in breast cancer where Granzyme B cleavage causes translocation of a truncated form of the receptor (Chioni and Grose, 2012). FGFR1 also localises with FGF2 within the nucleus, and may piggyback using the FGF2 nuclear localisation signal (Coleman et al., 2014b, Myers et al., 2003, Peng et al., 2002). Moreover, it has been confirmed that translocation of FGFR1 is dependent on importin-β (Reilly and Maher, 2001). FGFR1 travelling to the nucleus could be from receptor trafficking upon activation at the plasma membrane,

or alternatively translocation from an intracellular pool, possibly by retrograde transport from the endoplasmic reticulum (Stachowiak et al., 2007, Stachowiak and Stachowiak, 2016). This could be an area of future work to fully understand how this nuclear localisation is occurring, and furthermore, if there are other methods to target this translocation to avoid tyrosine kinase inhibitor resistance (Babina and Turner, 2017, Camidge et al., 2014). It will also be important to determine whether AZD4547 treatment prevents receptor translocation to the nucleus or if it interrupts its function whilst there, such as preventing DNA binding.

6.3.1.1 Transcriptional role of nFGFR1 in PSCs

Given that FGFR1 signalling is essential for stellate cell invasion and translocation of the receptor occurs in invasive cells in 3D models, as well as at the invasive edge of PDAC tumours, the novel role of nFGFR1 was investigated. Previous work demonstrated that FGFR1 in the nucleus co-localises with sc35 in nuclear speckles, indicating that it may play a role in transcriptional regulation (Section 1.6.3) (Coleman et al., 2014b). Moreover, nFGFR1 has been demonstrated to have a role in transcriptional regulation in neuronal and breast cancer cells (Chioni and Grose, 2012, Stachowiak and Stachowiak, 2016).

Therefore, chromatin immunoprecipitation was used to discover where FGFR1 may be binding to DNA or chromatin in stellate cells. This was a challenging aspect to develop, since the amount of FGFR1 translocating to the nucleus is small; and this is relevant since most ChIP-seq analysis has been developed for histone proteins to which DNA is bound in abundance (Kidder et al., 2011, Park, 2009). I tried different methods to enhance my yield whilst retaining specificity to FGFR1, such as HaloTag (Los et al., 2008), and using chemical and genetic manipulation of FGFR1 as well as

developing the steps to shear and isolate sufficient DNA. Finally, PS1 cells treated with AZD4547 compared to control, as well as three different shRNA cell lines were used to decipher the genes under transcriptional control of FGFR1. Excitingly, preliminary analyses showed that there was clear enrichment of peaks, indicating that FGFR1 is associating either directly or indirectly with the DNA. There was also overlap between the shRNA2 and shRNA3 samples across the biological repeats. I will be validating this in the near future.

6.3.1.2 Hippo signalling

Analysis of the ChIP-seq peaks from between either AZD4547 treated or FGFR1 knockdown, with their relevant control, demonstrated that one of the significantly enriched pathways was Hippo signalling (Figure 5.15 and Table 5.5). Peaks were identified in 152 proteins associated with this pathway, including BMP8A, SMAD3, PPP2R2C, SCRIB and LATS2. The Hippo signalling pathway is a key developmental regulatory kinase cascade that regulates organ size and can be switched on to drive cancer progression (Pan, 2010). I will, therefore, elaborate on Hippo signalling as one of the many novel leads from ChIP-seq data which I hope to take further to investigate PSC-mediated cancer cell invasion. I summarise the intra-cellular cascade involved in the Hippo pathway which can signal to the microenvironment, promote EMT, mediate angiogenesis and promote cell survival and proliferation (Figure 6.1).

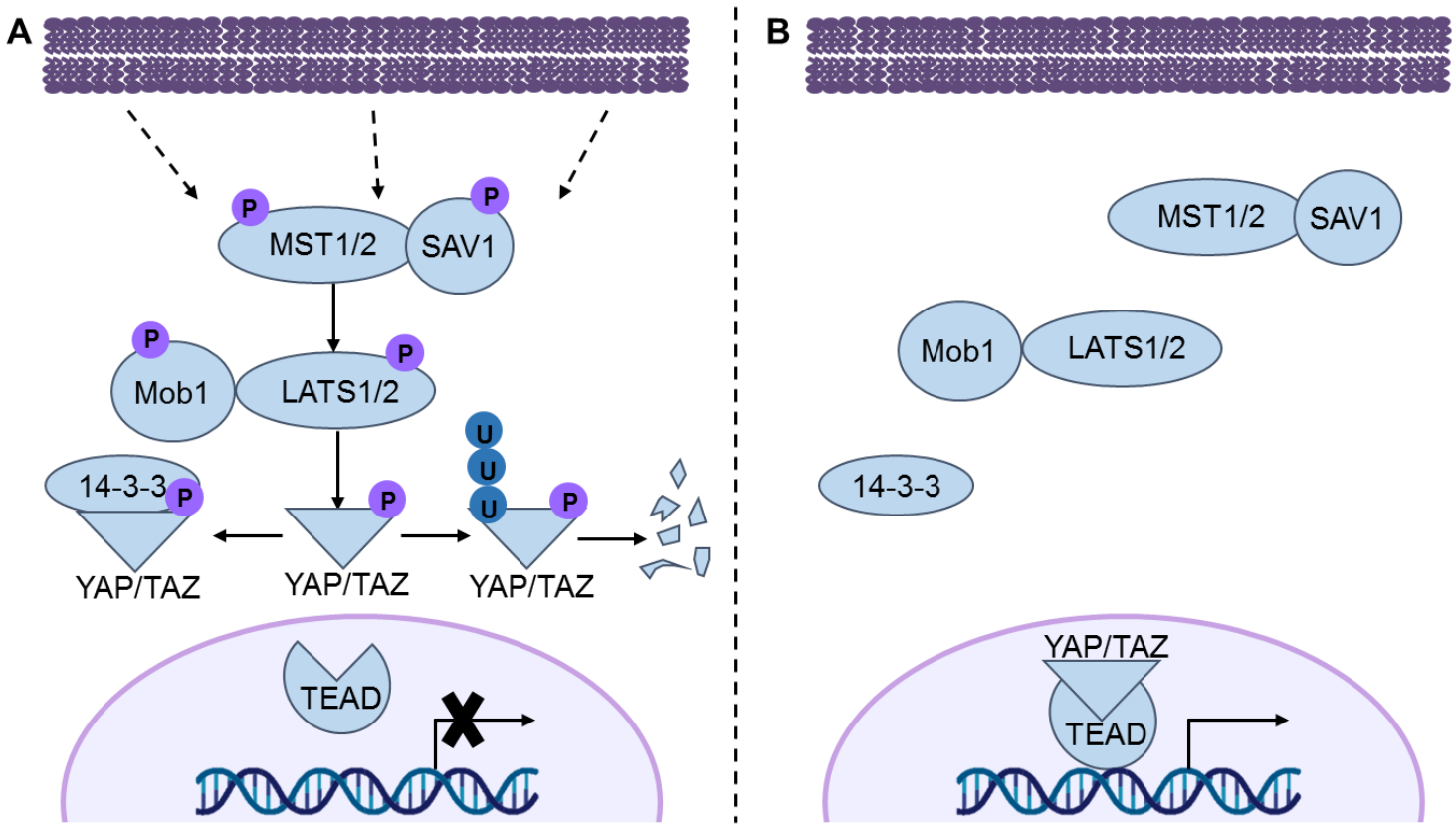

Figure 6.1 Hippo signalling pathway

Hippo signalling is a major regulator of cell survival and organ size. ***A.*** *When the core Hippo signalling pathway is switched on, signals feed into the cascade to phosphorylate MST1/2 and SAV1. These in turn phosphorylate LATS1/2 and Mob1, which then phosphorylate YAP/TAZ and sequester them in the cytoplasm. YAP/TAZ can then bind with other mediators, such as 14-3-3 to be retained in the cytoplasm or ubiquitinated for proteasome degradation.* ***B.*** *When Hippo signalling is switched off MST1/2, SAV1, LATS1/2 and Mob1 remain unphosphorylated. Therefore YAP/TAZ are not phosphorylated and translocate into the nucleus. YAP/TAZ can then bind to transcription factors, such as TEAD1-4, to trigger the expression of downstream proteins such as CTGF, BIRC5, CYR61, AREG, EDN2 and CXCL5 (Boopathy and Hong, 2019).*

6.3.1.3 Hippo signalling in PDAC

Novel cross-talk between FGF and Hippo signalling could be important to mediate PSC-led invasion and tumour progression. In fact, YAP/TAZ are overexpressed in PDAC patient tumours and have been described as a potential prognostic marker for patient survival (Ansari et al., 2019, Kapoor et al., 2014, Salcedo Allende et al., 2017). YAP has also been linked to acinar-to-ductal metaplasia (ADM) and PanIN progression in PDAC (Gruber et al., 2016, Jiang et al., 2018, Zhang et al., 2014b).

6.3.1.4 FGF and Hippo signalling cross-talk

The Hippo pathway can cross-talk with many other signalling cascades, such as BMP, TGF-β, Wnt, EGF and hedgehog signalling, as well as with other cells and the ECM through integrins and adhesion molecules present on the cell surface (Figures 6.2 and 6.3) (Alarcon et al., 2009, Barron and Kagey, 2014, Boopathy and Hong, 2019, Camargo et al., 2007, Cravo et al., 2015, Das Thakur et al., 2010, Fernandez et al., 2009, Grusche et al., 2010, He et al., 2015, Polesello et al., 2006, Varelas et al., 2010, Varelas et al., 2008, Zhao et al., 2010). The interaction between Hippo and FGF signalling remains unexplored and I would like to take this further to identify additional druggable options for PDAC.

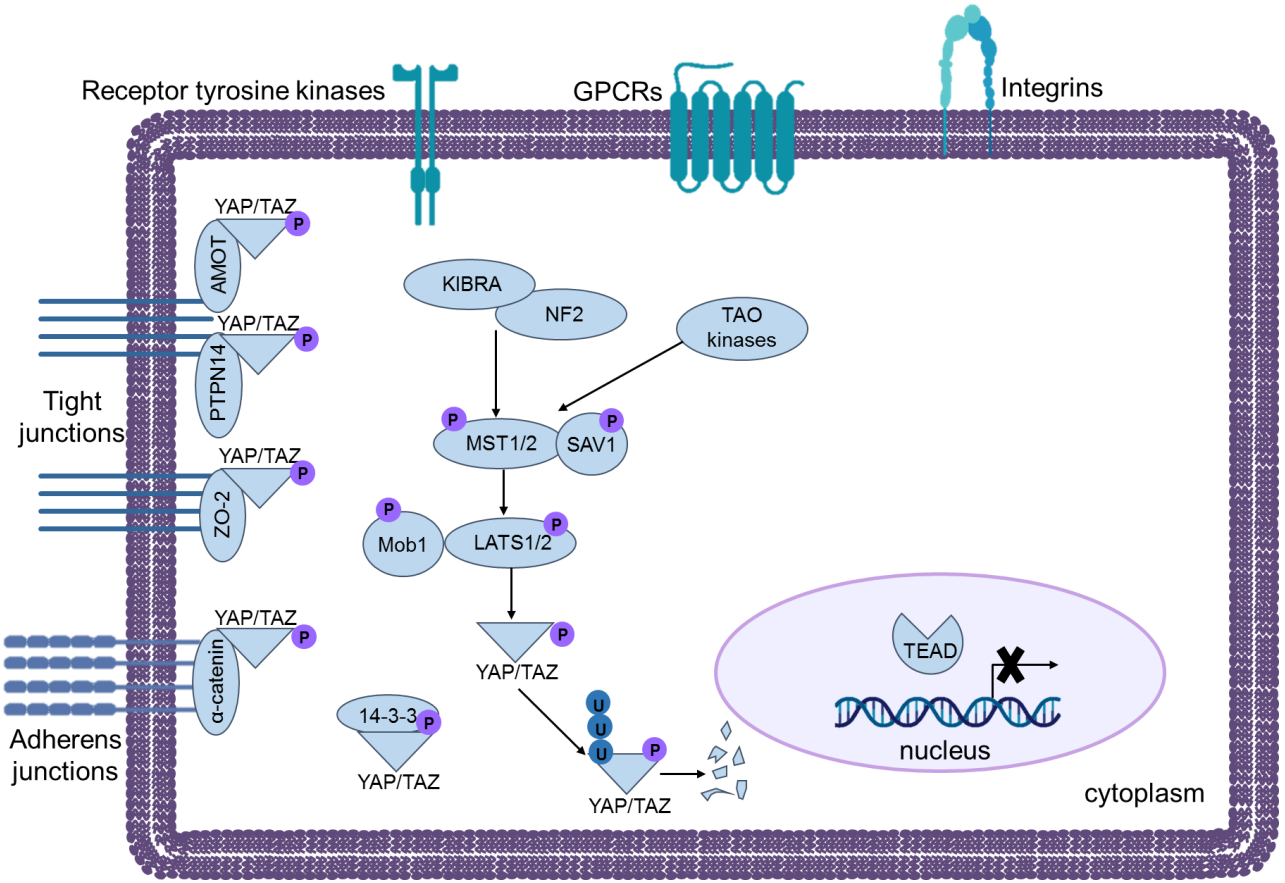

Figure 6.2 Activated Hippo signalling pathway interactions

Hippo signalling can be controlled by many different cell processes. When the pathway is switched on KIBRA, NF2 and TAOK1-3 can phosphorylate the MST1/2 and SAV1 complex to trigger the phosphorylation of Mob1 and LATS1/2, causing retention of YAP/TAZ in the cytoplasm, leading to ubiquitination and proteasomal degradation. Phosphorylated YAP/TAZ can also be retained within the cytoplasm by binding to mediators such as 14-3-3, or through cellular interactions by cadherins and tight junctions leading to activation of proteins such as α-catenin, ZO-2, PTPN14 and AMOT (Boopathy and Hong, 2019).

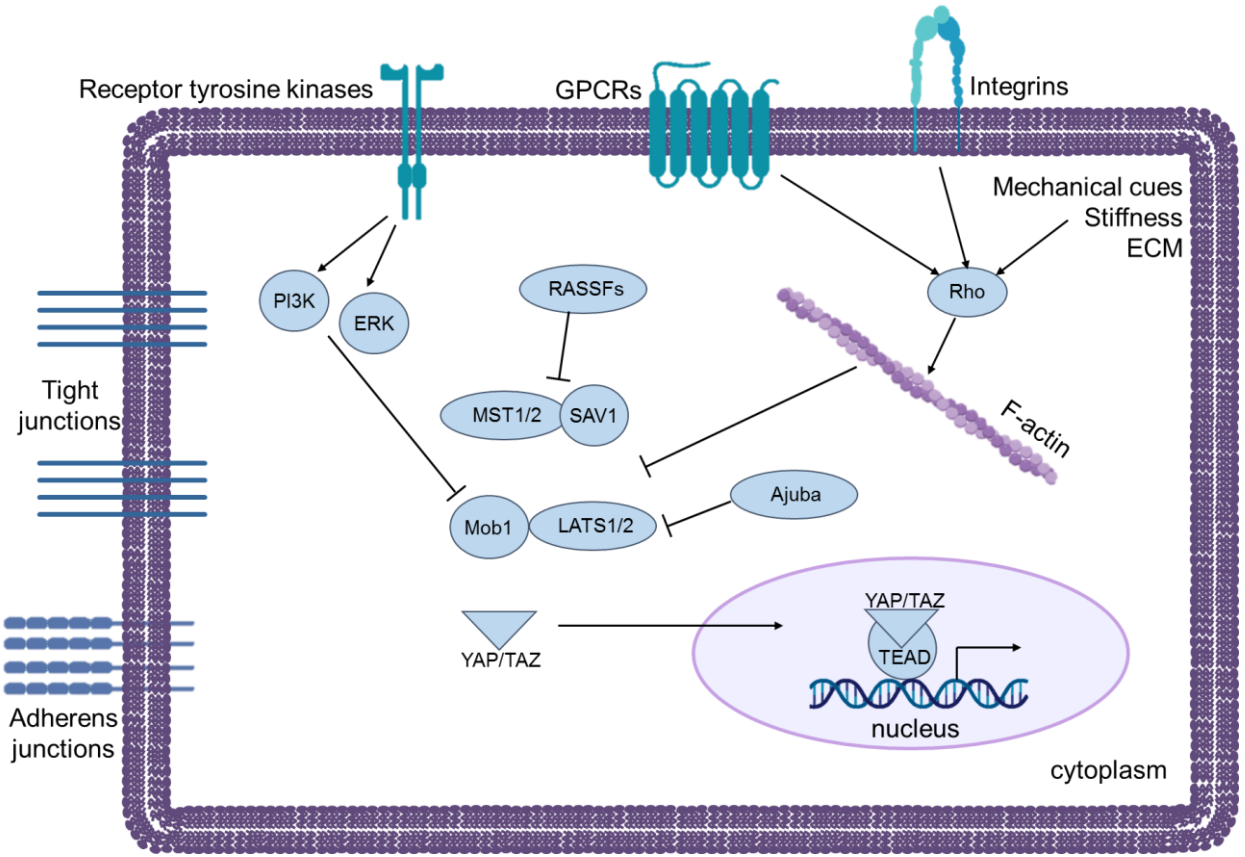

Figure 6.3 Un-activated Hippo signalling pathway interactions

Hippo signalling can be controlled by many different cell processes. Signalling through GPCRs, integrins and mechanical cues indicating ECM stiffness can activate Rho and reorganise F-actin within cells, which in turn can switch off the Hippo pathway and trigger nuclear localisation of YAP/TAZ. Additionally, receptor tyrosine kinase activation and downstream signalling, as well as adaptor proteins such as Ajuba and RASSFs, can inhibit the core Hippo complexes and activate gene transcription through YAP/TAZ nuclear translocation. In the nucleus, YAP/TAZ can bind with transcription factors, such as TEAD 1-4 and Smad1-3, to control gene expression (Boopathy and Hong, 2019).

This cross-talk may be relevant since FGF and Hippo signalling have been linked previously in studies in ovarian high grade serous carcinoma (HGSC), with a paracrine loop between FGF and YAP signalling in fallopian tube secretory epithelial cells (FTSECs) driving HGSC, presenting a novel combination therapeutic strategy (Hua et al., 2015). Moreover mutant FGFR3 in bladder cancer has been shown to increase TAZ levels through expression of the ETS-family transcription factor, ETV5 (di Martino et al., 2019). In breast cancer cells, YAP can bind to the KLF5 transcription factor, which in turn promotes cell survival. One of the downstream targets found to be activated through YAP-mediated KLF5 expression was FGFBP (Zhi et al., 2012). Additionally, MST1/2 have been identified as substrates for FGFR4 and in HER2 positive breast cancer cells FGFR4 expression has been correlated with increased nuclear YAP activity. Moreover, in 3D *in vitro* breast cancer sphere models FGFR4 knockdown increased phosphorylated MST1/2 and membrane-associated YAP (Turunen et al., 2019). In a study looking at genetic changes upon KRAS suppression, 147 genes were found to promote cell survival and rescue the KRAS phenotype. From these 147 genes, the highest hits were sterile α motif (SAM) post-transcriptional regulators, YAP1, WWTR1 and the FGF family (such as FGF3, 6 and 10) (Shao et al., 2014).

Cross-talk between these two pathways has also been described in the lung stem cell niche through YAP induced expression of FGF10, promoting regeneration and wound repair (Volckaert et al., 2017). Additionally, in colorectal cancer, YAP1 was identified as a downstream target of FGF8, which is correlated with a poor patient survival (Liu et al., 2015). In cholangiocarcinoma, YAP has been shown to play a key role in tumour progression and chemo-resistance (Marti et al., 2015). Nuclear YAP localisation and activation of TBX5 triggered the expression of FGFR1, -2 and -4. Additionally, FGF signalling in cell lines induced YAP expression and nuclear localisation, indicating

reciprocal cross-talk. Inhibition of FGF signalling with BGJ398 decreased YAP activation through FGF5-FGFR2, suggesting a novel clinical approach and demonstrating that YAP may be a biomarker of response to FGFR inhibition in these patients (Rizvi et al., 2016, Sugihara et al., 2019). Therefore, Hippo signalling may form complex cross-talk FGF signalling, to regulate cancer development and progression.

In addition to playing a key role in cancer cell survival, YAP1 has been reported to induce activation of CAFs within the stroma of breast and liver tumours (Calvo et al., 2013, Hao et al., 2017, Mannaerts et al., 2015). YAP1 was also found to be highly expressed in the nuclei of activated PSCs. Inhibition of YAP1 by RUNX1 or knockdown interrupted TGF-β signalling and caused PSCs to revert to a quiescent phenotype, indicating that Hippo signalling could play a key role in the desmoplastic stroma of PDAC. The stimulation of YAP1 expression in PSCs caused increased SPARC expression (Jiang et al., 2018, Xiao et al., 2019). High levels of SPARC within PDAC stroma has been correlated with poor patient prognosis (Guweidhi et al., 2005, Infante et al., 2007, Murakawa et al., 2019). However, the effect of SPARC in resectable compared to metastatic patients and how this affects response to treatment is complex and still not understood (Gundewar et al., 2015, Hidalgo et al., 2015, Mantoni et al., 2008, Miyoshi et al., 2010, Ormanns et al., 2016, Prenzel et al., 2006, Rossi et al., 2016, Sinn et al., 2014, Von Hoff et al., 2011). It has been shown that SPARC can decrease VEGF and Notch levels in cancer cells, decreasing angiogenesis and increasing stromal metabolic activity. Furthermore, SPARC levels can regulate MMP-2 expression. This contributes to tumour progression and the formation of the characteristic stiff, hypoxic tumour microenvironment in PDAC (Guweidhi et al., 2005). Additionally, studies have shown that conditioned media from PDAC cells can decrease endogenous PSC SPARC expression, whereas co-cultures

with PDAC cells can increase SPARC expression in stromal fibroblasts (Chen et al., 2010, Sato et al., 2003). This highlights the potential role of SPARC in mediating stromal-cancer cross-talk in tumours.

In contrast to stromal-derived SPARC, there has been a low level of expression detected in cancer cells (Mantoni et al., 2008). SPARC has been linked to increased invasiveness in cancer cells, evidenced by its expression in circulating tumour cells (Ting et al., 2014). However in other studies, SPARC expression in tumour cells has been associated with decreased invasion and proliferation. This was shown to be regulated by FGFR1 isoform expression, as FGFR1b increased SPARC levels whereas FGFR1c decreased expression (Chen et al., 2010). Therefore, cross-talk between FGF and Hippo signalling could modulate PDAC progression and invasion through secretion of proteins such as SPARC. This indicates the complexity of stromal-cancer cross-talk in PDAC and the difficulty in achieving effective stromal targeting in the clinic.

The novel role of nFGFR1 in PSCs in relation to Hippo signalling and other downstream targets will need to be validated. This will demonstrate if there are key nuclear targets that can be investigated further or if FGFR1 translocation triggers a total reprogramming of PSCs into invasive cells by multiple gene expression changes, such as the role of nFGFR1 in neural reprogramming (Stachowiak et al., 2007).

Hippo signalling is just one of the many promising avenues which could be explored further from my exciting, though preliminary, ChIP-seq data. Several other potential targets can be investigated, such as scribble planar cell polarity protein (SCRIB), myosin XVA (MYO15A), bone morphogenetic protein 8A (BMP8A), desert hedgehog

(DHH), mucin 2 (MUC2) and protocadherin beta 15 (PCDHB15), as well as the role of FGFR1 in ubiquitination and sub-cellular organisation pathways.

6.3.1.5 FGF and TGF-β signalling cross-talk

STRING analysis of networks enriched in the significant peaks from ChIP-seq analysis (Figure 5.15) identified SMAD3 as a central node, suggesting that this may be related to critical pathway changes upon FGFR inhibition or knockdown in PSCs. TGF-β signalling has been reported to interact with many other intracellular pathways to induce a range of responses, such as the Wnt, Hippo and Hedgehog pathways (Luo, 2017). It has been shown that activation of FGF signalling in smooth muscle cells causes a decrease in TGF-β signalling, switching the cells from a contractile to a proliferative phenotype (Chen et al., 2016a). Cross-talk between these pathways has also been confirmed in human atherosclerosis patients, where increased FGF and decreased TGF-β signalling causes more severe disease. This highlights the importance of the FGF driven phenotype switch in smooth muscle cells in the formation of atherosclerotic plaques (Chen et al., 2016b). Moreover, TGF-β signalling is a key driver of pancreatic fibrosis and pancreatic stellate cell activation (Bailey and Leach, 2012). Therefore, cross-talk between FGFR and SMAD3 in PSCs could be important for switching on the invasive phenotype and driving PDAC progression. This will warrant further investigation in the future.

6.3.2 FGF signalling in PSCs

In addition to the role of nFGFR1 in PSCs, sub-cellular fractionation and mass spectrometry was used to determine the protein flux upon FGFR inhibition. Proteomic analysis following FGFR1 inhibition with AZD4547 showed significant changes in both total peptide abundance and sub-cellular peptide localisation, compared to vehicle

control. Analysis showed that the most significantly decreased peptide was MARCKSL1, whilst the most significantly increased peptide was Zinc finger C3H1 domain-containing protein (ZFC3H1) (Figure 5.19). The results indicated that upon FGFR inhibition, there was a decrease in peptides related to actin cytoskeleton and cell migration (MARCKSL1 and FHOD1), as well as response to oxidative stress (GPX1). These hits, amongst other exciting mechanisms, are being validated currently in the laboratory. I will discuss the relevance and importance of these potential hits and their targeting.

6.3.2.1 Myristoylated alanine-rich c-kinase substrate-like protein 1

MARCKSL1 is a member of the MARCKS family of proteins, which play a role in cell migration and actin cytoskeleton remodelling (Aderem, 1992, El Amri et al., 2018, Yarmola et al., 2001). Phosphorylation of MARCKSL1 by PKC, or binding to calmodulin, causes the protein to dissociate from the plasma membrane and move into the cytosol (Hartwig et al., 1992). In the cytoplasm, MARCKSL1 can interact with actin or PLC and PI3K to trigger downstream signalling. It has been reported that MARCKS plays a role in cell motility, phagocytosis and membrane trafficking through its interaction with the actin cytoskeleton. It is also important for neural tube closure in early brain development and regulates fibroblast migration (Chen et al., 1996, Ott et al., 2013). Phosphorylation of MARCKS has been associated with cancer progression (Fong et al., 2017). However, it has been linked with both increasing and decreasing cancer cell invasion in different contexts (Bjorkblom et al., 2012, Dorris et al., 2017). Phosphorylated MARCKS is expressed by invasive lung cancer cell lines and promotes migration of melanoma cells (Chen and Rotenberg, 2010, Chen et al., 2014). It has been suggested that when the MARCKS family is phosphorylated, PIP_2 is available to PI3K and PLCγ and downstream Akt/PKC signalling is activated (Chin and Toker, 2009, El Amri et al., 2018).

Validation work has shown a decrease in invasion following siRNA-mediated knockdown of MARCKSL1 in the 3D spheroid co-culture *in vitro* model, replicating FGFR1 knockdown or inhibition (data not shown). Due to the opposing role of the MARCKS family in cell migration depending on the phosphorylation status, it may be imperative in future studies to investigate MARCKSL1 phosphorylation following FGFR1 knockdown or inhibition (Bjorkblom et al., 2012).

6.3.2.2 Formin homology-2-domain containing protein 1

FHOD1 is associated with actin cytoskeleton rearrangements in the process of EMT, contributing to cell migration (Gardberg et al., 2013). It can be modulated by PKC binding and MAPK signalling; therefore this may be a method of downstream signalling by FGFR1 within PSCs (Boehm et al., 2005). FHOD1 is also reported to be activated by ROCK by phosphorylation (Takeya et al., 2008) and can be upregulated in EMT during cancer cell migration (Gardberg et al., 2013). In particular, FHOD1 expression has been inversely correlated with miR200c, which can decrease invasion in cancer. The expression of miR200c has been shown to be decreased at the invasive front of PDAC tumours (Yu et al., 2010). Furthermore, overexpression of miR200c can decrease invasion and stress fibre formation in breast cancer cells, indicating that this could play an important role in tumour invasion and metastasis (Jurmeister et al., 2012). This points to a potential role for FHOD1 at the invasive edge of PDAC tumours, which is being validated in the context of nuclear FGFR1 signalling currently in the laboratory.

6.3.2.3 Glutathione peroxidase 1

GPX1 is a key protein involved in the response to oxidative stress and catalyses the conversion of glutathione and hydrogen peroxide into glutathione disulphide and

water (Mills, 1957). Activated FGF signalling in wound repair has been shown to regulate the expression of GPX1 (Frank et al., 1997, Munz et al., 1997). FGF7 can promote the expression of GPX1 to promote wound healing and protect keratinocytes from ROS in skin cancer formation (Marchese et al., 1995, Pentland, 1994). Moreover, following treatment with FGFR1 neutralising antisera, breast cancer and osteosarcoma cells displayed a decrease in GPX1 expression. This indicates a positive link between FGF signalling and GPX1 expression (Ling et al., 2015). GPX1 has been reported to be overexpressed in some cancers, such as colorectal, oesophageal and breast tumours (Hughes et al., 2018, Mahbouli et al., 2018, Peng et al., 2009). GPX1 expression has also been correlated with invasion in oesophageal cancer (Gan et al., 2014). Increased expression of GPX1 has been reported in activated hepatic stellate cells (HSCs) (Dunning et al., 2013). In PDAC, a decrease in GPX1 triggers EMT and chemotherapy resistance, indicating the complex response to ROS within tumours (Meng et al., 2018).

Validation work has shown that siRNA-mediated knockdown of GPX1 decreased invasion in the spheroid 3D co-culture *in vitro* model, replicating the results seen following FGFR1 knockdown or inhibition (data not shown). Oxidative stress is a central regulator of fibrosis and therefore GPX1 may be a key regulator in activated stellate cells in response to ROS (Richter and Kietzmann, 2016).

6.3.2.4 Sub-cellular peptide changes

Sub-cellular localisation of peptides upon FGFR inhibition was also determined using mass spectrometry. This highlighted many significant changes in different compartments within PSCs, which could indicate the critical role of FGFR1 within PDAC invasion and metastasis. Focusing on the changes occurring within the nuclear

compartment, potentially alongside, or as a result of, nuclear translocation of FGFR1, some key pathways are being altered (Table 5.7). In particular, epigenetic regulatory proteins are being changed, which could provide evidence for a role of nFGFR1 in regulating gene expression in PSCs (Figures 5.21 and 5.22). Furthermore, upon FGFR inhibition, the levels of the receptor tyrosine kinase c-MET within the nucleus are decreased (Figure 5.23). This could indicate a novel interaction between FGFR1 and c-Met in PSCs.

6.3.2.5 c-MET

The only known ligand of c-MET is hepatocyte growth factor (HGF). This binds to the receptor, triggering dimerization and phosphorylation to activate downstream signalling pathways (Organ and Tsao, 2011). Overexpression of c-MET has been detected in PDAC and correlated with decreased survival (Kim et al., 2017). Studies have also demonstrated that HGF produced by PSCs in PDAC stroma can activate c-MET on cancer cells, triggering proliferation and migration (Pothula et al., 2017). This c-MET mediated cross-talk can also promote perineural invasion of cancer cells (Nan et al., 2019). Furthermore, c-MET cross-talk in PDAC can enhance glycolysis and induce cancer stem cell properties in tumour cells (Yan et al., 2018).

Nuclear translocation of c-MET has been previously reported, triggering activation of calcium signals and downstream pathways. In particular c-MET translocation has been shown to be dependent on Gab1 and importin β1 (Gomes et al., 2008). Additionally, it has been shown that hydrogen peroxide can induce retrograde transport of c-MET into the nucleus in breast cancer cells, indicating a role of c-MET in ROS-induced DNA damage repair (Chen et al., 2019).

6.3.2.6 c-MET signalling cross-talk

c-MET can interact with EGFR in tumour cells, triggering receptor activation in the absence of HGF (Jo et al., 2000). Moreover, EGF stimulation of NSCLC cells can lead to phosphorylation of c-MET, indicating significant cross-talk between these two pathways (Puri and Salgia, 2008). Both ERBB2 and ERBB3 have also been shown to interact with and activate c-MET (Bachleitner-Hofmann et al., 2008, Khoury et al., 2005). Cross-talk has also been reported between c-MET and recepteur d'origine Nantais (RON) kinase, leading to transactivation in cancer cells (Benvenuti et al., 2011, Follenzi et al., 2000). In bladder cancer, cross-talk between c-MET, Axl and PDGFRα has been shown to cause tumour progression (Yeh et al., 2011). A study investigating the effect of FGFR inhibition with AZD4547 in lung cancer cell lines showed that upon acquired resistance developing, cells demonstrated overexpression and activation of c-MET. Using a combination therapy of FGFR inhibitors with the c-MET inhibitor crizotinib or c-MET knockdown restored sensitivity. This indicates that c-MET signalling may be used to bypass FGF inhibition in cells and there could be synergistic benefits of combining FGFR and c-MET inhibitors (Kim et al., 2016).

The downstream sub-cellular peptide changes discovered in PSCs following FGFR inhibition are now being validated and investigated, with a particular focus on the interaction with c-MET. This will demonstrate the functional importance of these hits in PDAC progression and invasion.

In summary, in Section 6.3, I have demonstrated that whilst elucidating intra-cellular mechanisms for FGFR1 signalling within PSCs is challenging, I have made significant

progress to yield many exciting and relevant biological leads which merit further investigation; thus opening new areas of research for PSC.

6.4 Introducing FGFR1-targeting into PDAC therapies

Following the exciting results showing a significant impact on stroma-cancer cross-talk in PDAC when targeting FGFR1 within PSCs, particularly in respect of invasion, I further validated this approach in the context of current and developing PDAC therapy combinations. A big focus in PDAC research is stromal targeting to improve treatment outcomes (Section 1.4). Therefore, I considered current stromal targeting combinations in promising PDAC clinical trials and investigated the effect of introducing FGFR1-targeting therapies to disrupt cellular cross-talk.

6.4.1 Stromal targeting

6.4.1.1 Stromal therapies in cancer

Tumours are not comprised of cancer cells alone, they include many other cell types, which can all make up the tumour microenvironment or stroma. It is now well accepted that the stroma can play a key role in tumour progression and contribute to therapeutic resistance (Section 1.3). Therefore, clinical targeting of the stromal compartment of tumours has attracted interest over recent years (Section 1.4) (Valkenburg et al., 2018). A number of stromal-targeting agents are in clinical trials, such as defactinib (a FAK kinase inhibitor) in ovarian cancer (NCT03287271) and fresolimumab (to target TGF-β) in NSCLC (NCT02581787).

Targeting the ECM is an area of interest in stromal therapies. In melanoma xenograft models treatment with halofuginone, a collagen type 1 inhibitor, was shown to reduce

metastasis (Juarez et al., 2012). Furthermore, lysyl oxidase catalyses collagen crosslinking and has been reported to play a role in metastasis, making it a potential therapeutic target (Erler et al., 2006).

Other approaches that are being considered are to target specific proteins on stromal cells, such as FAP on CAFs. Combining anti-FAP antibodies with drugs or radiotherapy to enhance delivery to the cancer stroma have demonstrated tumour regression in xenograft models of pancreatic, lung, colorectal and head and neck cancers, as well as melanoma (Erickson et al., 2006, Fischer et al., 2012, Ostermann et al., 2008). Another approach that demonstrates improved anti-tumour effects is to treat cancers with the prodrug promelittin, which is then cleaved by FAP to release a toxin within the tumour (LeBeau et al., 2009).

Immunotherapies have had significant success in a subset of tumours within the clinic. Immunotherapeutic targeting can include chimeric antigen receptor T (CAR T) cells, oncolytic virus therapy, adoptive cell therapy, cancer vaccines and antibodies (Farkona et al., 2016). Particular success has been achieved with immune checkpoint blockade of CTLA-4 or PD1/PDL1. Ipilimumab, an anti-CTLA4 antibody, has been approved for use in metastatic melanoma following successful trials showing an increase in overall survival (Hodi et al., 2010, Robert et al., 2011). Additionally anti-PD1 antibodies, pembrolizumab and nivolumab, have been approved for use in melanoma and NSCLC. Nivolumab has also been approved for renal cell carcinoma (Sharma and Allison, 2015, Topalian et al., 2012). Antibodies targeting PDL1 have also shown efficacy in melanoma, renal cell carcinoma, NSCLC and bladder cancer (Brahmer et al., 2012).

The explosion of stromal targeting therapies being investigated in the context of cancer, with translation into clinical trials, demonstrates the importance of the tumour microenvironment in a multitude of tumours. Clinical success of therapies such as immune checkpoint blockade antibodies highlights the significant benefit stromal-targeted therapies could have on patient prognosis.

6.4.1.2 Stromal therapies in PDAC

The characteristic desmoplastic stroma present in PDAC tumours has meant that stromal-therapeutic targeting has gathered significant interest in recent years, leading to several clinical trials, including hedgehog pathway inhibition, hyaluronic acid degradation, and a variety of immunotherapy concepts (summarised in Table 6.3 and Section 1.4) (Doherty et al., 2018, Gong et al., 2018, Jacobetz et al., 2013, Kabacaoglu et al., 2018, McCarroll et al., 2014, Merika et al., 2012, Olive et al., 2009, Richards et al., 2012, Thompson et al., 2010). PSCs, which form a key part of this desmoplastic stroma, become activated in response to tumour development. Activated PSCs engage in cross-talk with cancer cells to induce tumour cell proliferation and invasion, leading to metastatic spread, making these cells an attractive therapeutic target (Apte et al., 2013, Liu et al., 2019).

However, modifying the stroma has been shown to be more complicated than expected. Removal of activated PSCs in pancreatic tumours, or inhibition of hedgehog signalling, can lead to increased cancer cell proliferation and therefore result in shorter patient survival (Bailey et al., 2009, Feldmann et al., 2008, Rhim et al., 2014). This emphasises the importance of fully understanding the complex network of cellular interactions that characterise PDAC stroma, in particular the interactions between cancer cells and the activated PSCs.

I have shown that FGFR inhibition with AZD4547 does not affect the proliferation or survival of the cancer or stellate cells (Figure 3.6), but rather disrupts essential cellular cross-talk. Therefore the aim of treating patients with AZD4547 would be not to destroy the stroma but instead re-programme it into a less tumorigenic microenvironment.

Table 6.3 Stromal therapies in PDAC

Compound	Targets	Combination	Patient cohort	Trial phase	Ref
ATRA	CAFs	Gemcitabine, nab-paclitaxel	PDAC	Phase I	NCT03307148
Cabiralizumab	Colony-stimulating factor-1 receptor	Nivolumab	Solid tumour	Phase I	NCT02526017
EF-002	Macrophage activity	Dose escalation	Solid tumour	Phase I	NCT02052492
Paricalcitol	Metabolic pathway	Gemcitabine, nab-paclitaxel	Advanced PC	Phase I	NCT02030860
Pembrolizumab	PD-1	Paricalcitol, gemcitabine, nab-paclitaxel	Resectable PC	Phase I	NCT02930902
Defactinib	FAK signalling	PD-1	Solid tumour	Phase I/II	NCT02758587
MEDI4736	C-X-C chemokine receptor type 2	Gemcitabine, nab-paclitaxel	Stage IV PDAC	Phase I/II	NCT02583477
Sonidegib	Hedgehog signalling	Gemcitabine, nab-paclitaxel	Stage IV PDAC	Phase I/II	2013-002370-51
Vismodegib	Hedgehog signalling	Gemcitabine	Stage IV PDAC	Phase I/II	NCT01064622
GSK2256098	FAK signalling	Tremetinib	PDAC	Phase II	NCT02428270
PEGPH20	Hyaluronic acid	Gemcitabine, nab-paclitaxel	Stage IV PDAC	Phase II	NCT01839487
AM0010	IL-10	FOLFOX, 5-FU, leucovorin	Solid tumour	Phase III	NCT02923921

6.4.1.3 Targeting activated PSCs and cancer cells in combination

One of the most promising PDAC stromal targets is activated PSCs. Previous work carried out by our group showed that returning PSCs to their quiescent phenotype with all-trans retinoic acid (ATRA) improved response to gemcitabine in 3D *in vitro* models and the KPC mouse (Carapuça et al., 2016, Froeling et al., 2011). This work has now been translated into the STARPAC phase 1b clinical trial with the aim of re-educating stromal PSCs to improve response to current therapies (NCT03307148). This shows the importance of combining PSC targeting with current approved PDAC therapies in the clinic. Moreover, by re-educating the stroma rather than depleting it, the delivery of therapeutics to the tumour can be increased, without causing tumour progression.

Building on the successful translation of combining ATRA and gemcitabine to target PSCs and cancer cells, I selected these drugs to combine with AZD4547 to additionally target FGFR-mediated cellular cross-talk, with particular reference to reducing invasion.

6.4.2 Targeting FGFR-mediated cellular cross-talk

6.4.2.1 Addition of AZD4547 to current PDAC therapies

I have demonstrated that FGF signalling is a vital cross-talk mechanism between PSCs and cancer cells that leads to PDAC progression and invasion. Additionally, FGFR inhibition with AZD4547 can successfully disrupt FGF-mediated cellular cross-talk. Therefore, combination therapies of AZD4547, ATRA and gemcitabine were examined in the mini-organotypic 3D *in vitro* model, treating with ATRA and AZD4547 daily and gemcitabine weekly to match patient protocols. These results further demonstrated the importance of FGF signalling in PDAC invasion, with the

combinations containing AZD4547 displaying significantly reduced invasion (Figure 4.10). Additionally, AZD4547 treatment in combination with ATRA or both ATRA and gemcitabine resulted in a decreased cell layer on the surface of the gel, indicating that these treatment combinations may affect cell survival.

6.4.2.2 Development of triple therapy

The initial analysis combining ATRA, gemcitabine and AZD4547 therapeutically looks promising. However, these 3D models were only maintained for a short time (7 days) and the results obtained were a snapshot at one time-point, which may explain the lack of difference in proliferation and apoptosis between treatment conditions. The full effects of targeting the cancer, stroma and cross-talk still need to be determined, including a comprehensive investigation of the effect on cancer cell survival and PSC activation. Additionally, it will be useful to perform a dynamic analysis of cell behaviours with the different treatment combinations over time. Longer therapeutic regimens, with more treatments of relevant chemotherapies, may give a better representation of whether co-targeting the cross-talk alongside stellate and cancer cells is effective. Other 3D *in vitro* models could be used for this, such as organoids or microfluidic cultures. Furthermore, the effect of this combination treatment on tumour growth will be assessed using an *in vivo* model, which will give in-depth analysis of whether the three drugs together give an improved anti-tumour response. However, subcutaneous models in NSG mice will not include the response of all the surrounding stromal cells found within the pancreas, as well as not modelling the immune response, which could be extremely important in translating this data to patients in the clinic.

Any increased side effects will also need to be considered before applying these results to the clinic. Gemcitabine and ATRA are already being used in combination in patients in the STARPAC clinical trial (NCT03307148), however adding AZD4547 could increase side effects in patients. FGF tyrosine kinase inhibitors can have adverse effects on the cardiovascular system and the liver, as well as causing hypertension, bleeding and thrombosis due to their anti-angiogenetic action. Gastrointestinal and dermatological side effects have also been reported (Katoh, 2016, Paik et al., 2017, Saka et al., 2017).

6.5 Future work

Ongoing experiments are being performed to repeat and extend the mass spectrometry analysis to include FGFR1 shRNA knockdown cells. The results from these repeats will confirm which hits are important for mediating FGFR1 invasion in stellate cells. The full sub-cellular mass spectrometry and ChIP-seq results will also need to be analysed and validated, such as the role of MARCKSL1, GPX1, FHOD1, c-MET, epi-genetic regulators, Hippo signalling, ubiquitination and subcellular unit organisation. ChIP-PCR will confirm the validity of the ChIP hits. Furthermore, an siRNA screen will be used in the spheroid 3D *in vitro* model to confirm which hits are the most important for mediating stellate cell invasion in PDAC.

The critical role of nuclear FGFR1 could be determined in pancreatic stellate cells by further investigation into the upstream signalling causing this phenomenon at the invasive edge of tumours. This will provide a greater insight into the complex cross-talk that occurs in PDAC, improving understanding and therefore providing validation of therapeutic targeting that will lead to increased patient prognosis.

Using primary stellate cell cultures or patient-derived tissue will also provide further clinical validation of the importance of FGF-mediated cellular cross-talk and the potential for targeting this in the clinical setting. Longer term 3D *in vitro* models and *in vivo* targeting of FGF signalling cross-talk, alongside targeting cancer and stellate cells directly, will demonstrate whether this triple combination with gemcitabine, ATRA and AZD4547 is a valid clinical regimen to transfer into patients. By improving therapeutic targeting, especially of invasion, patient prognosis can be improved.

6.6 Conclusion

PDAC has a poor prognosis with a 5-year survival rate of less than 5 %. PDAC tumours consist of a desmoplastic stroma, which limits the effectiveness of chemotherapy. PSCs, which form a key part of this stroma, become activated in response to tumour development and enter a cross-talk with cancer cells to induce tumour cell proliferation and invasion, leading to metastatic spread. I have demonstrated that FGFR1 signalling is critical in mediating PSC-led invasion in PDAC. Inhibition or knockdown of FGFR1 in stellate cells decreases invasion in novel 3D co-culture *in vitro* models, highlighting this as a potential therapeutic target in patients.

Nuclear translocation of FGFR1 in PSCs appears to be a vital mechanism that triggers the transcription of key proteins involved in PDAC invasion. Chromatin immunoprecipitation (ChIP-seq) and sub-cellular mass spectrometry have been used to determine the potential role nFGFR1 and consequent sub-cellular protein flux upon FGFR inhibition in PSCs. These techniques have dissected the functional consequences of FGFR1 knockdown or inhibition in stellate cells. Candidate drivers

of invasion have been identified, as well as novel nuclear cross-talk mechanisms and these are now being validated in state-of-the-art 3D *in vitro* PDAC models.

Targeting cellular cross-talk with a clinically relevant FGFR inhibitor (AZD4547) has been extended to examine potential combination therapy regimens with the chemotherapeutic agent gemcitabine (targeting cancer cells) and ATRA (modulating PSCs), providing translational relevance for my findings. I am currently validating this novel strategy using *in vivo* co-culture xenograft models with specific reference to FGFR1.

Effectively disrupting FGFR-mediated cross-talk between the tumour and stroma, either alone or in combination with other therapies, could translate to improved therapeutic responses in PDAC patients by providing novel treatment options in the clinic.

References

AZD4547 & Anastrozole or Letrozole (NSAIs) in ER+ Breast Cancer Patients Who Have Progressed on NSAIs (RADICAL) [Online]. Available: https://ClinicalTrials.gov/show/NCT01791985 [Accessed].

Datasets in the Pancreatic Expression Database. [www.pancreasexpression.org/cgi-bin/pancexp/DataSets.pl].

Docetaxel With or Without FGFR Inhibitor AZD4547 in Treating Patients With Recurrent Non-Small Cell Lung Cancer [Online]. Available: https://ClinicalTrials.gov/show/NCT01824901 [Accessed].

Dose Escalation Study of OMP-54F28 in Combination With Nab-Paclitaxel and Gemcitabine in Patients With Previously Untreated Stage IV Pancreatic Cancer [Online]. Available: https://ClinicalTrials.gov/show/NCT02050178 [Accessed].

Efficacy and Safety of AZD4547 Versus Paclitaxel in Patients With Advanced Gastric or Gastro-oesophageal Cancer [Online]. Available: https://ClinicalTrials.gov/show/NCT01457846 [Accessed].

Lung-MAP: AZD4547 as Second-Line Therapy in Treating FGFR Positive Patients With Recurrent Stage IV Squamous Cell Lung Cancer [Online]. Available: https://ClinicalTrials.gov/show/NCT02965378 [Accessed].

Lung-MAP: Biomarker-Targeted Second-Line Therapy in Treating Patients With Recurrent Stage IV Squamous Cell Lung Cancer [Online]. Available: https://ClinicalTrials.gov/show/NCT02154490 [Accessed].

National Lung Matrix Trial: Multi-drug Phase II Trial in Non-Small Cell Lung Cancer [Online]. Available: https://ClinicalTrials.gov/show/NCT02664935 [Accessed].

Open-Label, Randomised, Multi-Drug, Biomarker-Directed, Phase 1b Study in Pts w/ Muscle Invasive Bladder Cancer [Online]. Available: https://ClinicalTrials.gov/show/NCT02546661 [Accessed].

Proof-of-Concept Study of AZD4547 in Patients With FGFR1 or FGFR2 Amplified Tumours [Online]. Available: https://ClinicalTrials.gov/show/NCT01795768 [Accessed].

ROCKIF Trial: Re-sensitization of Carboplatin-resistant Ovarian Cancer With Kinase Inhibition of FAK [Online]. Available: https://ClinicalTrials.gov/show/NCT03287271 [Accessed].

SABR-ATAC: A Trial of TGF-beta Inhibition and Stereotactic Ablative Radiotherapy for Early Stage Non-small Cell Lung Cancer [Online]. Available: https://ClinicalTrials.gov/show/NCT02581787 [Accessed].

Safety and Efficacy of AZD4547 in Combination With Fulvestrant vs. Fulvestrant Alone in ER+ Breast Cancer Patients [Online]. Available: https://ClinicalTrials.gov/show/NCT01202591 [Accessed].

SAFIR02_Breast - Efficacy of Genome Analysis as a Therapeutic Decision Tool for Patients With Metastatic Breast Cancer [Online]. Available: https://ClinicalTrials.gov/show/NCT02299999 [Accessed].

SAFIR02_Lung - Efficacy of Targeted Drugs Guided by Genomic Profiles in Metastatic NSCLC Patients [Online]. Available: https://ClinicalTrials.gov/show/NCT02117167 [Accessed].

Stromal TARgeting for PAncreatic Cancer (STAR_PAC) [Online]. Available: https://ClinicalTrials.gov/show/NCT03307148 [Accessed].

A Study Evaluating IPI-926 in Combination With Gemcitabine in Patients With Metastatic Pancreatic Cancer [Online]. Available: https://ClinicalTrials.gov/show/NCT01130142 [Accessed].

Study is Designed to Assess the Safety and Tolerability of AZD4547 at Increasing Doses in Patients With Advanced Tumours [Online]. Available: https://ClinicalTrials.gov/show/NCT00979134 [Accessed].

A Study of Vantictumab (OMP-18R5) in Combination With Nab-Paclitaxel and Gemcitabine in Previously Untreated Stage IV Pancreatic Cancer [Online]. Available: https://ClinicalTrials.gov/show/NCT02005315 [Accessed].

Study to Assess Safety and Tolerability of AZD4547 in Japanese Patient [Online]. Available: https://ClinicalTrials.gov/show/NCT01213160 [Accessed].

Targeted Therapy Directed by Genetic Testing in Treating Patients With Advanced Refractory Solid Tumors, Lymphomas, or Multiple Myeloma (The MATCH Screening Trial) [Online]. Available: https://ClinicalTrials.gov/show/NCT02465060 [Accessed].

Treatment With AZD4547 for Recurrent Malignant Glioma Expressing FGFR-TACC Gene Fusion" [Online]. Available: https://ClinicalTrials.gov/show/NCT02824133 [Accessed].

Aderem, A. 1992. The MARCKS brothers: a family of protein kinase C substrates. *Cell,* 71**,** 713-6.

Aebersold, R. & Mann, M. 2003. Mass spectrometry-based proteomics. *Nature,* 422**,** 198-207.

Aiello, N. M. & Stanger, B. Z. 2016. Echoes of the embryo: using the developmental biology toolkit to study cancer. *Disease Models & Mechanisms,* 9**,** 105-114.

Alarcon, C., Zaromytidou, A. I., Xi, Q., Gao, S., Yu, J., Fujisawa, S., Barlas, A., Miller, A. N., Manova-Todorova, K., Macias, M. J., Sapkota, G., Pan, D. & Massague, J. 2009. Nuclear CDKs drive Smad transcriptional activation and turnover in BMP and TGF-beta pathways. *Cell,* 139**,** 757-69.

Allenson, K., Castillo, J., San Lucas, F. A., Scelo, G., Kim, D. U., Bernard, V., Davis, G., Kumar, T., Katz, M., Overman, M. J., Foretova, L., Fabianova, E., Holcatova, I., Janout, V., Meric-Bernstam, F., Gascoyne, P., Wistuba, I., Varadhachary, G., Brennan, P., Hanash, S., Li, D., Maitra, A. & Alvarez, H. 2017. High prevalence of mutant KRAS in circulating exosome-derived DNA from early-stage pancreatic cancer patients. *Ann Oncol,* 28**,** 741-747.

Almawash, S. A., Mondal, G. & Mahato, R. I. 2018. Coadministration of Polymeric Conjugates of Docetaxel and Cyclopamine Synergistically Inhibits Orthotopic Pancreatic Cancer Growth and Metastasis. *Pharm Res,* 35**,** 17.

Altomare, D. A. & Testa, J. R. 2005. Perturbations of the AKT signaling pathway in human cancer. *Oncogene,* 24**,** 7455-64.

Ansari, D., Ohlsson, H., Althini, C., Bauden, M., Zhou, Q., Hu, D. & Andersson, R. 2019. The Hippo Signaling Pathway in Pancreatic Cancer. *Anticancer Res,* 39**,** 3317-3321.

Apte, M., Haber, P., Applegate, T., Norton, I., Mccaughan, G., Korsten, M., Pirola, R. & Wilson, J. 1998. Periacinar stellate shaped cells in rat pancreas: identification, isolation, and culture. *Gut,* 43**,** 128-133.

Apte, M. V. & Wilson, J. S. 2012. Dangerous liaisons: pancreatic stellate cells and pancreatic cancer cells. *J Gastroenterol Hepatol,* 27 Suppl 2**,** 69-74.

Apte, M. V., Wilson, J. S., Lugea, A. & Pandol, S. J. 2013. A Starring Role for Stellate Cells in the Pancreatic Cancer Microenvironment. *Gastroenterology,* 144**,** 1210-1219.

Arasada, R. R. & Carpenter, G. 2005. Secretase-dependent tyrosine phosphorylation of Mdm2 by the ErbB-4 intracellular domain fragment. *J Biol Chem,* 280**,** 30783-7.

Arasaradnam, R. P., Wicaksono, A., O'Brien, H., Kocher, H. M., Covington, J. A. & Crnogorac-Jurcevic, T. 2018. Noninvasive Diagnosis of Pancreatic Cancer Through Detection of Volatile Organic Compounds in Urine. *Gastroenterology,* 154**,** 485-487.e1.

Arumugam, T., Brandt, W., Ramachandran, V., Moore, T. T., Wang, H., May, F. E., Westley, B. R., Hwang, R. F. & Logsdon, C. D. 2011. Trefoil factor 1 stimulates both pancreatic cancer and stellate cells and increases metastasis. *Pancreas,* 40**,** 815-822.

Attieh, Y., Clark, A. G., Grass, C., Richon, S., Pocard, M., Mariani, P., Elkhatib, N., Betz, T., Gurchenkov, B. & Vignjevic, D. M. 2017. Cancer-associated fibroblasts lead tumor invasion through integrin-beta3-dependent fibronectin assembly. *J Cell Biol,* 216**,** 3509-3520.

Awasthi, N., Hinz, S., Brekken, R. A., Schwarz, M. A. & Schwarz, R. E. 2015. Nintedanib, a triple angiokinase inhibitor, enhances cytotoxic therapy response in pancreatic cancer. *Cancer Lett,* 358**,** 59-66.

Babina, I. S. & Turner, N. C. 2017. Advances and challenges in targeting FGFR signalling in cancer. *Nat Rev Cancer,* 17**,** 318-332.

Bachem, M. G., Schneider, E., Gross, H., Weidenbach, H., Schmid, R. M., Menke, A., Siech, M., Beger, H., Grunert, A. & Adler, G. 1998. Identification, culture, and characterization of pancreatic stellate cells in rats and humans. *Gastroenterology,* 115**,** 421-32.

Bachleitner-Hofmann, T., Sun, M. Y., Chen, C. T., Tang, L., Song, L., Zeng, Z., Shah, M., Christensen, J. G., Rosen, N., Solit, D. B. & Weiser, M. R. 2008. HER kinase activation confers resistance to MET tyrosine kinase inhibition in MET oncogene-addicted gastric cancer cells. *Mol Cancer Ther,* 7**,** 3499-508.

Bahleda, R., Hollebecque, A., Varga, A., Gazzah, A., Massard, C., Deutsch, E., Amellal, N., Farace, F., Ould-Kaci, M., Roux, F., Marzin, K. & Soria, J. C. 2015. Phase I study of afatinib combined with nintedanib in patients with advanced solid tumours. *Br J Cancer,* 113**,** 1413-20.

Bailey, J. M. & Leach, S. D. 2012. Signaling pathways mediating epithelial-mesenchymal crosstalk in pancreatic cancer: Hedgehog, Notch and TGFbeta. *In:* Grippo, P. J. & Munshi, H. G. (eds.) *Pancreatic Cancer and Tumor Microenvironment.* Trivandrum (India): Transworld Research Network.

Bailey, J. M., Mohr, A. M. & Hollingsworth, M. A. 2009. Sonic hedgehog paracrine signaling regulates metastasis and lymphangiogenesis in pancreatic cancer. *Oncogene,* 28**,** 3513-25.

Bailey, J. M., Swanson, B. J., Hamada, T., Eggers, J. P., Singh, P. K., Caffery, T., Ouellette, M. M. & Hollingsworth, M. A. 2008. Sonic hedgehog promotes desmoplasia in pancreatic cancer. *Clin Cancer Res,* 14**,** 5995-6004.

Bailey, P., Chang, D. K., Nones, K., Johns, A. L., Patch, A. M., Gingras, M. C., Miller, D. K., Christ, A. N., Bruxner, T. J., Quinn, M. C., Nourse, C., Murtaugh, L. C., Harliwong, I., Idrisoglu, S., Manning, S., Nourbakhsh, E., Wani, S., Fink, L., Holmes, O., Chin, V., Anderson, M. J., Kazakoff, S., Leonard, C., Newell, F., Waddell, N., Wood, S., Xu, Q., Wilson, P. J., Cloonan, N., Kassahn, K. S., Taylor, D., Quek, K., Robertson, A., Pantano, L., Mincarelli, L., Sanchez, L. N., Evers, L., Wu, J., Pinese, M., Cowley, M. J., Jones, M. D., Colvin, E. K., Nagrial, A. M., Humphrey, E. S., Chantrill, L. A., Mawson, A., Humphris, J., Chou, A., Pajic, M., Scarlett, C. J., Pinho, A. V., Giry-Laterriere, M., Rooman, I., Samra, J. S., Kench, J. G., Lovell, J. A., Merrett, N. D., Toon, C. W., Epari, K., Nguyen, N. Q., Barbour, A., Zeps, N., Moran-Jones, K., Jamieson, N. B., Graham, J. S., Duthie, F., Oien, K., Hair, J., Grutzmann, R., Maitra, A., Iacobuzio-Donahue, C. A., Wolfgang, C. L., Morgan, R. A., Lawlor, R. T., Corbo, V., Bassi, C., Rusev, B., Capelli, P., Salvia, R., Tortora, G., Mukhopadhyay, D., Petersen, G. M., Munzy, D. M., Fisher, W. E., Karim, S. A., Eshleman, J. R., Hruban, R. H., Pilarsky, C., Morton, J. P., Sansom, O. J., Scarpa, A., Musgrove, E. A., Bailey, U. M., Hofmann, O., Sutherland, R. L., Wheeler, D. A., Gill, A. J., Gibbs, R. A., Pearson, J. V., Waddell, N., et al. 2016. Genomic analyses identify molecular subtypes of pancreatic cancer. *Nature,* 531**,** 47-52.

Baker, L. A., Tiriac, H., Clevers, H. & Tuveson, D. A. 2016. Modeling pancreatic cancer with organoids. *Trends Cancer,* 2**,** 176-190.

Baldia, P. H., Maurer, A., Heide, T., Rose, M., Stoehr, R., Hartmann, A., Williams, S. V., Knowles, M. A., Knuechel, R. & Gaisa, N. T. 2016. Fibroblast growth factor receptor (FGFR) alterations in squamous differentiated bladder cancer: a putative therapeutic target for a small subgroup. *Oncotarget,* 7**,** 71429-71439.

Barbazán, J. & Matic Vignjevic, D. 2019. Cancer associated fibroblasts: is the force the path to the dark side? *Current Opinion in Cell Biology,* 56**,** 71-79.

Bard, L., Boscher, C., Lambert, M., Mège, R.-M., Choquet, D. & Thoumine, O. 2008. A Molecular Clutch between the Actin Flow and N-Cadherin Adhesions Drives Growth Cone Migration. *The Journal of Neuroscience,* 28**,** 5879-5890.

Bardeesy, N. & Depinho, R. A. 2002. Pancreatic cancer biology and genetics. *Nat Rev Cancer,* 2**,** 897-909.

Baron, O., Förthmann, B., Lee, Y.-W., Terranova, C., Ratzka, A., Stachowiak, E. K., Grothe, C., Claus, P. & Stachowiak, M. K. 2012. Cooperation of Nuclear Fibroblast Growth Factor Receptor 1 and Nurr1 Offers New Interactive Mechanism in Postmitotic Development of Mesencephalic Dopaminergic Neurons. *The Journal of Biological Chemistry,* 287**,** 19827-19840.

Barron, D. A. & Kagey, J. D. 2014. The role of the Hippo pathway in human disease and tumorigenesis. *Clinical and Translational Medicine,* 3**,** 25.

Bazhin, A. V., Shevchenko, I., Umansky, V., Werner, J. & Karakhanova, S. 2014. Two immune faces of pancreatic adenocarcinoma: possible implication for immunotherapy. *Cancer Immunol Immunother,* 63**,** 59-65.

Becker, A. E., Hernandez, Y. G., Frucht, H. & Lucas, A. L. 2014. Pancreatic ductal adenocarcinoma: Risk factors, screening, and early detection. *World Journal of Gastroenterology : WJG,* 20**,** 11182-11198.

Beer, L. A., Liu, P., Ky, B., Barnhart, K. T. & Speicher, D. W. 2017a. Efficient Quantitative Comparisons of Plasma Proteomes Using Label-Free Analysis with MaxQuant. *Methods in molecular biology (Clifton, N.J.),* 1619**,** 339-352.

Beer, M., Kuppalu, N., Stefanini, M., Becker, H., Schulz, I., Manoli, S., Schuette, J., Schmees, C., Casazza, A., Stelzle, M. & Arcangeli, A. 2017b. A novel microfluidic 3D platform for culturing pancreatic ductal adenocarcinoma cells: comparison with in vitro cultures and in vivo xenografts. *Scientific Reports,* 7**,** 1325.

Benvenuti, S., Lazzari, L., Arnesano, A., Li Chiavi, G., Gentile, A. & Comoglio, P. M. 2011. Ron kinase transphosphorylation sustains MET oncogene addiction. *Cancer Res,* 71**,** 1945-55.

Berberat, P. O., Friess, H., Wang, L., Zhu, Z., Bley, T., Frigeri, L., Zimmermann, A. & Buchler, M. W. 2001. Comparative analysis of galectins in primary tumors and tumor metastasis in human pancreatic cancer. *J Histochem Cytochem,* 49**,** 539-49.

Bettegowda, C., Sausen, M., Leary, R. J., Kinde, I., Wang, Y., Agrawal, N., Bartlett, B. R., Wang, H., Luber, B., Alani, R. M., Antonarakis, E. S., Azad, N. S., Bardelli, A., Brem, H., Cameron, J. L., Lee, C. C., Fecher, L. A., Gallia, G. L., Gibbs, P., Le, D., Giuntoli, R. L., Goggins, M., Hogarty, M. D., Holdhoff, M., Hong, S. M., Jiao, Y., Juhl, H. H., Kim, J. J., Siravegna, G., Laheru, D. A., Lauricella, C., Lim, M., Lipson, E. J., Marie, S. K., Netto, G. J., Oliner, K. S., Olivi, A., Olsson, L., Riggins, G. J., Sartore-Bianchi, A., Schmidt, K., Shih L, M., Oba-Shinjo, S. M., Siena, S., Theodorescu, D., Tie, J., Harkins, T. T., Veronese, S., Wang, T. L., Weingart, J. D., Wolfgang, C. L., Wood, L. D., Xing, D., Hruban, R. H., Wu, J., Allen, P. J., Schmidt, C. M., Choti, M. A., Velculescu, V. E., Kinzler, K. W., Vogelstein, B., Papadopoulos, N. & Diaz, L. A., Jr. 2014. Detection of circulating tumor DNA in early- and late-stage human malignancies. *Sci Transl Med,* 6**,** 224ra24.

Bharali, D. J., Klejbor, I., Stachowiak, E. K., Dutta, P., Roy, I., Kaur, N., Bergey, E. J., Prasad, P. N. & Stachowiak, M. K. 2005. Organically modified silica nanoparticles: a nonviral vector for in vivo gene delivery and expression in the brain. *Proc Natl Acad Sci U S A,* 102**,** 11539-44.

Bill, R., Fagiani, E., Zumsteg, A., Antoniadis, H., Johansson, D., Haefliger, S., Albrecht, I., Hilberg, F. & Christofori, G. 2015. Nintedanib Is a Highly Effective Therapeutic for Neuroendocrine Carcinoma of the Pancreas (PNET) in the Rip1Tag2 Transgenic Mouse Model. *Clin Cancer Res,* 21**,** 4856-67.

Birrer, M. J., Johnson, M. E., Hao, K., Wong, K. K., Park, D. C., Bell, A., Welch, W. R., Berkowitz, R. S. & Mok, S. C. 2007. Whole genome oligonucleotide-based array comparative genomic hybridization analysis identified fibroblast growth factor 1 as a prognostic marker for advanced-stage serous ovarian adenocarcinomas. *J Clin Oncol,* 25**,** 2281-7.

Bixby, J. L. & Zhang, R. 1990. Purified N-cadherin is a potent substrate for the rapid induction of neurite outgrowth. *The Journal of Cell Biology,* 110**,** 1253-1260.

Bjorkblom, B., Padzik, A., Mohammad, H., Westerlund, N., Komulainen, E., Hollos, P., Parviainen, L., Papageorgiou, A. C., Iljin, K., Kallioniemi, O., Kallajoki, M., Courtney, M. J., Magard, M., James, P. & Coffey, E. T. 2012. c-Jun N-terminal kinase phosphorylation of MARCKSL1 determines actin stability and migration in neurons and in cancer cells. *Mol Cell Biol,* 32**,** 3513-26.

Boehm, M. B., Milius, T. J., Zhou, Y., Westendorf, J. J. & Koka, S. 2005. The mammalian formin FHOD1 interacts with the ERK MAP kinase pathway. *Biochem Biophys Res Commun,* 335**,** 1090-4.

Boj, S. F., Hwang, C. I., Baker, L. A., Chio, I. C., Engle, D. D., Corbo, V., Jager, M., Ponz-Sarvise, M., Tiriac, H., Spector, M. S., Gracanin, A., Oni, T., Yu, K. H., Van Boxtel, R., Huch, M., Rivera, K. D., Wilson, J. P., Feigin, M. E., Öhlund, D., Handly-Santana, A., Ardito-Abraham, C. M., Ludwig, M., Elyada, E., Alagesan, B., Biffi, G., Yordanov, G. N., Delcuze, B., Creighton, B., Wright, K., Park, Y., Morsink, F. H. M., Molenaar, I. Q., Borel Rinkes, I. H., Cuppen, E., Hao, Y., Jin, Y., Nijman, I. J., Iacobuzio-Donahue, C., Leach, S. D., Pappin, D. J., Hammell, M., Klimstra, D. S., Basturk, O., Hruban, R. H., Offerhaus, G. J., Vries, R. G. J., Clevers, H. & Tuveson, D. A. 2015. Organoid Models of Human and Mouse Ductal Pancreatic Cancer. *Cell,* 160**,** 324-338.

Bono, F., De Smet, F., Herbert, C., De Bock, K., Georgiadou, M., Fons, P., Tjwa, M., Alcouffe, C., Ny, A., Bianciotto, M., Jonckx, B., Murakami, M., Lanahan, A. A., Michielsen, C., Sibrac, D., Dol-Gleizes, F., Mazzone, M., Zacchigna, S., Herault, J. P., Fischer, C., Rigon, P., Ruiz De Almodovar, C., Claes, F., Blanc, I., Poesen, K., Zhang, J., Segura, I., Gueguen, G., Bordes, M. F., Lambrechts, D., Broussy, R., Van De Wouwer, M., Michaux, C., Shimada, T., Jean, I., Blacher, S., Noel, A., Motte, P., Rom, E., Rakic, J. M., Katsuma, S., Schaeffer, P., Yayon, A., Van Schepdael, A., Schwalbe, H., Gervasio, F. L., Carmeliet, G., Rozensky, J., Dewerchin, M., Simons, M., Christopoulos, A., Herbert, J. M. & Carmeliet, P. 2013. Inhibition of tumor angiogenesis and growth by a small-molecule multi-FGF receptor blocker with allosteric properties. *Cancer Cell,* 23**,** 477-88.

Boopathy, G. T. K. & Hong, W. 2019. Role of Hippo Pathway-YAP/TAZ Signaling in Angiogenesis. *Frontiers in cell and developmental biology,* 7**,** 49-49.

Bosetti, C., Bertuccio, P., Malvezzi, M., Levi, F., Chatenoud, L., Negri, E. & La Vecchia, C. 2013. Cancer mortality in Europe, 2005-2009, and an overview of trends since 1980. *Ann Oncol,* 24**,** 2657-71.

Brahmer, J. R., Tykodi, S. S., Chow, L. Q., Hwu, W. J., Topalian, S. L., Hwu, P., Drake, C. G., Camacho, L. H., Kauh, J., Odunsi, K., Pitot, H. C., Hamid, O., Bhatia, S., Martins, R., Eaton, K., Chen, S., Salay, T. M., Alaparthy, S., Grosso, J. F., Korman, A. J., Parker, S. M., Agrawal, S., Goldberg, S. M., Pardoll, D. M., Gupta, A. & Wigginton, J. M. 2012. Safety and activity of anti-PD-L1 antibody in patients with advanced cancer. *N Engl J Med,* 366**,** 2455-65.

Brooks, J. C., Shavelle, R. M. & Vavra-Musser, K. N. 2019. Life expectancy in pancreatic neuroendocrine cancer. *Clinics and Research in Hepatology and Gastroenterology,* 43**,** 88-97.

Bruno, I. G., Jin, W. & Cote, G. J. 2004. Correction of aberrant FGFR1 alternative RNA splicing through targeting of intronic regulatory elements. *Hum Mol Genet,* 13**,** 2409-20.

Bryant, D. M. & Stow, J. L. 2005. Nuclear Translocation of Cell-Surface Receptors: Lessons from Fibroblast Growth Factor. *Traffic,* 6**,** 947-953.

Bryant, D. M., Wylie, F. G. & Stow, J. L. 2005. Regulation of endocytosis, nuclear translocation, and signaling of fibroblast growth factor receptor 1 by E-cadherin. *Mol Biol Cell,* 16**,** 14-23.

Buchler, P., Reber, H. A., Roth, M. M., Shiroishi, M., Friess, H. & Hines, O. J. 2007. Target therapy using a small molecule inhibitor against angiogenic receptors in pancreatic cancer. *Neoplasia,* 9**,** 119-27.

Bueter, W., Dammann, O., Zscheppang, K., Korenbaum, E. & Dammann, C. E. 2006. ErbB receptors in fetal endothelium--a potential linkage point for inflammation-associated neonatal disorders. *Cytokine,* 36**,** 267-75.

Bynigeri, R. R., Jakkampudi, A., Jangala, R., Subramanyam, C., Sasikala, M., Rao, G. V., Reddy, D. N. & Talukdar, R. 2017. Pancreatic stellate cell: Pandora's box for pancreatic disease biology. *World Journal of Gastroenterology,* 23**,** 382-405.

Calvo, F., Ege, N., Grande-Garcia, A., Hooper, S., Jenkins, R. P., Chaudhry, S. I., Harrington, K., Williamson, P., Moeendarbary, E., Charras, G. & Sahai, E. 2013. Mechanotransduction and YAP-dependent matrix remodelling is required for the generation and maintenance of cancer-associated fibroblasts. *Nature Cell Biology,* 15**,** 637.

Camargo, F. D., Gokhale, S., Johnnidis, J. B., Fu, D., Bell, G. W., Jaenisch, R. & Brummelkamp, T. R. 2007. YAP1 increases organ size and expands undifferentiated progenitor cells. *Curr Biol,* 17**,** 2054-60.

Camidge, D. R., Pao, W. & Sequist, L. V. 2014. Acquired resistance to TKIs in solid tumours: learning from lung cancer. *Nat Rev Clin Oncol,* 11**,** 473-81.

Cappellen, D., De Oliveira, C., Ricol, D., De Medina, S., Bourdin, J., Sastre-Garau, X., Chopin, D., Thiery, J. P. & Radvanyi, F. 1999. Frequent activating mutations of FGFR3 in human bladder and cervix carcinomas. *Nature Genetics,* 23**,** 18.

Carapuça, E. F., Gemenetzidis, E., Feig, C., Bapiro, T. E., Williams, M. D., Wilson, A. S., Delvecchio, F. R., Arumugam, P., Grose, R. P., Lemoine, N. R., Richards, F. M. & Kocher, H. M. 2016. Anti-stromal treatment together with chemotherapy targets multiple signalling pathways in pancreatic adenocarcinoma. *The Journal of Pathology,* 239**,** 286-296.

Carey, M. F., Peterson, C. L. & Smale, S. T. 2009. Chromatin immunoprecipitation (ChIP). *Cold Spring Harb Protoc,* 2009**,** pdb.prot5279.

Carpenter, G. & Liao, H.-J. 2013. Receptor Tyrosine Kinases in the Nucleus. *Cold Spring Harbor Perspectives in Biology,* 5**,** a008979.

Carter, E. P., Fearon, A. E. & Grose, R. P. 2015. Careless talk costs lives: fibroblast growth factor receptor signalling and the consequences of pathway malfunction. *Trends Cell Biol,* 25**,** 221-33.

Cavallaro, U., Niedermeyer, J., Fuxa, M. & Christofori, G. 2001. N-CAM modulates tumour-cell adhesion to matrix by inducing FGF-receptor signalling. *Nat Cell Biol,* 3**,** 650-7.

Charrier, A. & Brigstock, D. R. 2013. Regulation of pancreatic function by connective tissue growth factor (CTGF, CCN2). *Cytokine & growth factor reviews,* 24**,** 59-68.

Chen, C. H., Thai, P., Yoneda, K., Adler, K. B., Yang, P. C. & Wu, R. 2014. A peptide that inhibits function of Myristoylated Alanine-Rich C Kinase Substrate (MARCKS) reduces lung cancer metastasis. *Oncogene,* 33**,** 3696-706.

Chen, G., Tian, X., Liu, Z., Zhou, S., Schmidt, B., Henne-Bruns, D., Bachem, M. & Kornmann, M. 2010. Inhibition of endogenous SPARC enhances pancreatic cancer cell growth: modulation by FGFR1-III isoform expression. *British Journal of Cancer,* 102**,** 188-195.

Chen, J., Chang, S., Duncan, S. A., Okano, H. J., Fishell, G. & Aderem, A. 1996. Disruption of the MacMARCKS gene prevents cranial neural tube closure and results in anencephaly. *Proc Natl Acad Sci U S A,* 93**,** 6275-9.

Chen, M. K., Du, Y., Sun, L., Hsu, J. L., Wang, Y. H., Gao, Y., Huang, J. & Hung, M. C. 2019. H2O2 induces nuclear transport of the receptor tyrosine kinase c-MET in breast cancer cells via a membrane-bound retrograde trafficking mechanism. *J Biol Chem,* 294**,** 8516-8528.

Chen, M. K. & Hung, M. C. 2015. Proteolytic cleavage, trafficking, and functions of nuclear receptor tyrosine kinases. *Febs J,* 282**,** 3693-721.

Chen, P.-Y., Qin, L., Li, G., Tellides, G. & Simons, M. 2016a. Fibroblast growth factor (FGF) signaling regulates transforming growth factor beta (TGFβ)-dependent smooth muscle cell phenotype modulation. *Scientific Reports,* 6**,** 33407.

Chen, P.-Y., Qin, L., Li, G., Tellides, G. & Simons, M. 2016b. Smooth muscle FGF/TGFβ cross talk regulates atherosclerosis progression. *EMBO molecular medicine,* 8**,** 712-728.

Chen, W. H., Horoszewicz, J. S., Leong, S. S., Shimano, T., Penetrante, R., Sanders, W. H., Berjian, R., Douglass, H. O., Martin, E. W. & Chu, T. M. 1982. Human pancreatic adenocarcinoma: in vitro and in vivo morphology of a new tumor line established from ascites. *In Vitro,* 18**,** 24-34.

Chen, X. & Rotenberg, S. A. 2010. PhosphoMARCKS drives motility of mouse melanoma cells. *Cell Signal,* 22**,** 1097-103.

Cheng, X.-B., Kohi, S., Koga, A., Hirata, K. & Sato, N. 2016. Hyaluronan stimulates pancreatic cancer cell motility. *Oncotarget,* 7**,** 4829-4840.

Chin, Y. R. & Toker, A. 2009. Function of Akt/PKB signaling to cell motility, invasion and the tumor stroma in cancer. *Cell Signal,* 21**,** 470-6.

Chioni, A.-M. & Grose, R. 2012. FGFR1 cleavage and nuclear translocation regulates breast cancer cell behavior. *The Journal of Cell Biology,* 197**,** 801-817.

Chronopoulos, A., Robinson, B., Sarper, M., Cortes, E., Auernheimer, V., Lachowski, D., Attwood, S., García, R., Ghassemi, S., Fabry, B. & Del Río Hernández, A. 2016. ATRA mechanically reprograms pancreatic stellate cells to suppress matrix remodelling and inhibit cancer cell invasion. *Nature Communications,* 7**,** 12630.

Cicenas, J., Kvederaviciute, K., Meskinyte, I., Meskinyte-Kausiliene, E., Skeberdyte, A. & Cicenas, J. 2017. KRAS, TP53, CDKN2A, SMAD4, BRCA1, and BRCA2 Mutations in Pancreatic Cancer. *Cancers,* 9**,** 42.

Clayton, N. S., Wilson, A. S., Laurent, E. P., Grose, R. P. & Carter, E. P. 2017. Fibroblast growth factor-mediated crosstalk in cancer etiology and treatment. *Dev Dyn,* 246**,** 493-501.

Coetzee, A., Grose, R. & Kocher, H. 2019. Pancreatic Cancer Organotypic Models. *Curr Top Microbiol Immunol*.

Cohn, M. J., Izpisua-Belmonte, J. C., Abud, H., Heath, J. K. & Tickle, C. 1995. Fibroblast growth factors induce additional limb development from the flank of chick embryos. *Cell,* 80**,** 739-46.

Coleman, S. J., Bruce, C., Chioni, A. M., Kocher, H. M. & Grose, R. P. 2014a. The ins and outs of fibroblast growth factor receptor signalling. *Clin Sci (Lond),* 127**,** 217-31.

Coleman, S. J., Chioni, A.-M., Ghallab, M., Anderson, R. K., Lemoine, N. R., Kocher, H. M. & Grose, R. P. 2014b. Nuclear translocation of FGFR1 and FGF2 in pancreatic stellate cells facilitates pancreatic cancer cell invasion. *EMBO Molecular Medicine,* 6**,** 467-481.

Coleman, S. J., Watt, J., Arumugam, P., Solaini, L., Carapuca, E., Ghallab, M., Grose, R. P. & Kocher, H. M. 2014c. Pancreatic cancer organotypics: High throughput, preclinical models for pharmacological agent evaluation. *World Journal of Gastroenterology : WJG,* 20**,** 8471-8481.

Collisson, E. A., Sadanandam, A., Olson, P., Gibb, W. J., Truitt, M., Gu, S., Cooc, J., Weinkle, J., Kim, G. E., Jakkula, L., Feiler, H. S., Ko, A. H., Olshen, A. B., Danenberg, K. L., Tempero, M. A., Spellman, P. T., Hanahan, D. & Gray, J. W. 2011. Subtypes of pancreatic ductal adenocarcinoma and their differing responses to therapy. *Nat Med,* 17**,** 500-503.

Conroy, T., Desseigne, F., Ychou, M., Bouché, O., Guimbaud, R., Bécouarn, Y., Adenis, A., Raoul, J.-L., Gourgou-Bourgade, S., De La Fouchardière, C., Bennouna, J., Bachet, J.-B., Khemissa-Akouz, F., Péré-Vergé, D., Delbaldo, C., Assenat, E., Chauffert, B., Michel, P., Montoto-Grillot, C. & Ducreux, M. 2011. FOLFIRINOX versus Gemcitabine for Metastatic Pancreatic Cancer. *New England Journal of Medicine,* 364**,** 1817-1825.

Cordero, J. B., Cozzolino, M., Lu, Y., Vidal, M., Slatopolsky, E., Stahl, P. D., Barbieri, M. A. & Dusso, A. 2002. 1,25-Dihydroxyvitamin D down-regulates cell membrane growth- and nuclear growth-promoting signals by the epidermal growth factor receptor. *J Biol Chem,* 277**,** 38965-71.

Cortes, E., Sarper, M., Robinson, B., Lachowski, D., Chronopoulos, A., Thorpe, S. D., Lee, D. A. & Del Río Hernández, A. E. 2019. GPER is a mechanoregulator of pancreatic stellate cells and the tumor microenvironment. *EMBO reports,* 20**,** e46556.

Cox, T. R., Bird, D., Baker, A. M., Barker, H. E., Ho, M. W., Lang, G. & Erler, J. T. 2013. LOX-mediated collagen crosslinking is responsible for fibrosis-enhanced metastasis. *Cancer Res,* 73**,** 1721-32.

Cravo, A. S., Carter, E., Erkan, M., Harvey, E., Furutani-Seiki, M. & Mrsny, R. 2015. Hippo pathway elements Co-localize with Occludin: A possible sensor system in pancreatic epithelial cells. *Tissue Barriers,* 3**,** e1037948.

Crippa, S., Salvia, R., Warshaw, A. L., Domínguez, I., Bassi, C., Falconi, M., Thayer, S. P., Zamboni, G., Lauwers, G. Y., Mino-Kenudson, M., Capelli, P., Pederzoli, P. & Castillo, C. F.-D. 2008. Mucinous cystic neoplasm of the pancreas is not an aggressive entity: lessons from 163 resected patients. *Annals of surgery,* 247**,** 571-579.

Cunningham, D., Chau, I., Stocken, D. D., Valle, J. W., Smith, D., Steward, W., Harper, P. G., Dunn, J., Tudur-Smith, C., West, J., Falk, S., Crellin, A., Adab, F., Thompson, J., Leonard, P., Ostrowski, J., Eatock, M., Scheithauer, W., Herrmann, R. & Neoptolemos, J. P. 2009. Phase III Randomized Comparison of Gemcitabine Versus Gemcitabine Plus Capecitabine in Patients With Advanced Pancreatic Cancer. *Journal of Clinical Oncology,* 27**,** 5513-5518.

Das Thakur, M., Feng, Y., Jagannathan, R., Seppa, M. J., Skeath, J. B. & Longmore, G. D. 2010. Ajuba LIM proteins are negative regulators of the Hippo signaling pathway. *Curr Biol,* 20**,** 657-62.

Dayon, L., Hainard, A., Licker, V., Turck, N., Kuhn, K., Hochstrasser, D. F., Burkhard, P. R. & Sanchez, J. C. 2008. Relative quantification of proteins in human cerebrospinal fluids by MS/MS using 6-plex isobaric tags. *Anal Chem,* 80**,** 2921-31.

De La Iglesia, N., Konopka, G., Puram, S. V., Chan, J. A., Bachoo, R. M., You, M. J., Levy, D. E., Depinho, R. A. & Bonni, A. 2008. Identification of a PTEN-regulated STAT3 brain tumor suppressor pathway. *Genes Dev,* 22**,** 449-62.

De Oca B, P. M., Malardé, V., Proust, R., Dautry-Varsat, A. & Gesbert, F. 2010. Ectodomain Shedding of Interleukin-2 Receptor β and Generation of an Intracellular Functional Fragment. *The Journal of Biological Chemistry,* 285**,** 22050-22058.

Debernardi, S., Massat, N. J., Radon, T. P., Sangaralingam, A., Banissi, A., Ennis, D. P., Dowe, T., Chelala, C., Pereira, S. P., Kocher, H. M., Young, B. D., Bond-Smith, G., Hutchins, R. & Crnogorac-Jurcevic, T. 2015. Noninvasive urinary miRNA biomarkers for early detection of pancreatic adenocarcinoma. *American Journal of Cancer Research,* 5**,** 3455-3466.

Debiais, F., Lemonnier, J., Hay, E., Delannoy, P., Caverzasio, J. & Marie, P. J. 2001. Fibroblast growth factor-2 (FGF-2) increases N-cadherin expression through protein kinase C and Src-kinase pathways in human calvaria osteoblasts. *Journal of Cellular Biochemistry,* 81**,** 68-81.

Deer, E. L., Gonzalez-Hernandez, J., Coursen, J. D., Shea, J. E., Ngatia, J., Scaife, C. L., Firpo, M. A. & Mulvihill, S. J. 2010. Phenotype and genotype of pancreatic cancer cell lines. *Pancreas,* 39**,** 425-35.

Degnin, C. R., Laederich, M. B. & Horton, W. A. 2011. Ligand activation leads to regulated intramembrane proteolysis of fibroblast growth factor receptor 3. *Mol Biol Cell,* 22**,** 3861-73.

Delehedde, M., Lyon, M., Gallagher, J. T., Rudland, P. S. & Fernig, D. G. 2002. Fibroblast growth factor-2 binds to small heparin-derived oligosaccharides and stimulates a sustained phosphorylation of p42/44 mitogen-activated protein kinase and proliferation of rat mammary fibroblasts. *Biochem J,* 366**,** 235-44.

Delehedde, M., Seve, M., Sergeant, N., Wartelle, I., Lyon, M., Rudland, P. S. & Fernig, D. G. 2000. Fibroblast growth factor-2 stimulation of p42/44MAPK phosphorylation and IkappaB degradation is regulated by heparan sulfate/heparin in rat mammary fibroblasts. *J Biol Chem,* 275**,** 33905-10.

Deplanque, G., Demarchi, M., Hebbar, M., Flynn, P., Melichar, B., Atkins, J., Nowara, E., Moye, L., Piquemal, D., Ritter, D., Dubreuil, P., Mansfield, C. D., Acin, Y., Moussy, A., Hermine, O. & Hammel, P. 2015. A randomized, placebo-controlled phase III trial of masitinib plus gemcitabine in the treatment of advanced pancreatic cancer. *Ann Oncol,* 26**,** 1194-200.

Derycke, L. D. & Bracke, M. E. 2004. N-cadherin in the spotlight of cell-cell adhesion, differentiation, embryogenesis, invasion and signalling. *Int J Dev Biol,* 48**,** 463-76.

Desai, N., Trieu, V., Yao, Z., Louie, L., Ci, S., Yang, A., Tao, C., De, T., Beals, B., Dykes, D., Noker, P., Yao, R., Labao, E., Hawkins, M. & Soon-Shiong, P. 2006. Increased antitumor activity, intratumor paclitaxel concentrations, and endothelial cell transport of cremophor-free, albumin-bound paclitaxel, ABI-007, compared with cremophor-based paclitaxel. *Clin Cancer Res,* 12**,** 1317-24.

Di Gangi, I. M., Mazza, T., Fontana, A., Copetti, M., Fusilli, C., Ippolito, A., Mattivi, F., Latiano, A., Andriulli, A., Vrhovsek, U. & Pazienza, V. 2016. Metabolomic profile in pancreatic cancer patients: a consensus-based approach to identify highly discriminating metabolites. *Oncotarget,* 7**,** 5815-29.

Di Martino, E., Alder, O., Hurst, C. D. & Knowles, M. A. 2019. ETV5 links the FGFR3 and Hippo signalling pathways in bladder cancer. *Scientific Reports,* 9**,** 5740.

Diamandis, E. P. 2004. Mass Spectrometry as a Diagnostic and a Cancer Biomarker Discovery Tool. *Opportunities and Potential Limitations,* 3**,** 367-378.

Distler, M., Aust, D., Weitz, J., Pilarsky, C. & Grutzmann, R. 2014. Precursor lesions for sporadic pancreatic cancer: PanIN, IPMN, and MCN. *Biomed Res Int,* 2014**,** 474905.

Distler, M., Kersting, S., Niedergethmann, M., Aust, D. E., Franz, M., Ruckert, F., Ehehalt, F., Pilarsky, C., Post, S., Saeger, H. D. & Grutzmann, R. 2013. Pathohistological subtype predicts survival in patients with intraductal papillary mucinous neoplasm (IPMN) of the pancreas. *Ann Surg,* 258**,** 324-30.

Doherty, G. J., Tempero, M. & Corrie, P. G. 2018. HALO-109-301: a Phase III trial of PEGPH20 (with gemcitabine and nab-paclitaxel) in hyaluronic acid-high stage IV pancreatic cancer. *Future Oncol,* 14**,** 13-22.

Dorris, E., O'Neill, A., Hanrahan, K., Treacy, A. & Watson, R. W. 2017. MARCKS promotes invasion and is associated with biochemical recurrence in prostate cancer. *Oncotarget,* 8**,** 72021-72030.

Dourado, M. R., Korvala, J., Åström, P., De Oliveira, C. E., Cervigne, N. K., Mofatto, L. S., Campanella Bastos, D., Pereira Messetti, A. C., Graner, E., Paes Leme, A. F., Coletta, R. D. & Salo, T. 2019. Extracellular vesicles derived from cancer-associated fibroblasts induce the migration and invasion of oral squamous cell carcinoma. *Journal of Extracellular Vesicles,* 8**,** 1578525.

Duchesne, L., Tissot, B., Rudd, T. R., Dell, A. & Fernig, D. G. 2006. N-glycosylation of fibroblast growth factor receptor 1 regulates ligand and heparan sulfate co-receptor binding. *J Biol Chem,* 281**,** 27178-89.

Dunham-Ems, S. M., Lee, Y.-W., Stachowiak, E. K., Pudavar, H., Claus, P., Prasad, P. N. & Stachowiak, M. K. 2009. Fibroblast growth factor receptor-1 (FGFR1) nuclear dynamics reveal a novel mechanism in transcription control. *Molecular Biology of the Cell,* 20**,** 2401-2412.

Dunham-Ems, S. M., Pudavar, H. E., Myers, J. M., Maher, P. A., Prasad, P. N. & Stachowiak, M. K. 2006. Factors controlling fibroblast growth factor receptor-1's cytoplasmic trafficking and its regulation as revealed by FRAP analysis. *Mol Biol Cell,* 17**,** 2223-35.

Dunning, S., Ur Rehman, A., Tiebosch, M. H., Hannivoort, R. A., Haijer, F. W., Woudenberg, J., Van Den Heuvel, F. A., Buist-Homan, M., Faber, K. N. & Moshage, H. 2013. Glutathione and antioxidant enzymes serve complementary roles in protecting activated hepatic stellate cells against hydrogen peroxide-induced cell death. *Biochim Biophys Acta,* 1832**,** 2027-34.

Dutt, A., Salvesen, H. B., Chen, T. H., Ramos, A. H., Onofrio, R. C., Hatton, C., Nicoletti, R., Winckler, W., Grewal, R., Hanna, M., Wyhs, N., Ziaugra, L., Richter, D. J., Trovik, J., Engelsen, I. B., Stefansson, I. M., Fennell, T., Cibulskis, K., Zody, M. C., Akslen, L. A., Gabriel, S., Wong, K. K., Sellers, W. R., Meyerson, M. & Greulich, H. 2008. Drug-sensitive FGFR2 mutations in endometrial carcinoma. *Proc Natl Acad Sci U S A,* 105**,** 8713-7.

Duxbury, M. S., Ito, H., Zinner, M. J., Ashley, S. W. & Whang, E. E. 2004. EphA2: a determinant of malignant cellular behavior and a potential therapeutic target in pancreatic adenocarcinoma. *Oncogene,* 23**,** 1448-56.

Edwards, J., Traynor, P., Munro, A. F., Pirret, C. F., Dunne, B. & Bartlett, J. M. 2006. The role of HER1-HER4 and EGFRvIII in hormone-refractory prostate cancer. *Clin Cancer Res,* 12**,** 123-30.

Egbivwie, N., Cockle, J. V., Humphries, M., Ismail, A., Esteves, F., Taylor, C., Karakoula, K., Morton, R., Warr, T., Short, S. C. & Brüning-Richardson, A. 2019. FGFR1 Expression and Role in Migration in Low and High Grade Pediatric Gliomas. *Frontiers in Oncology,* 9**,** 103-103.

Ekerot, M., Stavridis, M. P., Delavaine, L., Mitchell, M. P., Staples, C., Owens, D. M., Keenan, I. D., Dickinson, R. J., Storey, K. G. & Keyse, S. M. 2008. Negative-feedback regulation of FGF signalling by DUSP6/MKP-3 is driven by ERK1/2 and mediated by Ets factor binding to a conserved site within the DUSP6/MKP-3 gene promoter. *The Biochemical Journal,* 412**,** 287-298.

El-Hariry, I., Pignatelli, M. & Lemoine, N. R. 2001a. FGF-1 and FGF-2 modulate the E-cadherin/catenin system in pancreatic adenocarcinoma cell lines. *Br J Cancer,* 84**,** 1656-63.

El-Hariry, I., Pignatelli, M. & Lemoine, N. R. 2001b. FGF-1 and FGF-2 regulate the expression of E-cadherin and catenins in pancreatic adenocarcinoma. *Int J Cancer,* 94**,** 652-61.

El Amri, M., Fitzgerald, U. & Schlosser, G. 2018. MARCKS and MARCKS-like proteins in development and regeneration. *Journal of Biomedical Science,* 25**,** 43.

Elbauomy Elsheikh, S., Green, A. R., Lambros, M. B., Turner, N. C., Grainge, M. J., Powe, D., Ellis, I. O. & Reis-Filho, J. S. 2007. FGFR1 amplification in breast carcinomas: a chromogenic in situ hybridisation analysis. *Breast Cancer Res,* 9**,** R23.

Elkharwily, A. & Gottlieb, K. 2008. The pancreas in familial adenomatous polyposis. *Journal of the Pancreas,* 9**,** 9-18.

Ellenrieder, V., Hendler, S. F., Ruhland, C., Boeck, W., Adler, G. & Gress, T. M. 2001. TGF-beta-induced invasiveness of pancreatic cancer cells is mediated by matrix metalloproteinase-2 and the urokinase plasminogen activator system. *Int J Cancer,* 93**,** 204-11.

Erickson, H. K., Park, P. U., Widdison, W. C., Kovtun, Y. V., Garrett, L. M., Hoffman, K., Lutz, R. J., Goldmacher, V. S. & Blattler, W. A. 2006. Antibody-maytansinoid conjugates are activated in targeted cancer cells by lysosomal degradation and linker-dependent intracellular processing. *Cancer Res,* 66**,** 4426-33.

Erler, J. T., Bennewith, K. L., Nicolau, M., Dornhofer, N., Kong, C., Le, Q. T., Chi, J. T., Jeffrey, S. S. & Giaccia, A. J. 2006. Lysyl oxidase is essential for hypoxia-induced metastasis. *Nature,* 440**,** 1222-6.

Escaffit, F., Estival, A., Bertrand, C., Vaysse, N., Hollande, E. & Clemente, F. 2000. FGF-2 isoforms of 18 and 22.5 kDa differentially modulate t-PA and PAI-1 expressions on the pancreatic carcinoma cells AR4-2J: consequences on cell spreading and invasion. *Int J Cancer,* 85**,** 555-62.

Escobar Galvis, M. L., Jia, J., Zhang, X., Jastrebova, N., Spillmann, D., Gottfridsson, E., Van Kuppevelt, T. H., Zcharia, E., Vlodavsky, I., Lindahl, U. & Li, J. P. 2007. Transgenic or tumor-induced expression of heparanase upregulates sulfation of heparan sulfate. *Nat Chem Biol,* 3**,** 773-8.

Esko, J. D. & Selleck, S. B. 2002. Order Out of Chaos: Assembly of Ligand Binding Sites in Heparan Sulfate. *Annual Review of Biochemistry,* 71**,** 435-471.

Eswarakumar, V. P., Lax, I. & Schlessinger, J. 2005. Cellular signaling by fibroblast growth factor receptors. *Cytokine Growth Factor Rev,* 16**,** 139-49.

Fang, X., Stachowiak, E. K., Dunham-Ems, S. M., Klejbor, I. & Stachowiak, M. K. 2005. Control of CREB-binding protein signaling by nuclear fibroblast growth factor receptor-1: a novel mechanism of gene regulation. *J Biol Chem,* 280**,** 28451-62.

Farkona, S., Diamandis, E. P. & Blasutig, I. M. 2016. Cancer immunotherapy: the beginning of the end of cancer? *BMC Medicine,* 14**,** 73.

Fearon, A. E., Carter, E. P., Clayton, N. S., Wilkes, E. H., Baker, A. M., Kapitonova, E., Bakhouche, B. A., Tanner, Y., Wang, J., Gadaleta, E., Chelala, C., Moore, K. M., Marshall, J. F., Chupin, J., Schmid, P., Jones, J. L., Lockley, M., Cutillas, P. R. & Grose, R. P. 2018. PHLDA1 Mediates Drug Resistance in Receptor Tyrosine Kinase-Driven Cancer. *Cell Rep,* 22**,** 2469-2481.

Feig, C., Gopinathan, A., Neesse, A., Chan, D. S., Cook, N. & Tuveson, D. A. 2012. The pancreas cancer microenvironment. *Clinical cancer research : an official journal of the American Association for Cancer Research,* 18**,** 4266-4276.

Feldmann, G., Fendrich, V., Mcgovern, K., Bedja, D., Bisht, S., Alvarez, H., Koorstra, J. B., Habbe, N., Karikari, C., Mullendore, M., Gabrielson, K. L., Sharma, R., Matsui, W. & Maitra, A. 2008. An orally bioavailable small-molecule inhibitor of Hedgehog signaling inhibits tumor initiation and metastasis in pancreatic cancer. *Mol Cancer Ther,* 7**,** 2725-35.

Fernandez, L. A., Northcott, P. A., Dalton, J., Fraga, C., Ellison, D., Angers, S., Taylor, M. D. & Kenney, A. M. 2009. YAP1 is amplified and up-regulated in hedgehog-associated medulloblastomas and mediates Sonic hedgehog-driven neural precursor proliferation. *Genes Dev,* 23**,** 2729-41.

Fischer, E., Chaitanya, K., Wuest, T., Wadle, A., Scott, A. M., Van Den Broek, M., Schibli, R., Bauer, S. & Renner, C. 2012. Radioimmunotherapy of fibroblast activation

protein positive tumors by rapidly internalizing antibodies. *Clin Cancer Res,* 18**,** 6208-18.

Fogelman, D. R., Wolff, R. A., Kopetz, S., Javle, M., Bradley, C., Mok, I., Cabanillas, F. & Abbruzzese, J. L. 2011. Evidence for the efficacy of Iniparib, a PARP-1 inhibitor, in BRCA2-associated pancreatic cancer. *Anticancer Res,* 31**,** 1417-20.

Follenzi, A., Bakovic, S., Gual, P., Stella, M. C., Longati, P. & Comoglio, P. M. 2000. Cross-talk between the proto-oncogenes Met and Ron. *Oncogene,* 19**,** 3041-9.

Fong, L. W. R., Yang, D. C. & Chen, C. H. 2017. Myristoylated alanine-rich C kinase substrate (MARCKS): a multirole signaling protein in cancers. *Cancer Metastasis Rev,* 36**,** 737-747.

Frank, S., Munz, B. & Werner, S. 1997. The human homologue of a bovine non-selenium glutathione peroxidase is a novel keratinocyte growth factor-regulated gene. *Oncogene,* 14**,** 915-21.

Frese, K. K., Neesse, A., Cook, N., Bapiro, T. E., Lolkema, M. P., Jodrell, D. I. & Tuveson, D. A. 2012. nab-Paclitaxel potentiates gemcitabine activity by reducing cytidine deaminase levels in a mouse model of pancreatic cancer. *Cancer Discov,* 2**,** 260-9.

Froeling, F. E., Feig, C., Chelala, C., Dobson, R., Mein, C. E., Tuveson, D. A., Clevers, H., Hart, I. R. & Kocher, H. M. 2011. Retinoic acid-induced pancreatic stellate cell quiescence reduces paracrine Wnt-beta-catenin signaling to slow tumor progression. *Gastroenterology,* 141**,** 1486-97, 1497.e1-14.

Fürthauer, M., Lin, W., Ang, S.-L., Thisse, B. & Thisse, C. 2002. Sef is a feedback-induced antagonist of Ras/MAPK-mediated FGF signalling. *Nature Cell Biology,* 4**,** 170.

Furukawa, T., Kloppel, G., Volkan Adsay, N., Albores-Saavedra, J., Fukushima, N., Horii, A., Hruban, R. H., Kato, Y., Klimstra, D. S., Longnecker, D. S., Luttges, J., Offerhaus, G. J., Shimizu, M., Sunamura, M., Suriawinata, A., Takaori, K. & Yonezawa, S. 2005. Classification of types of intraductal papillary-mucinous neoplasm of the pancreas: a consensus study. *Virchows Arch,* 447**,** 794-9.

Gaggioli, C., Hooper, S., Hidalgo-Carcedo, C., Grosse, R., Marshall, J. F., Harrington, K. & Sahai, E. 2007. Fibroblast-led collective invasion of carcinoma cells with differing roles for RhoGTPases in leading and following cells. *Nature Cell Biology,* 9**,** 1392.

Gan, X., Chen, B., Shen, Z., Liu, Y., Li, H., Xie, X., Xu, X., Li, H., Huang, Z. & Chen, J. 2014. High GPX1 expression promotes esophageal squamous cell carcinoma invasion, migration, proliferation and cisplatin-resistance but can be reduced by vitamin D. *Int J Clin Exp Med,* 7**,** 2530-40.

Gao, G., Tian, Z., Zhu, H.-Y. & Ouyang, X.-Y. 2018. miRNA-133b targets FGFR1 and presents multiple tumor suppressor activities in osteosarcoma. *Cancer Cell International,* 18**,** 210.

Gardberg, M., Kaipio, K., Lehtinen, L., Mikkonen, P., Heuser, V. D., Talvinen, K., Iljin, K., Kampf, C., Uhlen, M., Grenman, R., Koivisto, M. & Carpen, O. 2013. FHOD1, a formin upregulated in epithelial-mesenchymal transition, participates in cancer cell migration and invasion. *PLoS One,* 8**,** e74923.

Gavine, P. R., Mooney, L., Kilgour, E., Thomas, A. P., Al-Kadhimi, K., Beck, S., Rooney, C., Coleman, T., Baker, D., Mellor, M. J., Brooks, A. N. & Klinowska, T. 2012. AZD4547: An Orally Bioavailable, Potent, and Selective Inhibitor of the Fibroblast Growth Factor Receptor Tyrosine Kinase Family. *Cancer Research,* 72**,** 2045-2056.

Ge, H., Gong, X. & Tang, C. K. 2002. Evidence of high incidence of EGFRvIII expression and coexpression with EGFR in human invasive breast cancer by laser capture microdissection and immunohistochemical analysis. *Int J Cancer,* 98**,** 357-61.

Geerts, A. 2001. History, heterogeneity, developmental biology, and functions of quiescent hepatic stellate cells. *Semin Liver Dis,* 21**,** 311-35.

Ghaemmaghami, S., Huh, W. K., Bower, K., Howson, R. W., Belle, A., Dephoure, N., O'Shea, E. K. & Weissman, J. S. 2003. Global analysis of protein expression in yeast. *Nature,* 425**,** 737-41.

Gilmour, D. S. & Lis, J. T. 1984. Detecting protein-DNA interactions in vivo: distribution of RNA polymerase on specific bacterial genes. *Proceedings of the National Academy of Sciences of the United States of America,* 81**,** 4275-4279.

Gilmour, D. S., Pflugfelder, G., Wang, J. C. & Lis, J. T. 1986. Topoisomerase I interacts with transcribed regions in Drosophila cells. *Cell,* 44**,** 401-407.

Giri, D., Ropiquet, F. & Ittmann, M. 1999. Alterations in expression of basic fibroblast growth factor (FGF) 2 and its receptor FGFR-1 in human prostate cancer. *Clin Cancer Res,* 5**,** 1063-71.

Gittes, G. K. 2009. Developmental biology of the pancreas: A comprehensive review. *Developmental Biology,* 326**,** 4-35.

Gnatenko, D. A., Kopantzev, E. P. & Sverdlov, E. D. 2018. Variable Effects of Growth Factors on Developmental Gene Expression in Pancreatic Cancer Cells. *Dokl Biochem Biophys,* 481**,** 217-218.

Goetz, R. & Mohammadi, M. 2013. Exploring mechanisms of FGF signalling through the lens of structural biology. *Nat Rev Mol Cell Biol,* 14**,** 166-80.

Goldfarb, M. 2005. Fibroblast growth factor homologous factors: evolution, structure, and function. *Cytokine Growth Factor Rev,* 16**,** 215-20.

Gomes, D. A., Rodrigues, M. A., Leite, M. F., Gomez, M. V., Varnai, P., Balla, T., Bennett, A. M. & Nathanson, M. H. 2008. c-Met Must Translocate to the Nucleus to Initiate Calcium Signals. *Journal of Biological Chemistry,* 283**,** 4344-4351.

Gong, J., Hendifar, A., Tuli, R., Chuang, J., Cho, M., Chung, V., Li, D. & Salgia, R. 2018. Combination systemic therapies with immune checkpoint inhibitors in pancreatic cancer: overcoming resistance to single-agent checkpoint blockade. *Clin Transl Med,* 7**,** 32.

Gong, S. G. 2014. Isoforms of receptors of fibroblast growth factors. *J Cell Physiol,* 229**,** 1887-95.

Goriely, A., Hansen, R. M. S., Taylor, I. B., Olesen, I. A., Jacobsen, G. K., McGowan, S. J., Pfeifer, S. P., McVean, G. A. T., Rajpert-De Meyts, E. & Wilkie, A. O. M. 2009. Activating mutations in FGFR3 and HRAS reveal a shared genetic origin for congenital disorders and testicular tumors. *Nature Genetics,* 41**,** 1247-1252.

Gotoh, N. 2008. Regulation of growth factor signaling by FRS2 family docking/scaffold adaptor proteins. *Cancer Sci,* 99**,** 1319-25.

Greer, J. B. & Whitcomb, D. C. 2007. Role of BRCA1 and BRCA2 mutations in pancreatic cancer. *Gut,* 56**,** 601-605.

Greggio, C., De Franceschi, F., Figueiredo-Larsen, M., Gobaa, S., Ranga, A., Semb, H., Lutolf, M. & Grapin-Botton, A. 2013. Artificial three-dimensional niches deconstruct pancreas development in vitro. *Development (Cambridge, England),* 140**,** 4452-4462.

Gruber, R., Panayiotou, R., Nye, E., Spencer-Dene, B., Stamp, G. & Behrens, A. 2016. YAP1 and TAZ Control Pancreatic Cancer Initiation in Mice by Direct Up-regulation of JAK–STAT3 Signaling. *Gastroenterology,* 151**,** 526-539.

Grusche, F. A., Richardson, H. E. & Harvey, K. F. 2010. Upstream Regulation of the Hippo Size Control Pathway. *Current Biology,* 20**,** R574-R582.

Grützmann, R., Post, S., Saeger, H. D. & Niedergethmann, M. 2011. Intraductal papillary mucinous neoplasia (IPMN) of the pancreas: its diagnosis, treatment, and prognosis. *Deutsches Arzteblatt International,* 108**,** 788-794.

Gu, T. L., Goss, V. L., Reeves, C., Popova, L., Nardone, J., Macneill, J., Walters, D. K., Wang, Y., Rush, J., Comb, M. J., Druker, B. J. & Polakiewicz, R. D. 2006. Phosphotyrosine profiling identifies the KG-1 cell line as a model for the study of FGFR1 fusions in acute myeloid leukemia. *Blood,* 108**,** 4202-4.

Guagnano, V., Kauffmann, A., Wohrle, S., Stamm, C., Ito, M., Barys, L., Pornon, A., Yao, Y., Li, F., Zhang, Y., Chen, Z., Wilson, C. J., Bordas, V., Le Douget, M., Gaither, L. A., Borawski, J., Monahan, J. E., Venkatesan, K., Brummendorf, T., Thomas, D. M., Garcia-Echeverria, C., Hofmann, F., Sellers, W. R. & Graus-Porta, D. 2012. FGFR genetic alterations predict for sensitivity to NVP-BGJ398, a selective pan-FGFR inhibitor. *Cancer Discov,* 2**,** 1118-33.

Guan, Z., Lan, H., Sun, D., Wang, X. & Jin, K. 2019. A potential novel therapy for FGFR1-amplified pancreatic cancer with bone metastasis, screened by next-generation sequencing and a patient-derived xenograft model. *Oncol Lett,* 17**,** 2303-2307.

Guimond, S. E. & Turnbull, J. E. 1999. Fibroblast growth factor receptor signalling is dictated by specific heparan sulphate saccharides. *Curr Biol,* 9**,** 1343-6.

Gundewar, C., Sasor, A., Hilmersson, K. S., Andersson, R. & Ansari, D. 2015. The role of SPARC expression in pancreatic cancer progression and patient survival. *Scand J Gastroenterol,* 50**,** 1170-4.

Guweidhi, A., Kleeff, J., Adwan, H., Giese, N. A., Wente, M. N., Giese, T., Büchler, M. W., Berger, M. R. & Friess, H. 2005. Osteonectin influences growth and invasion of pancreatic cancer cells. *Annals of Surgery,* 242**,** 224-234.

Haage, A. & Schneider, I. C. 2014. Cellular contractility and extracellular matrix stiffness regulate matrix metalloproteinase activity in pancreatic cancer cells. *Faseb j,* 28**,** 3589-99.

Habisch, H., Zhou, S., Siech, M. & Bachem, M. G. 2010. Interaction of Stellate Cells with Pancreatic Carcinoma Cells. *Cancers,* 2**,** 1661-1682.

Hacohen, N., Kramer, S., Sutherland, D., Hiromi, Y. & Krasnow, M. A. 1998. sprouty encodes a novel antagonist of FGF signaling that patterns apical branching of the Drosophila airways. *Cell,* 92**,** 253-63.

Hadari, Y. R., Gotoh, N., Kouhara, H., Lax, I. & Schlessinger, J. 2001. Critical role for the docking-protein FRS2 alpha in FGF receptor-mediated signal transduction pathways. *Proc Natl Acad Sci U S A,* 98**,** 8578-83.

Hafner, C., Van Oers, J. M., Vogt, T., Landthaler, M., Stoehr, R., Blaszyk, H., Hofstaedter, F., Zwarthoff, E. C. & Hartmann, A. 2006. Mosaicism of activating

FGFR3 mutations in human skin causes epidermal nevi. *J Clin Invest,* 116**,** 2201-2207.

Hamaguchi, A., Tooyama, I., Yoshiki, T. & Kimura, H. 1995. Demonstration of fibroblast growth factor receptor-I in human prostate by polymerase chain reaction and immunohistochemistry. *Prostate,* 27**,** 141-7.

Hanada, N., Lo, H. W., Day, C. P., Pan, Y., Nakajima, Y. & Hung, M. C. 2006. Co-regulation of B-Myb expression by E2F1 and EGF receptor. *Mol Carcinog,* 45**,** 10-7.

Hao, F., Xu, Q., Zhao, Y., Stevens, J. V., Young, S. H., Sinnett-Smith, J. & Rozengurt, E. 2017. Insulin Receptor and GPCR Crosstalk Stimulates YAP via PI3K and PKD in Pancreatic Cancer Cells. *Molecular Cancer Research,* 15**,** 929-941.

Haq, F., Sung, Y.-N., Park, I., Kayani, M. A., Yousuf, F., Hong, S.-M. & Ahn, S.-M. 2018. FGFR1 expression defines clinically distinct subtypes in pancreatic cancer. *Journal of Translational Medicine,* 16**,** 374.

Hariharan, D., Saied, A. & Kocher, H. M. 2008. Analysis of mortality rates for pancreatic cancer across the world. *HPB : The Official Journal of the International Hepato Pancreato Biliary Association,* 10**,** 58-62.

Hart, K. C., Robertson, S. C., Kanemitsu, M. Y., Meyer, A. N., Tynan, J. A. & Donoghue, D. J. 2000. Transformation and Stat activation by derivatives of FGFR1, FGFR3, and FGFR4. *Oncogene,* 19**,** 3309-20.

Hartwig, J. H., Thelen, M., Rosen, A., Janmey, P. A., Nairn, A. C. & Aderem, A. 1992. MARCKS is an actin filament crosslinking protein regulated by protein kinase C and calcium-calmodulin. *Nature,* 356**,** 618-22.

Hasegawa, Y., Takada, M., Yamamoto, M. & Saitoh, Y. 1994. The gradient of basic fibroblast growth factor concentration in human pancreatic cancer cell invasion. *Biochem Biophys Res Commun,* 200**,** 1435-9.

He, C., Lv, X., Hua, G., Lele, S. M., Remmenga, S., Dong, J., Davis, J. S. & Wang, C. 2015. YAP forms autocrine loops with the ERBB pathway to regulate ovarian cancer initiation and progression. *Oncogene,* 34**,** 6040-54.

Hebbes, T. R., Thorne, A. W. & Crane-Robinson, C. 1988. A direct link between core histone acetylation and transcriptionally active chromatin. *The EMBO Journal,* 7**,** 1395-1402.

Heinemann, V., Hertel, L. W., Grindey, G. B. & Plunkett, W. 1988. Comparison of the Cellular Pharmacokinetics and Toxicity of 2′,2′-Difluorodeoxycytidine and 1-β-Arabinofuranosylcytosine. *Cancer Research,* 48**,** 4024-4031.

Helsten, T., Elkin, S., Arthur, E., Tomson, B. N., Carter, J. & Kurzrock, R. 2016. The FGFR Landscape in Cancer: Analysis of 4,853 Tumors by Next-Generation Sequencing. *Clin Cancer Res,* 22**,** 259-67.

Hernandez, S., De Muga, S., Agell, L., Juanpere, N., Esgueva, R., Lorente, J. A., Mojal, S., Serrano, S. & Lloreta, J. 2009. FGFR3 mutations in prostate cancer: association with low-grade tumors. *Mod Pathol,* 22**,** 848-56.

Hezel, A. F., Kimmelman, A. C., Stanger, B. Z., Bardeesy, N. & Depinho, R. A. 2006. Genetics and biology of pancreatic ductal adenocarcinoma. *Genes Dev,* 20**,** 1218-49.

Hidalgo, M., Plaza, C., Musteanu, M., Illei, P., Brachmann, C. B., Heise, C., Pierce, D., Lopez-Casas, P. P., Menendez, C., Tabernero, J., Romano, A., Wei, X., Lopez-Rios, F. & Von Hoff, D. D. 2015. SPARC Expression Did Not Predict Efficacy of nab-Paclitaxel plus Gemcitabine or Gemcitabine Alone for Metastatic Pancreatic Cancer in an Exploratory Analysis of the Phase III MPACT Trial. *Clin Cancer Res,* 21**,** 4811-8.

Hingorani, S. R., Harris, W. P., Beck, J. T., Berdov, B. A., Wagner, S. A., Pshevlotsky, E. M., Tjulandin, S., Gladkov, O., Holcombe, R. F., Jiang, P., Maneval, D. C., Zhu, J. & Devoe, C. E. 2013. A phase Ib study of gemcitabine plus PEGPH20 (pegylated recombinant human hyaluronidase) in patients with stage IV previously untreated pancreatic cancer. *Journal of Clinical Oncology,* 31**,** 4010-4010.

Hingorani, S. R., Harris, W. P., Hendifar, A. E., Bullock, A. J., Wu, X. W., Huang, Y. & Jiang, P. 2015. High response rate and PFS with PEGPH20 added to nab-paclitaxel/gemcitabine in stage IV previously untreated pancreatic cancer patients with high-HA tumors: Interim results of a randomized phase II study. *Journal of Clinical Oncology,* 33**,** 4006-4006.

Hingorani, S. R., Harris, W. P., Seery, T. E., Zheng, L., Sigal, D., Hendifar, A. E., Braiteh, F. S., Zalupski, M., Baron, A. D., Bahary, N., Wang-Gillam, A., Loconte, N. K., Springett, G. M., Ritch, P. S., Hezel, A. F., Ma, W. W., Bathini, V. G., Wu, X. W., Jiang, P. & Bullock, A. J. 2016. Interim results of a randomized phase II study of PEGPH20 added to nab-paclitaxel/gemcitabine in patients with stage IV previously untreated pancreatic cancer. *Journal of Clinical Oncology,* 34**,** 439-439.

Hitosugi, T., Fan, J., Chung, T. W., Lythgoe, K., Wang, X., Xie, J., Ge, Q., Gu, T. L., Polakiewicz, R. D., Roesel, J. L., Chen, G. Z., Boggon, T. J., Lonial, S., Fu, H., Khuri, F. R., Kang, S. & Chen, J. 2011. Tyrosine phosphorylation of mitochondrial pyruvate dehydrogenase kinase 1 is important for cancer metabolism. *Mol Cell,* 44**,** 864-77.

Ho, H. K., Pok, S., Streit, S., Ruhe, J. E., Hart, S., Lim, K. S., Loo, H. L., Aung, M. O., Lim, S. G. & Ullrich, A. 2009. Fibroblast growth factor receptor 4 regulates proliferation, anti-apoptosis and alpha-fetoprotein secretion during hepatocellular carcinoma progression and represents a potential target for therapeutic intervention. *J Hepatol,* 50**,** 118-27.

Hodi, F. S., O'day, S. J., Mcdermott, D. F., Weber, R. W., Sosman, J. A., Haanen, J. B., Gonzalez, R., Robert, C., Schadendorf, D., Hassel, J. C., Akerley, W., Van Den Eertwegh, A. J., Lutzky, J., Lorigan, P., Vaubel, J. M., Linette, G. P., Hogg, D., Ottensmeier, C. H., Lebbe, C., Peschel, C., Quirt, I., Clark, J. I., Wolchok, J. D., Weber, J. S., Tian, J., Yellin, M. J., Nichol, G. M., Hoos, A. & Urba, W. J. 2010. Improved survival with ipilimumab in patients with metastatic melanoma. *N Engl J Med,* 363**,** 711-23.

Hoffman, E. A., Frey, B. L., Smith, L. M. & Auble, D. T. 2015. Formaldehyde crosslinking: a tool for the study of chromatin complexes. *J Biol Chem,* 290**,** 26404-11.

Hopkins, A., Coatham, M. L. & Berry, F. B. 2017. FOXC1 Regulates FGFR1 Isoform Switching to Promote Invasion Following TGFbeta-Induced EMT. *Mol Cancer Res,* 15**,** 1341-1353.

Hoshino, M., Fukui, H., Ono, Y., Sekikawa, A., Ichikawa, K., Tomita, S., Imai, Y., Imura, J., Hiraishi, H. & Fujimori, T. 2007. Nuclear expression of phosphorylated EGFR is associated with poor prognosis of patients with esophageal squamous cell carcinoma. *Pathobiology,* 74**,** 15-21.

Hsueh, C.-T., Selim, J. H., Tsai, J. Y. & Hsueh, C.-T. 2016. Nanovectors for anti-cancer drug delivery in the treatment of advanced pancreatic adenocarcinoma. *World Journal of Gastroenterology,* 22**,** 7080-7090.

Hu, Y., Fang, X., Dunham, S. M., Prada, C., Stachowiak, E. K. & Stachowiak, M. K. 2004. 90-kDa ribosomal S6 kinase is a direct target for the nuclear fibroblast growth factor receptor 1 (FGFR1): role in FGFR1 signaling. *J Biol Chem,* 279**,** 29325-35.

Hua, G., Lv, X., He, C., Remmenga, S. W., Rodabough, K. J., Dong, J., Yang, L., Lele, S. M., Yang, P., Zhou, J., Karst, A., Drapkin, R. I., Davis, J. S. & Wang, C. 2015. YAP induces high-grade serous carcinoma in fallopian tube secretory epithelial cells. *Oncogene,* 35**,** 2247.

Huang, C., Qiu, Z., Wang, L., Peng, Z., Jia, Z., Logsdon, C. D., Le, X., Wei, D., Huang, S. & Xie, K. 2012. A novel FoxM1-caveolin signaling pathway promotes pancreatic cancer invasion and metastasis. *Cancer Res,* 72**,** 655-65.

Huang, L., Holtzinger, A., Jagan, I., Begora, M., Lohse, I., Ngai, N., Nostro, C., Wang, R., Muthuswamy, L. B., Crawford, H. C., Arrowsmith, C., Kalloger, S. E., Renouf, D. J., Connor, A. A., Cleary, S., Schaeffer, D. F., Roehrl, M., Tsao, M.-S., Gallinger, S., Keller, G. & Muthuswamy, S. K. 2015. Ductal pancreatic cancer modeling and drug screening using human pluripotent stem cell- and patient-derived tumor organoids. *Nat Med,* 21**,** 1364-1371.

Hughes, D. J., Kunicka, T., Schomburg, L., Liska, V., Swan, N. & Soucek, P. 2018. Expression of Selenoprotein Genes and Association with Selenium Status in Colorectal Adenoma and Colorectal Cancer. *Nutrients,* 10.

Humbert, M., Casteran, N., Letard, S., Hanssens, K., Iovanna, J., Finetti, P., Bertucci, F., Bader, T., Mansfield, C. D., Moussy, A., Hermine, O. & Dubreuil, P. 2010. Masitinib combined with standard gemcitabine chemotherapy: in vitro and in vivo studies in human pancreatic tumour cell lines and ectopic mouse model. *PLoS One,* 5**,** e9430.

Hung, L. Y., Tseng, J. T., Lee, Y. C., Xia, W., Wang, Y. N., Wu, M. L., Chuang, Y. H., Lai, C. H. & Chang, W. C. 2008. Nuclear epidermal growth factor receptor (EGFR) interacts with signal transducer and activator of transcription 5 (STAT5) in activating Aurora-A gene expression. *Nucleic Acids Res,* 36**,** 4337-51.

Hwang, R. F., Moore, T. T., Hattersley, M. M., Scarpitti, M., Yang, B., Devereaux, E., Ramachandran, V., Arumugam, T., Ji, B., Logsdon, C. D., Brown, J. L. & Godin, R. 2012. Inhibition of the Hedgehog Pathway Targets the Tumor-Associated Stroma in Pancreatic Cancer. *Molecular Cancer Research,* 10**,** 1147-1157.

Iioka, H., Saito, K., Sakaguchi, M., Tachibana, T., Homma, K. & Kondo, E. 2019. Crumbs3 is a critical factor that regulates invasion and metastasis of colon adenocarcinoma via the specific interaction with FGFR1. *International Journal of Cancer,* 10, 2740-2753.

Ilic, M. & Ilic, I. 2016. Epidemiology of pancreatic cancer. *World J Gastroenterol,* 22**,** 9694-9705.

Infante, J. R., Matsubayashi, H., Sato, N., Tonascia, J., Klein, A. P., Riall, T. A., Yeo, C., Iacobuzio-Donahue, C. & Goggins, M. 2007. Peritumoral Fibroblast SPARC Expression and Patient Outcome With Resectable Pancreatic Adenocarcinoma. *Journal of Clinical Oncology,* 25**,** 319-325.

Inman, K. S., Francis, A. A. & Murray, N. R. 2014. Complex role for the immune system in initiation and progression of pancreatic cancer. *World Journal of Gastroenterology : WJG,* 20**,** 11160-11181.

Ishikawa, F., Yasukawa, M., Lyons, B., Yoshida, S., Miyamoto, T., Yoshimoto, G., Watanabe, T., Akashi, K., Shultz, L. D. & Harada, M. 2005. Development of functional human blood and immune systems in NOD/SCID/IL2 receptor {gamma} chain(null) mice. *Blood,* 106**,** 1565-73.

Ishiwata, T., Matsuda, Y., Yamamoto, T., Uchida, E., Korc, M. & Naito, Z. 2012. Enhanced expression of fibroblast growth factor receptor 2 IIIc promotes human pancreatic cancer cell proliferation. *Am J Pathol,* 180**,** 1928-41.

Jackson, C. C., Medeiros, L. J. & Miranda, R. N. 2010. 8p11 myeloproliferative syndrome: a review. *Hum Pathol,* 41**,** 461-76.

Jacobetz, M. A., Chan, D. S., Neesse, A., Bapiro, T. E., Cook, N., Frese, K. K., Feig, C., Nakagawa, T., Caldwell, M. E., Zecchini, H. I., Lolkema, M. P., Jiang, P., Kultti, A., Thompson, C. B., Maneval, D. C., Jodrell, D. I., Frost, G. I., Shepard, H. M., Skepper, J. N. & Tuveson, D. A. 2013. Hyaluronan impairs vascular function and drug delivery in a mouse model of pancreatic cancer. *Gut,* 62**,** 112-20.

Jang, M., Kim, E., Choi, Y., Lee, H., Kim, Y., Kim, J., Kang, E., Kim, S. W., Kim, I. & Park, S. 2012. FGFR1 is amplified during the progression of in situ to invasive breast carcinoma. *Breast Cancer Res,* 14**,** R115.

Jaster, R., Lichte, P., Fitzner, B., Brock, P., Glass, A., Karopka, T., Gierl, L., Koczan, D., Thiesen, H. J., Sparmann, G., Emmrich, J. & Liebe, S. 2005. Peroxisome proliferator-activated receptor gamma overexpression inhibits pro-fibrogenic activities of immortalised rat pancreatic stellate cells. *J Cell Mol Med,* 9**,** 670-82.

Jesnowski, R., Furst, D., Ringel, J., Chen, Y., Schrodel, A., Kleeff, J., Kolb, A., Schareck, W. D. & Lohr, M. 2005. Immortalization of pancreatic stellate cells as an in vitro model of pancreatic fibrosis: deactivation is induced by matrigel and N-acetylcysteine. *Lab Invest,* 85**,** 1276-91.

Jiang, X., Seo, Y. D., Chang, J. H., Coveler, A., Nigjeh, E. N., Pan, S., Jalikis, F., Yeung, R. S., Crispe, I. N. & Pillarisetty, V. G. 2017. Long-lived pancreatic ductal adenocarcinoma slice cultures enable precise study of the immune microenvironment. *Oncoimmunology,* 6**,** 210.

Jiang, Z., Zhou, C., Cheng, L., Yan, B., Chen, K., Chen, X., Zong, L., Lei, J., Duan, W., Xu, Q., Li, X., Wang, Z., Ma, Q. & Ma, J. 2018. Inhibiting YAP expression suppresses pancreatic cancer progression by disrupting tumor-stromal interactions. *Journal of Experimental & Clinical Cancer Research,* 37**,** 69.

Jo, M., Stolz, D. B., Esplen, J. E., Dorko, K., Michalopoulos, G. K. & Strom, S. C. 2000. Cross-talk between epidermal growth factor receptor and c-Met signal pathways in transformed cells. *J Biol Chem,* 275**,** 8806-11.

Johannesson, M., Stahlberg, A., Ameri, J., Sand, F. W., Norrman, K. & Semb, H. 2009. FGF4 and retinoic acid direct differentiation of hESCs into PDX1-expressing foregut endoderm in a time- and concentration-dependent manner. *PLoS One,* 4**,** e4794.

Johnson, D. S., Mortazavi, A., Myers, R. M. & Wold, B. 2007. Genome-Wide Mapping of In Vivo Protein-DNA Interactions. *Science,* 316**,** 1497-1502.

Juarez, P., Mohammad, K. S., Yin, J. J., Fournier, P. G., Mckenna, R. C., Davis, H. W., Peng, X. H., Niewolna, M., Javelaud, D., Chirgwin, J. M., Mauviel, A. & Guise, T. A. 2012. Halofuginone inhibits the establishment and progression of melanoma bone metastases. *Cancer Res,* 72**,** 6247-56.

Jurmeister, S., Baumann, M., Balwierz, A., Keklikoglou, I., Ward, A., Uhlmann, S., Zhang, J. D., Wiemann, S. & Sahin, Ö. 2012. MicroRNA-200c Represses Migration and Invasion of Breast Cancer Cells by Targeting Actin-Regulatory Proteins FHOD1 and PPM1F. *Molecular and Cellular Biology,* 32**,** 633-651.

Kabacaoglu, D., Ciecielski, K. J., Ruess, D. A. & Algül, H. 2018. Immune Checkpoint Inhibition for Pancreatic Ductal Adenocarcinoma: Current Limitations and Future Options. *Frontiers in Immunology,* 9**,** 1878-1878.

Kadaba, R., Birke, H., Wang, J., Hooper, S., Andl, C. D., Di Maggio, F., Soylu, E., Ghallab, M., Bor, D., Froeling, F. E. M., Bhattacharya, S., Rustgi, A. K., Sahai, E., Chelala, C., Sasieni, P. & Kocher, H. M. 2013. Imbalance of desmoplastic stromal cell numbers drives aggressive cancer processes. *The Journal of pathology,* 230**,** 107-117.

Kalluri, R. 2016. The biology and function of fibroblasts in cancer. *Nat Rev Cancer,* 16**,** 582-598.

Kang, J., Choi, Y. J., Seo, B. Y., Jo, U., Park, S. I., Kim, Y. H. & Park, K. H. 2019a. A Selective FGFR inhibitor AZD4547 suppresses RANKL/M-CSF/OPG-dependent ostoclastogenesis and breast cancer growth in the metastatic bone microenvironment. *Scientific Reports,* 9**,** 8726.

Kang, X., Lin, Z., Xu, M., Pan, J. & Wang, Z.-W. 2019b. Deciphering role of FGFR signalling pathway in pancreatic cancer. *Cell Proliferation,* 52**,** e12605.

Kang, Y. E., Kim, J. T., Lim, M. A., Oh, C., Liu, L., Jung, S.-N., Won, H.-R., Lee, K., Chang, J. W., Yi, H.-S., Kim, H. J., Ku, B. J., Shong, M. & Koo, B. S. 2019c. Association between Circulating Fibroblast Growth Factor 21 and Aggressiveness in Thyroid Cancer. *Cancers,* 11**,** 1154.

Kapałczyńska, M., Kolenda, T., Przybyła, W., Zajączkowska, M., Teresiak, A., Filas, V., Ibbs, M., Bliźniak, R., Łuczewski, Ł. & Lamperska, K. 2018. 2D and 3D cell cultures - a comparison of different types of cancer cell cultures. *Archives of Medical Science,* 14**,** 910-919.

Kapoor, A., Yao, W., Ying, H., Hua, S., Liewen, A., Wang, Q., Zhong, Y., Wu, C.-J., Sadanandam, A., Hu, B., Chang, Q., Chu, Gerald c., Al-Khalil, R., Jiang, S., Xia, H., Fletcher-Sananikone, E., Lim, C., Horwitz, Gillian i., Viale, A., Pettazzoni, P., Sanchez, N., Wang, H., Protopopov, A., Zhang, J., Heffernan, T., Johnson, Randy l., Chin, L., Wang, Y. A., Draetta, G. & Depinho, Ronald a. 2014. Yap1 Activation

Enables Bypass of Oncogenic Kras Addiction in Pancreatic Cancer. *Cell,* 158**,** 185-197.

Karbownik, M. S. & Nowak, J. Z. 2013. Hyaluronan: towards novel anti-cancer therapeutics. *Pharmacol Rep,* 65**,** 1056-74.

Kastrinos, F., Mukherjee, B., Tayob, N., Wang, F., Sparr, J., Raymond, V. M., Bandipalliam, P., Stoffel, E. M., Gruber, S. B. & Syngal, S. 2009. The Risk of Pancreatic Cancer in Families with Lynch Syndrome. *JAMA : the journal of the American Medical Association,* 302**,** 1790-1795.

Katoh, M. 2016. FGFR inhibitors: Effects on cancer cells, tumor microenvironment and whole-body homeostasis (Review). *Int J Mol Med,* 38**,** 3-15.

Katoh, M. 2019. Fibroblast growth factor receptors as treatment targets in clinical oncology. *Nat Rev Clin Oncol,* 16**,** 105-122.

Katoh, M. & Nakagama, H. 2014. FGF receptors: cancer biology and therapeutics. *Med Res Rev,* 34**,** 280-300.

Kelleher, F. C., O'sullivan, H., Smyth, E., Mcdermott, R. & Viterbo, A. 2013. Fibroblast growth factor receptors, developmental corruption and malignant disease. *Carcinogenesis,* 34**,** 2198-2205.

Khoury, H., Naujokas, M. A., Zuo, D., Sangwan, V., Frigault, M. M., Petkiewicz, S., Dankort, D. L., Muller, W. J. & Park, M. 2005. HGF converts ErbB2/Neu epithelial morphogenesis to cell invasion. *Mol Biol Cell,* 16**,** 550-61.

Kidder, B. L., Hu, G. & Zhao, K. 2011. ChIP-Seq: technical considerations for obtaining high-quality data. *Nat Immunol,* 12**,** 918-22.

Kikuta, K., Masamune, A., Watanabe, T., Ariga, H., Itoh, H., Hamada, S., Satoh, K., Egawa, S., Unno, M. & Shimosegawa, T. 2010. Pancreatic stellate cells promote epithelial-mesenchymal transition in pancreatic cancer cells. *Biochem Biophys Res Commun,* 403**,** 380-4.

Kim, H. P., Yoon, Y. K., Kim, J. W., Han, S. W., Hur, H. S., Park, J., Lee, J. H., Oh, D. Y., Im, S. A., Bang, Y. J. & Kim, T. Y. 2009. Lapatinib, a dual EGFR and HER2 tyrosine kinase inhibitor, downregulates thymidylate synthase by inhibiting the nuclear translocation of EGFR and HER2. *PLoS One,* 4**,** e5933.

Kim, J. H., Kim, H. S., Kim, B. J., Lee, J. & Jang, H. J. 2017. Prognostic value of c-Met overexpression in pancreatic adenocarcinoma: a meta-analysis. *Oncotarget,* 8**,** 73098-73104.

Kim, S. H., Turnbull, J. & Guimond, S. 2011. Extracellular matrix and cell signalling: the dynamic cooperation of integrin, proteoglycan and growth factor receptor. *J Endocrinol,* 209**,** 139-51.

Kim, S. K. & Hebrok, M. 2001. Intercellular signals regulating pancreas development and function. *Genes Dev,* 15**,** 111-27.

Kim, S. M., Kim, H., Yun, M. R., Kang, H. N., Pyo, K. H., Park, H. J., Lee, J. M., Choi, H. M., Ellinghaus, P., Ocker, M., Paik, S., Kim, H. R. & Cho, B. C. 2016. Activation of the Met kinase confers acquired drug resistance in FGFR-targeted lung cancer therapy. *Oncogenesis,* 5**,** e241.

Kobrin, M. S., Yamanaka, Y., Friess, H., Lopez, M. E. & Korc, M. 1993. Aberrant expression of type I fibroblast growth factor receptor in human pancreatic adenocarcinomas. *Cancer Res,* 53**,** 4741-4.

Koikawa, K., Ohuchida, K., Ando, Y., Kibe, S., Nakayama, H., Takesue, S., Endo, S., Abe, T., Okumura, T., Iwamoto, C., Moriyama, T., Nakata, K., Miyasaka, Y., Ohtsuka, T., Nagai, E., Mizumoto, K., Hashizume, M. & Nakamura, M. 2018. Basement membrane destruction by pancreatic stellate cells leads to local invasion in pancreatic ductal adenocarcinoma. *Cancer Lett,* 425**,** 65-77.

Koole, K., Brunen, D., Van Kempen, P. M., Noorlag, R., De Bree, R., Lieftink, C., Van Es, R. J., Bernards, R. & Willems, S. M. 2016a. FGFR1 Is a Potential Prognostic Biomarker and Therapeutic Target in Head and Neck Squamous Cell Carcinoma. *Clin Cancer Res,* 22**,** 3884-93.

Koole, K., Van Kempen, P. M., Swartz, J. E., Peeters, T., Van Diest, P. J., Koole, R., Van Es, R. J. & Willems, S. M. 2016b. Fibroblast growth factor receptor 3 protein is overexpressed in oral and oropharyngeal squamous cell carcinoma. *Cancer Med,* 5**,** 275-84.

Kornmann, M., Ishiwata, T., Beger, H. G. & Korc, M. 1997. Fibroblast growth factor-5 stimulates mitogenic signaling and is overexpressed in human pancreatic cancer: evidence for autocrine and paracrine actions. *Oncogene,* 15**,** 1417-24.

Kornmann, M., Ishiwata, T., Matsuda, K., Lopez, M. E., Fukahi, K., Asano, G., Beger, H. G. & Korc, M. 2002. IIIc isoform of fibroblast growth factor receptor 1 is overexpressed in human pancreatic cancer and enhances tumorigenicity of hamster ductal cells. *Gastroenterology,* 123**,** 301-13.

Kornmann, M., Lopez, M., Beger, H. & Korc, M. 2001. Expression of the IIIc Variant of FGF Receptor-1 Confers Mitogenic Responsiveness to Heparin and FGF-5 in TAKA-1 Pancreatic Ductal Cells. *Int J Gastrointest Cancer,* 29**,** 85-92.

Kotteas, E., Saif, M. W. & Syrigos, K. 2016. Immunotherapy for pancreatic cancer. *Journal of Cancer Research and Clinical Oncology,* 142**,** 1795-1805.

Krejci, P., Salazar, L., Kashiwada, T. A., Chlebova, K., Salasova, A., Thompson, L. M., Bryja, V., Kozubik, A. & Wilcox, W. R. 2008. Analysis of STAT1 activation by six FGFR3 mutants associated with skeletal dysplasia undermines dominant role of STAT1 in FGFR3 signaling in cartilage. *PLoS One,* 3**,** e3961.

Kultti, A., Pasonen-Seppänen, S., Jauhiainen, M., Rilla, K. J., Kärnä, R., Pyöriä, E., Tammi, R. H. & Tammi, M. I. 2009. 4-Methylumbelliferone inhibits hyaluronan synthesis by depletion of cellular UDP-glucuronic acid and downregulation of hyaluronan synthase 2 and 3. *Experimental Cell Research,* 315**,** 1914-1923.

Kultti, A., Zhao, C., Singha, N. C., Zimmerman, S., Osgood, R. J., Symons, R., Jiang, P., Li, X., Thompson, C. B., Infante, J. R., Jacobetz, M. A., Tuveson, D. A., Frost, G. I., Shepard, H. M. & Huang, Z. 2014. Accumulation of extracellular hyaluronan by hyaluronan synthase 3 promotes tumor growth and modulates the pancreatic cancer microenvironment. *Biomed Res Int,* 2014**,** 817613.

Kunii, K., Davis, L., Gorenstein, J., Hatch, H., Yashiro, M., Di Bacco, A., Elbi, C. & Lutterbach, B. 2008. FGFR2-amplified gastric cancer cell lines require FGFR2 and Erbb3 signaling for growth and survival. *Cancer Res,* 68**,** 2340-8.

Kuniyasu, H., Abbruzzese, J. L., Cleary, K. R. & Fidler, I. J. 2001. Induction of ductal and stromal hyperplasia by basic fibroblast growth factor produced by human pancreatic carcinoma. *Int J Oncol,* 19**,** 681-5.

Kutluk Cenik, B., Ostapoff, K. T., Gerber, D. E. & Brekken, R. A. 2013. BIBF 1120 (nintedanib), a triple angiokinase inhibitor, induces hypoxia but not EMT and blocks progression of preclinical models of lung and pancreatic cancer. *Mol Cancer Ther,* 12**,** 992-1001.

Kuwahara, K., Sasaki, T., Kuwada, Y., Murakami, M., Yamasaki, S. & Chayama, K. 2003. Expressions of angiogenic factors in pancreatic ductal carcinoma: a correlative study with clinicopathologic parameters and patient survival. *Pancreas,* 26**,** 344-9.

Labernadie, A., Kato, T., Brugues, A., Serra-Picamal, X., Derzsi, S., Arwert, E., Weston, A., Gonzalez-Tarrago, V., Elosegui-Artola, A., Albertazzi, L., Alcaraz, J., Roca-Cusachs, P., Sahai, E. & Trepat, X. 2017. A mechanically active heterotypic E-cadherin/N-cadherin adhesion enables fibroblasts to drive cancer cell invasion. *Nat Cell Biol,* 19**,** 224-237.

Lai, S. W., Bamodu, O. A., Tsai, W. C., Chang, Y. M., Lee, W. H., Yeh, C. T. & Chao, T. Y. 2018. The therapeutic targeting of the FGFR1/Src/NF-kappaB signaling axis inhibits pancreatic ductal adenocarcinoma stemness and oncogenicity. *Clin Exp Metastasis,* 35**,** 663-677.

Landt, S. G., Marinov, G. K., Kundaje, A., Kheradpour, P., Pauli, F., Batzoglou, S., Bernstein, B. E., Bickel, P., Brown, J. B., Cayting, P., Chen, Y., Desalvo, G., Epstein, C., Fisher-Aylor, K. I., Euskirchen, G., Gerstein, M., Gertz, J., Hartemink, A. J., Hoffman, M. M., Iyer, V. R., Jung, Y. L., Karmakar, S., Kellis, M., Kharchenko, P. V., Li, Q., Liu, T., Liu, X. S., Ma, L., Milosavljevic, A., Myers, R. M., Park, P. J., Pazin, M. J., Perry, M. D., Raha, D., Reddy, T. E., Rozowsky, J., Shoresh, N., Sidow, A., Slattery, M., Stamatoyannopoulos, J. A., Tolstorukov, M. Y., White, K. P., Xi, S., Farnham, P. J., Lieb, J. D., Wold, B. J. & Snyder, M. 2012. ChIP-seq guidelines and practices of the ENCODE and modENCODE consortia. *Genome Res,* 22**,** 1813-31.

Le, T., New, J., Jones, J. W., Usman, S., Yalamanchali, S., Tawfik, O., Hoover, L., Bruegger, D. E. & Thomas, S. M. 2017. Inhibition of fibroblast growth factor receptor with AZD4547 mitigates juvenile nasopharyngeal angiofibroma. *International Forum of Allergy & Rhinology,* 7**,** 973-979.

Lebeau, A. M., Brennen, W. N., Aggarwal, S. & Denmeade, S. R. 2009. Targeting the cancer stroma with a fibroblast activation protein-activated promelittin protoxin. *Mol Cancer Ther,* 8**,** 1378-86.

Lee, H. J., Seo, A. N., Park, S. Y., Kim, J. Y., Park, J. Y., Yu, J. H., Ahn, J. H. & Gong, G. 2014. Low prognostic implication of fibroblast growth factor family activation in triple-negative breast cancer subsets. *Ann Surg Oncol,* 21**,** 1561-8.

Lee, J., Condello, S., Yakubov, B., Emerson, R., Caperell-Grant, A., Hitomi, K., Xie, J. & Matei, D. 2015. Tissue Transglutaminase Mediated Tumor-Stroma Interaction Promotes Pancreatic Cancer Progression. *Clin Cancer Res,* 21**,** 4482-93.

Lee, Y. W., Stachowiak, E. K., Birkaya, B., Terranova, C., Capacchietti, M., Claus, P., Aletta, J. M. & Stachowiak, M. K. 2013. NGF-induced cell differentiation and gene activation is mediated by integrative nuclear FGFR1 signaling (INFS). *PLoS One,* 8**,** e68931.

Lee, Y. W., Terranova, C., Birkaya, B., Narla, S., Kehoe, D., Parikh, A., Dong, S., Ratzka, A., Brinkmann, H., Aletta, J. M., Tzanakakis, E. S., Stachowiak, E. K., Claus, P. & Stachowiak, M. K. 2012. A novel nuclear FGF Receptor-1 partnership with retinoid and Nur receptors during developmental gene programming of embryonic stem cells. *J Cell Biochem,* 113**,** 2920-36.

Lehnen, N. C., Von Massenhausen, A., Kalthoff, H., Zhou, H., Glowka, T., Schutte, U., Holler, T., Riesner, K., Boehm, D., Merkelbach-Bruse, S., Kirfel, J., Perner, S. & Gutgemann, I. 2013. Fibroblast growth factor receptor 1 gene amplification in pancreatic ductal adenocarcinoma. *Histopathology,* 63**,** 157-66.

Leichtle, A. B., Ceglarek, U., Weinert, P., Nakas, C. T., Nuoffer, J. M., Kase, J., Conrad, T., Witzigmann, H., Thiery, J. & Fiedler, G. M. 2013. Pancreatic carcinoma, pancreatitis, and healthy controls: metabolite models in a three-class diagnostic dilemma. *Metabolomics,* 9**,** 677-687.

Leung, H. Y., Gullick, W. J. & Lemoine, N. R. 1994. Expression and functional activity of fibroblast growth factors and their receptors in human pancreatic cancer. *Int J Cancer,* 59**,** 667-75.

Li, D. 2012. Diabetes and pancreatic cancer. *Molecular carcinogenesis,* 51**,** 64-74.

Li, M., Seki, Y., Freitas, P. H. L., Nagata, M., Kojima, T., Sultana, S., Ubaidus, S., Maeda, T., Shimomura, J., Henderson, J. E., Tamura, M., Oda, K., Liu, Z., Guo, Y., Suzuki, R., Yamamoto, T., Takagi, R. & Amizuka, N. 2010. FGFR3 down-regulates PTH/PTHrP receptor gene expression by mediating JAK/STAT signaling in chondrocytic cell line. *Journal of Electron Microscopy,* 59**,** 227-236.

Li, N. F., Kocher, H. M., Salako, M. A., Obermueller, E., Sandle, J. & Balkwill, F. 2009. A novel function of colony-stimulating factor 1 receptor in hTERT immortalization of human epithelial cells. *Oncogene,* 28**,** 773-80.

Li, X., Nadauld, L., Ootani, A., Corney, D. C., Pai, R. K., Gevaert, O., Cantrell, M. A., Rack, P. G., Neal, J. T., Chan, C. W. M., Yeung, T., Gong, X., Yuan, J., Wilhelmy, J., Robine, S., Attardi, L. D., Plevritis, S. K., Hung, K. E., Chen, C.-Z., Ji, H. P. & Kuo, C. J. 2014. Oncogenic transformation of diverse gastrointestinal tissues in primary organoid culture. *Nature medicine,* 20**,** 769-777.

Li, Z., Adams, R. M., Chourey, K., Hurst, G. B., Hettich, R. L. & Pan, C. 2012. Systematic comparison of label-free, metabolic labeling, and isobaric chemical labeling for quantitative proteomics on LTQ Orbitrap Velos. *J Proteome Res,* 11**,** 1582-90.

Lieber, M., Mazzetta, J., Nelson-Rees, W., Kaplan, M. & Todaro, G. 1975. Establishment of a continuous tumor-cell line (panc-1) from a human carcinoma of the exocrine pancreas. *Int J Cancer,* 15**,** 741-7.

Lievens, P. M.-J., Mutinelli, C., Baynes, D. & Liboi, E. 2004. The Kinase Activity of Fibroblast Growth Factor Receptor 3 with Activation Loop Mutations Affects Receptor Trafficking and Signaling. *Journal of Biological Chemistry,* 279**,** 43254-43260.

Liggett, T., Melnikov, A., Yi, Q. L., Replogle, C., Brand, R., Kaul, K., Talamonti, M., Abrams, R. A. & Levenson, V. 2010. Differential methylation of cell-free circulating DNA among patients with pancreatic cancer versus chronic pancreatitis. *Cancer,* 116**,** 1674-80.

Lim, S. A., Kim, J., Jeon, S., Shin, M. H., Kwon, J., Kim, T.-J., Im, K., Han, Y., Kwon, W., Kim, S.-W., Yee, C., Kim, S.-J., Jang, J.-Y. & Lee, K.-M. 2019. Defective Localization With Impaired Tumor Cytotoxicity Contributes to the Immune Escape of NK Cells in Pancreatic Cancer Patients. *Frontiers in Immunology,* 10.

Lin, S.-Y., Makino, K., Xia, W., Matin, A., Wen, Y., Kwong, K. Y., Bourguignon, L. & Hung, M.-C. 2001. Nuclear localization of EGF receptor and its potential new role as a transcription factor. *Nat Cell Biol,* 3**,** 802-808.

Lin, Y. Z., Yao, S. Y. & Hawiger, J. 1996. Role of the nuclear localization sequence in fibroblast growth factor-1-stimulated mitogenic pathways. *J Biol Chem,* 271**,** 5305-8.

Linder, S., Castanos-Velez, E., Von Rosen, A. & Biberfeld, P. 2001. Immunohistochemical expression of extracellular matrix proteins and adhesion molecules in pancreatic carcinoma. *Hepatogastroenterology,* 48**,** 1321-7.

Ling, J., Kang, Y., Zhao, R., Xia, Q., Lee, D. F., Chang, Z., Li, J., Peng, B., Fleming, J. B., Wang, H., Liu, J., Lemischka, I. R., Hung, M. C. & Chiao, P. J. 2012. KrasG12D-induced IKK2/beta/NF-kappaB activation by IL-1alpha and p62 feedforward loops is required for development of pancreatic ductal adenocarcinoma. *Cancer Cell,* 21**,** 105-20.

Ling, L., Tan, S. K., Goh, T. H., Cheung, E., Nurcombe, V., Van Wijnen, A. J. & Cool, S. M. 2015. Targeting the heparin-binding domain of fibroblast growth factor receptor 1 as a potential cancer therapy. *Mol Cancer,* 14**,** 136.

Linggi, B. & Carpenter, G. 2006. ErbB-4 s80 intracellular domain abrogates ETO2-dependent transcriptional repression. *J Biol Chem,* 281**,** 25373-80.

Liu, L., Ye, T. H., Han, Y. P., Song, H., Zhang, Y. K., Xia, Y., Wang, N. Y., Xiong, Y., Song, X. J., Zhu, Y. X., Li, D. L., Zeng, J., Ran, K., Peng, C. T., Wei, Y. Q. & Yu, L. T. 2014. Reductions in Myeloid-Derived Suppressor Cells and Lung Metastases using AZD4547 Treatment of a Metastatic Murine Breast Tumor Model. *Cellular Physiology and Biochemistry,* 33**,** 633-645.

Liu, R., Huang, S., Lei, Y., Zhang, T., Wang, K., Liu, B., Nice, E. C., Xiang, R., Xie, K., Li, J. & Huang, C. 2015. FGF8 promotes colorectal cancer growth and metastasis by activating YAP1. *Oncotarget,* 6**,** 935-52.

Liu, S.-L., Cao, S.-G., Li, Y., Sun, B., Chen, D., Wang, D.-S. & Zhou, Y.-B. 2019. Pancreatic stellate cells facilitate pancreatic cancer cell viability and invasion. *Oncology letters,* 17**,** 2057-2062.

Liu, Z., Neiss, N., Zhou, S., Henne-Bruns, D., Korc, M., Bachem, M. & Kornmann, M. 2007. Identification of a fibroblast growth factor receptor 1 splice variant that inhibits pancreatic cancer cell growth. *Cancer Res,* 67**,** 2712-9.

Lo, H. W., Hsu, S. C., Ali-Seyed, M., Gunduz, M., Xia, W., Wei, Y., Bartholomeusz, G., Shih, J. Y. & Hung, M. C. 2005. Nuclear interaction of EGFR and STAT3 in the activation of the iNOS/NO pathway. *Cancer Cell,* 7**,** 575-89.

Longley, D. B., Harkin, D. P. & Johnston, P. G. 2003. 5-Fluorouracil: mechanisms of action and clinical strategies. *Nat Rev Cancer,* 3**,** 330-338.

Los, G. V., Encell, L. P., McDougall, M. G., Hartzell, D. D., Karassina, N., Zimprich, C., Wood, M. G., Learish, R., Ohana, R. F., Urh, M., Simpson, D., Mendez, J., Zimmerman, K., Otto, P., Vidugiris, G., Zhu, J., Darzins, A., Klaubert, D. H., Bulleit, R. F. & Wood, K. V. 2008. HaloTag: a novel protein labeling technology for cell imaging and protein analysis. *ACS Chem Biol,* 3**,** 373-82.

Lowenfels, A. B. & Maisonneuve, P. 2006. Epidemiology and risk factors for pancreatic cancer. *Best Pract Res Clin Gastroenterol,* 20**,** 197-209.

Lu, C.-H., Tang, W.-C., Liu, Y.-T., Chang, S.-W., Wu, F. C. M., Chen, C.-Y., Tsai, Y.-C., Yang, S.-M., Kuo, C.-W., Okada, Y., Hwu, Y.-K., Chen, P. & Chen, B.-C. 2019. Lightsheet localization microscopy enables fast, large-scale, and three-dimensional super-resolution imaging. *Communications Biology,* 2**,** 177.

Luo, K. 2017. Signaling Cross Talk between TGF-β/Smad and Other Signaling Pathways. *Cold Spring Harbor perspectives in biology,* 9**,** a022137.

Ma, W. W., Xie, H., Fetterly, G., Pitzonka, L., Whitworth, A., Levea, C., Wilton, J., Mantione, K., Schihl, S., Dy, G. K., Boland, P., Iyer, R., Tan, W., Brady, W., Straubinger, R. M. & Adjei, A. A. 2019. A Phase Ib Study of the FGFR/VEGFR Inhibitor Dovitinib With Gemcitabine and Capecitabine in Advanced Solid Tumor and Pancreatic Cancer Patients. *Am J Clin Oncol,* 42**,** 184-189.

Mahadevan, D. & Von Hoff, D. D. 2007. Tumor-stroma interactions in pancreatic ductal adenocarcinoma. *Molecular Cancer Therapeutics,* 6**,** 1186-1197.

Mahbouli, S., Talvas, J., Der Vartanian, A., Ortega, S., Rouge, S., Vasson, M. P. & Rossary, A. 2018. Activation of antioxidant defences of human mammary epithelial cells under leptin depend on neoplastic state. *BMC Cancer,* 18**,** 1264.

Maher, P. A. 1996. Nuclear Translocation of fibroblast growth factor (FGF) receptors in response to FGF-2. *J Cell Biol,* 134**,** 529-36.

Mahipal, A. & Malafa, M. 2016. Importins and exportins as therapeutic targets in cancer. *Pharmacol Ther,* 164**,** 135-43.

Mannaerts, I., Leite, S. B., Verhulst, S., Claerhout, S., Eysackers, N., Thoen, L. F. R., Hoorens, A., Reynaert, H., Halder, G. & Van Grunsven, L. A. 2015. The Hippo pathway effector YAP controls mouse hepatic stellate cell activation. *Journal of Hepatology,* 63**,** 679-688.

Mano, Y., Takahashi, K., Ishikawa, N., Takano, A., Yasui, W., Inai, K., Nishimura, H., Tsuchiya, E., Nakamura, Y. & Daigo, Y. 2007. Fibroblast growth factor receptor 1 oncogene partner as a novel prognostic biomarker and therapeutic target for lung cancer. *Cancer Sci,* 98**,** 1902-13.

Mantoni, T. S., Schendel, R. R., Rodel, F., Niedobitek, G., Al-Assar, O., Masamune, A. & Brunner, T. B. 2008. Stromal SPARC expression and patient survival after chemoradiation for non-resectable pancreatic adenocarcinoma. *Cancer Biol Ther,* 7**,** 1806-15.

Marangon, E., Sala, F., Caffo, O., Galligioni, E., D'Incalci, M. & Zucchetti, M. 2008. Simultaneous determination of gemcitabine and its main metabolite, dFdU, in plasma of patients with advanced non-small-cell lung cancer by high-performance liquid chromatography-tandem mass spectrometry. *J Mass Spectrom,* 43**,** 216-23.

Marchesan, S. & Prato, M. 2015. Under the lens: carbon nanotube and protein interaction at the nanoscale. *Chemical Communications,* 51**,** 4347-4359.

Marchese, C., Chedid, M., Dirsch, O. R., Csaky, K. G., Santanelli, F., Latini, C., Larochelle, W. J., Torrisi, M. R. & Aaronson, S. A. 1995. Modulation of keratinocyte growth factor and its receptor in reepithelializing human skin. *J Exp Med,* 182**,** 1369-76.

Marek, L., Ware, K. E., Fritzsche, A., Hercule, P., Helton, W. R., Smith, J. E., Mcdermott, L. A., Coldren, C. D., Nemenoff, R. A., Merrick, D. T., Helfrich, B. A., Bunn, P. A., Jr. & Heasley, L. E. 2009. Fibroblast growth factor (FGF) and FGF receptor-mediated autocrine signaling in non-small-cell lung cancer cells. *Mol Pharmacol,* 75**,** 196-207.

Marti, P., Stein, C., Blumer, T., Abraham, Y., Dill, M. T., Pikiolek, M., Orsini, V., Jurisic, G., Megel, P., Makowska, Z., Agarinis, C., Tornillo, L., Bouwmeester, T., Ruffner, H., Bauer, A., Parker, C. N., Schmelzle, T., Terracciano, L. M., Heim, M. H. & Tchorz, J. S. 2015. YAP promotes proliferation, chemoresistance, and angiogenesis in human cholangiocarcinoma through TEAD transcription factors. *Hepatology,* 62**,** 1497-510.

Marti, U., Burwen, S. J., Wells, A., Barker, M. E., Huling, S., Feren, A. M. & Jones, A. L. 1991. Localization of epidermal growth factor receptor in hepatocyte nuclei. *Hepatology,* 13**,** 15-20.

Marzec, J., Dayem Ullah, A. Z., Pirro, S., Gadaleta, E., Crnogorac-Jurcevic, T., Lemoine, N. R., Kocher, H. M. & Chelala, C. 2018. The Pancreatic Expression Database: 2018 update. *Nucleic Acids Res,* 46**,** D1107-d1110.

Masamune, A., Satoh, M., Kikuta, K., Suzuki, N. & Shimosegawa, T. 2003. Establishment and characterization of a rat pancreatic stellate cell line by spontaneous immortalization. *World Journal of Gastroenterology,* 9**,** 2751-2758.

Matsuda, Y., Yoshimura, H., Suzuki, T., Uchida, E., Naito, Z. & Ishiwata, T. 2014. Inhibition of fibroblast growth factor receptor 2 attenuates proliferation and invasion of pancreatic cancer. *Cancer Sci,* 105**,** 1212-9.

Matsumoto, K., Arao, T., Hamaguchi, T., Shimada, Y., Kato, K., Oda, I., Taniguchi, H., Koizumi, F., Yanagihara, K., Sasaki, H., Nishio, K. & Yamada, Y. 2012. FGFR2 gene amplification and clinicopathological features in gastric cancer. *Br J Cancer,* 106**,** 727-32.

Matsuo, I. & Kimura-Yoshida, C. 2013. Extracellular modulation of Fibroblast Growth Factor signaling through heparan sulfate proteoglycans in mammalian development. *Curr Opin Genet Dev,* 23**,** 399-407.

McCarroll, J. A., Naim, S., Sharbeen, G., Russia, N., Lee, J., Kavallaris, M., Goldstein, D. & Phillips, P. A. 2014. Role of pancreatic stellate cells in chemoresistance in pancreatic cancer. *Front Physiol,* 5**,** 141.

McCarroll, J. A., Phillips, P. A., Santucci, N., Pirola, R. C., Wilson, J. S. & Apte, M. V. 2006. Vitamin A inhibits pancreatic stellate cell activation: implications for treatment of pancreatic fibrosis. *Gut,* 55**,** 79-89.

McCarthy, J. B., El-Ashry, D. & Turley, E. A. 2018. Hyaluronan, Cancer-Associated Fibroblasts and the Tumor Microenvironment in Malignant Progression. *Front Cell Dev Biol,* 6**,** 48.

Megger, D. A., Pott, L. L., Ahrens, M., Padden, J., Bracht, T., Kuhlmann, K., Eisenacher, M., Meyer, H. E. & Sitek, B. 2014. Comparison of label-free and label-based strategies for proteome analysis of hepatoma cell lines. *Biochim Biophys Acta,* 1844**,** 967-76.

Memon, B., Karam, M., Al-Khawaga, S. & Abdelalim, E. M. 2018. Enhanced differentiation of human pluripotent stem cells into pancreatic progenitors co-expressing PDX1 and NKX6.1. *Stem Cell Res Ther,* 9**,** 15.

Meng, Q., Shi, S., Liang, C., Liang, D., Hua, J., Zhang, B., Xu, J. & Yu, X. 2018. Abrogation of glutathione peroxidase-1 drives EMT and chemoresistance in pancreatic cancer by activating ROS-mediated Akt/GSK3beta/Snail signaling. *Oncogene,* 37**,** 5843-5857.

Merika, E. E., Syrigos, K. N. & Saif, M. W. 2012. Desmoplasia in Pancreatic Cancer. Can We Fight It? *Gastroenterology Research and Practice,* 2012**,** 781765.

Metzner, T., Bedeir, A., Held, G., Peter-Vorosmarty, B., Ghassemi, S., Heinzle, C., Spiegl-Kreinecker, S., Marian, B., Holzmann, K., Grasl-Kraupp, B., Pirker, C., Micksche, M., Berger, W., Heffeter, P. & Grusch, M. 2011. Fibroblast growth factor

receptors as therapeutic targets in human melanoma: synergism with BRAF inhibition. *J Invest Dermatol,* 131**,** 2087-95.

Mfopou, J. K., Chen, B., Mateizel, I., Sermon, K. & Bouwens, L. 2010. Noggin, retinoids, and fibroblast growth factor regulate hepatic or pancreatic fate of human embryonic stem cells. *Gastroenterology,* 138**,** 2233-45, 2245.e1-14.

Miller, B. W., Morton, J. P., Pinese, M., Saturno, G., Jamieson, N. B., Mcghee, E., Timpson, P., Leach, J., Mcgarry, L., Shanks, E., Bailey, P., Chang, D., Oien, K., Karim, S., Au, A., Steele, C., Carter, C. R., Mckay, C., Anderson, K., Evans, T. R., Marais, R., Springer, C., Biankin, A., Erler, J. T. & Sansom, O. J. 2015. Targeting the LOX/hypoxia axis reverses many of the features that make pancreatic cancer deadly: inhibition of LOX abrogates metastasis and enhances drug efficacy. *EMBO Mol Med,* 7**,** 1063-76.

Mills, G. C. 1957. Hemoglobin Catabolism: I. Glutathione Peroxidase, an erythrocyte enzyme which protects hemoglobin from oxidative breakdown. *Journal of Biological Chemistry,* 229**,** 189-197.

Mini, E., Nobili, S., Caciagli, B., Landini, I. & Mazzei, T. 2006. Cellular pharmacology of gemcitabine. *Ann Oncol,* 17 Suppl 5**,** v7-12.

Missiaglia, E., Dalai, I., Barbi, S., Beghelli, S., Falconi, M., Della Peruta, M., Piemonti, L., Capurso, G., Di Florio, A., Delle Fave, G., Pederzoli, P., Croce, C. M. & Scarpa, A. 2010. Pancreatic endocrine tumors: expression profiling evidences a role for AKT-mTOR pathway. *J Clin Oncol,* 28**,** 245-55.

Missiaglia, E., Selfe, J., Hamdi, M., Williamson, D., Schaaf, G., Fang, C., Koster, J., Summersgill, B., Messahel, B., Versteeg, R., Pritchard-Jones, K., Kool, M. & Shipley, J. 2009. Genomic imbalances in rhabdomyosarcoma cell lines affect expression of genes frequently altered in primary tumors: an approach to identify candidate genes involved in tumor development. *Genes Chromosomes Cancer,* 48**,** 455-67.

Mitry, E., Hammel, P., Deplanque, G., Mornex, F., Levy, P., Seitz, J. F., Moussy, A., Kinet, J. P., Hermine, O., Rougier, P. & Raymond, E. 2010. Safety and activity of masitinib in combination with gemcitabine in patients with advanced pancreatic cancer. *Cancer Chemother Pharmacol,* 66**,** 395-403.

Miyoshi, K., Sato, N., Ohuchida, K., Mizumoto, K. & Tanaka, M. 2010. SPARC mRNA expression as a prognostic marker for pancreatic adenocarcinoma patients. *Anticancer Res,* 30**,** 867-71.

Moffitt, R. A., Marayati, R., Flate, E. L., Volmar, K. E., Loeza, S. G., Hoadley, K. A., Rashid, N. U., Williams, L. A., Eaton, S. C., Chung, A. H., Smyla, J. K., Anderson, J. M., Kim, H. J., Bentrem, D. J., Talamonti, M. S., Iacobuzio-Donahue, C. A., Hollingsworth, M. A. & Yeh, J. J. 2015. Virtual microdissection identifies distinct

tumor- and stroma-specific subtypes of pancreatic ductal adenocarcinoma. *Nat Genet,* 47**,** 1168-78.

Mohammadi, M., Froum, S., Hamby, J. M., Schroeder, M. C., Panek, R. L., Lu, G. H., Eliseenkova, A. V., Green, D., Schlessinger, J. & Hubbard, S. R. 1998. Crystal structure of an angiogenesis inhibitor bound to the FGF receptor tyrosine kinase domain. *The EMBO journal,* 17**,** 5896-5904.

Mohammed, S., Van Buren, G., Ii & Fisher, W. E. 2014. Pancreatic cancer: advances in treatment. *World Journal of Gastroenterology,* 20**,** 9354-9360.

Moreira, L., Bakir, B., Chatterji, P., Dantes, Z., Reichert, M. & Rustgi, A. K. 2018. Pancreas 3D Organoids: Current and Future Aspects as a Research Platform for Personalized Medicine in Pancreatic Cancer. *Cellular and Molecular Gastroenterology and Hepatology,* 5**,** 289-298.

Morgan, R. T., Woods, L. K., Moore, G. E., Quinn, L. A., Mcgavran, L. & Gordon, S. G. 1980. Human cell line (COLO 357) of metastatic pancreatic adenocarcinoma. *Int J Cancer,* 25**,** 591-8.

Mori, S., Hatori, N., Kawaguchi, N., Hamada, Y., Shih, T.-C., Wu, C.-Y., Lam, K. S., Matsuura, N., Yamamoto, H., Takada, Y. K. & Takada, Y. 2017. The integrin-binding defective FGF2 mutants potently suppress FGF2 signalling and angiogenesis. *Bioscience reports,* 37**,** BSR20170173.

Mori, S., Saegusa, J., Yamaji, S., Wu, C.-Y., Akakura, N., Shi, B., Kuwabara, Y., Chan, B., Takada, Y., Lam, K., Cheung, A., Isseroff, R. & Takada, Y. 2008a. FGF receptor-integrin crosstalk by direct binding of αvβ3 to FGF1: A dominant-negative inhibitory action of the integrin-binding-defective FGF1 mutant in FGF signaling. *Cancer Research,* 68**,** 143-143.

Mori, S. & Takada, Y. 2013. Crosstalk between Fibroblast Growth Factor (FGF) Receptor and Integrin through Direct Integrin Binding to FGF and Resulting Integrin-FGF-FGFR Ternary Complex Formation. *Medical Sciences,* 1**,** 20-36.

Mori, S., Wu, C.-Y., Yamaji, S., Saegusa, J., Shi, B., Ma, Z., Kuwabara, Y., Lam, K. S., Isseroff, R. R., Takada, Y. K. & Takada, Y. 2008b. Direct binding of integrin alphavbeta3 to FGF1 plays a role in FGF1 signaling. *The Journal of biological chemistry,* 283**,** 18066-18075.

Motoda, N., Matsuda, Y., Onda, M., Ishiwata, T., Uchida, E. & Naito, Z. 2011. Overexpression of fibroblast growth factor receptor 4 in high-grade pancreatic intraepithelial neoplasia and pancreatic ductal adenocarcinoma. *Int J Oncol,* 38**,** 133-43.

Munz, B., Frank, S., Hübner, G., Olsen, E. & Werner, S. 1997. A novel type of glutathione peroxidase: expression and regulation during wound repair. *The Biochemical Journal,* 326 (Pt 2)**,** 579-585.

Murakawa, M., Aoyama, T., Miyagi, Y., Kobayashi, S., Ueno, M., Morimoto, M., Numata, M., Yamamoto, N., Tamagawa, H., Yukawa, N., Rino, Y., Masuda, M. & Morinaga, S. 2019. The impact of SPARC expression on the survival of pancreatic ductal adenocarcinoma patients after curative resection. *J Cancer,* 10**,** 627-633.

Musumeci, F., Greco, C., Grossi, G., Molinari, A. & Schenone, S. 2018. Recent Studies on Ponatinib in Cancers Other Than Chronic Myeloid Leukemia. *Cancers (Basel),* 10.

Myers, J. M., Martins, G. G., Ostrowski, J. & Stachowiak, M. K. 2003. Nuclear trafficking of FGFR1: a role for the transmembrane domain. *J Cell Biochem,* 88**,** 1273-91.

Nakazawa, H., Yoshihara, S., Kudo, D., Morohashi, H., Kakizaki, I., Kon, A., Takagaki, K. & Sasaki, M. 2006. 4-methylumbelliferone, a hyaluronan synthase suppressor, enhances the anticancer activity of gemcitabine in human pancreatic cancer cells. *Cancer Chemother Pharmacol,* 57**,** 165-70.

Nan, L., Qin, T., Xiao, Y., Qian, W., Li, J., Wang, Z., Ma, J., Ma, Q. & Wu, Z. 2019. Pancreatic Stellate Cells Facilitate Perineural Invasion of Pancreatic Cancer via HGF/c-Met Pathway. *Cell Transplant***,** 963689719851772.

Naresh, A., Thor, A. D., Edgerton, S. M., Torkko, K. C., Kumar, R. & Jones, F. E. 2008. The HER4/4ICD estrogen receptor coactivator and BH3-only protein is an effector of tamoxifen-induced apoptosis. *Cancer Res,* 68**,** 6387-95.

Neuzillet, C., Tijeras-Raballand, A., Ragulan, C., Cros, J., Patil, Y., Martinet, M., Erkan, M., Kleeff, J., Wilson, J., Apte, M., Tosolini, M., Wilson, A. S., Delvecchio, F. R., Bousquet, C., Paradis, V., Hammel, P., Sadanandam, A. & Kocher, H. M. 2019. Inter- and intra-tumoural heterogeneity in cancer-associated fibroblasts of human pancreatic ductal adenocarcinoma. *J Pathol,* 248**,** 51-65.

Nguyen, P. T., Tsunematsu, T., Yanagisawa, S., Kudo, Y., Miyauchi, M., Kamata, N. & Takata, T. 2013. The FGFR1 inhibitor PD173074 induces mesenchymal-epithelial transition through the transcription factor AP-1. *British Journal of Cancer,* 109**,** 2248-2258.

Nguyen, T., Duchesne, L., Sankara Narayana, G. H. N., Boggetto, N., Fernig, D. D., Uttamrao Murade, C., Ladoux, B. & Mège, R.-M. 2019. Enhanced cell–cell contact stability and decreased N-cadherin-mediated migration upon fibroblast growth factor receptor-N-cadherin cross talk. *Oncogene,* 38**,** 6283-6300.

Nielsen, M. F. B., Mortensen, M. B. & Detlefsen, S. 2016. Key players in pancreatic cancer-stroma interaction: Cancer-associated fibroblasts, endothelial and inflammatory cells. *World Journal of Gastroenterology,* 22**,** 2678-2700.

Niu, J., Chang, Z., Peng, B., Xia, Q., Lu, W., Huang, P., Tsao, M. S. & Chiao, P. J. 2007. Keratinocyte growth factor/fibroblast growth factor-7-regulated cell migration and invasion through activation of NF-kappaB transcription factors. *J Biol Chem,* 282**,** 6001-11.

Nomura, S., Yoshitomi, H., Takano, S., Shida, T., Kobayashi, S., Ohtsuka, M., Kimura, F., Shimizu, H., Yoshidome, H., Kato, A. & Miyazaki, M. 2008. FGF10/FGFR2 signal induces cell migration and invasion in pancreatic cancer. *Br J Cancer,* 99**,** 305-13.

O'Neill, L. P. & Turner, B. M. 2003. Immunoprecipitation of native chromatin: NChIP. *Methods,* 31**,** 76-82.

Ohlund, D., Handly-Santana, A., Biffi, G., Elyada, E., Almeida, A. S., Ponz-Sarvise, M., Corbo, V., Oni, T. E., Hearn, S. A., Lee, E. J., Chio, Ii, Hwang, C. I., Tiriac, H., Baker, L. A., Engle, D. D., Feig, C., Kultti, A., Egeblad, M., Fearon, D. T., Crawford, J. M., Clevers, H., Park, Y. & Tuveson, D. A. 2017. Distinct populations of inflammatory fibroblasts and myofibroblasts in pancreatic cancer. *J Exp Med,* 214**,** 579-596.

Ohta, T., Yamamoto, M., Numata, M., Iseki, S., Tsukioka, Y., Miyashita, T., Kayahara, M., Nagakawa, T., Miyazaki, I., Nishikawa, K. & Yoshitake, Y. 1995. Expression of basic fibroblast growth factor and its receptor in human pancreatic carcinomas. *Br J Cancer,* 72**,** 824-31.

Olive, K. P., Jacobetz, M. A., Davidson, C. J., Gopinathan, A., Mcintyre, D., Honess, D., Madhu, B., Goldgraben, M. A., Caldwell, M. E., Allard, D., Frese, K. K., Denicola, G., Feig, C., Combs, C., Winter, S. P., Ireland-Zecchini, H., Reichelt, S., Howat, W. J., Chang, A., Dhara, M., Wang, L., Rückert, F., Grützmann, R., Pilarsky, C., Izeradjene, K., Hingorani, S. R., Huang, P., Davies, S. E., Plunkett, W., Egorin, M., Hruban, R. H., Whitebread, N., Mcgovern, K., Adams, J., Iacobuzio-Donahue, C., Griffiths, J. & Tuveson, D. A. 2009. Inhibition of Hedgehog Signaling Enhances Delivery of Chemotherapy in a Mouse Model of Pancreatic Cancer. *Science,* 324**,** 1457-1461.

Olive, K. P. & Tuveson, D. A. 2006. The Use of Targeted Mouse Models for Preclinical Testing of Novel Cancer Therapeutics. *Clinical Cancer Research,* 12**,** 5277-5287.

Olsen, S. K., Li, J. Y., Bromleigh, C., Eliseenkova, A. V., Ibrahimi, O. A., Lao, Z., Zhang, F., Linhardt, R. J., Joyner, A. L. & Mohammadi, M. 2006. Structural basis by which alternative splicing modulates the organizer activity of FGF8 in the brain. *Genes Dev,* 20**,** 185-98.

Omary, M. B., Lugea, A., Lowe, A. W. & Pandol, S. J. 2007. The pancreatic stellate cell: a star on the rise in pancreatic diseases. *J Clin Invest,* 117**,** 50-9.

Ootani, A., Li, X., Sangiorgi, E., Ho, Q. T., Ueno, H., Toda, S., Sugihara, H., Fujimoto, K., Weissman, I. L., Capecchi, M. R. & Kuo, C. J. 2009. Sustained in vitro intestinal epithelial culture within a Wnt-dependent stem cell niche. *Nature medicine,* 15**,** 701-706.

Organ, S. L. & Tsao, M. S. 2011. An overview of the c-MET signaling pathway. *Ther Adv Med Oncol,* 3**,** 7-19.

Orlando, V. 2000. Mapping chromosomal proteins in vivo by formaldehyde-crosslinked-chromatin immunoprecipitation. *Trends in Biochemical Sciences,* 2*5***,** 99-104.

Ormanns, S., Haas, M., Baechmann, S., Altendorf-Hofmann, A., Remold, A., Quietzsch, D., Clemens, M. R., Bentz, M., Geissler, M., Lambertz, H., Kruger, S., Kirchner, T., Heinemann, V. & Boeck, S. 2016. Impact of SPARC expression on outcome in patients with advanced pancreatic cancer not receiving nab-paclitaxel: a pooled analysis from prospective clinical and translational trials. *British Journal of Cancer,* 115**,** 1520.

Ornitz, D. M. & Itoh, N. 2015. The Fibroblast Growth Factor signaling pathway. *Wiley interdisciplinary reviews. Developmental biology,* 4**,** 215-266.

Ornitz, D. M., Yayon, A., Flanagan, J. G., Svahn, C. M., Levi, E. & Leder, P. 1992. Heparin is required for cell-free binding of basic fibroblast growth factor to a soluble receptor and for mitogenesis in whole cells. *Mol Cell Biol,* 12**,** 240-7.

Ostermann, E., Garin-Chesa, P., Heider, K. H., Kalat, M., Lamche, H., Puri, C., Kerjaschki, D., Rettig, W. J. & Adolf, G. R. 2008. Effective immunoconjugate therapy in cancer models targeting a serine protease of tumor fibroblasts. *Clin Cancer Res,* 14**,** 4584-92.

Ott, L. E., Sung, E. J., Melvin, A. T., Sheats, M. K., Haugh, J. M., Adler, K. B. & Jones, S. L. 2013. Fibroblast Migration Is Regulated by Myristoylated Alanine-Rich C-Kinase Substrate (MARCKS) Protein. *PLoS One,* 8**,** e66512.

Paauwe, M., Schoonderwoerd, M. J. A., Helderman, R. F. C. P., Harryvan, T. J., Groenewoud, A., Van Pelt, G. W., Bor, R., Hemmer, D. M., Versteeg, H. H., Snaar-Jagalska, B. E., Theuer, C. P., Hardwick, J. C. H., Sier, C. F. M., Ten Dijke, P. & Hawinkels, L. J. a. C. 2018. Endoglin Expression on Cancer-Associated Fibroblasts Regulates Invasion and Stimulates Colorectal Cancer Metastasis. *Clinical Cancer Research,* 24**,** 6331-6344.

Paik, P. K., Shen, R., Berger, M. F., Ferry, D., Soria, J.-C., Mathewson, A., Rooney, C., Smith, N. R., Cullberg, M., Kilgour, E., Landers, D., Frewer, P., Brooks, N. & André, F. 2017. A Phase Ib Open-Label Multicenter Study of AZD4547 in Patients with Advanced Squamous Cell Lung Cancers. *Clinical Cancer Research,* 23**,** 5366-5373.

Pal, A., Dziubinski, M., Di Magliano, M. P., Simeone, D. M., Owens, S., Thomas, D., Peterson, L., Potu, H., Talpaz, M. & Donato, N. J. 2018. Usp9x promotes survival in human pancreatic cancer and its inhibition suppresses pancreatic ductal adenocarcinoma in vivo tumor growth. *Neoplasia,* 20**,** 152-164.

Pan, D. 2010. The hippo signaling pathway in development and cancer. *Dev Cell,* 19**,** 491-505.

Pan, F. C. & Brissova, M. 2014. Pancreas development in humans. *Current opinion in endocrinology, diabetes, and obesity,* 21**,** 77-82.

Park, P. J. 2009. ChIP-seq: advantages and challenges of a maturing technology. *Nat Rev Genet,* 10**,** 669-680.

Patel, V. J., Thalassinos, K., Slade, S. E., Connolly, J. B., Crombie, A., Murrell, J. C. & Scrivens, J. H. 2009. A comparison of labeling and label-free mass spectrometry-based proteomics approaches. *J Proteome Res,* 8**,** 3752-9.

Patel, V. N., Likar, K. M., Zisman-Rozen, S., Cowherd, S. N., Lassiter, K. S., Sher, I., Yates, E. A., Turnbull, J. E., Ron, D. & Hoffman, M. P. 2008. Specific heparan sulfate structures modulate FGF10-mediated submandibular gland epithelial morphogenesis and differentiation. *J Biol Chem,* 283**,** 9308-17.

Peifer, M., Fernandez-Cuesta, L., Sos, M. L., George, J., Seidel, D., Kasper, L. H., Plenker, D., Leenders, F., Sun, R., Zander, T., Menon, R., Koker, M., Dahmen, I., Muller, C., Di Cerbo, V., Schildhaus, H. U., Altmuller, J., Baessmann, I., Becker, C., De Wilde, B., Vandesompele, J., Bohm, D., Ansen, S., Gabler, F., Wilkening, I., Heynck, S., Heuckmann, J. M., Lu, X., Carter, S. L., Cibulskis, K., Banerji, S., Getz, G., Park, K. S., Rauh, D., Grutter, C., Fischer, M., Pasqualucci, L., Wright, G., Wainer, Z., Russell, P., Petersen, I., Chen, Y., Stoelben, E., Ludwig, C., Schnabel, P., Hoffmann, H., Muley, T., Brockmann, M., Engel-Riedel, W., Muscarella, L. A., Fazio, V. M., Groen, H., Timens, W., Sietsma, H., Thunnissen, E., Smit, E., Heideman, D. A., Snijders, P. J., Cappuzzo, F., Ligorio, C., Damiani, S., Field, J., Solberg, S., Brustugun, O. T., Lund-Iversen, M., Sanger, J., Clement, J. H., Soltermann, A., Moch, H., Weder, W., Solomon, B., Soria, J. C., Validire, P., Besse, B., Brambilla, E., Brambilla, C., Lantuejoul, S., Lorimier, P., Schneider, P. M., Hallek, M., Pao, W., Meyerson, M., Sage, J., Shendure, J., Schneider, R., Buttner, R., Wolf, J., Nurnberg, P., Perner, S., Heukamp, L. C., Brindle, P. K., Haas, S. & Thomas, R. K. 2012. Integrative genome analyses identify key somatic driver mutations of small-cell lung cancer. *Nat Genet,* 44**,** 1104-10.

Peng, D. F., Razvi, M., Chen, H., Washington, K., Roessner, A., Schneider-Stock, R. & El-Rifai, W. 2009. DNA hypermethylation regulates the expression of members of the Mu-class glutathione S-transferases and glutathione peroxidases in Barrett's adenocarcinoma. *Gut,* 58**,** 5-15.

Peng, H., Myers, J., Fang, X., Stachowiak, E. K., Maher, P. A., Martins, G. G., Popescu, G., Berezney, R. & Stachowiak, M. K. 2002. Integrative nuclear FGFR1 signaling (INFS) pathway mediates activation of the tyrosine hydroxylase gene by angiotensin II, depolarization and protein kinase C. *J Neurochem,* 81**,** 506-24.

Pentland, A. P. 1994. Active oxygen mechanisms of UV inflammation. *Adv Exp Med Biol,* 366**,** 87-97.

Pérez–Mancera, P. A., Guerra, C., Barbacid, M. & Tuveson, D. A. 2012. What We Have Learned About Pancreatic Cancer From Mouse Models. *Gastroenterology,* 142**,** 1079-1092.

Peters, K. G., Marie, J., Wilson, E., Ives, H. E., Escobedo, J., Del Rosario, M., Mirda, D. & Williams, L. T. 1992. Point mutation of an FGF receptor abolishes phosphatidylinositol turnover and Ca2+ flux but not mitogenesis. *Nature,* 358**,** 678-81.

Pistol-Tanase, C., Raducan, E., Dima, S. O., Albulescu, L., Alina, I., Marius, P., Cruceru, L. M., Codorean, E., Neagu, T. M. & Popescu, I. 2008. Assessment of soluble angiogenic markers in pancreatic cancer. *Biomark Med,* 2**,** 447-55.

Plunkett, W. & Gandhi, V. 1996. Pharmacology of purine nucleoside analogues. *Hematol Cell Ther,* 38 Suppl 2**,** S67-74.

Plunkett, W., Huang, P. & Gandhi, V. 1995a. Preclinical characteristics of gemcitabine. *Anticancer Drugs,* 6 Suppl 6**,** 7-13.

Plunkett, W., Huang, P., Xu, Y. Z., Heinemann, V., Grunewald, R. & Gandhi, V. 1995b. Gemcitabine: metabolism, mechanisms of action, and self-potentiation. *Seminars in Oncology,* 22**,** 3-10.

Polanska, U. M., Duchesne, L., Harries, J. C., Fernig, D. G. & Kinnunen, T. K. 2009. N-Glycosylation regulates fibroblast growth factor receptor/EGL-15 activity in Caenorhabditis elegans in vivo. *The Journal of biological chemistry,* 284**,** 33030-33039.

Polesello, C., Huelsmann, S., Brown, N. H. & Tapon, N. 2006. The Drosophila RASSF homolog antagonizes the hippo pathway. *Curr Biol,* 16**,** 2459-65.

Pollock, P. M., Gartside, M. G., Dejeza, L. C., Powell, M. A., Mallon, M. A., Davies, H., Mohammadi, M., Futreal, P. A., Stratton, M. R., Trent, J. M. & Goodfellow, P. J. 2007. Frequent activating FGFR2 mutations in endometrial carcinomas parallel germline mutations associated with craniosynostosis and skeletal dysplasia syndromes. *Oncogene,* 26**,** 7158-62.

Poon, R. T., Fan, S. T. & Wong, J. 2001. Clinical implications of circulating angiogenic factors in cancer patients. *J Clin Oncol,* 19**,** 1207-25.

Porębska, N., Latko, M., Kucińska, M., Zakrzewska, M., Otlewski, J. & Opaliński, Ł. 2018. Targeting Cellular Trafficking of Fibroblast Growth Factor Receptors as a Strategy for Selective Cancer Treatment. *Journal of Clinical Medicine,* 8**,** 7.

Pothula, S. P., Xu, Z., Goldstein, D., Merrett, N., Pirola, R. C., Wilson, J. S. & Apte, M. V. 2017. Targeting the HGF/c-MET pathway: stromal remodelling in pancreatic cancer. *Oncotarget,* 8**,** 76722-76739.

Potthoff, M. J., Kliewer, S. A. & Mangelsdorf, D. J. 2012. Endocrine fibroblast growth factors 15/19 and 21: from feast to famine. *Genes Dev,* 26**,** 312-24.

Pouessel, D., Neuzillet, Y., Mertens, L. S., Van Der Heijden, M. S., De Jong, J., Sanders, J., Peters, D., Leroy, K., Manceau, A., Maille, P., Soyeux, P., Moktefi, A., Semprez, F., Vordos, D., De La Taille, A., Hurst, C. D., Tomlinson, D. C., Harnden, P., Bostrom, P. J., Mirtti, T., Horenblas, S., Loriot, Y., Houede, N., Chevreau, C., Beuzeboc, P., Shariat, S. F., Sagalowsky, A. I., Ashfaq, R., Burger, M., Jewett, M. A., Zlotta, A. R., Broeks, A., Bapat, B., Knowles, M. A., Lotan, Y., Van Der Kwast, T. H., Culine, S., Allory, Y. & Van Rhijn, B. W. 2016. Tumor heterogeneity of fibroblast growth factor receptor 3 (FGFR3) mutations in invasive bladder cancer: implications for perioperative anti-FGFR3 treatment. *Ann Oncol,* 27**,** 1311-6.

Prenzel, K. L., Warnecke-Eberz, U., Xi, H., Brabender, J., Baldus, S. E., Bollschweiler, E., Gutschow, C. A., Holscher, A. H. & Schneider, P. M. 2006. Significant overexpression of SPARC/osteonectin mRNA in pancreatic cancer compared to cancer of the papilla of Vater. *Oncol Rep,* 15**,** 1397-401.

Provenzano, P. P., Cuevas, C., Chang, A. E., Goel, V. K., Von Hoff, D. D. & Hingorani, S. R. 2012. Enzymatic Targeting of the Stroma Ablates Physical Barriers to Treatment of Pancreatic Ductal Adenocarcinoma. *Cancer Cell,* 21**,** 418-429.

Psyrri, A., Egleston, B., Weinberger, P., Yu, Z., Kowalski, D., Sasaki, C., Haffty, B., Rimm, D. & Burtness, B. 2008. Correlates and determinants of nuclear epidermal growth factor receptor content in an oropharyngeal cancer tissue microarray. *Cancer Epidemiol Biomarkers Prev,* 17**,** 1486-92.

Puls, T. J., Tan, X., Whittington, C. F. & Voytik-Harbin, S. L. 2017. 3D collagen fibrillar microstructure guides pancreatic cancer cell phenotype and serves as a critical design parameter for phenotypic models of EMT. *PLoS One,* 12**,** e0188870.

Puri, N. & Salgia, R. 2008. Synergism of EGFR and c-Met pathways, cross-talk and inhibition, in non-small cell lung cancer. *J Carcinog,* 7**,** 9.

Qiu, W., Sahin, F., Iacobuzio-Donahue, C. A., Garcia-Carracedo, D., Wang, W. M., Kuo, C.-Y., Chen, D., Arking, D. E., Lowy, A. M., Hruban, R. H., Remotti, H. E. & Su, G. H. 2011. Disruption of p16 and activation of Kras in pancreas increase ductal adenocarcinoma formation and metastasis in vivo. *Oncotarget,* 2**,** 862-873.

Radon, T. P., Massat, N. J., Jones, R., Alrawashdeh, W., Dumartin, L., Ennis, D., Duffy, S. W., Kocher, H. M., Pereira, S. P., Guarner Posthumous, L., Murta-Nascimento, C., Real, F. X., Malats, N., Neoptolemos, J., Costello, E., Greenhalf, W., Lemoine, N. R. & Crnogorac-Jurcevic, T. 2015. Identification of a Three-Biomarker Panel in Urine for Early Detection of Pancreatic Adenocarcinoma. *Clin Cancer Res,* 21**,** 3512-21.

Rahib, L., Smith, B. D., Aizenberg, R., Rosenzweig, A. B., Fleshman, J. M. & Matrisian, L. M. 2014. Projecting Cancer Incidence and Deaths to 2030: The Unexpected Burden of Thyroid, Liver, and Pancreas Cancers in the United States. *Cancer Research,* 74**,** 2913.

Raivio, T., Sidis, Y., Plummer, L., Chen, H., Ma, J., Mukherjee, A., Jacobson-Dickman, E., Quinton, R., Van Vliet, G., Lavoie, H., Hughes, V. A., Dwyer, A., Hayes, F. J., Xu, S., Sparks, S., Kaiser, U. B., Mohammadi, M. & Pitteloud, N. 2009. Impaired fibroblast growth factor receptor 1 signaling as a cause of normosmic idiopathic hypogonadotropic hypogonadism. *J Clin Endocrinol Metab,* 94**,** 4380-90.

Rauniyar, N., Gao, B., McClatchy, D. B. & Yates, J. R., 3rd 2013. Comparison of protein expression ratios observed by sixplex and duplex TMT labeling method. *Journal of Proteome Research,* 12**,** 1031-1039.

Rauniyar, N. & Yates, J. R., 3rd 2014. Isobaric labeling-based relative quantification in shotgun proteomics. *Journal of Proteome Research,* 13**,** 5293-5309.

Rawla, P., Sunkara, T. & Gaduputi, V. 2019. Epidemiology of Pancreatic Cancer: Global Trends, Etiology and Risk Factors. *World Journal of Oncology,* 10**,** 10-27.

Raymond, E., Faivre, S., Chaney, S., Woynarowski, J. & Cvitkovic, E. 2002. Cellular and Molecular Pharmacology of Oxaliplatin. *Molecular Cancer Therapeutics,* 1**,** 227-235.

Reece-Hoyes, J. S. & Walhout, A. J. M. 2018. Gateway Recombinational Cloning. *Cold Spring Harbor Protocols,* 2018.

Regeenes, R., Silva, P. N., Chang, H. H., Arany, E. J., Shukalyuk, A. I., Audet, J., Kilkenny, D. M. & Rocheleau, J. V. 2018. Fibroblast growth factor receptor 5 (FGFR5)

is a co-receptor for FGFR1 that is up-regulated in beta-cells by cytokine-induced inflammation. *J Biol Chem,* 293**,** 17218-17228.

Reilly, J. F. & Maher, P. A. 2001. Importin β–Mediated Nuclear Import of Fibroblast Growth Factor Receptor: Role in Cell Proliferation. *The Journal of Cell Biology,* 152**,** 1307-1312.

Reis-Filho, J. S., Simpson, P. T., Turner, N. C., Lambros, M. B., Jones, C., Mackay, A., Grigoriadis, A., Sarrio, D., Savage, K., Dexter, T., Iravani, M., Fenwick, K., Weber, B., Hardisson, D., Schmitt, F. C., Palacios, J., Lakhani, S. R. & Ashworth, A. 2006. FGFR1 emerges as a potential therapeutic target for lobular breast carcinomas. *Clin Cancer Res,* 12**,** 6652-62.

Rhim, A. D., Oberstein, P. E., Thomas, D. H., Mirek, E. T., Palermo, C. F., Sastra, S. A., Dekleva, E. N., Saunders, T., Becerra, C. P., Tattersall, I. W., Westphalen, C. B., Kitajewski, J., Fernandez-Barrena, M. G., Fernandez-Zapico, M. E., Iacobuzio-Donahue, C., Olive, K. P. & Stanger, B. Z. 2014. Stromal elements act to restrain, rather than support, pancreatic ductal adenocarcinoma. *Cancer Cell,* 25**,** 735-47.

Rhim, A. D. & Stanger, B. Z. 2010. Molecular biology of pancreatic ductal adenocarcinoma progression: aberrant activation of developmental pathways. *Prog Mol Biol Transl Sci,* 97**,** 41-78.

Richards, D. A., Stephenson, J., Wolpin, B. M., Becerra, C., Hamm, J. T., Messersmith, W. A., Devens, S., Cushing, J., Schmalbach, T. & Fuchs, C. S. 2012. A phase Ib trial of IPI-926, a hedgehog pathway inhibitor, plus gemcitabine in patients with metastatic pancreatic cancer. *Journal of Clinical Oncology,* 30**,** 213.

Richter, K. & Kietzmann, T. 2016. Reactive oxygen species and fibrosis: further evidence of a significant liaison. *Cell Tissue Res,* 365**,** 591-605.

Rizvi, S., Yamada, D., Hirsova, P., Bronk, S. F., Werneburg, N. W., Krishnan, A., Salim, W., Zhang, L., Trushina, E., Truty, M. J. & Gores, G. J. 2016. A Hippo and Fibroblast Growth Factor Receptor Autocrine Pathway in Cholangiocarcinoma. *Journal of Biological Chemistry,* 291**,** 8031-8047.

Robert, C., Thomas, L., Bondarenko, I., O'day, S., Weber, J., Garbe, C., Lebbe, C., Baurain, J. F., Testori, A., Grob, J. J., Davidson, N., Richards, J., Maio, M., Hauschild, A., Miller, W. H., Jr., Gascon, P., Lotem, M., Harmankaya, K., Ibrahim, R., Francis, S., Chen, T. T., Humphrey, R., Hoos, A. & Wolchok, J. D. 2011. Ipilimumab plus dacarbazine for previously untreated metastatic melanoma. *N Engl J Med,* 364**,** 2517-26.

Robert, J. & Rivory, L. 1998. Pharmacology of irinotecan. *Drugs Today (Barc),* 34**,** 777-803.

Roidl, A., Foo, P., Wong, W., Mann, C., Bechtold, S., Berger, H. J., Streit, S., Ruhe, J. E., Hart, S., Ullrich, A. & Ho, H. K. 2010. The FGFR4 Y367C mutant is a dominant oncogene in MDA-MB453 breast cancer cells. *Oncogene,* 29**,** 1543-52.

Ropiquet, F., Giri, D., Kwabi-Addo, B., Mansukhani, A. & Ittmann, M. 2000. Increased expression of fibroblast growth factor 6 in human prostatic intraepithelial neoplasia and prostate cancer. *Cancer Res,* 60**,** 4245-50.

Rossi, M. K., Gnanamony, M. & Gondi, C. S. 2016. The 'SPARC' of life: Analysis of the role of osteonectin/SPARC in pancreatic cancer (Review). *Int J Oncol,* 48**,** 1765-71.

Rusnati, M., Tanghetti, E., Dell'era, P., Gualandris, A. & Presta, M. 1997. alphavbeta3 integrin mediates the cell-adhesive capacity and biological activity of basic fibroblast growth factor (FGF-2) in cultured endothelial cells. *Molecular biology of the cell,* 8**,** 2449-2461.

Ryan , D. P., Hong , T. S. & Bardeesy , N. 2014. Pancreatic Adenocarcinoma. *New England Journal of Medicine,* 371**,** 1039-1049.

Sahu, N., Chan, E., Chu, F., Pham, T., Koeppen, H., Forrest, W., Merchant, M. & Settleman, J. 2017. Cotargeting of MEK and PDGFR/STAT3 Pathways to Treat Pancreatic Ductal Adenocarcinoma. *Mol Cancer Ther,* 16**,** 1729-1738.

Saka, H., Kitagawa, C., Kogure, Y., Takahashi, Y., Fujikawa, K., Sagawa, T., Iwasa, S., Takahashi, N., Fukao, T., Tchinou, C., Landers, D. & Yamada, Y. 2017. Safety, tolerability and pharmacokinetics of the fibroblast growth factor receptor inhibitor AZD4547 in Japanese patients with advanced solid tumours: a Phase I study. *Invest New Drugs,* 35**,** 451-462.

Sakai, A., Suzuki, M., Kobayashi, T., Nishiumi, S., Yamanaka, K., Hirata, Y., Nakagawa, T., Azuma, T. & Yoshida, M. 2016. Pancreatic cancer screening using a multiplatform human serum metabolomics system. *Biomark Med,* 10**,** 577-86.

Salcedo Allende, M. T., Zeron-Medina, J., Hernandez, J., Macarulla, T., Balsells, J., Merino, X., Allende, H., Tabernero, J. & Ramon, Y. C. S. 2017. Overexpression of Yes Associated Protein 1, an Independent Prognostic Marker in Patients With Pancreatic Ductal Adenocarcinoma, Correlated With Liver Metastasis and Poor Prognosis. *Pancreas,* 46**,** 913-920.

Santolla, M. F., Vivacqua, A., Lappano, R., Rigiracciolo, D. C., Cirillo, F., Galli, G. R., Talia, M., Brunetti, G., Miglietta, A. M., Belfiore, A. & Maggiolini, M. 2019. GPER Mediates a Feedforward FGF2/FGFR1 Paracrine Activation Coupling CAFs to Cancer Cells toward Breast Tumor Progression. *Cells,* 8**,** 223.

Sanz-Moreno, V., Gaggioli, C., Yeo, M., Albrengues, J., Wallberg, F., Viros, A., Hooper, S., Mitter, R., Féral, Chloé c., Cook, M., Larkin, J., Marais, R., Meneguzzi, G., Sahai, E. & Marshall, Chris j. 2011. ROCK and JAK1 Signaling Cooperate to Control Actomyosin Contractility in Tumor Cells and Stroma. *Cancer Cell,* 20**,** 229-245.

Sato, N., Cheng, X.-B., Kohi, S., Koga, A. & Hirata, K. 2016. Targeting hyaluronan for the treatment of pancreatic ductal adenocarcinoma. *Acta Pharmaceutica Sinica. B,* 6**,** 101-105.

Sato, N., Fukushima, N., Maehara, N., Matsubayashi, H., Koopmann, J., Su, G. H., Hruban, R. H. & Goggins, M. 2003. SPARC/osteonectin is a frequent target for aberrant methylation in pancreatic adenocarcinoma and a mediator of tumor-stromal interactions. *Oncogene,* 22**,** 5021-30.

Scavini, M., Dugnani, E., Pasquale, V., Liberati, D., Aleotti, F., Di Terlizzi, G., Petrella, G., Balzano, G. & Piemonti, L. 2015. Diabetes After Pancreatic Surgery: Novel Issues. *Current Diabetes Reports,* 15**,** 16.

Scavuzzo, M. A., Yang, D. & Borowiak, M. 2017. Organotypic pancreatoids with native mesenchyme develop Insulin producing endocrine cells. *Sci Rep,* 7**,** 10810.

Schmaus, A., Klusmeier, S., Rothley, M., Dimmler, A., Sipos, B., Faller, G., Thiele, W., Allgayer, H., Hohenberger, P., Post, S. & Sleeman, J. P. 2014. Accumulation of small hyaluronan oligosaccharides in tumour interstitial fluid correlates with lymphatic invasion and lymph node metastasis. *Br J Cancer,* 111**,** 559-67.

Serls, A. E., Doherty, S., Parvatiyar, P., Wells, J. M. & Deutsch, G. H. 2005. Different thresholds of fibroblast growth factors pattern the ventral foregut into liver and lung. *Development,* 132**,** 35-47.

Shannon, H. E., Fishel, M. L., Xie, J., Gu, D., Mccarthy, B. P., Riley, A. A., Sinn, A. L., Silver, J. M., Peterman, K., Kelley, M. R., Hanenberg, H., Korc, M., Pollok, K. E. & Territo, P. R. 2015. Longitudinal Bioluminescence Imaging of Primary Versus Abdominal Metastatic Tumor Growth in Orthotopic Pancreatic Tumor Models in NSG Mice. *Pancreas,* 44**,** 64-75.

Shao, D. D., Xue, W., Krall, E. B., Bhutkar, A., Piccioni, F., Wang, X., Schinzel, A. C., Sood, S., Rosenbluh, J., Kim, J. W., Zwang, Y., Roberts, T. M., Root, D. E., Jacks, T. & Hahn, W. C. 2014. KRAS and YAP1 Converge to Regulate EMT and Tumor Survival. *Cell,* 158**,** 171-184.

Sharma, P. & Allison, J. P. 2015. Immune checkpoint targeting in cancer therapy: toward combination strategies with curative potential. *Cell,* 161**,** 205-214.

Shaw, V. E., Lane, B., Jenkinson, C., Cox, T., Greenhalf, W., Halloran, C. M., Tang, J., Sutton, R., Neoptolemos, J. P. & Costello, E. 2014. Serum cytokine biomarker panels for discriminating pancreatic cancer from benign pancreatic disease. *Mol Cancer,* 13**,** 114.

Sherman, M. H., Yu, R. T., Engle, D. D., Ding, N., Atkins, A. R., Tiriac, H., Collisson, E. A., Connor, F., Van Dyke, T., Kozlov, S., Martin, P., Tseng, T. W., Dawson, D. W., Donahue, T. R., Masamune, A., Shimosegawa, T., Apte, M. V., Wilson, J. S., Ng, B., Lau, S. L., Gunton, J. E., Wahl, G. M., Hunter, T., Drebin, J. A., O'dwyer, P. J., Liddle, C., Tuveson, D. A., Downes, M. & Evans, R. M. 2014. Vitamin D Receptor-Mediated Stromal Reprogramming Suppresses Pancreatitis and Enhances Pancreatic Cancer Therapy. *Cell,* 159**,** 80-93.

Shibata, W., Kinoshita, H., Hikiba, Y., Sato, T., Ishii, Y., Sue, S., Sugimori, M., Suzuki, N., Sakitani, K., Ijichi, H., Mori, R., Endo, I. & Maeda, S. 2018. Overexpression of HER2 in the pancreas promotes development of intraductal papillary mucinous neoplasms in mice. *Scientific Reports,* 8**,** 6150-6150.

Shultz, L. D., Lyons, B. L., Burzenski, L. M., Gott, B., Chen, X., Chaleff, S., Kotb, M., Gillies, S. D., King, M., Mangada, J., Greiner, D. L. & Handgretinger, R. 2005. Human lymphoid and myeloid cell development in NOD/LtSz-scid IL2R gamma null mice engrafted with mobilized human hemopoietic stem cells. *J Immunol,* 174**,** 6477-89.

Sia, D., Losic, B., Moeini, A., Cabellos, L., Hao, K., Revill, K., Bonal, D., Miltiadous, O., Zhang, Z., Hoshida, Y., Cornella, H., Castillo-Martin, M., Pinyol, R., Kasai, Y., Roayaie, S., Thung, S. N., Fuster, J., Schwartz, M. E., Waxman, S., Cordon-Cardo, C., Schadt, E., Mazzaferro, V. & Llovet, J. M. 2015. Massive parallel sequencing uncovers actionable FGFR2-PPHLN1 fusion and ARAF mutations in intrahepatic cholangiocarcinoma. *Nat Commun,* 6**,** 6087.

Siegel, R. L., Miller, K. D. & Jemal, A. 2018. Cancer statistics, 2018. *CA: A Cancer Journal for Clinicians,* 68**,** 7-30.

Singh, D., Chan, J. M., Zoppoli, P., Niola, F., Sullivan, R., Castano, A., Liu, E. M., Reichel, J., Porrati, P., Pellegatta, S., Qiu, K., Gao, Z., Ceccarelli, M., Riccardi, R., Brat, D. J., Guha, A., Aldape, K., Golfinos, J. G., Zagzag, D., Mikkelsen, T., Finocchiaro, G., Lasorella, A., Rabadan, R. & Iavarone, A. 2012. Transforming fusions of FGFR and TACC genes in human glioblastoma. *Science,* 337**,** 1231-5.

Sinn, M., Sinn, B. V., Striefler, J. K., Lindner, J. L., Stieler, J. M., Lohneis, P., Bischoff, S., Blaker, H., Pelzer, U., Bahra, M., Dietel, M., Dorken, B., Oettle, H., Riess, H. & Denkert, C. 2014. SPARC expression in resected pancreatic cancer patients treated with gemcitabine: results from the CONKO-001 study. *Ann Oncol,* 25**,** 1025-32.

Smith, E. R., Mcmahon, L. P. & Holt, S. G. 2014. Fibroblast growth factor 23. *Ann Clin Biochem,* 51**,** 203-27.

Sohal, J., Chase, A., Mould, S., Corcoran, M., Oscier, D., Iqbal, S., Parker, S., Welborn, J., Harris, R. I., Martinelli, G., Montefusco, V., Sinclair, P., Wilkins, B. S., Van Den Berg, H., Vanstraelen, D., Goldman, J. M. & Cross, N. C. 2001. Identification of four new translocations involving FGFR1 in myeloid disorders. *Genes Chromosomes Cancer,* 32**,** 155-63.

Solomon, M. J., Larsen, P. L. & Varshavsky, A. 1988. Mapping proteinDNA interactions in vivo with formaldehyde: Evidence that histone H4 is retained on a highly transcribed gene. *Cell,* 53**,** 937-947.

Sparmann, G., Hohenadl, C., Tornoe, J., Jaster, R., Fitzner, B., Koczan, D., Thiesen, H. J., Glass, A., Winder, D., Liebe, S. & Emmrich, J. 2004. Generation and characterization of immortalized rat pancreatic stellate cells. *Am J Physiol Gastrointest Liver Physiol,* 287**,** G211-9.

Spooner, R. A. & Lord, J. M. 2015. Ricin trafficking in cells. *Toxins (Basel),* 7**,** 49-65.

Staal, B., Liu, Y., Barnett, D., Hsueh, P., He, Z., Gao, C. F., Partyka, K., Hurd, M. W., Singhi, A. D., Drake, R. R., Huang, Y., Maitra, A., Brand, R. E. & Haab, B. B. 2019. The sTRA Plasma Biomarker: Blinded Validation of Improved Accuracy over CA19-9 in Pancreatic Cancer Diagnosis. *Clin Cancer Res***,** 2745-2754.

Stachowiak, E. K., Roy, I., Lee, Y. W., Capacchietti, M., Aletta, J. M., Prasad, P. N. & Stachowiak, M. K. 2009. Targeting novel integrative nuclear FGFR1 signaling by nanoparticle-mediated gene transfer stimulates neurogenesis in the adult brain. *Integr Biol (Camb),* 1**,** 394-403.

Stachowiak, M. K., Maher, P. A., Joy, A., Mordechai, E. & Stachowiak, E. K. 1996. Nuclear accumulation of fibroblast growth factor receptors is regulated by multiple signals in adrenal medullary cells. *Mol Biol Cell,* 7**,** 1299-317.

Stachowiak, M. K., Maher, P. A. & Stachowiak, E. K. 2007. Integrative nuclear signaling in cell development--a role for FGF receptor-1. *DNA Cell Biol,* 26**,** 811-26.

Stachowiak, M. K. & Stachowiak, E. K. 2016. Evidence-Based Theory for Integrated Genome Regulation of Ontogeny—An Unprecedented Role of Nuclear FGFR1 Signaling. *Journal of Cellular Physiology,* 231**,** 1199-1218.

Stahle, M., Veit, C., Bachfischer, U., Schierling, K., Skripczynski, B., Hall, A., Gierschik, P. & Giehl, K. 2003. Mechanisms in LPA-induced tumor cell migration: critical role of phosphorylated ERK. *J Cell Sci,* 116**,** 3835-46.

Strobel, O., Neoptolemos, J., Jäger, D. & Büchler, M. W. 2019. Optimizing the outcomes of pancreatic cancer surgery. *Nature Reviews Clinical Oncology,* 16**,** 11-26.

Sudo, K., Nakamura, K. & Yamaguchi, T. 2014. S-1 in the treatment of pancreatic cancer. *World Journal of Gastroenterology : WJG,* 20**,** 15110-15118.

Sugihara, T., Isomoto, H., Gores, G. & Smoot, R. 2019. YAP and the Hippo pathway in cholangiocarcinoma. *J Gastroenterol,* 54**,** 485-491.

Sugiyama, T., Benitez, C. M., Ghodasara, A., Liu, L., Mclean, G. W., Lee, J., Blauwkamp, T. A., Nusse, R., Wright, C. V., Gu, G. & Kim, S. K. 2013. Reconstituting pancreas development from purified progenitor cells reveals genes essential for islet differentiation. *Proc Natl Acad Sci U S A,* 110**,** 12691-6.

Sun, H., Ma, H., Hong, G., Sun, H. & Wang, J. 2014. Survival improvement in patients with pancreatic cancer by decade: A period analysis of the SEER database, 1981–2010. *Scientific Reports,* 4**,** 6747.

Sun, H., Tu, X., Prisco, M., Wu, A., Casiburi, I. & Baserga, R. 2003. Insulin-Like Growth Factor I Receptor Signaling and Nuclear Translocation of Insulin Receptor Substrates 1 and 2. *Molecular Endocrinology,* 17**,** 472-486.

Suyama, K., Shapiro, I., Guttman, M. & Hazan, R. B. 2002. A signaling pathway leading to metastasis is controlled by N-cadherin and the FGF receptor. *Cancer Cell,* 2**,** 301-314.

Szadvari, I., Krizanova, O. & Babula, P. 2016. Athymic nude mice as an experimental model for cancer treatment. *Physiol Res,* 65**,** 441-453.

Taeger, J., Moser, C., Hellerbrand, C., Mycielska, M. E., Glockzin, G., Schlitt, H. J., Geissler, E. K., Stoeltzing, O. & Lang, S. A. 2011. Targeting FGFR/PDGFR/VEGFR impairs tumor growth, angiogenesis, and metastasis by effects on tumor cells, endothelial cells, and pericytes in pancreatic cancer. *Mol Cancer Ther,* 10**,** 2157-67.

Takada, M., Nakamura, Y., Koizumi, T., Toyama, H., Kamigaki, T., Suzuki, Y., Takeyama, Y. & Kuroda, Y. 2002. Suppression of human pancreatic carcinoma cell growth and invasion by epigallocatechin-3-gallate. *Pancreas,* 25**,** 45-8.

Takehara, T., Teramura, T., Onodera, Y., Frampton, J. & Fukuda, K. 2015. Cdh2 stabilizes FGFR1 and contributes to primed-state pluripotency in mouse epiblast stem cells. *Scientific Reports,* 5**,** 14722.

Takeya, R., Taniguchi, K., Narumiya, S. & Sumimoto, H. 2008. The mammalian formin FHOD1 is activated through phosphorylation by ROCK and mediates thrombin-induced stress fibre formation in endothelial cells. *EMBO,* 27**,** 618-28.

Tan, M., Jing, T., Lan, K. H., Neal, C. L., Li, P., Lee, S., Fang, D., Nagata, Y., Liu, J., Arlinghaus, R., Hung, M. C. & Yu, D. 2002. Phosphorylation on tyrosine-15 of

p34(Cdc2) by ErbB2 inhibits p34(Cdc2) activation and is involved in resistance to taxol-induced apoptosis. *Mol Cell,* 9**,** 993-1004.

Tanghetti, E., Ria, R., Dell'era, P., Urbinati, C., Rusnati, M., Ennas, M. G. & Presta, M. 2002. Biological activity of substrate-bound basic fibroblast growth factor (FGF2): recruitment of FGF receptor-1 in endothelial cell adhesion contacts. *Oncogene,* 21**,** 3889-3897.

Tanner, Y. & Grose, R. P. 2016. Dysregulated FGF signalling in neoplastic disorders. *Seminars in Cell & Developmental Biology,* 53**,** 126-135.

Tassi, E., Henke, R. T., Bowden, E. T., Swift, M. R., Kodack, D. P., Kuo, A. H., Maitra, A. & Wellstein, A. 2006. Expression of a fibroblast growth factor-binding protein during the development of adenocarcinoma of the pancreas and colon. *Cancer Res,* 66**,** 1191-8.

Terranova, C., Narla, S. T., Lee, Y. W., Bard, J., Parikh, A., Stachowiak, E. K., Tzanakakis, E. S., Buck, M. J., Birkaya, B. & Stachowiak, M. K. 2015. Global Developmental Gene Programing Involves a Nuclear Form of Fibroblast Growth Factor Receptor-1 (FGFR1). *PLoS One,* 10**,** e0123380.

Theelen, W. S., Mittempergher, L., Willems, S. M., Bosma, A. J., Peters, D. D., Van Der Noort, V., Japenga, E. J., Peeters, T., Koole, K., Sustic, T., Blaauwgeers, J. L., Van Noesel, C. J., Bernards, R. & Van Den Heuvel, M. M. 2016. FGFR1, 2 and 3 protein overexpression and molecular aberrations of FGFR3 in early stage non-small cell lung cancer. *J Pathol Clin Res,* 2**,** 223-233.

Thien, C. B. F. & Langdon, W. Y. 2001. Cbl: many adaptations to regulate protein tyrosine kinases. *Nature Reviews Molecular Cell Biology,* 2**,** 294.

Thomas, D. & Radhakrishnan, P. 2019. Tumor-stromal crosstalk in pancreatic cancer and tissue fibrosis. *Mol Cancer,* 18**,** 14.

Thompson, A., Schafer, J., Kuhn, K., Kienle, S., Schwarz, J., Schmidt, G., Neumann, T., Johnstone, R., Mohammed, A. K. & Hamon, C. 2003. Tandem mass tags: a novel quantification strategy for comparative analysis of complex protein mixtures by MS/MS. *Anal Chem,* 75**,** 1895-904.

Thompson, C. B., Shepard, H. M., O'Connor, P. M., Kadhim, S., Jiang, P., Osgood, R. J., Bookbinder, L. H., Li, X., Sugarman, B. J., Connor, R. J., Nadjsombati, S. & Frost, G. I. 2010. Enzymatic depletion of tumor hyaluronan induces antitumor responses in preclinical animal models. *Mol Cancer Ther,* 9**,** 3052-64.

Thompson, M., Lauderdale, S., Webster, M. J., Chong, V. Z., McClintock, B., Saunders, R. & Weickert, C. S. 2007. Widespread expression of ErbB2, ErbB3 and ErbB4 in non-human primate brain. *Brain Res,* 1139**,** 95-109.

Tian, X., Chen, G., Zhou, S., Henne-Bruns, D., Bachem, M. & Kornmann, M. 2012. Interactions of pancreatic cancer and stellate cells are mediated by FGFR1-III isoform expression. *Hepatogastroenterology,* 59**,** 1604-8.

Ting, D. T., Wittner, B. S., Ligorio, M., Vincent Jordan, N., Shah, A. M., Miyamoto, D. T., Aceto, N., Bersani, F., Brannigan, B. W., Xega, K., Ciciliano, J. C., Zhu, H., Mackenzie, O. C., Trautwein, J., Arora, K. S., Shahid, M., Ellis, H. L., Qu, N., Bardeesy, N., Rivera, M. N., Deshpande, V., Ferrone, C. R., Kapur, R., Ramaswamy, S., Shioda, T., Toner, M., Maheswaran, S. & Haber, D. A. 2014. Single-cell RNA sequencing identifies extracellular matrix gene expression by pancreatic circulating tumor cells. *Cell Rep,* 8**,** 1905-1918.

Tomlinson, D. C., Lamont, F. R., Shnyder, S. D. & Knowles, M. A. 2009. Fibroblast growth factor receptor 1 promotes proliferation and survival via activation of the mitogen-activated protein kinase pathway in bladder cancer. *Cancer Res,* 69**,** 4613-20.

Toole, B. P. 2004. Hyaluronan: from extracellular glue to pericellular cue. *Nat Rev Cancer,* 4**,** 528-539.

Topalian, S. L., Hodi, F. S., Brahmer, J. R., Gettinger, S. N., Smith, D. C., Mcdermott, D. F., Powderly, J. D., Carvajal, R. D., Sosman, J. A., Atkins, M. B., Leming, P. D., Spigel, D. R., Antonia, S. J., Horn, L., Drake, C. G., Pardoll, D. M., Chen, L., Sharfman, W. H., Anders, R. A., Taube, J. M., Mcmiller, T. L., Xu, H., Korman, A. J., Jure-Kunkel, M., Agrawal, S., Mcdonald, D., Kollia, G. D., Gupta, A., Wigginton, J. M. & Sznol, M. 2012. Safety, activity, and immune correlates of anti-PD-1 antibody in cancer. *N Engl J Med,* 366**,** 2443-54.

Torres, C., Perales, S., Alejandre, M. J., Iglesias, J., Palomino, R. J., Martin, M., Caba, O., Prados, J. C., Aranega, A., Delgado, J. R., Irigoyen, A., Ortuno, F. M., Rojas, I. & Linares, A. 2014. Serum cytokine profile in patients with pancreatic cancer. *Pancreas,* 43**,** 1042-9.

Trolice, M. P., Pappalardo, A. & Peluso, J. J. 1997. Basic Fibroblast Growth Factor and N-Cadherin Maintain Rat Granulosa Cell and Ovarian Surface Epithelial Cell Viability by Stimulating the Tyrosine Phosphorylation of the Fibroblast Growth Factor Receptors. *Endocrinology,* 138**,** 107-113.

Trueb, B. 2011. Biology of FGFRL1, the fifth fibroblast growth factor receptor. *Cell Mol Life Sci,* 68**,** 951-64.

Tsai, S., Mcolash, L., Palen, K., Johnson, B., Duris, C., Yang, Q., Dwinell, M. B., Hunt, B., Evans, D. B., Gershan, J. & James, M. A. 2018. Development of primary human pancreatic cancer organoids, matched stromal and immune cells and 3D tumor microenvironment models. *BMC Cancer,* 18**,** 335.

Turner, N. & Grose, R. 2010. Fibroblast growth factor signalling: from development to cancer. *Nat Rev Cancer,* 10**,** 116-129.

Turner, N., Lambros, M. B., Horlings, H. M., Pearson, A., Sharpe, R., Natrajan, R., Geyer, F. C., Van Kouwenhove, M., Kreike, B., Mackay, A., Ashworth, A., Van De Vijver, M. J. & Reis-Filho, J. S. 2010. Integrative molecular profiling of triple negative breast cancers identifies amplicon drivers and potential therapeutic targets. *Oncogene,* 29**,** 2013-23.

Turunen, S. P., Von Nandelstadh, P., Öhman, T., Gucciardo, E., Seashore-Ludlow, B., Martins, B., Rantanen, V., Li, H., Höpfner, K., Östling, P., Varjosalo, M. & Lehti, K. 2019. FGFR4 phosphorylates MST1 to confer breast cancer cells resistance to MST1/2-dependent apoptosis. *Cell Death & Differentiation*.

Uemura, T., Hibi, K., Kaneko, T., Takeda, S., Inoue, S., Okochi, O., Nagasaka, T. & Nakao, A. 2004. Detection of K-ras mutations in the plasma DNA of pancreatic cancer patients. *J Gastroenterol,* 39**,** 56-60.

Uesaka, K., Boku, N., Fukutomi, A., Okamura, Y., Konishi, M., Matsumoto, I., Kaneoka, Y., Shimizu, Y., Nakamori, S., Sakamoto, H., Morinaga, S., Kainuma, O., Imai, K., Sata, N., Hishinuma, S., Ojima, H., Yamaguchi, R., Hirano, S., Sudo, T. & Ohashi, Y. 2016. Adjuvant chemotherapy of S-1 versus gemcitabine for resected pancreatic cancer: a phase 3, open-label, randomised, non-inferiority trial (JASPAC 01). *Lancet,* 388**,** 248-57.

Vaira, V., Fedele, G., Pyne, S., Fasoli, E., Zadra, G., Bailey, D., Snyder, E., Faversani, A., Coggi, G., Flavin, R., Bosari, S. & Loda, M. 2010. Preclinical model of organotypic culture for pharmacodynamic profiling of human tumors. *Proc Natl Acad Sci U S A,* 107**,** 8352-6.

Valkenburg, K. C., De Groot, A. E. & Pienta, K. J. 2018. Targeting the tumour stroma to improve cancer therapy. *Nature Reviews Clinical Oncology,* 15**,** 366-381.

Van Heek, N. T., Meeker, A. K., Kern, S. E., Yeo, C. J., Lillemoe, K. D., Cameron, J. L., Offerhaus, G. J. A., Hicks, J. L., Wilentz, R. E., Goggins, M. G., De Marzo, A. M., Hruban, R. H. & Maitra, A. 2002. Telomere shortening is nearly universal in pancreatic intraepithelial neoplasia. *The American Journal of Pathology,* 161**,** 1541-1547.

Van Rhijn, B. W., Lurkin, I., Radvanyi, F., Kirkels, W. J., Van Der Kwast, T. H. & Zwarthoff, E. C. 2001. The fibroblast growth factor receptor 3 (FGFR3) mutation is a strong indicator of superficial bladder cancer with low recurrence rate. *Cancer Res,* 61**,** 1265-8.

Varelas, X., Miller, B. W., Sopko, R., Song, S., Gregorieff, A., Fellouse, F. A., Sakuma, R., Pawson, T., Hunziker, W., Mcneill, H., Wrana, J. L. & Attisano, L. 2010. The Hippo pathway regulates Wnt/beta-catenin signaling. *Dev Cell,* 18**,** 579-91.

Varelas, X., Sakuma, R., Samavarchi-Tehrani, P., Peerani, R., Rao, B. M., Dembowy, J., Yaffe, M. B., Zandstra, P. W. & Wrana, J. L. 2008. TAZ controls Smad nucleocytoplasmic shuttling and regulates human embryonic stem-cell self-renewal. *Nat Cell Biol,* 10**,** 837-48.

Veelken, C., Bakker, G.-J., Drell, D. & Friedl, P. 2017. Single cell-based automated quantification of therapy responses of invasive cancer spheroids in organotypic 3D culture. *Methods,* 128**,** 139-149.

Vickers, S. M., Huang, Z. Q., Macmillan-Crow, L., Greendorfer, J. S. & Thompson, J. A. 2002. Ligand activation of alternatively spliced fibroblast growth factor receptor-1 modulates pancreatic adenocarcinoma cell malignancy. *J Gastrointest Surg,* 6**,** 546-53.

Vickers, S. M., Macmillan-Crow, L. A., Green, M., Ellis, C. & Thompson, J. A. 1999. Association of increased immunostaining for inducible nitric oxide synthase and nitrotyrosine with fibroblast growth factor transformation in pancreatic cancer. *Arch Surg,* 134**,** 245-51.

Volckaert, T., Yuan, T., Chao, C. M., Bell, H., Sitaula, A., Szimmtenings, L., El Agha, E., Chanda, D., Majka, S., Bellusci, S., Thannickal, V. J., Fassler, R. & De Langhe, S. P. 2017. Fgf10-Hippo Epithelial-Mesenchymal Crosstalk Maintains and Recruits Lung Basal Stem Cells. *Dev Cell,* 43**,** 48-59.e5.

Von Hoff, D. D., Ervin, T., Arena, F. P., Chiorean, E. G., Infante, J., Moore, M., Seay, T., Tjulandin, S. A., Ma, W. W., Saleh, M. N., Harris, M., Reni, M., Dowden, S., Laheru, D., Bahary, N., Ramanathan, R. K., Tabernero, J., Hidalgo, M., Goldstein, D., Van Cutsem, E., Wei, X., Iglesias, J. & Renschler, M. F. 2013. Increased Survival in Pancreatic Cancer with nab-Paclitaxel plus Gemcitabine. *New England Journal of Medicine,* 369**,** 1691-1703.

Von Hoff, D. D., Ramanathan, R. K., Borad, M. J., Laheru, D. A., Smith, L. S., Wood, T. E., Korn, R. L., Desai, N., Trieu, V., Iglesias, J. L., Zhang, H., Soon-Shiong, P., Shi, T., Rajeshkumar, N. V., Maitra, A. & Hidalgo, M. 2011. Gemcitabine plus nab-paclitaxel is an active regimen in patients with advanced pancreatic cancer: a phase I/II trial. *J Clin Oncol,* 29**,** 4548-54.

Vonlaufen, A., Joshi, S., Qu, C., Phillips, P. A., Xu, Z., Parker, N. R., Toi, C. S., Pirola, R. C., Wilson, J. S., Goldstein, D. & Apte, M. V. 2008a. Pancreatic Stellate Cells: Partners in Crime with Pancreatic Cancer Cells. *Cancer Research,* 68**,** 2085-2093.

Vonlaufen, A., Phillips, P. A., Xu, Z., Goldstein, D., Pirola, R. C., Wilson, J. S. & Apte, M. V. 2008b. Pancreatic stellate cells and pancreatic cancer cells: an unholy alliance. *Cancer Res,* 68**,** 7707-10.

Waddell, N., Pajic, M., Patch, A.-M., Chang, D. K., Kassahn, K. S., Bailey, P., Johns, A. L., Miller, D., Nones, K., Quek, K., Quinn, M. C. J., Robertson, A. J., Fadlullah, M.

Z. H., Bruxner, T. J. C., Christ, A. N., Harliwong, I., Idrisoglu, S., Manning, S., Nourse, C., Nourbakhsh, E., Wani, S., Wilson, P. J., Markham, E., Cloonan, N., Anderson, M. J., Fink, J. L., Holmes, O., Kazakoff, S. H., Leonard, C., Newell, F., Poudel, B., Song, S., Taylor, D., Waddell, N., Wood, S., Xu, Q., Wu, J., Pinese, M., Cowley, M. J., Lee, H. C., Jones, M. D., Nagrial, A. M., Humphris, J., Chantrill, L. A., Chin, V., Steinmann, A. M., Mawson, A., Humphrey, E. S., Colvin, E. K., Chou, A., Scarlett, C. J., Pinho, A. V., Giry-Laterriere, M., Rooman, I., Samra, J. S., Kench, J. G., Pettitt, J. A., Merrett, N. D., Toon, C., Epari, K., Nguyen, N. Q., Barbour, A., Zeps, N., Jamieson, N. B., Graham, J. S., Niclou, S. P., Bjerkvig, R., Grutzmann, R., Aust, D., Hruban, R. H., Maitra, A., Iacobuzio-Donahue, C. A., Wolfgang, C. L., Morgan, R. A., Lawlor, R. T., Corbo, V., Bassi, C., Falconi, M., Zamboni, G., Tortora, G., Tempero, M. A., Australian Pancreatic Cancer Genome, I., Gill, A. J., Eshleman, J. R., Pilarsky, C., Scarpa, A., Musgrove, E. A., Pearson, J. V., Biankin, A. V. & Grimmond, S. M. 2015. Whole genomes redefine the mutational landscape of pancreatic cancer. *Nature,* 518**,** 495-501.

Waheed, A., Purvey, S. & Saif, M. W. 2018. Masitinib in treatment of pancreatic cancer. *Expert Opin Pharmacother,* 19**,** 759-764.

Walsh, A. J., Castellanos, J. A., Nagathihalli, N. S., Merchant, N. B. & Skala, M. C. 2016. Optical Imaging of Drug-Induced Metabolism Changes in Murine and Human Pancreatic Cancer Organoids Reveals Heterogeneous Drug Response. *Pancreas,* 45**,** 863-869.

Wang, F., Yang, L., Shi, L., Li, Q., Zhang, G., Wu, J., Zheng, J. & Jiao, B. 2015. Nuclear translocation of fibroblast growth factor-2 (FGF2) is regulated by Karyopherin-β2 and Ran GTPase in human glioblastoma cells. *Oncotarget,* 6**,** 21468-21478.

Wang, S. C. & Hung, M. C. 2009. Nuclear translocation of the epidermal growth factor receptor family membrane tyrosine kinase receptors. *Clin Cancer Res,* 15**,** 6484-9.

Wang, S. C., Lien, H. C., Xia, W., Chen, I. F., Lo, H. W., Wang, Z., Ali-Seyed, M., Lee, D. F., Bartholomeusz, G., Ou-Yang, F., Giri, D. K. & Hung, M. C. 2004. Binding at and transactivation of the COX-2 promoter by nuclear tyrosine kinase receptor ErbB-2. *Cancer Cell,* 6**,** 251-61.

Wang, S. C., Nakajima, Y., Yu, Y. L., Xia, W., Chen, C. T., Yang, C. C., Mcintush, E. W., Li, L. Y., Hawke, D. H., Kobayashi, R. & Hung, M. C. 2006. Tyrosine phosphorylation controls PCNA function through protein stability. *Nat Cell Biol,* 8**,** 1359-68.

Wang, Y. & Becker, D. 1997. Antisense targeting of basic fibroblast growth factor and dibroblast growth factor receptor-1 in human melanomas blocks intratumoral angiogenesis and tumor growth. *Nature Medicine,* 3**,** 887-893.

Wardle, F. & Tan, H. 2015. A ChIP on the shoulder? Chromatin immunoprecipitation and validation strategies for ChIP antibodies. *F1000Research,* 4**,** 235.

Watari, N., Hotta, Y. & Mabuchi, Y. 1982. Morphological studies on a vitamin A-storing cell and its complex with macrophage observed in mouse pancreatic tissues following excess vitamin A administration. *Okajimas Folia Anat Jpn,* 58**,** 837-58.

Wehr, A. Y., Furth, E. E., Sangar, V., Blair, I. A. & Yu, K. H. 2011. Analysis of the human pancreatic stellate cell secreted proteome. *Pancreas,* 40**,** 557-566.

Weiss, J., Sos, M. L., Seidel, D., Peifer, M., Zander, T., Heuckmann, J. M., Ullrich, R. T., Menon, R., Maier, S., Soltermann, A., Moch, H., Wagener, P., Fischer, F., Heynck, S., Koker, M., Schottle, J., Leenders, F., Gabler, F., Dabow, I., Querings, S., Heukamp, L. C., Balke-Want, H., Ansen, S., Rauh, D., Baessmann, I., Altmuller, J., Wainer, Z., Conron, M., Wright, G., Russell, P., Solomon, B., Brambilla, E., Brambilla, C., Lorimier, P., Sollberg, S., Brustugun, O. T., Engel-Riedel, W., Ludwig, C., Petersen, I., Sanger, J., Clement, J., Groen, H., Timens, W., Sietsma, H., Thunnissen, E., Smit, E., Heideman, D., Cappuzzo, F., Ligorio, C., Damiani, S., Hallek, M., Beroukhim, R., Pao, W., Klebl, B., Baumann, M., Buettner, R., Ernestus, K., Stoelben, E., Wolf, J., Nurnberg, P., Perner, S. & Thomas, R. K. 2010. Frequent and focal FGFR1 amplification associates with therapeutically tractable FGFR1 dependency in squamous cell lung cancer. *Sci Transl Med,* 2**,** 62ra93.

Wen, S., Hou, Y., Fu, L., Xi, L., Yang, D., Zhao, M., Qin, Y., Sun, K., Teng, Y. & Liu, M. 2019. Cancer-associated fibroblast (CAF)-derived IL32 promotes breast cancer cell invasion and metastasis via integrin β3–p38 MAPK signalling. *Cancer Letters,* 442**,** 320-332.

Weniger, M., Honselmann, K. C. & Liss, A. S. 2018. The Extracellular Matrix and Pancreatic Cancer: A Complex Relationship. *Cancers,* 10**,** 316.

Wiedemann, M. & Trueb, B. 2000. Characterization of a novel protein (FGFRL1) from human cartilage related to FGF receptors. *Genomics,* 69**,** 275-9.

Wiley, H. S. & Burke, P. M. 2001. Regulation of receptor tyrosine kinase signaling by endocytic trafficking. *Traffic,* 2**,** 12-8.

Williams, C. C., Allison, J. G., Vidal, G. A., Burow, M. E., Beckman, B. S., Marrero, L. & Jones, F. E. 2004. The ERBB4/HER4 receptor tyrosine kinase regulates gene expression by functioning as a STAT5A nuclear chaperone. *J Cell Biol,* 167**,** 469-78.

Williams, E. J., Furness, J., Walsh, F. S. & Doherty, P. 1994. Activation of the FGF receptor underlies neurite outgrowth stimulated by L1, N-CAM, and N-cadherin. *Neuron,* 13**,** 583-594.

Williams, S. V., Hurst, C. D. & Knowles, M. A. 2013. Oncogenic FGFR3 gene fusions in bladder cancer. *Hum Mol Genet,* 22**,** 795-803.

Wingren, C., Sandstrom, A., Segersvard, R., Carlsson, A., Andersson, R., Lohr, M. & Borrebaeck, C. A. 2012. Identification of serum biomarker signatures associated with pancreatic cancer. *Cancer Res,* 72**,** 2481-90.

Wu, M., Arimura, G. K. & Yunis, A. A. 1977. Purification and characterization of a plasminogen activator secreted by cultured human pancreatic carcinoma cells. *Biochemistry,* 16**,** 1908-13.

Wu, R., Connolly, D., Ngelangel, C., Bosch, F. X., Muñoz, N. & Cho, K. R. 2000. Somatic mutations of fibroblast growth factor receptor 3 (FGFR3) are uncommon in carcinomas of the uterine cervix. *Oncogene,* 19**,** 5543.

Wu, Y. M., Su, F., Kalyana-Sundaram, S., Khazanov, N., Ateeq, B., Cao, X., Lonigro, R. J., Vats, P., Wang, R., Lin, S. F., Cheng, A. J., Kunju, L. P., Siddiqui, J., Tomlins, S. A., Wyngaard, P., Sadis, S., Roychowdhury, S., Hussain, M. H., Feng, F. Y., Zalupski, M. M., Talpaz, M., Pienta, K. J., Rhodes, D. R., Robinson, D. R. & Chinnaiyan, A. M. 2013. Identification of targetable FGFR gene fusions in diverse cancers. *Cancer Discov,* 3**,** 636-47.

Xiao, W., Jiang, W., Shen, J., Yin, G., Fan, Y., Wu, D., Qiu, L., Yu, G., Xing, M., Hu, G., Wang, X. & Wan, R. 2015. Retinoic Acid Ameliorates Pancreatic Fibrosis and Inhibits the Activation of Pancreatic Stellate Cells in Mice with Experimental Chronic Pancreatitis via Suppressing the Wnt/beta-Catenin Signaling Pathway. *PLoS One,* 10**,** e0141462.

Xiao, Y., Zhang, H., Ma, Q., Huang, R., Lu, J., Liang, X., Liu, X., Zhang, Z., Yu, L., Pang, J., Zhou, L., Liu, T., Wu, H. & Liang, Z. 2019. YAP1-mediated pancreatic stellate cell activation inhibits pancreatic cancer cell proliferation. *Cancer Letters,* 462**,** 51-60.

Xu, Z., Vonlaufen, A., Phillips, P. A., Fiala-Beer, E., Zhang, X., Yang, L., Biankin, A. V., Goldstein, D., Pirola, R. C., Wilson, J. S. & Apte, M. V. 2010. Role of pancreatic stellate cells in pancreatic cancer metastasis. *Am J Pathol,* 177**,** 2585-96.

Xue, X., Lu, Z., Tang, D., Yao, J., An, Y., Wu, J., Li, Q., Gao, W., Xu, Z., Qian, Z., Dai, C., Wei, J., Miao, Y. & Jiang, K. 2011. Galectin-1 secreted by activated stellate cells in pancreatic ductal adenocarcinoma stroma promotes proliferation and invasion of pancreatic cancer cells: an in vitro study on the microenvironment of pancreatic ductal adenocarcinoma. *Pancreas,* 40**,** 832-9.

Yamaji, S., Saegusa, J., Ieguchi, K., Fujita, M., Mori, S., Takada, Y. K. & Takada, Y. 2010. A Novel Fibroblast Growth Factor-1 (FGF1) Mutant that Acts as an FGF Antagonist. *PLOS ONE,* 5**,** e10273.

Yamamoto, Y., Matsui, J., Matsushima, T., Obaishi, H., Miyazaki, K., Nakamura, K., Tohyama, O., Semba, T., Yamaguchi, A., Hoshi, S. S., Mimura, F., Haneda, T., Fukuda, Y., Kamata, J. I., Takahashi, K., Matsukura, M., Wakabayashi, T., Asada, M., Nomoto, K. I., Watanabe, T., Dezso, Z., Yoshimatsu, K., Funahashi, Y. & Tsuruoka, A. 2014. Lenvatinib, an angiogenesis inhibitor targeting VEGFR/FGFR, shows broad antitumor activity in human tumor xenograft models associated with microvessel density and pericyte coverage. *Vasc Cell,* 6**,** 18.

Yamanaka, Y., Friess, H., Buchler, M., Beger, H. G., Uchida, E., Onda, M., Kobrin, M. S. & Korc, M. 1993. Overexpression of acidic and basic fibroblast growth factors in human pancreatic cancer correlates with advanced tumor stage. *Cancer Res,* 53**,** 5289-96.

Yamazaki, K., Nagao, T., Yamaguchi, T., Saisho, H. & Kondo, Y. 1997. Expression of basic fibroblast growth factor (FGF-2)-associated with tumour proliferation in human pancreatic carcinoma. *Virchows Arch,* 431**,** 95-101.

Yan, B., Jiang, Z., Cheng, L., Chen, K., Zhou, C., Sun, L., Qian, W., Li, J., Cao, J., Xu, Q., Ma, Q. & Lei, J. 2018. Paracrine HGF/c-MET enhances the stem cell-like potential and glycolysis of pancreatic cancer cells via activation of YAP/HIF-1alpha. *Exp Cell Res,* 371**,** 63-71.

Yang, J. Y., Sun, Y. W., Liu, D. J., Zhang, J. F., Li, J. & Hua, R. 2014. MicroRNAs in stool samples as potential screening biomarkers for pancreatic ductal adenocarcinoma cancer. *Am J Cancer Res,* 4**,** 663-73.

Yang, S., Che, S. P., Kurywchak, P., Tavormina, J. L., Gansmo, L. B., Correa de Sampaio, P., Tachezy, M., Bockhorn, M., Gebauer, F., Haltom, A. R., Melo, S. A., Lebleu, V. S. & Kalluri, R. 2017. Detection of mutant KRAS and TP53 DNA in circulating exosomes from healthy individuals and patients with pancreatic cancer. *Cancer Biol Ther,* 18**,** 158-165.

Yarmola, E. G., Edison, A. S., Lenox, R. H. & Bubb, M. R. 2001. Actin filament cross-linking by MARCKS: characterization of two actin-binding sites within the phosphorylation site domain. *J Biol Chem,* 276**,** 22351-8.

Yeh, C. Y., Shin, S. M., Yeh, H. H., Wu, T. J., Shin, J. W., Chang, T. Y., Raghavaraju, G., Lee, C. T., Chiang, J. H., Tseng, V. S., Lee, Y. C., Shen, C. H., Chow, N. H. & Liu, H. S. 2011. Transcriptional activation of the Axl and PDGFR-alpha by c-Met through a ras- and Src-independent mechanism in human bladder cancer. *BMC Cancer,* 11**,** 139.

Yi, J. M., Guzzetta, A. A., Bailey, V. J., Downing, S. R., Van Neste, L., Chiappinelli, K. B., Keeley, B. P., Stark, A., Herrera, A., Wolfgang, C., Pappou, E. P., Iacobuzio-Donahue, C. A., Goggins, M. G., Herman, J. G., Wang, T.-H., Baylin, S. B. & Ahuja, N. 2013. Novel methylation biomarker panel for the early detection of pancreatic cancer. *Clinical Cancer Research,* 19**,** 6544-6555.

Yu, J., Ohuchida, K., Mizumoto, K., Sato, N., Kayashima, T., Fujita, H., Nakata, K. & Tanaka, M. 2010. MicroRNA, hsa-miR-200c, is an independent prognostic factor in pancreatic cancer and its upregulation inhibits pancreatic cancer invasion but increases cell proliferation. *Mol Cancer,* 9**,** 169.

Yuan, C., Clish, C. B., Wu, C., Mayers, J. R., Kraft, P., Townsend, M. K., Zhang, M., Tworoger, S. S., Bao, Y., Qian, Z. R., Rubinson, D. A., Ng, K., Giovannucci, E. L., Ogino, S., Stampfer, M. J., Gaziano, J. M., Ma, J., Sesso, H. D., Anderson, G. L., Cochrane, B. B., Manson, J. E., Torrence, M. E., Kimmelman, A. C., Amundadottir, L. T., Vander Heiden, M. G., Fuchs, C. S. & Wolpin, B. M. 2016. Circulating Metabolites and Survival Among Patients With Pancreatic Cancer. *J Natl Cancer Inst,* 108**,** djv409.

Yuan, Y., Jiang, J.-Y., Wang, J.-M., Sun, J., Li, C., Liu, B.-Q., Yan, J., Meng, X.-N. & Wang, H.-Q. 2019. BAG3-positive pancreatic stellate cells promote migration and invasion of pancreatic ductal adenocarcinoma. *Journal of Cellular and Molecular Medicine,* 23**,** 5006-5016.

Yunis, A. A., Arimura, G. K. & Russin, D. J. 1977. Human pancreatic carcinoma (MIA PaCa-2) in continuous culture: sensitivity to asparaginase. *Int J Cancer,* 19**,** 128-35.

Zhang, H., Hylander, B. L., Levea, C., Repasky, E. A., Straubinger, R. M., Adjei, A. A. & Ma, W. W. 2014a. Enhanced FGFR signalling predisposes pancreatic cancer to the effect of a potent FGFR inhibitor in preclinical models. *British Journal of Cancer,* 110**,** 320-329.

Zhang, W., Nandakumar, N., Shi, Y., Manzano, M., Smith, A., Graham, G., Gupta, S., Vietsch, E. E., Laughlin, S. Z., Wadhwa, M., Chetram, M., Joshi, M., Wang, F., Kallakury, B., Toretsky, J., Wellstein, A. & Yi, C. 2014b. Downstream of Mutant KRAS, the Transcription Regulator YAP Is Essential for Neoplastic Progression to Pancreatic Ductal Adenocarcinoma. *Science Signaling,* 7**,** 42.

Zhang, X., Shi, S., Zhang, B., Ni, Q., Yu, X. & Xu, J. 2018. Circulating biomarkers for early diagnosis of pancreatic cancer: facts and hopes. *American Journal of Cancer Research,* 8**,** 332-353.

Zhang, Y., Morris, J. P., Yan, W., Schofield, H. K., Gurney, A., Simeone, D. M., Millar, S. E., Hoey, T., Hebrok, M. & Pasca Di Magliano, M. 2013. Canonical Wnt Signaling Is Required for Pancreatic Carcinogenesis. *Cancer Research,* 73**,** 4909-4922.

Zhao, B., Li, L. & Guan, K.-L. 2010. Hippo signaling at a glance. *Journal of Cell Science,* 123**,** 4001-4006.

Zhi, X., Zhao, D., Zhou, Z., Liu, R. & Chen, C. 2012. YAP Promotes Breast Cell Proliferation and Survival Partially through Stabilizing the KLF5 Transcription Factor. *The American Journal of Pathology,* 180**,** 2452-2461.

Zhu, H., Duchesne, L., Rudland, P. S. & Fernig, D. G. 2010. The heparan sulfate co-receptor and the concentration of fibroblast growth factor-2 independently elicit different signalling patterns from the fibroblast growth factor receptor. *Cell communication and signaling : CCS,* 8**,** 14-14.

Appendix

Appendix 1: PDAC Cell Lines

Appendix 1.1 Cell line details

The details of all the PDAC cell lines used during this project are described in Appendix Table 1.1

Appendix 1.2 STR profiles

All of the STR profiles for the PDAC cell lines and the PS1 cell line are in Appendix Figures 1.1-1.5.

Appendix Table 1.1 PDAC cell line characteristics

Cell Line	Origin	Site	Differentiation	Mutations
AsPC-1	Female age 62	Ascites	Poor	*KRAS*, *TP53*, *INK4A*
MIA PaCa-2	Male age 65	Primary	Poor	*KRAS*, *TP53*, *INK4A*
PANC-1	Male age 56	Primary	Poor	*KRAS*, *TP53*, *INK4A*
COLO 357	Female age 77	Lymph node metastasis	Well	*KRAS*, *SMAD4*

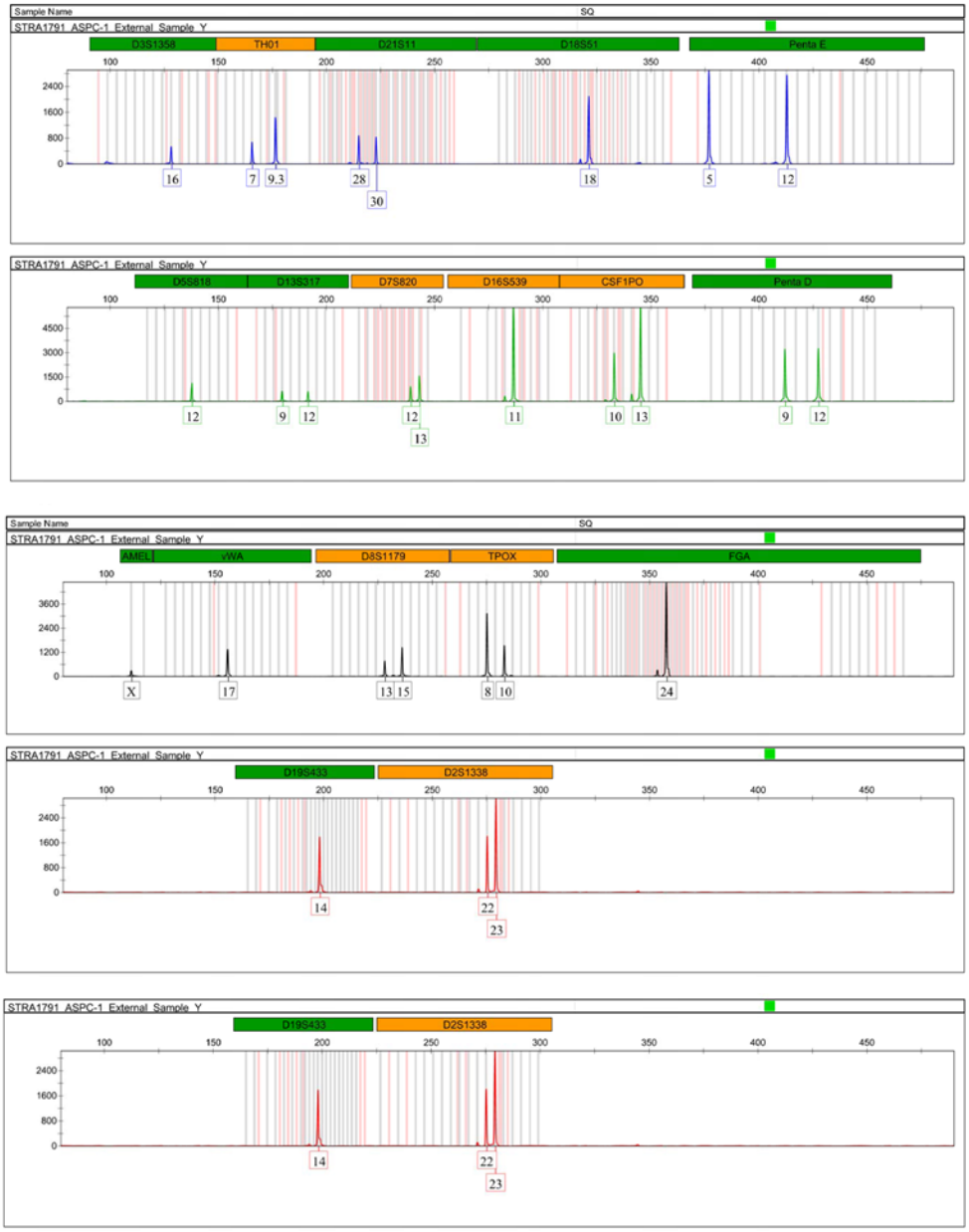

Appendix Figure 1.1 STR profile of AsPC-1 cells

This confirmed the identity of the AsPC-1 cell line.

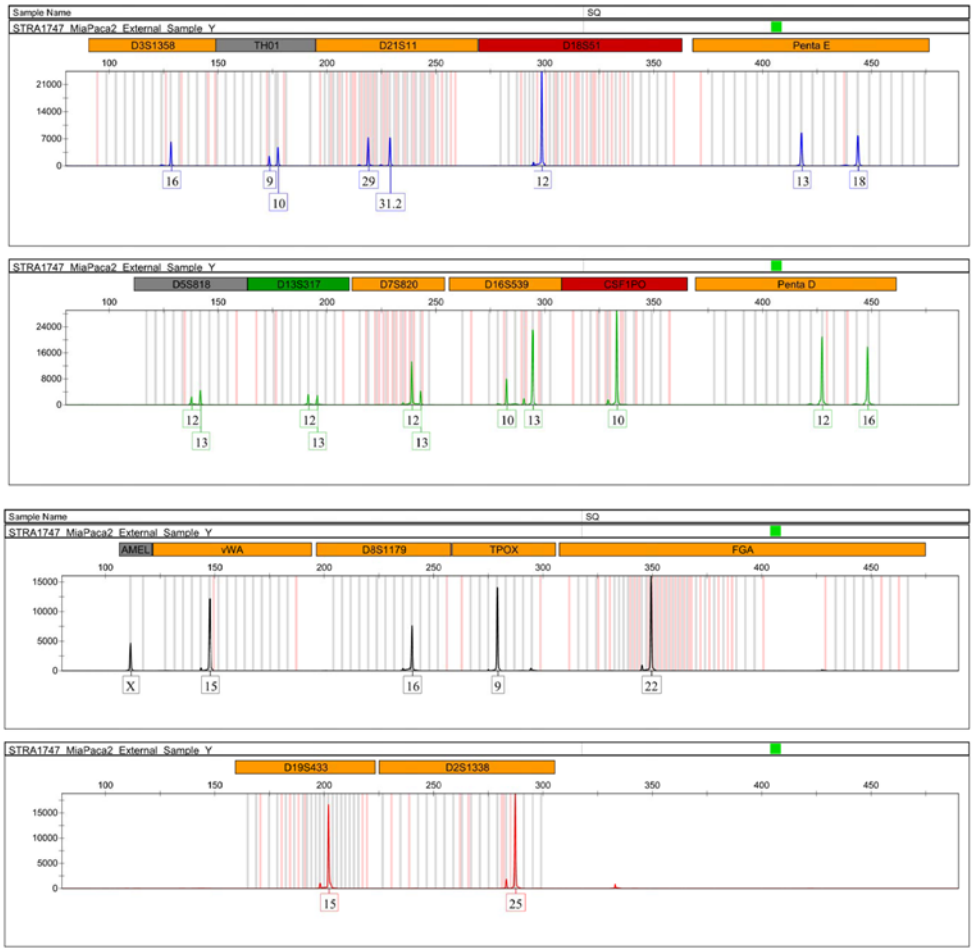

Appendix Figure 1.2 STR profile of MIA PaCa-2 cells

This confirmed the identity of the MIA PaCa-2 cell line.

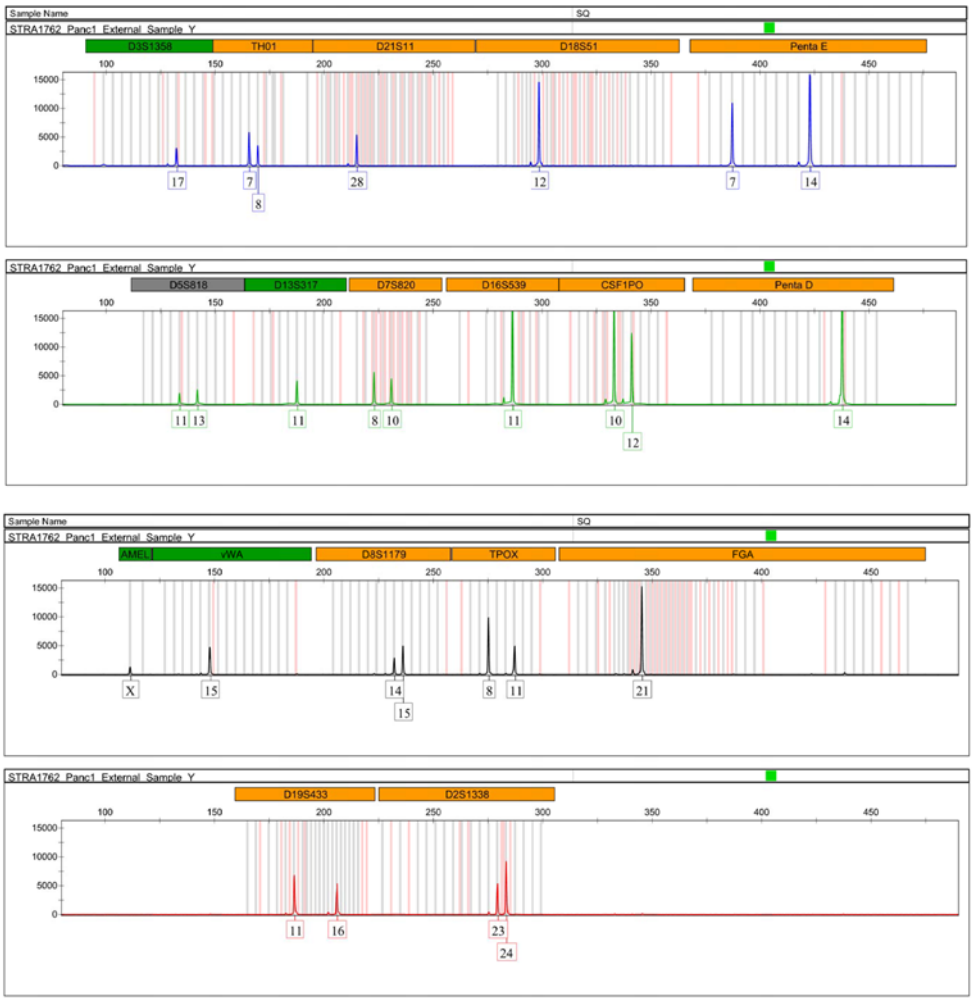

Appendix Figure 1.3 STR profile of PANC-1 cells

This confirmed the identity of the PANC-1 cell line.

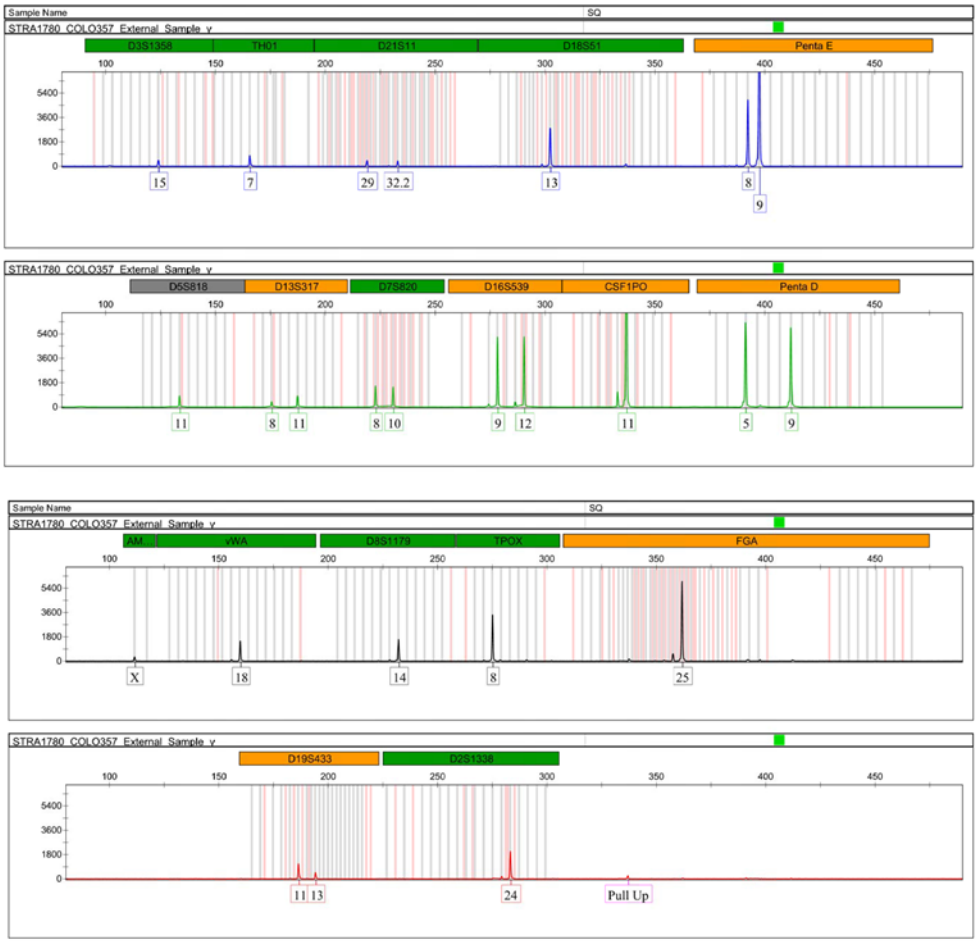

Appendix Figure 1.4 STR profile of COLO 357 cells

This confirmed the identity of the COLO 357 cell line.

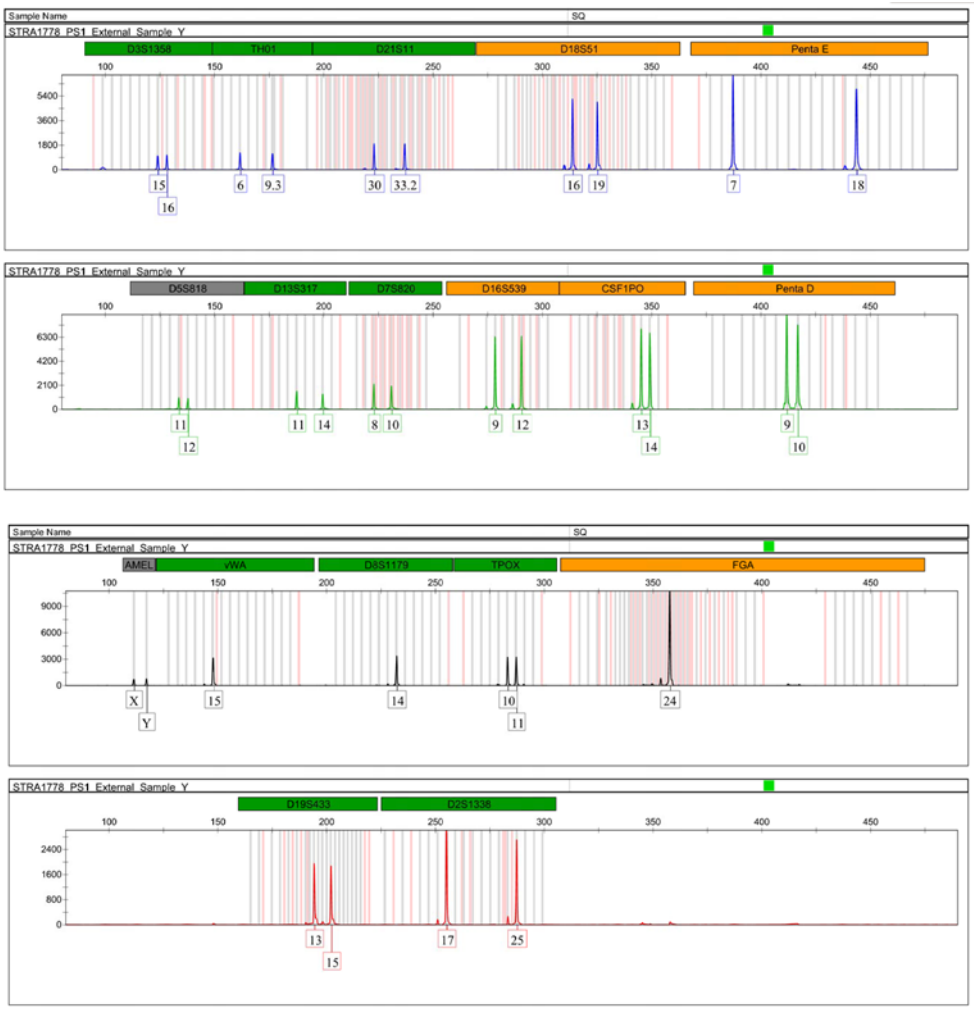

Appendix Figure 1.5 STR profile of PS1 cells

This confirmed the identity of the PS1 cell line, it did not match any other cell lines in the published databases.

Appendix 2: Gemcitabine response

Appendix 2.1 Cell viability

MTS cell viability assays were used to determine the GI_{50} of all the PDAC cancer cells and the PS1 stellate cell line to gemcitabine treatment

Appendix 2.1.1 Method

MTS cell viability assays were carried out according to Section 2.2.1. Serial dilutions of gemcitabine were prepared to treat the cell cultures after 24 hours. In total, 17 drug solutions were added to the 96 well plates (10 µl per well) to give a final drug concentration ranging from 1.22 pM to 50 µM.

Appendix 2.1.2 Results

Cell viability was determined using standard MTS assays. The growth inhibition to 50 % viability (GI_{50}) of gemcitabine, for PS1, AsPC-1, MIA PaCa-2, COLO 357 and PANC-1 cell lines in 2D culture was calculated (Appendix Figure 2.1).

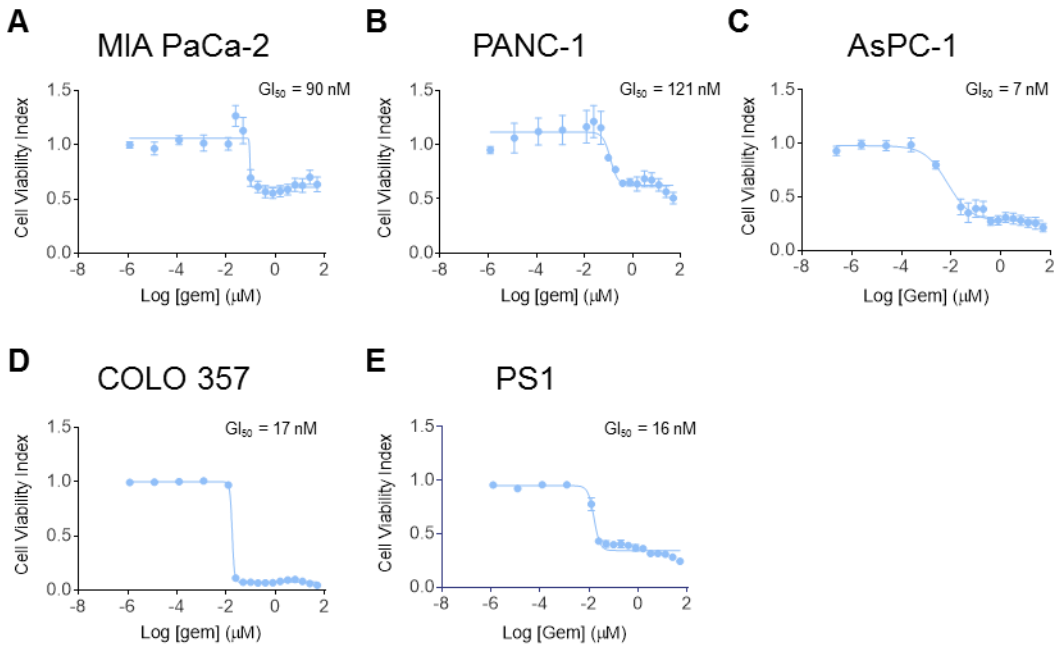

Appendix Figure 2.1 MTS assay dose response following gemcitabine treatment

MTS cell viability assays gave a GI_{50} value of 90 nM (A), 121 nM (B), 7 nM (C), 17 nM (D) and 16 nM (E) for gemcitabine with the MIA PaCa-2, PANC-1, AsPC-1, COLO 357 and PS1 cell lines respectively. These values provide a starting value to use for drug treatment moving into co-culture and 3D models. The graphs represent the mean cell viability from three technical repeats on each plate from at least three biological replicates.

Appendix 2.2 Cell proliferation

Flow cytometry analysis was used to determine AsPC-1 and PS1 response to gemcitabine in both mono- and co-cultures.

Appendix 2.2.1 Method

Cell proliferation assays of PS1 and AsPC-1 proliferation in response to increasing concentrations of gemcitabine in mono- and co-culture conditions were carried out using CellTracker dyes and Flow Cytometry analysis.

Appendix 2.2.2 Results

Geometric mean was used to determine the change in proliferation of both cell lines in response to gemcitabine treatment. There was no difference in the response of either cell line to drug in mono- or co-culture in 2D (Appendix Figure 2.2).

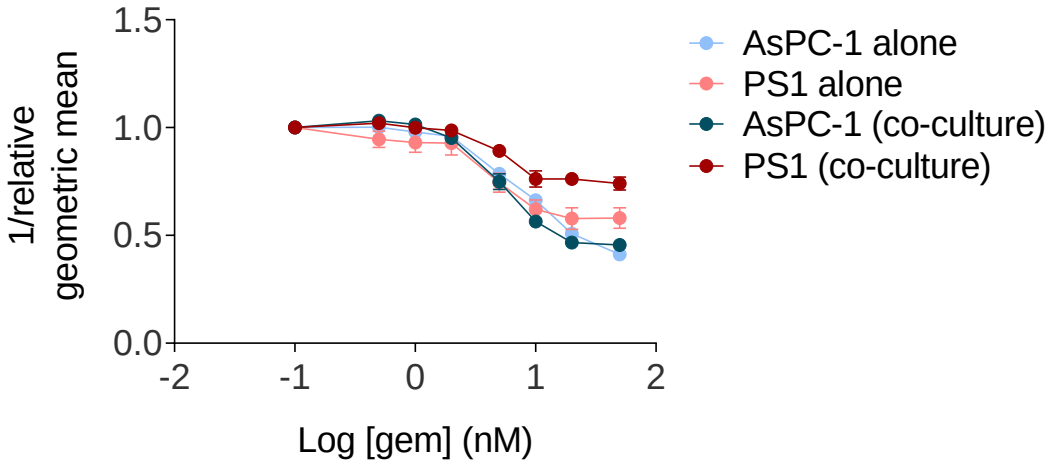

Appendix Figure 2.2 Flow Cytometry analysis of gemcitabine dose response

Flow Cytometry analysis assays showed that as the drug concentration increased, the proliferation of the cells decreased (measured by an increasing geometric mean indicating less cell division). The graph shows the change in cell proliferation of both cell lines in mono- or co-culture to gemcitabine treatment. The average geometric mean value from three biological replicates has been plotted. Two-way ANOVA analysis was carried out to analyse the data. There was no significant difference in response to gemcitabine treatment of each cell line in mono- or co-culture.

Appendix 3: Small interfering RNA (siRNA) transfection

To determine the specificity of FGFR1 antibodies, siRNA-mediated knockdown was performed.

Appendix 3.1 Method

AsPC-1 and PS1 cells were seeded into 100 mm dishes at a density of 6 x 10^5 and 2.5 x 10^5 cells per dish respectively. After 24 hours, siRNA was diluted in optiMEM (31985-062, Gibco) to give a final concentration of 10 nM. InterferIN (24µl) (409-10, Polyplus) was used as the transfection reagent and appropriate controls were included (Appendix Table 3.1). RNA extraction was carried out after 48 hours (Section 2.5.5) and cell lysates were harvested after 72 hours (Section 2.4). Western blot analysis was performed with antibodies listed in Table 2.3 and Appendix Table 3.2. Primers used to analyse gene expression by qPCR are listed in Table 2.1 and Appendix Table 3.3.

Appendix 3.2 Results

Successful knockdown of FGFR1 was confirmed by Western blot (Section 2.4 and Appendix Figure 3.1) and qPCR (Section 2.5.5 and Appendix Figures 3.2). Fibronectin and pleckstrin homology-like domain family A member 1 (PHLDA1) knockdown were used as positive controls in PS1 and AsPC-1 cells respectively.

Appendix Table 3.1 siRNA knockdown conditions and controls

Condition	PS1	AsPC-1
Negative control	optiMEM only	optiMEM only
Non-targeting negative control	nt siRNA pool (D-001810-10-20, Dharmacon)	nt siRNA pool (D-001810-10-20, Dharmacon)
Positive control	Fibronectin siRNA pool (M-009853-01, Dharmacon)	PHLDA1 siRNA pool (L-012389-00, Dharmacon)
Targeted knockdown	FGFR1 siRNA pool (L-003131-00, Dharmacon)	FGFR1 siRNA pool (L-003131-00, Dharmacon)

Appendix Table 3.2 Positive control antibodies for siRNA-mediated knockdown

Antibody	Species	Incubation conditions	Dilution for IF/IHC	Dilution for WB
Fibronectin (sc-73601, Santa Cruz)	Mouse	O/N 4ºC		1:1000
PHLDA1 (HPA019000-100UL, Sigma-Aldrich)	Rabbit	O/N 4ºC		1:1000

Appendix Table 3.3 Positive control primers for siRNA-mediated knockdown

Target	Sequence – Forward	Sequence – Reverse
PHLDA1	CAG-AGG-GCA-AGG-AGA-TCG-AC	GTG-GAT-TTG-ACC-GCC-AGG-AT
Fibronectin	AAC-AAA-CAC-TAA-TGT-TAA-TTG-CCC-A	TCG-GGA-ATC-TTC-TCT-GTC-AGC

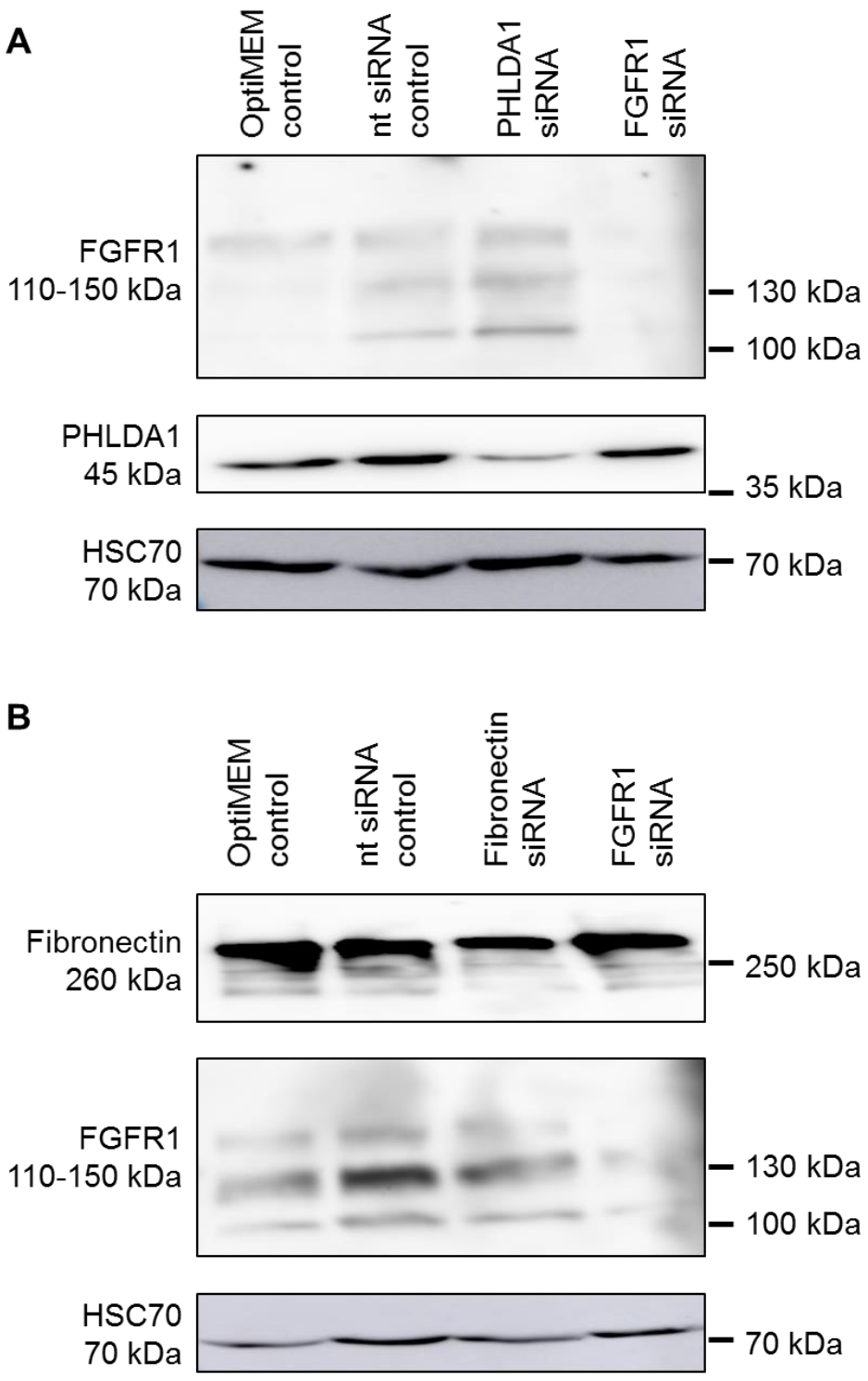

Appendix Figure 3.1 Western blot analysis of siRNA-mediated knockdown

*Western blot analysis of protein levels following siRNA-mediated knockdown of FGFR1 in AsPC-1 (**A**) and PS1 (**B**) cells. Negative controls of OptiMEM only and non-targeting (nt) siRNA were used, as well as a relevant positive control siRNA for each cell line (PHLDA1 for AsPC-1 cells and fibronectin for PS1 cells).*

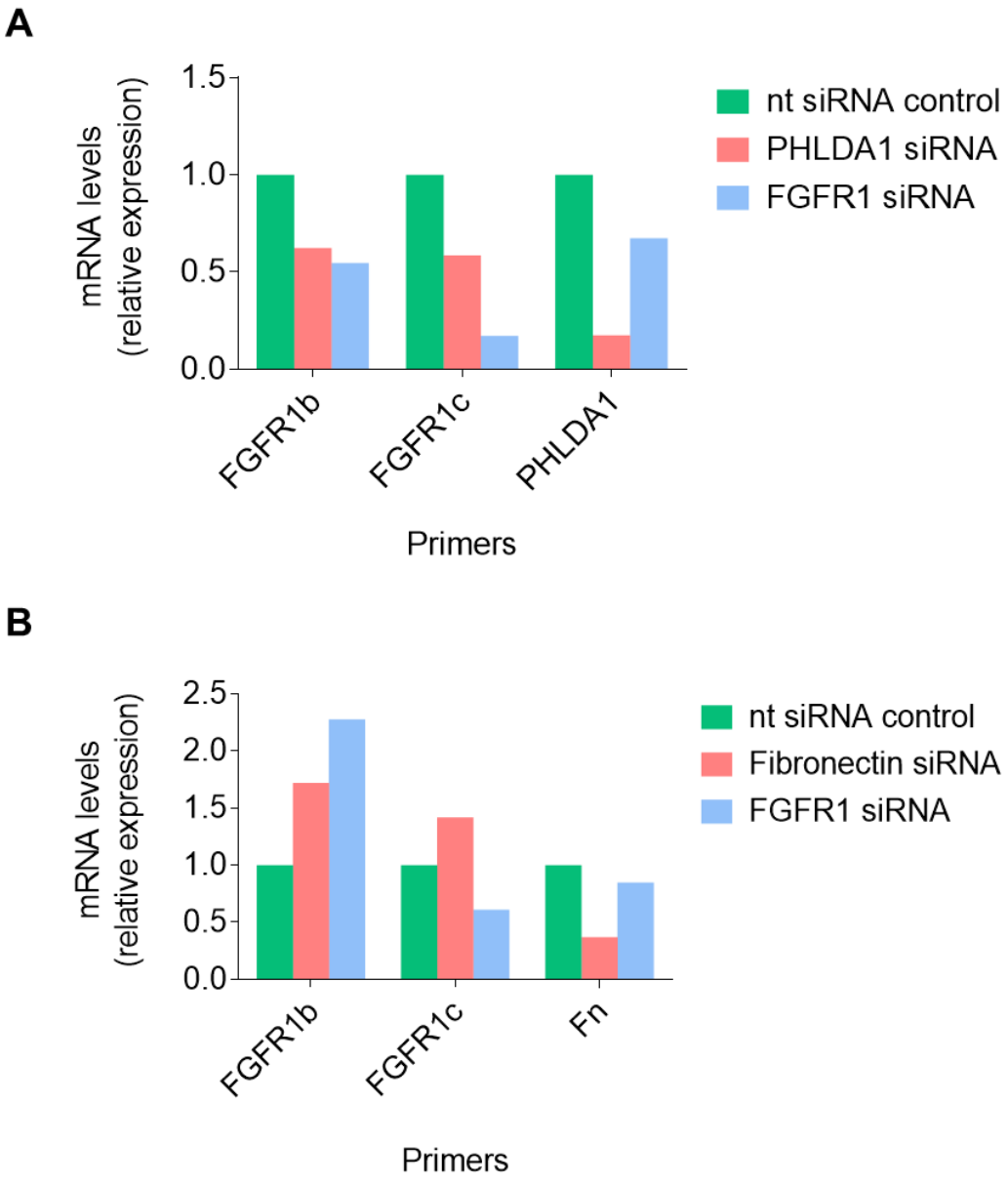

Appendix Figure 3.2 qPCR analysis of siRNA-mediated knockdown

*Gene expression analysis of RNA levels by qPCR following siRNA-mediated knockdown of FGFR1 in AsPC-1 (**A**) and PS1 (**B**) cells. All samples were normalised to the relevant housekeeping primer (B2M and HPRT-1) and then to the non-targeting (nt) siRNA negative control. The expression of both the FGFR1b and FGFR1c isoform was analysed, as well as a relevant positive control for each cell line (PHLDA1 for AsPC-1 cells and fibronectin (Fn) for PS1 cells).*

Appendix 4: Western blots

Appendix Figure 4.1, 4.2, 4.3, 4.4 and 4.5 show the full Western blot images for all antibodies from Figures 4.7, 5.6 and 5.9 and Appendix Figure 3.1 respectively.

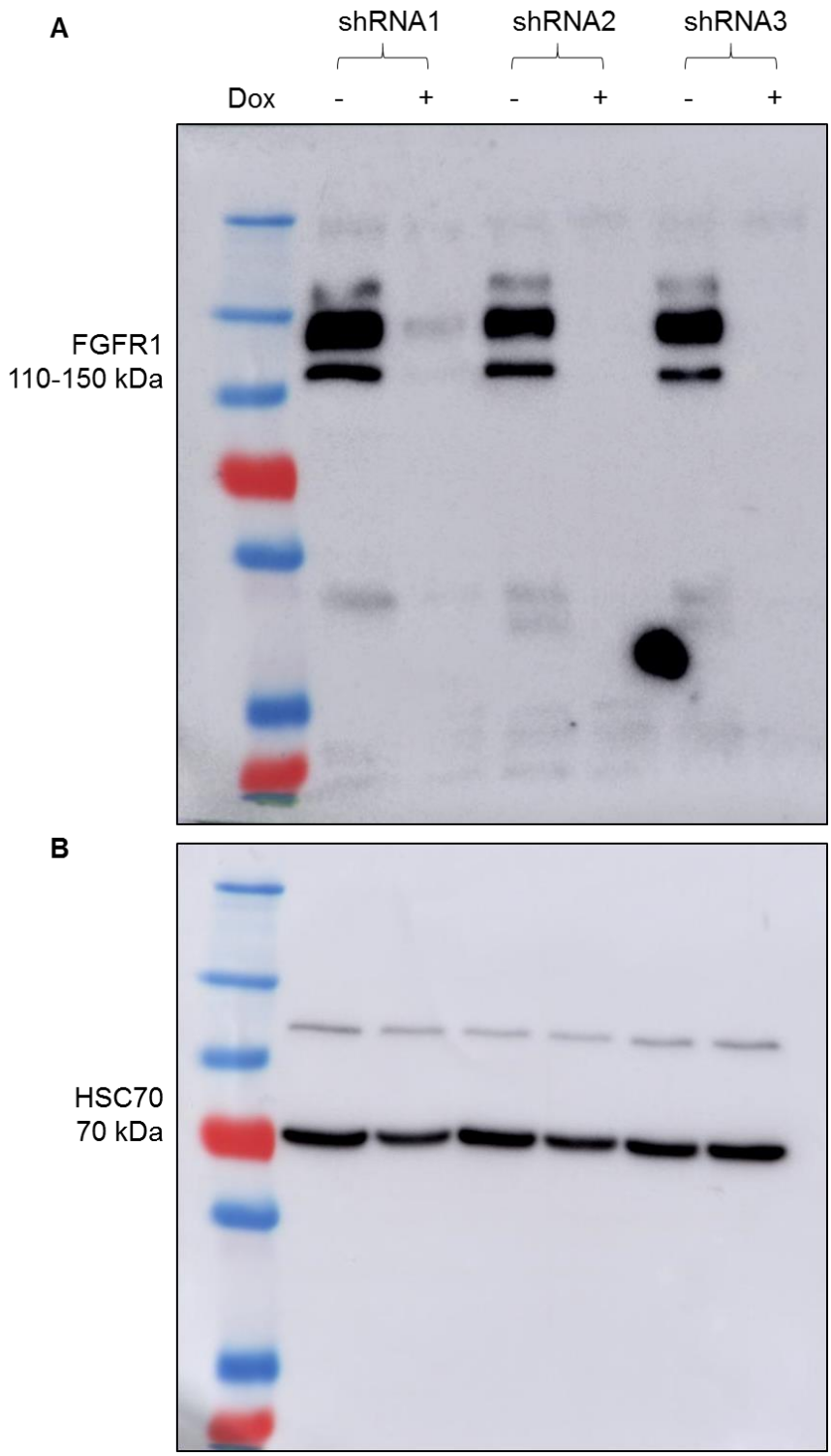

Appendix Figure 4.1 FGFR1 shRNA knockdown Western blot

*Full Western blot images of the antibodies used in Figure 4.7 to confirm FGFR1 knockdown following doxycycline (dox) induction of shRNA for 48 hours. FGFR1 antibody (**A**) was blotted with HSC70 (**B**) as a loading control.*

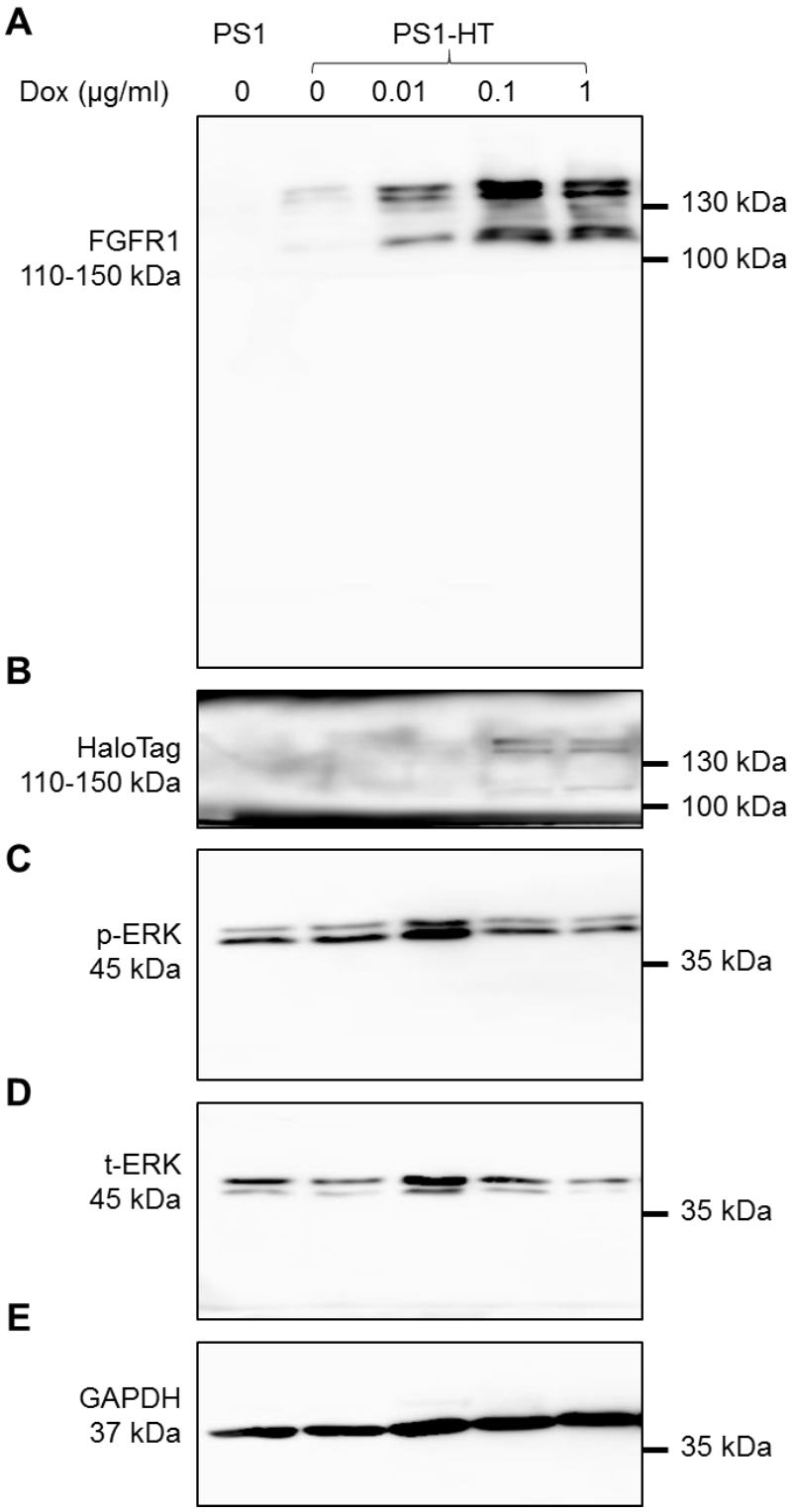

Appendix Figure 4.2 Inducible FGFR1-HT expression Western blot

*Full Western blot images of the antibodies used in Figure 5.6 to confirm FGFR1-HT expression following treatment with increasing concentrations of doxycycline (dox) for 48 hours. FGFR1 (**A**), HaloTag (**B**), p-ERK (**C**), t-ERK (**D**) antibodies were blotted with GAPDH (**E**) as a loading control.*

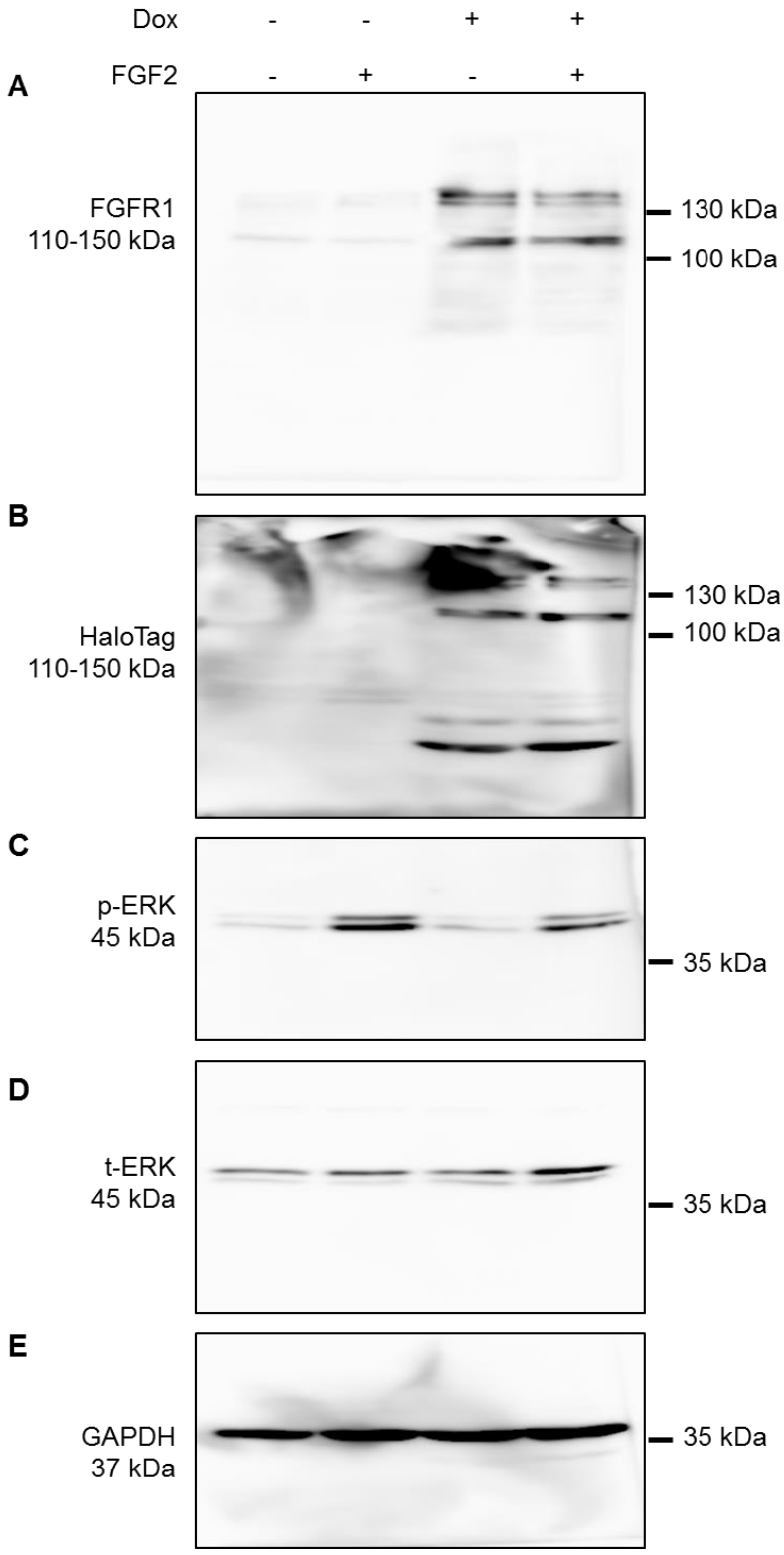

Appendix Figure 4.3 Functionality of FGFR1-HT construct Western blot

*Full Western blot images of the antibodies used in Figure 5.9 to confirm FGFR1-HT functionality following treatment with doxycycline (dox) for 48 hours to induce FGFR1-HT expression and then stimulation with 100 ng/ml FGF2 for 15 minutes. FGFR1 (**A**), HaloTag (**B**), p-ERK (**C**), t-ERK (**D**) antibodies were blotted with GAPDH (**E**) as a loading control.*

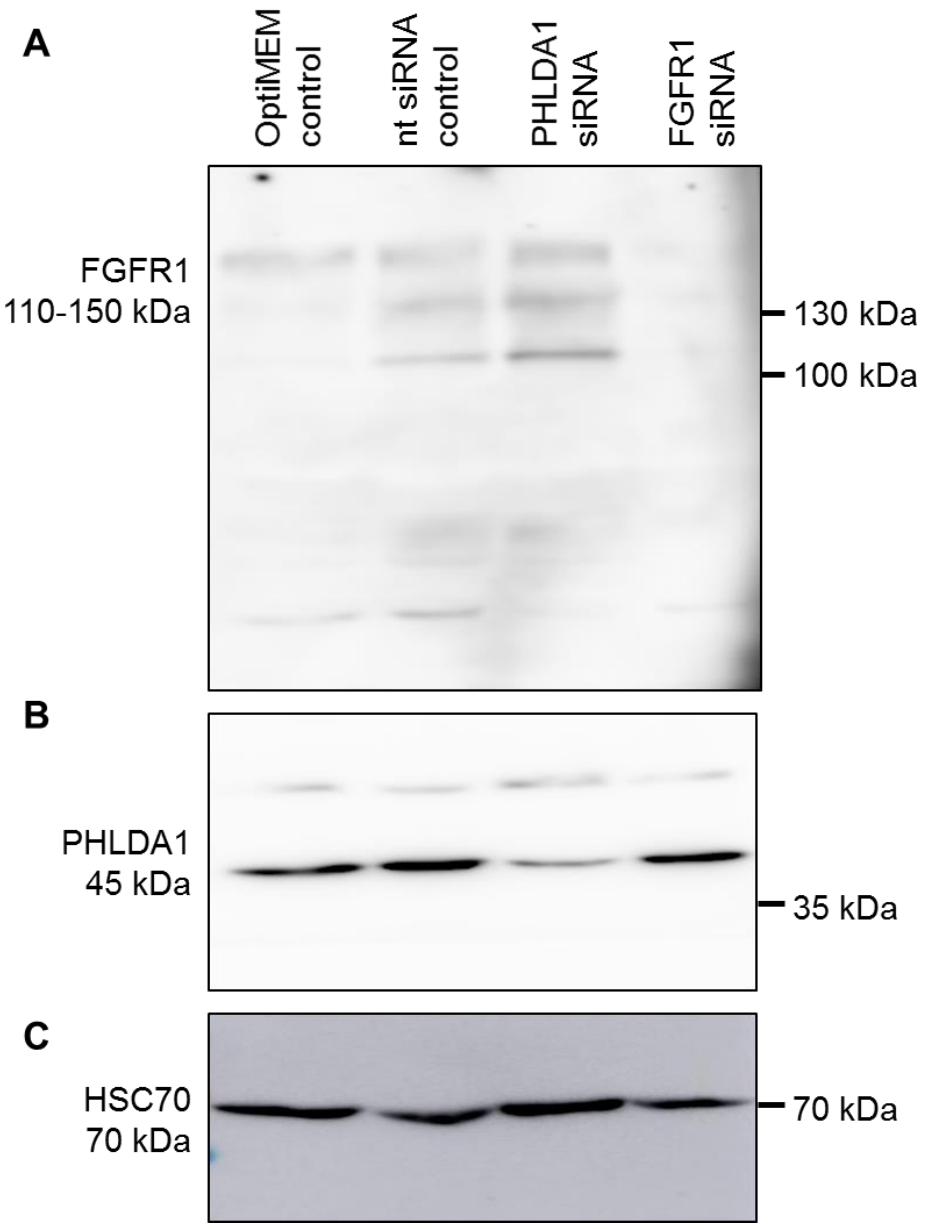

Appendix Figure 4.4 AsPC-1 siRNA knockdown Western blot

*Full Western blot images of the antibodies used in Appendix Figure 3.1**A** to confirm siRNA-mediated knockdown of FGFR1. Negative controls of OptiMEM only and non-targeting (nt) siRNA were used, as well as PHLDA1 siRNA as a positive control. FGFR1 (**A**) and PHLDA1 (**B**) antibodies were blotted with HSC70 (**C**) as a loading control.*

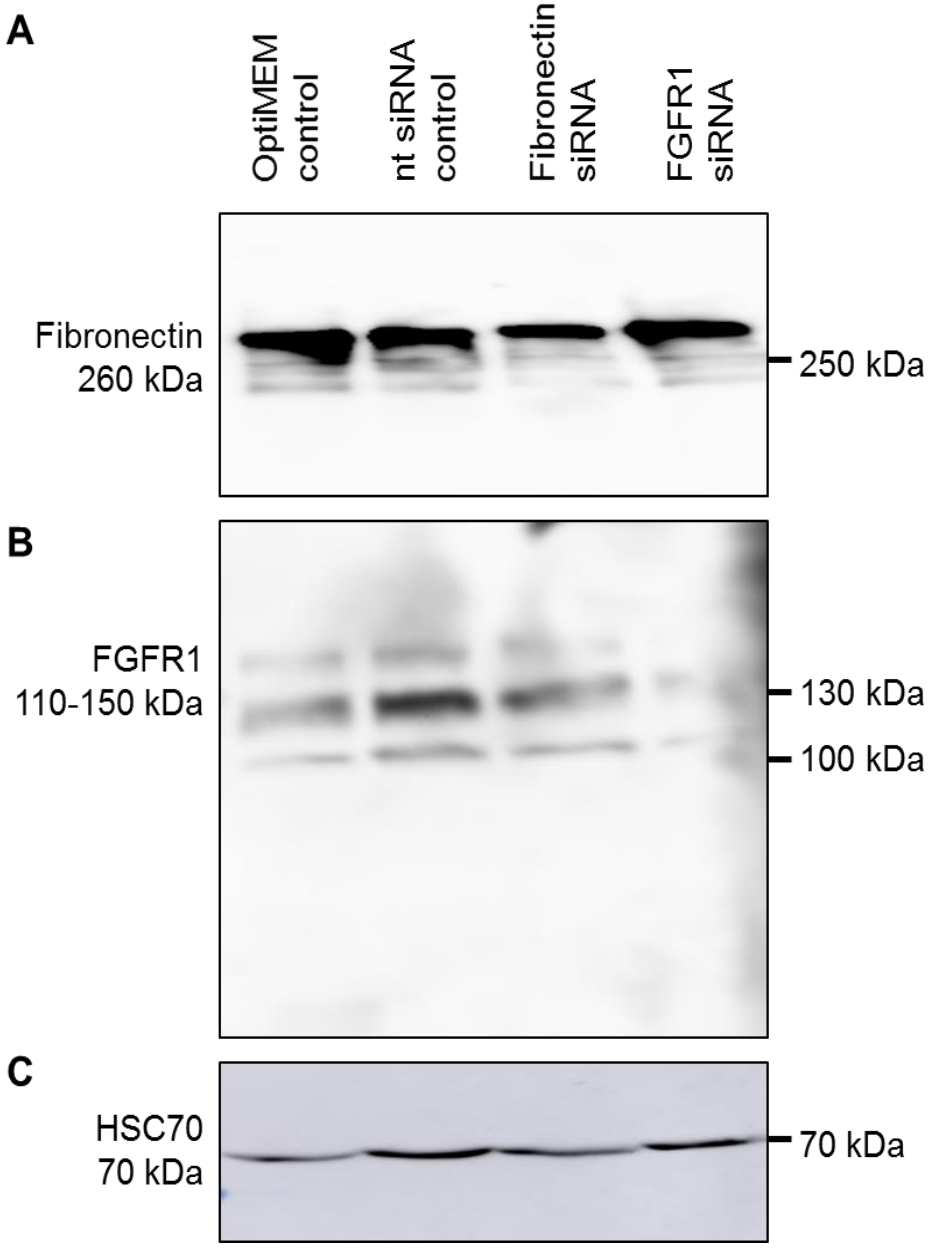

Appendix Figure 4.5 PS1 siRNA knockdown Western blot

*Full Western blot images of the antibodies used in Appendix Figure 3.1**B** to confirm siRNA-mediated knockdown of FGFR1. Negative controls of OptiMEM only and non-targeting (nt) siRNA were used, as well as Fibronectin siRNA as a positive control. Fibronectin (**A**) and FGFR1 (**B**) antibodies were blotted with HSC70 (**C**) as a loading control.*

Appendix 5: ChIP

Appendix 5.1 ChIP optimisation

In early optimisation of cell number for ChIP, chromatin harvesting and sonication of PS1 cells was compared to the positive control MFE-296 (FGFR2 mutant endometrial cancer).

Appendix 5.1.1 Method

MFE-296 cells were grown in minimum essential medium (MEM) (M7278, Sigma) plus 10 % (v/v) FBS. Cells were harvested and sonicated according to the Millipore protocol (Section 2.7.3). One flask of MFE-296 cells was used (positive control) compared to 14 flasks of PS1 cells.

Appendix 5.1.2 Results

Input DNA of unsonicated and sonicated chromatin isolated from PS1 and MFE-296 cells was run on an agarose gel. The sonication had fragmented the chromatin in both samples to a sufficient range of sizes (150-500 bp), however the MFE-296 range went up to 1,000 bp, indicating that more sonication may be required (Appendix Figure 4.1). The amount of DNA extracted from PS1 cells was much lower than from MFE-296 cells, despite having many more flasks of starting material. This indicated that a high cell number of cells (20 million) would be needed to have enough chromatin to analyse by ChIP-seq.

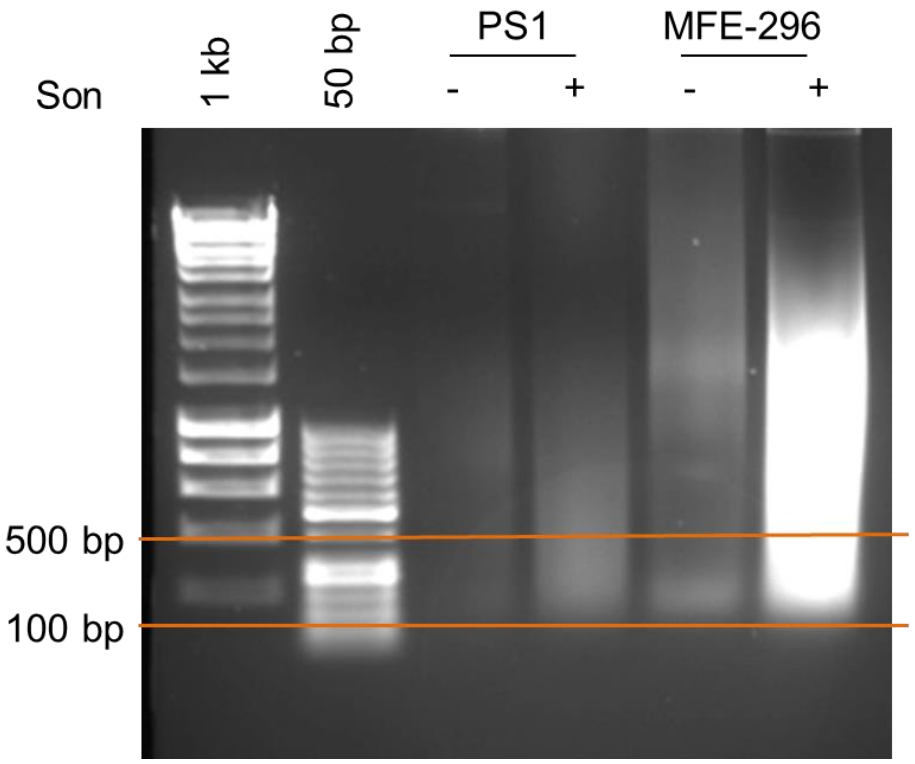

Appendix Figure 5.1 Chromatin harvesting optimisation

Cell number required for efficient chromatin isolation and sonication for ChIP-seq was optimised using MFE-296 cells as a positive control. Fragmentation of both cells lines after 10 sonication cycles can be seen after sonication (son), however, the DNA band for MFE-296 cells is much brighter than PS1 cells. Also, further sonication would have been required to enrich the fragment size within the 100-500 bp acceptable range.

Appendix 5.2 ChIP-PCR

During the optimisation for ChIP-seq experiments, ChIP-PCR analysis was carried out to analyse the expression of some previous FGFR1-targeted hits shown in PSCs.

Appendix 5.2.1 Method

PS1 cells (20 million) were seeded in a series of 150 mm^3 dishes. After 24 hours, cells were placed in serum free media overnight and FGF2 stimulation was carried out according to Section 2.1.3. Chromatin was harvested and fragmented from both FGF2 stimulated and unstimulated control cells according to Section 2.7.4.2. Immunoprecipitation with an FGFR1 and relevant IgG antibody (Table 2.3) and DNA extraction were performed according to Sections 2.7.4.3 and Section 2.7.4.4. Analysis of potential FGFR1 targets from previous work was performed by qPCR using relevant primers (Section 2.5.5, Table 2.1 and Appendix Table 4.1).

Appendix 5.2.2 Results

The levels of relevant FGFR1 targets in each sample were normalised to the IgG negative control. Cells stimulated with FGF2 had increased levels of these target genes, compared to unstimulated control samples, apart from *JunB* (Appendix Figure 4.2). This indicates that when cells are stimulated with FGF2, there is increased nuclear localisation of FGFR1 and therefore more binding to relevant target genes. However, this experiment was only performed once as ChIP-seq analysis is more detailed and allowed new FGFR1 target genes to be identified.

Appendix Table 5.1 FGFR1 target gene primers

Target	Sequence – Forward	Sequence – Reverse
SP2	GGC-CTC-ACC-CTA-AGG-ACT-TC	GGG-GAC-CGA-CAG-CAC-TAT-TA
ZN384	GCC-CCT-CTT-TCT-CCA-TTA-GC	CTT-CTG-GAG-CGA-GAC-AGA-CC
ROCK1	GCA-AGA-AGC-CTT-TTC-GTC-GG	CGT-AAA-TGG-GTT-CAA-CGC-CG
JUNB	GCT-GAC-TAG-CGC-GGT-ATA-AA	GTG-CGC-AAA-AGC-CCT-GTC
CDK12	TCG-CGT-TGT-TTG-ATA-AGC-AG	CTT-TCT-TGC-CTC-CGT-TTC-AC
GLI1	ACA-GGG-AGA-CAC-CGA-AGA-TG	AAG-AGC-CTC-CAA-GGA-AAT-GG

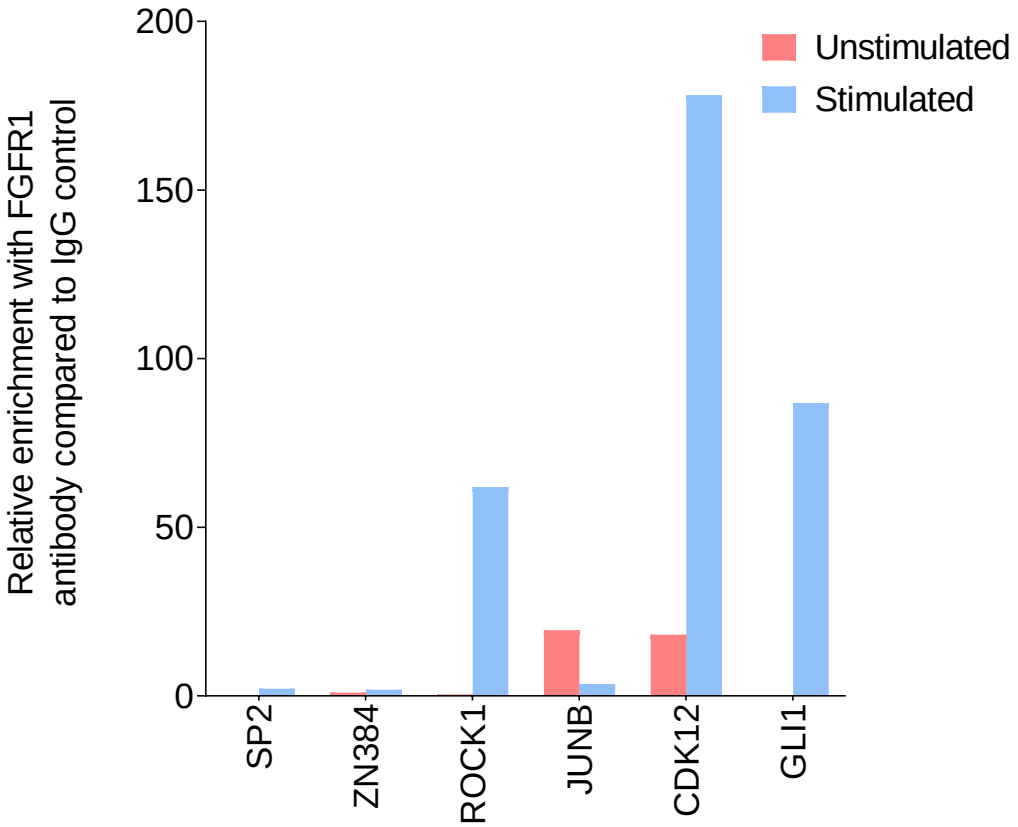

Appendix Figure 5.2 ChIP-PCR of potential FGFR1 target genes

ChIP-PCR analysis was performed on chromatin isolated from PS1 cells stimulated with FGF2, compared to unstimulated controls. FGFR1 binding to potential target genes was analysed by qPCR and enrichment levels were plotted relative to the IgG control sample. Most of the target genes showed enriched FGFR1 binding upon FGF2 stimulation.

Appendix 6: Tables of hits

Appendix 6.1 Total peptide changes

Appendix Table 6.1 Most decreased peptides upon FGFR inhibition

Log2 (AZD/DMSO) total protein levels	Protein names	Gene names	Function
-4.89711	MARCKS-related protein	MARCKSL1	Controls cell movement by regulating actin cytoskeleton homeostasis and filopodium and lamellipodium formation
-4.32754	Nuclear factor 1 X-type;Nuclear factor 1	NFIX	These proteins are individually capable of activating transcription and replication
-3.98183	Sodium-dependent phosphate transporter 2	SLC20A2	Sodium-phosphate symporter which seems to play a fundamental housekeeping role in phosphate transport by absorbing phosphate from interstitial fluid for normal cellular functions such as cellular metabolism, signal transduction, and nucleic acid and lipid synthesis
-3.91147	FH1/FH2 domain-containing protein 1	FHOD1	Required for the assembly of F-actin structures, such as stress fibers
-3.56177	Protein-tyrosine sulfotransferase 1	TPST1	Catalyzes the O-sulfation of tyrosine residues within acidic motifs of polypeptides, using 3'-phosphoadenylyl sulfate (PAPS) as cosubstrate
-3.51652	Cytochrome c oxidase assembly factor 7	COA7	Required for assembly of mitochondrial respiratory chain complex I and complex IV
-3.30857	Tetratricopeptide repeat protein 7A	TTC7A	Component of a complex required to localize phosphatidylinositol 4-kinase (PI4K) to the plasma membrane
-3.00918	Glutathione peroxidase 1	GPX1	May constitute a glutathione peroxidase-like protective system against oxidative stresses
-2.93539	Intersectin-2	ITSN2	Adapter protein that may provide indirect link between the endocytic membrane traffic and the actin assembly machinery
-2.92123	Replication factor C subunit 1	RFC1	Plays a role in DNA transcription regulation, DNA replication and repair
-2.91835	BUB3-interacting and GLEBS motif-containing protein ZNF207	ZNF207	Kinetochore- and microtubule-binding protein that plays a key role in spindle assembly
-2.54075	Ras-related protein Rab-31	RAB31	Key regulator of intracellular membrane trafficking
-2.35453	Histone deacetylase complex subunit SAP130	SAP130	Acts as a transcriptional repressor
-2.25421	Selenoprotein S	VIMP;SELS	Involved in the degradation process of misfolded endoplasmic reticulum (ER) luminal proteins

Log2 (AZD/DMSO) total protein levels	Protein names	Gene names	Function
-2.23287	NADH dehydrogenase [ubiquinone] iron-sulfur protein 8, mitochondrial	NDUFS8	Part of the mitochondrial membrane respiratory chain
-2.1943	Amyloid beta A4 precursor protein-binding family B member 2	APBB2	May modulate the internalization of amyloid-beta precursor protein
-2.18975	Transmembrane protein 51	TMEM51	
-2.15253	Pre-rRNA-processing protein TSR1 homolog	TSR1	Required during maturation of the 40S ribosomal subunit in the nucleolus
-2.14636	Volume-regulated anion channel subunit LRRC8E	LRRC8E	Component of the anion channel VRAC
-2.13332	Sorting nexin-17	SNX17	Regulator of endosomal recycling
-2.13287	Calcium-independent phospholipase A2-gamma	PNPLA8	Cleaves membrane phospholipids
-2.11054	Inositol 1,4,5-trisphosphate receptor type 2	ITPR2	Mediates the release of intracellular calcium
-2.10362	Serine/threonine-protein phosphatase 2A regulatory subunit B subunit alpha	PPP2R3A	Phosphatase – B subunit determines target and activity
-2.08795	Sodium/hydrogen exchanger 6	SLC9A6	Electroneutral exchange of protons for Na+ and K+ across the early and recycling endosome membranes
-2.04367	Titin	TTN	Connects microfilaments affecting the function of striated muscles
-2.03418	NADH dehydrogenase [ubiquinone] 1 beta subcomplex subunit 1	NDUFB1	Part of the mitochondrial membrane respiratory chain
-2.02466	ER membrane protein complex subunit 2	EMC2	
-2.00131	Thrombospondin-3	THBS3	Adhesive glycoprotein that mediates cell-to-cell and cell-to-matrix interactions. Can bind to fibrinogen, fibronectin, laminin and type V collagen.

Appendix Table 6.2 Most increased peptides upon FGFR inhibition

Log2 (AZD/DMSO) total protein levels	Protein names	Gene names	Function
2.07153	Pre-mRNA-processing factor 17	CDC40	Involved in mRNA splicing
2.1054	Active breakpoint cluster region-related protein	ABR	GTPase-activating protein for RAC and CDC42
2.11896	DNA dC->dU-editing enzyme APOBEC-3C	APOBEC3C	DNA deaminase (cytidine deaminase) which acts as an inhibitor of retrovirus replication
2.25082	Absent in melanoma 1 protein	AIM1	
2.38664	Dehydrogenase/reductase SDR family member on chromosome X	DHRSX	Involved in the positive regulation of starvation-induced autophagy
2.39439	Centromere-associated protein E;Kinesin-like protein	CENPE	Microtubule plus-end-directed kinetochore motor which plays an important role in chromosome congression, microtubule-kinetochore conjugation and spindle assembly checkpoint activation
2.47182	ATP-binding cassette sub-family B member 7, mitochondrial	ABCB7	Involved in transport of heme from the mitochondria to the cytosol
2.5983	Glycosylated lysosomal membrane protein	GLMP	Transcription factor
2.66223	UAP56-interacting factor	FYTTD1	Required for mRNA export from the nucleus to the cytoplasm
2.72045	Deoxyribonuclease-1-like 1	DNASE1L1	deoxyribonuclease
2.724	Zinc finger protein 808	ZNF808	Involved in transcriptional regulation
2.8061	Death domain-associated protein 6	DAXX	Transcriptional repressor
2.80693	Core histone macro-H2A.2	H2AFY2	Transcriptional repressor
2.82514	Ubiquitin carboxyl-terminal hydrolase;Ubiquitin carboxyl-terminal hydrolase 30	USP30	Deubiquitinating enzyme tethered to the mitochondrial outer membrane that acts as a key inhibitor of mitophagy by counteracting the action of parkin (PRKN)
2.93415	Sorting nexin-13	SNX13	Involved in intracellular trafficking
2.94608	Lysozyme; Lysozyme C	LYZ	Lysozyme C is capable of both hydrolysis and transglycosylation; it shows also a slight esterase activity. Bacteriolytic function
3.25699	39S ribosomal protein L10, mitochondrial	MRPL10	RNA binding
3.64192	BCL2/adenovirus E1B 19 kDa protein-interacting protein 3	BNIP3	Induces apoptosis

Log2 (AZD/DMSO) total protein levels	Protein names	Gene names	Function
4.91431	Zinc finger C3H1 domain-containing protein	ZFC3H1	Subunit of the trimeric poly(A) tail exosome targeting (PAXT) complex, a complex that directs a subset of long and polyadenylated poly(A) RNAs for exosomal degradation

Appendix 6.2 Nuclear peptide changes

Appendix Table 6.3 Most decreased nuclear peptides upon FGFR inhibition

Percentage change	Protein names	Significant in another fraction?	Which Direction	Peptides	Gene names
-45.8485	Histone-lysine N-methyltransferase NSD2	Plasma Membrane (33 %)	Opposite - increase in PM with AZD	6	WHSC1
-43.1173	WD repeat-containing protein 43	IM (22 %)	Opposite - increase in IM with AZD	5	WDR43
-40.9542	Zinc finger protein 318	Cytoplasm (45 %)	Opposite - increase in Cyt with AZD	3	ZNF318
-40.2951	Protein SON	Plasma Membrane (55 %)	Opposite - increase in PM with AZD	14	SON
-39.5653	Heterogeneous nuclear ribonucleoprotein U	Cytoplasm (36 %)	Opposite - increase in Cyt with AZD	38	HNRNPU
-38.4907	Zinc finger C3H1 domain-containing protein	Plasma Membrane (20 %)	Opposite - increase in PM with AZD	3	ZFC3H1
-37.8679	Regulation of nuclear pre-mRNA domain-containing protein 2			6	RPRD2
-37.5041	Histone-lysine N-methyltransferase 2D	Cytoplasm (28 %)	Opposite - increase in Cyt with AZD	2	KMT2D
-33.763	Ribosome biogenesis regulatory protein homolog	Cytoplasm (23 %)	Opposite - increase in Cyt with AZD	10	RRS1
-31.2712	Hepatocyte growth factor receptor	IM (20 %)	Opposite - increase in IM with AZD	2	MET
-30.741	Eukaryotic translation initiation factor 6	Plasma Membrane (23 %)	Opposite - increase in PM with AZD	6	EIF6
-30.7352	Zinc finger MYM-type protein 4			4	ZMYM4
-30.2354	Protein DEK			10	DEK
-29.7403	Protein ENL	Cytoplasm (26 %)	Opposite - increase in Cyt with AZD	3	MLLT1

Percentage change	Protein names	Significant in another fraction?	Which Direction	Peptides	Gene names
-29.4794	PHD finger-like domain-containing protein 5A			2	PHF5A
-28.6006	pre-rRNA processing protein FTSJ3	Cytoplasm (29 %)	Opposite - increase in Cyt with AZD	10	FTSJ3
-27.6277	DNA ligase 3			3	LIG3
-27.3851	Integrator complex subunit 3			5	INTS3
-27.1325	Fos-related antigen 1			4	FOSL1
-26.827	Barrier-to-autointegration factor;Barrier-to-autointegration factor, N-terminally processed	IM (19 %)	Opposite - increase in IM with AZD	2	BANF1

Appendix Table 6.4 Most increased nuclear peptides upon FGFR inhibition

Percentage change	Protein names	Significant in another fraction?	Which Direction	Peptides	Gene names
20.0689	Cleavage and polyadenylation specificity factor subunit 4			1	CPSF4
20.1101	FH1/FH2 domain-containing protein 1			2	FHOD1
20.3297	Ubiquitin-like protein ISG15			3	ISG15
20.4251	Centromere-associated protein E;Kinesin-like protein	Cytoplasm (40 %)	Opposite - decrease in Cyt with AZD	2	CENPE
21.26094	Ras-related GTP-binding protein A	Cytoplasm (27 %)	Opposite - decrease in Cyt with AZD	2	RRAGA; RRAGB
21.2845	NHL repeat-containing protein 3	Cytoplasm (25 %)	Opposite - decrease in Cyt with AZD	2	NHLRC3
21.3897	Phosphatidylinositol 5-phosphate 4-kinase type-2 beta			3	PIP4K2B
21.5724	HD domain-containing protein 2	Cytoplasm (25 %)	Opposite - decrease in Cyt with AZD	2	HDDC2
21.7991	Activator of 90 kDa heat shock protein ATPase homolog 1			5	AHSA1
22.6076	Protein cornichon homolog 4			1	CNIH4
23.1148	A-kinase anchor protein 2	Cytoplasm (25 %)	Opposite - decrease in Cyt with AZD	20	AKAP2
23.1816	Protein SCO1 homolog, mitochondrial	Cytoplasm (35 %)	Opposite - decrease in Cyt with AZD	2	SCO1
23.2109	Fibronectin;Anastellin; Ugl-Y1;Ugl-Y2;Ugl-Y3	IM (20 %)	Opposite - decrease in IM with AZD	94	FN1
23.3054	Lysosomal-associated transmembrane protein 4A			2	LAPTM4A
23.3125	Ankyrin-2			3	ANK2
23.6622	Probable Xaa-Pro aminopeptidase 3	IM (19 %)	Opposite - decrease in IM with AZD	2	XPNPEP3

Percentage change	Protein names	Significant in another fraction?	Which Direction	Peptides	Gene names
26.1964	Suppressor of SWI4 1 homolog			3	PPAN
27.8245	Latrophilin-2			3	ADGRL2; LPHN2
30.8725	Tropomyosin alpha-3 chain	Cytoplasm (35 %)	Opposite - decrease in Cyt with AZD	18	TPM3
43.4746	Kinesin-like protein KIF3B;Kinesin-like protein KIF3B, N-terminally processed;Kinesin-like protein;Kinesin-like protein KIF3A			2	KIF3B; KIF3A

Appendix 6.3 ChIP-seq peak enrichment

Appendix Table 6.5 ChIP-seq enriched peaks across shRNA2 and shRNA3

Symbol	Gene Name
CAPN15	calpain 15
SH2B3	SH2B adaptor protein 3
NTN3	netrin 3
MC5R	melanocortin 5 receptor
CHPF	chondroitin polymerizing factor
TUB	TUB bipartite transcription factor
RNF4	ring finger protein 4
ZFYVE9	zinc finger FYVE-type containing 9
BAIAP2L2	BAI1 associated protein 2 like 2
CYP2D7	cytochrome P450 family 2 subfamily D member 7 (gene/pseudogene)
EPPK1	epiplakin 1
LATS2	large tumor suppressor kinase 2
ADORA2A	adenosine A2a receptor
SPECC1	sperm antigen with calponin homology and coiled-coil domains 1
RAP2B	RAP2B, member of RAS oncogene family
DPRXP4	divergent-paired related homeobox pseudogene 4
DLX3	distal-less homeobox 3
TTLL11	tubulin tyrosine ligase like 11
ZYG11A	zyg-11 family member A, cell cycle regulator
RREB1	ras responsive element binding protein 1
ARHGAP27	Rho GTPase activating protein 27
RUNX2	RUNX family transcription factor 2
SIM2	SIM bHLH transcription factor 2
PML	promyelocytic leukemia
SHANK2	SH3 and multiple ankyrin repeat domains 2
CCDC68	coiled-coil domain containing 68
LINC01140	long intergenic non-protein coding RNA 1140
ERG	ETS transcription factor ERG
KCNJ9	potassium voltage-gated channel subfamily J member 9
ERICH5	glutamate rich 5
ADARB1	adenosine deaminase RNA specific B1
BTBD6	BTB domain containing 6
ISM2	isthmin 2
TSPAN9	tetraspanin 9
FBXL14	F-box and leucine rich repeat protein 14
DNAAF5	dynein axonemal assembly factor 5
SIVA1	SIVA1 apoptosis inducing factor
PANX2	pannexin 2
EPS8L2	EPS8 like 2
CD248	CD248 molecule
FAM110A	family with sequence similarity 110 member A
SCRIB	scribble planar cell polarity protein

Symbol	Gene Name
MYO15A	myosin XVA
PLXND1	plexin D1
RNF223	ring finger protein 223
PAX8-AS1	PAX8 antisense RNA 1
RYR2	ryanodine receptor 2
EML5	EMAP like 5
RASA3	RAS p21 protein activator 3
PJA2	praja ring finger ubiquitin ligase 2
CYP2W1	cytochrome P450 family 2 subfamily W member 1
SYNGR3	synaptogyrin 3
NFIL3	nuclear factor, interleukin 3 regulated
LINC00235	long intergenic non-protein coding RNA 235
FAM83H	family with sequence similarity 83 member H
BMS1P17	BMS1 pseudogene 17
DNAJB6	DnaJ heat shock protein family (Hsp40) member B6
BMP8A	bone morphogenetic protein 8a
DHH	desert hedgehog signaling molecule
SLC25A37	solute carrier family 25 member 37
SEPT5-GP1BB	SEPT5-GP1BB readthrough
HAGLR	HOXD antisense growth-associated long non-coding RNA
HTRA4	HtrA serine peptidase 4
PTPN23	protein tyrosine phosphatase non-receptor type 23
SARM1	sterile alpha and TIR motif containing 1
MATN4	matrilin 4
HID1	HID1 domain containing
MRPL38	mitochondrial ribosomal protein L38
FAM162B	family with sequence similarity 162 member B
TRIML2	tripartite motif family like 2
KRTCAP3	keratinocyte associated protein 3
SCIN	scinderin
LMF1	lipase maturation factor 1
TBCD	tubulin folding cofactor D
NPNT	nephronectin
ZAR1	zygote arrest 1
HBQ1	hemoglobin subunit theta 1
ZMIZ1	zinc finger MIZ-type containing 1
A4GALT	alpha 1,4-galactosyltransferase (P blood group)
UTP6	UTP6 small subunit processome component
LYPD6	LY6/PLAUR domain containing 6
TMEM249	transmembrane protein 249
ANKRD30B	ankyrin repeat domain 30B
BEGAIN	brain enriched guanylate kinase associated
KIF16B	kinesin family member 16B
CBY3	chibby family member 3
STRN4	striatin 4

Symbol	Gene Name
INPP5F	inositol polyphosphate-5-phosphatase F
HAGLR	HOXD antisense growth-associated long non-coding RNA
IMPA2	inositol monophosphatase 2
MUC2	mucin 2, oligomeric mucus/gel-forming
SIVA1	SIVA1 apoptosis inducing factor
C5orf66	chromosome 5 open reading frame 66
ST13P4	ST13, Hsp70 interacting protein pseudogene 4
CEP131	centrosomal protein 131
MIR638	microRNA 638
KCTD17	potassium channel tetramerization domain containing 17
KCNH3	potassium voltage-gated channel subfamily H member 3
SLC25A12	solute carrier family 25 member 12
ELFN2	extracellular leucine rich repeat and fibronectin type III domain containing 2
ZMYND19	zinc finger MYND-type containing 19
RASIP1	Ras interacting protein 1
MIR939	microRNA 939
ADPRHL1	ADP-ribosylhydrolase like 1
GPR62	G protein-coupled receptor 62
TUBBP5	tubulin beta pseudogene 5
ZNF737	zinc finger protein 737
LOC154449	uncharacterized LOC154449
RNH1	ribonuclease/angiogenin inhibitor 1
PCDHB15	protocadherin beta 15
ZNF414	zinc finger protein 414
TRIM11	tripartite motif containing 11
ADAMTS10	ADAM metallopeptidase with thrombospondin type 1 motif 10
NABP1	nucleic acid binding protein 1
GABBR2	gamma-aminobutyric acid type B receptor subunit 2